# Mass Spectrometry Methods for Bacterial Infection Diagnosis and Cancer Analysis

**Thèse N° 9322**

## YINGDI ZHU

Acceptée sur proposition du jury

Dr T. Meyer, président du jury
Prof. H. Girault, Dr L. Qiao, directeurs de thèse
Prof. G. Greub, rapporteur
Dr L. Dayon, rapporteur
Prof. R. Zenobi, rapporteur

2019

**EPFL**
ÉCOLE POLYTECHNIQUE
FÉDÉRALE DE LAUSANNE

*A salute to science*
致敬科学


*To my dear father and mother*
献给我亲爱的爸爸妈妈


*To my dear thesis advisor Prof. Hubert H. Girault*
献给我敬爱的导师 *Hubert H. Girault* 教授

# Acknowledgements

# Abstract

Matrix-assisted laser desorption/ionisation (MALDI) time-of-flight (TOF) mass spectrometry is an important analytical tool in chemistry and biology. Bearing the advantages of easy-to-use, fast measurements and relatively simple data interpretation, MALDI-TOF mass spectrometry has been expanded from research laboratories to clinical applications. In this thesis, methods based on MALDI-TOF mass spectrometry are developed for the purpose of bacterial infection diagnosis and cancer analysis.

Magnetic beads coated with antibodies specific to bacterial species are used to isolate and enrich bacterial cells from complex matrices. This immuno-affinity bacterial capture/enrichment procedure is combined with MALDI-TOF mass spectrometry for the fast identification of bacterial pathogens in human blood.

Titanium dioxide nanoparticles-modified target plates are designed to improve the MALDI efficiency for measuring bacterial cellular components by extending the mass range and lowering the detection sensitivity. This titanium dioxide-facilitated MALDI-TOF mass spectrometry method allows the detection of antimicrobial resistance-associated proteins directly from intact bacterial cells.

A combination of immuno-affinity enrichment strategy and redox indicators-mediated amperometric read-out is implemented in a point-of-care platform for bacteria detection. The platform provides bacterial species determination, living cell quantification and antimicrobial susceptibility testing. It could serve as a supplement to MALDI-TOF mass spectrometry to speed up bacterial infection diagnosis.

MALDI-TOF mass spectrometry detection of exosomes is proposed as a potential tool for cancer analysis. It allows the classification of cancer cells, tracking of target proteins, detection of cancer biomarkers and exploring cancer progression *via* exosomes-mediated intercellular communication. Targeting blood-circulating exosomes, it also opens new ways for fast detection of cancer diseases and dynamic monitoring of the disease status.

Cells are recovered from human skin using adhesive tapes, and the skin cells-bearing tapes are directly transferred onto a MALDI target for skin cell fingerprinting using MALDI-TOF mass spectrometry. This tape stripping mass spectrometry approach is proposed for rapid and non-invasive detection of skin diseases like skin cancers.

**Keywords:** matrix-assisted laser desorption/ionisation; mass spectrometry; bacteria; bloodstream infections; immuno-affinity; antimicrobial resistance; amperometry; exosomes; cancer; adhesive tape

# Résumé

La spectrométrie de masse par "Matrix-assisted laser desorption/ionisation (MALDI) time-of-flight (TOF)" est un outil analytique important en chimie et en biologie. Facile d'utilisation, rapide et donnante des spectres assez faciles à interpréter, la spectrométrie de masse MALDI-TOF est utilisée non seulement dans les laboratoires de recherche mais aussi pour les analyses médicales. Dans cette thèse, différents méthodes analytiques basées sur la spectrométrie de masse MALDI-TOF ont été développées pour la détection de bactéries et comme outil de diagnostic du cancer.

Des billes magnétiques recouvertes d'anticorps spécifiques aux bactéries ont été utilisées pour isoler et enrichir des bactéries à partir de matrices biologiques complexes. Cette méthode d'immuno-affinité et d'enrichissement a été combinée à la spectrométrie de masse MALDI-TOF pour une identification rapide des bactéries pathogènes dans le sang humain.

Des plaques MALDI modifiées avec des couches de dioxyde de titane ont été développées pour améliorer l'efficacité des mesures des spectres de masse en élargissant la gamme des rapports masse/charge et en baissant les seuils de détection. Cette nouvelle approche permet la détection des protéines associées à la résistance aux antibiotiques directement à partir des bactéries intactes.

La combinaison des stratégies d'enrichissement par immuno-affinité et l'utilisation des indicateurs rédox a permis de développer une approche ampérométrique « point-of-care, POC » de la détection des bactéries. Cette méthode permet de mesurer non seulement la présence des bactéries mais aussi directement leur résistance aux antibiotiques et représente un complément aux analyses par spectrométrie de masse pour le diagnostic des infections.

La détection des exosomes dans le sang par spectrométrie de masse MALDI-TOF est proposée comme un outil potentiel pour le diagnostic du cancer. En effet, cette approche permet de classifier les cellules cancéreuses, de traquer des protéines caractéristiques, et de suivre la progression d'un cancer en suivant la communication intercellulaire des exosomes. En mesurant la présence des exosomes circulant dans le sang, on peut en effet avoir une mesure rapide de la présence et de la dynamique d'un cancer.

Des cellules de peau humaine ont été prélevées par un ruban adhésif et ont pu être mesurées par spectrométrie de masse MALDI-TOF donnant une signature spectrale. Cette approche est proposée pour une détection rapide et non-invasive des maladies de peau comme les mélanomes.

# List of Abbreviations

| | |
|---|---|
| Ab | Antibody |
| AST | Antimicrobial susceptibility testing |
| ATCC | American type culture collection |
| BSA | Bovine serum albumin |
| BSI | Bloodstream infections |
| CE | Counter electrode |
| CFU | Colony-forming unit |
| CHCA | α-Cyano-4-hydroxycinnamic acid |
| CLSI | Clinical and laboratory standards institute |
| CNT | Carbon nanotube |
| CTC | 5-Cyano-2,3-di-(p-tolyl) tetrazolium chloride |
| CV | Cyclic voltammetry |
| DHB | 2,5-Dihydroxybenzoic acid |
| DPV | Differential pulse voltammetry |
| ER | Endoplasmic reticulum |
| ESBL | Extended-spectrum β-lactamase |
| ESI | Electrospray ionisation |
| EUCAST | European committee on antimicrobial susceptibility testing |
| FA | *trans*-Ferulic acid |
| GFP | Green fluorescence protein |
| HPLC | High-performance liquid chromatography |
| INT | 2-(4-Iodophenyl)-3-(4-nitrophenyl)-5-(phenyl) tetrazolium chloride |
| LC | Liquid chromatography |
| LDI | Laser desorption/ionisation |
| MALDI | Matrix-assisted laser desorption/ionisation |
| MB | Magnetic bead |

| | |
|---|---|
| MCP | Microchannel plate |
| MDR | Multidrug-resistant |
| MIC | Minimal inhibitory concentration |
| mPMS | 1-Methoxy-5-methyl-phenazium methyl sulfate |
| MRSA | Methicillin-resistant *Staphylococcus aureus* |
| MS | Mass spectrometry |
| PAGE | Polyacrylamide gel electrophoresis |
| PBS | Phosphate buffered saline |
| PBST | Phosphate buffered saline containing tween-20 |
| PRC | Polymerase chain reaction |
| RE | Reference electrode |
| RS | Resazurin |
| SA | Sinapinic acid |
| SDS | Sodium dodecyl sulphate- |
| $TiO_2$ | Titanium dioxide |
| TOF | Time-of-flight |
| TTC | 2,3,5-Triphenyl tetrazolium chloride |
| USP | United States pharmacopeia |
| UV | Ultraviolet |
| WE | Working electrode |
| WST-1 | 2-(4-Iodophenyl)-3-(4-nitrophenyl)-5-(2,4-disulfophenyl)-2*H* tetrazolium monosodium salt |
| WST-8 | 2-(2-Methoxy-4-nitrophenyl)-3-(4-nitrophenyl)-5-(2,4-disulfophenyl)-2*H* tetrazolium monosodium salt |

# List of Symbols

| | |
|---|---|
| A | Area |
| C | Concentration |
| $d$ | Distance |
| $E$ | Energy |
| L | Length |
| m | Mass |
| $m/z$ | Mass-to-charge ratio |
| R | Resolution |
| $S/N$ | Signal-to-noise ratio |
| t | Time |
| U | Potential |
| $v$ | Velocity |
| $\lambda$ | Wavelength |

# Table of Contents

# CHAPTER I. Introduction

On May 26th, 1981, a Marine EA-6B Prowler jet fighter plane crashed on the deck of the aircraft carrier Nimitz off the northern coast of Florida in the U.S. The crash led to 14 crewmen killed and around 48 injured. The subsequent fire and explosions destroyed 3 other fighters and damaged 16, causing heavy economic losses (source: May 28, 1981, Page 00001, The New York Times Archives). Subsequent immunoassay tests told that most of the 14 killed crewman had traces of illicit drugs in their bodies, pointing to the use of marijuana (source: June 17, 1981, Page 00020, The New York Times Archives). Although unclear whether the drug use would have directly contributed to the crash, U.S. President Ronald Reagan afterwards instituted a "Zero Tolerance" drug policy across the armed service, starting the mandatory drug testing of all U.S. service personnel (Executive Order 12564–Drug-Free Federal Workplace, September 15, 1986). Due to the high false-positive rate resulting from the conventional immunoassays, the drug testing results were required to be confirmed by gas chromatography–mass spectrometry (Mandatory Guidelines for Federal Workplace Drug Testing Programs, firstly published in the Federal Register on April 11, 1988). Since then, mass spectrometry has been used in both research laboratory and clinical laboratory.

Historically, the success of gas chromatography–mass spectrometry in clinics has focused on the confirmation of immunoassay-positive drug screening, the identification of inborn errors of metabolism and the analysis of steroid hormones.[1] Years of clinical practice made evident the limitation of this technique, which measures volatile analytes and thus requires multiple extraction/purification steps to make the analytes sufficiently volatile for analysis. The use of mass spectrometry for biospecimen analysis grew rapidly during the middle and late 1990s, seeing a shift from gas chromatography as a mass spectrometry frond-end technique to liquid chromatography. Measuring liquid analytes, liquid chromatography mass spectrometry or tandem mass spectrometry eliminates the need for volatile analytes and thus simplifies the sample preparation process, significantly improving the analysis throughput and cost-effectiveness. Its applications in clinical laboratory have spanned hundreds of tests in drug/toxicology, newborn screening and endocrinology.[2] The combination of the soft ionisation technique electrospray ionisation (ESI) with high performance liquid chromatography mass spectrometry provides sensitive measurements at femtomole ($10^{-15}$ mole) quantities in microliter sample volumes. The soft ionisation technique allows the formation of analyte

ions without the loss of analyte molecular integrity, playing important roles in clinical metabolomics and proteomics.[3] In the late 1990s, the coupling of matrix-assisted laser desorption/ionisation (MALDI), another soft ionisation technique, with time-of-flight (TOF) mass analyser has transformed the practice of clinical microbiology.[4] Compared to ESI mass spectrometry, MALDI-TOF mass spectrometry has certain advantages. The samples on the target plate can be kept for a certain period of time for re-analysis to gain more information or to valid the previously obtained information. Also, it produces mostly singly charged analyte ions, and thus makes the spectrum interpretation much easier. MALDI-TOF mass spectrometry enables the identification of microorganisms at the genus, species or even strain level by directly measuring the intact microbes. This fast microorganism identification technique has been approved by many countries for the diagnosis of infectious diseases.[5] Additionally, MALDI-TOF mass spectrometry is also powerful for biomarker discovery and detection, showing potentials for the management of diseases like cancers.[6] This thesis is mainly focused on the development of methods to improve bacterial infection diagnosis and to facilitate cancer analysis on the basis of MALDI-TOF mass spectrometry.

# 1. MALDI-TOF mass spectrometry

## 1.1 What is MALDI-TOF mass spectrometry?

In the past decades MALDI-TOF mass spectrometry has become one of the most powerful tools for the analysis of biomolecules like metabolites, lipids, peptides and proteins, as well as biological entities like bacteria, fungi, virus and mammalian cells. It has been employed not only in fundamental scientific research but also in practical clinical diagnosis. The importance of this mass spectrometry technique has been recognized by the Nobel Prize in Chemistry in 2002. The Google Scholar search of "MALDI-TOF mass spectrometry" gives about 368,000 hits, indicating its wide usage. What is MALDI-TOF mass spectrometry? This is an apparently simple but not yet fully understood analytical technique. Dating back to the year of 1969 when TOF mass analyser was in its infancy, H. Kienitz, *et al.*, gave the following definition for mass spectrometry:

"*The basic principle of mass spectrometry is to generate ions from either inorganic or organic compounds by any suitable method, to separate these ions by their mass-to-charge ratio (m/z) and to detect them qualitatively and quantitatively by their respective m/z and abundance. The analyte may be ionized thermally, by electric fields or by impacting energetic electrons, ions or photons. The ions can be single ionized atoms, clusters, molecules or their fragments or associates. Ion separation is effected by static or dynamic electric or magnetic fields.*"[7]

After fifty years of development, the definition is still valid. Ionisation of analyte and separation/detection of analyte ions remain the basic steps of all mass spectrometry techniques. Generally, a mass spectrometer comprises five parts, including *i)* an inlet to introduce the sample, *e.g.* a liquid chromatograph or gas chromatograph, an injection pump, or a direct insert target plate; *ii)* an ion source to produce ions from the sample, with the ionisation technique varies from hard gas phase ionisation to soft condensed phase ionisation; *iii)* one or several mass analysers to separate ions according to their mass-to-charge ratio, sometimes also including steps of ion selection and fragmentation; *iv)* an ion detector to "receive" or "count" the ions coming from the mass analyser and convert the ions into electrical signals; *v)* a digital data acquisition system to process the signals from the detector and create a mass spectrum.[8] In the case of MALDI-TOF mass spectrometers, the general compositions are shown in **Figure 1.1**. The analyte is introduced by directly inserting an electrically conductive target plate, which bears 48, 96, 192 or 384 sample spots and allows high-throughput analysis. Thereafter, the analyte is ionized by the soft ionisation technique of matrix-assisted laser desorption/ionisation (MALDI), which employs pulsed laser to irradiate the co-crystals of analyte and a laser energy absorbing matrix to generate protonated or deprotonated ions. The generated ions are then separated by a time-of-flight (TOF) analyser according to their mass-to-charge ratios, and finally detected by a mass detector, which often is a microchannel plate (MCP) detector. The mass spectrometer is software-controlled for spectrum acquisition and instrumental parameter adjustment. All the mass spectra present in this thesis were obtained with the Bruker microflex[TM] LRF instrument, which is currently one of the most powerful benchtop MALDI-TOF mass spectrometer.
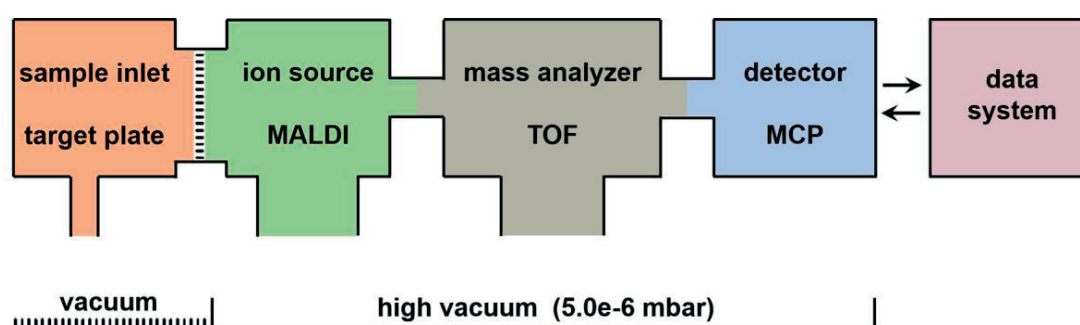


**Figure 1.1** General structure of a MALDI-TOF mass spectrometer. The measurements are conducted under high vacuum condition. The exact vacuum level depends on the individual instrument. For instance, the Bruker microflex[TM] LRF requires the ion source vacuum lower than $5 \cdot 10^{-6}$ mbar.

The generated mass spectrum is the two-dimensional representation of signal intensity *versus* the mass-to-charge ratio (*m/z*), with the observation of a panel of mass spectral peaks, with an example shown in **Figure 1.2**. In many cases, the mass spectrum is normalized to make the most intense peak 100% relative intensity. The normalization facilitates the comparison of mass spectra. Mass spectrometry measurements are "ion counting" processes, with the peak intensities greatly dependent on the numbers of ions reaching the detector. Thereby, during the measurement of a mixture analyte, the peak intensities represent, to a large extent, the relative molecular abundance of the analyte components. The performance of a mass spectrometer is usually characterized by the terms of *sensitivity* and *detection limit*.[9] *Sensitivity* is the change in peak intensity in response to analyte amount, reported as electric charge of a particular ion species reaching the detector per mass of the analyte. It is given in the unit of $C \cdot \mu g^{-1}$ for solid analytes. The *detection limit* is defined as the smallest amount of an analyte required to generate a mass spectral peak that can be distinguished from the background noise. The detection limit can be improved by adjusting the sample preparation protocol, as illustrated in Chapter II of this thesis. A good quality mass spectrum makes the data explanation easy. The spectrum quality is evaluated according to the *signal-to-noise* ratio and the *peak resolution*. The *signal-to-noise* ratio represents the ability to read an analyte from the mass spectrum. The noise mainly comes from the matrix, especially in the mass range lower than 2,000 *m/z*. *Peak resolution* is defined as the observed mass value (*m/z*) divided by the smallest mass difference (Δ(*m/z*) allowing the separation of two nearby peaks, *i.e. (m/z)/*Δ(*m/z*). Higher resolution refers to the higher possibility to distinguish two adjacent peaks.
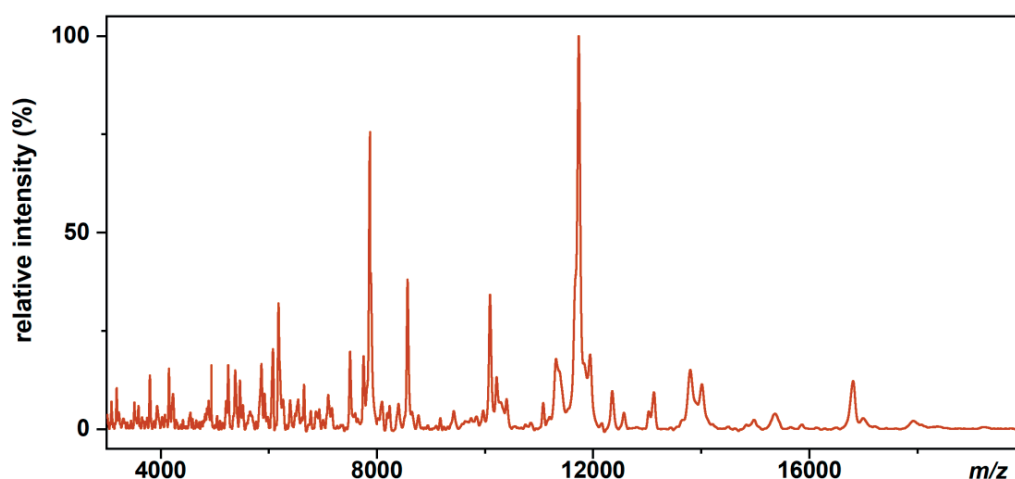


**Figure 1.2** An example of MALDI-TOF mass spectrum. The spectrum was collected from exosomes that were secreted by human melanoma cell line SBCl2.

## 1.2. MALDI principle

The technique of laser desorption/ionisation (LDI) was introduced in the late 1960s, which is easily achievable for low-mass organic salts and light absorbing organic molecules.[10-12] However, the ionisation of biological macromolecules such as proteins are hardly achievable with the LDI technique. The situation greatly improved since the year 1988 when the concept of MALDI was introduced by Karas and Hillenkamap.[13,14] After that, MALDI has become a widely used technique for the generation of ions from a wide range of molecules, especially the larger, non-volatile and thermally labile compounds like lipids, polymers, oligonucleotides and proteins.[15,16] It benefits from an easy sample preparation and large tolerance to contamination from salts, buffers, detergents, *etc.*, and significantly promotes the development of modern life science and polymer synthesis science.
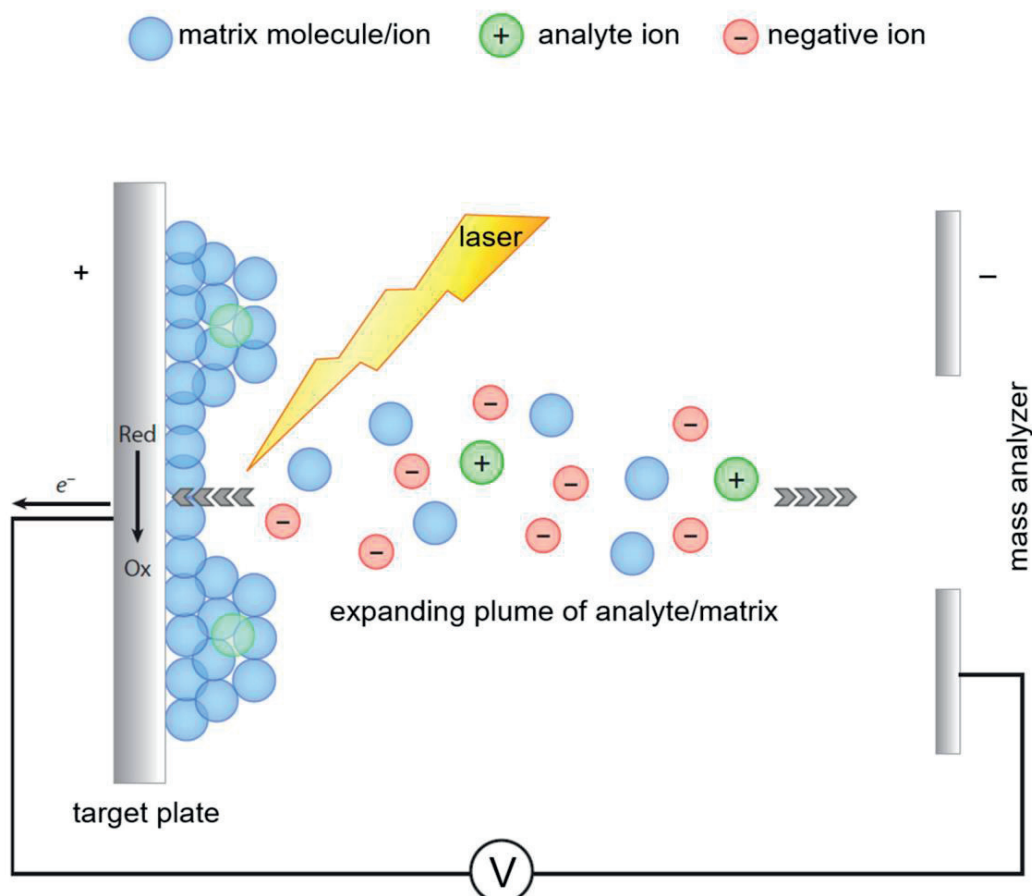
**Figure 1.3** Scheme of the MALDI process in positive ion mode.[18] Copyright © 2010 Annual Reviews.

MALDI is a soft condensed phase ionisation process, which is achieved in two steps. In the first step, the analytes are dissolved in an aqueous/organic solvent containing small organic molecules, the so-called matrix. The matrix molecules have strong ability to absorb energy from laser. The mixture of analyte and matrix is dried on the target plate at room temperature to remove any liquid solvent, resulting in the formation of a "solid solution" where analyte molecules are doped in the crystals of matrix molecules. The analyte molecules are embedded throughout the matrix crystals so that they are separated from each other. The target plate bearing the analyte/matrix mixture is inserted into the sample inlet of the mass spectrometer, and is transferred to the ion source under high vacuum condition. In the ion source, the analyte/matrix mixture is irradiated with intense laser pulses. Each of the pulses lasts a short time, usually a few nanoseconds to a few hundred nanoseconds. Under the laser irradiation, the mixture of analyte/matrix is rapidly heated by the accumulation of laser energy in the condensed phase. The rapid heating excites the matrix crystals, and leads to localized ablation of the analyte/matrix surface, expansion of analyte/matrix into the gas phase, formation of analyte/matrix expanding plume and thus the generation of analyte ions.[17,18] The produced analyte ions in the gas phase are thereafter accelerated by an electrostatic field towards the mass analyser. In a Bruker microflex[TM] LRF mass spectrometer, the acceleration voltage is mostly 20 kV. The scheme of the general MALDI process is presented in **Figure 1.3**.

The exact mechanism of the ion formation process is still not fully understood. Numerous chemical and physical ionisation pathways have been proposed. [19] Among them, the most widely accepted are the preformation of analyte ions in the solid phase before desorption and the gas-phase proton transfer in the expanding plume. It has been found that decreased pH of the matrix aqueous/organic solution can increase the production yield of protonated analyte ions $[M+H]^+$. A similar phenomenon was observed for cationisation products like $[M+alkali]^+$ from oxygen-rich analytes. These discoveries indicated the incorporation of analyte molecules as preformed ions into the matrix crystals, and the preformed ions are afterwards desorbed from the condensed phase and released into the gas phase under laser irradiation.[20-22] Nonetheless, the preformation of analyte ions in the solid phase does not exclude the possibility of gas-phase ionisation. In the expanding plume, protons can be transferred from the photo-ionized matrix molecules to the analyte molecules. The proton transfer process is accompanied with a series of in-plume matrix-matrix reactions and matrix-analyte reactions. This is especially the case when a non-carboxylic acid matrix is used, where the excited state of matrix molecules, or the protonated matrix ions, account for the proton transfer to the slightly basic analyte molecules.[23,24] To be noted, deprotonated matrix ions can also be generated, most probably through dissociative electron capture. These matrix anions are generally not able to deprotonate the analyte molecules, especially for analyte classes like hydrocarbons,

thiols and nitro-containing compounds.[25] Therefore, the formation of analyte anions [M-H]$^-$ often results from dissociated electron capture reactions, as is the case for the formation of matrix anions. For analytes that can absorb energy from the laser, direct photo-ionisation can happen. Usually, the ionisation of an individual sample stems from several ion formation pathways, rather than from only a single process. Which process contributes the most is dependent on the exact combination of the analyte, matrix, solvent and other possible additives.

The expanding plume of analyte/matrix emerging from the solid mixture upon laser irradiation is globally neutral, containing both positive and negative ions. One can extract either positive or negative ions by adjusting the polarity of the acceleration voltage, which corresponds to the positive ion mode or the negative ion mode of MALDI. On a MALDI-TOF mass spectrum, almost all the observed peaks are singly charged. But in the starting conditions of MALDI, the analyte molecules can be multiply charged, by either protonation, deprotonation, or ion attachment in the matrix solution before embedding into the matrix crystals. The preferential detection of only singly charged analyte ions can be explained by the so-called *lucky survivor model*.[26,27] This model explains the happening of mutual neutralization by recombination of the positive ions and the negative ions in the expanding plume. The rate of mutual neutralization is high if the initial charges of an ion are high. Thereby, the mutual neutralization rate of singly charged ions is generally much lower than that of multiply charged ions. The singly charged ions are thus the "lucky survivors" from the mutual neutralization conflict, and finally enter into the mass analyser. Moreover, during a MALDI mass spectrometry detection, negative ions are often observed in lower abundance than positive ions. This phenomenon can be explained by the rapid loss of most fast moving electrons from the laser plume, which leads to the excess presence of positive ions over time. Also, a mass spectrum often displays lower resolution at high mass range, which could be explained by the initial ion velocity. The initial velocities of analyte ions are reported in the range of 400-1200 m·s$^{-1}$.[28-30] The initial velocity is dependent on the matrix utilized and the analyte compound types, but almost irrelevant to the analyte mass. Thereby, compared to analyte ions with low mass, the analyte ions with higher mass would carry higher translational energy before ion acceleration in electrostatic field. And the velocity range of the higher mass ions is wider after they pass through the acceleration region, leading to the formation of thicker ion packet when they are approaching the detector, which could cause considerable loss of peak resolution.[31]

During a MALDI process, the ionisation process will not happen if the laser fluence is lower than the threshold value.[32] Above the threshold, desorption/ionisation is switched on with a sudden rising of ion abundance. The fluence threshold depends on the molar ratio of matrix-to-analyte and the absolute amount of analyte. For instance, the minimum

threshold for cytochrome c is obtained when the matrix-to-cytochrome c molar ratio is 4000:1.[33] Lower concentrations of the analyte would decrease the detection efficiency as a large volume of analyte/matrix mixture is required to be ablated to generate enough amount of analyte ions. While too high concentrations of analytes are also unfavorable for the detection, because the dilution of matrix leads to a reduced energy absorption per volume of analyte/matrix and thus an elevated laser fluence threshold. A good quality mass spectrum with high peak resolution and less (or no) fragmentation is obtained when the laser irradiation is performed with the laser fluence slightly above the threshold value.

Beside of the laser fluence, the laser beam size also affects the spectrum quality. The ideal laser beam size, or laser spot size, is 100-200 μm.[34] Such a laser spot size can generate an evenly distributed shallow ablation of the upper layer of the analyte/matrix solid mixture, also can simultaneously irradiate a large number of micrometer-sized matrix crystals to average out the influence from mutual orientation of crystal surface and laser beam axis. The utilization of an extremely narrow laser beam should be avoided, as it will cause a deep crater on the analyte/matrix mixture surface and lead to an heterogeneous eruption of analyte/matrix.[35]

The laser commonly used for MALDI are ultraviolet lasers, including the nitrogen lasers ($\lambda = 337$ nm, $E = 3.68$ eV) and Nd:YAG lasers ($\lambda = 266$ or $355$ nm, $E = 4.66$ or $3.49$ eV), due to their convenient operation and low cost.[36,37] Infrared lasers such as Er:YAG lasers ($\lambda = 2.94$ μm, $E = 0.42$ eV) and TEA-CO$_2$ lasers ($\lambda = 10.6$ μm, $E = 0.12$ eV) are also used but limited to the applications where the deeper penetration of infrared radiation is required, $e.g.$ for the detection of analytes direct from sodium dodecyl sulfate gels.[38] The pulse widths of ultraviolet lasers are often about 3-10 ns. This short laser pulse results in a short time interval of ion production, and avoids the thermal degradation of the analytes.[39]

### 1.3. TOF analyser

The concept of time-of-flight (TOF) mass analyser was firstly described by W. E. Stephens in 1946.[40] Nine years later, in 1955, the design of a liner TOF, which later became the first commercial instrument through the effort from Bendix, was published by Wiley and McLaren.[41] The first generation of TOF analysers were designed for the coupling with gas chromatography-mass spectrometry, but their performance was quite poor at that time.[42] Then, it was only in the later 1980s that the pulsed ionisation method of MALDI was developed. MALDI generated a great demand for mass analysers that could be compatible with its pulsed ionisation nature and able to manage ions with wide range of mass. Thereafter, the development of TOF analysers has been greatly push forward.[43]

Generally, TOF analysers separate ions according to their velocities.[8] **Figure 1.4** displays the scheme of a linear TOF for the analysis of ions produced by MALDI. Upon

generation, the ions are accelerated to the flight tube by a potential difference (*U*) applied between the target plate and the extraction grid. In a Bruker microflex™ LRF mass spectrometer, the potential difference, or the acceleration voltage, is usually 20 kV. When leaving the acceleration region, all the ions acquire a certain velocity and fly into a field-free region, *i.e.* the flight tube, where they are separated according to their velocities. Ions with different velocities reach the detector at different time points. The *m/z* of ions is determined by measuring the time that ions take to fly through the flight tube.
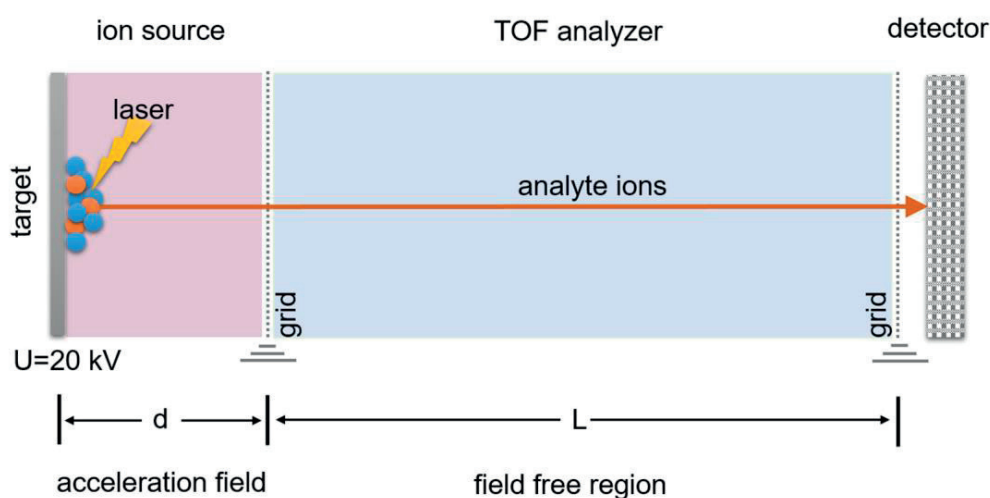


**Figure 1.4** Scheme of liner TOF for the analysis of ions produced by MALDI under positive mode. Copyright © 2007 John Wiley & Sons Ltd.

Ignoring the initial velocity, the velocity (*v*) of ions with mass *m* and total charge *q* (*q=ze*) when leaving the acceleration region can be calculated as:

$$\frac{1}{2} mv^2 = zeU$$

$$v = \sqrt{2zeU/m}$$

The flight time (*t*) to pass through the flight tube (length *L*) to reach the detector is:

$$t = L/v = L\sqrt{m/2zeU}$$

Taking into account the length (*d*) of the acceleration region, the total flight time (*t′*) is:

$$t' = (2d + L)\sqrt{m/2zeU}$$

Accordingly, *m/z* is given by:

$$^{m}/_{z} = 2eU(^{t'}/_{2d + L})^2$$

The above equation shows *m/z* can be calculated by measuring the total flight time, as all other terms are constant. As most of the detected ions are single charged, this equation also shows that under the same condition ions with a lower mass will reach the detector faster. In principle, the mass range of a TOF analyser has no limit, and various types of analyte can be detected.[44] The analysis speed of TOF is very fast, because the velocities of ions are generally quite high and the flight time is quite short. As a result, a spectrum over a broad mass range can be obtained within microseconds in theory.

As previously mentioned, resolution is one of the crucial characteristics of a mass spectrometer. It indicates the ability of the mass spectrometer to yield distinct peaks for two ions with small mass difference. The resolution (R) is defined as:

$$R = ^{(m/z)}/_{\Delta(m/z)}$$

As

$$^{m}/_{z} = 2eU (^{t'}/_{2d + L})^2$$

Thus

$$\Delta(m/z) = 2eU(^{1}/_{2d + L})^2 \cdot 2t'\Delta t'$$

Therefore

$$R = ^{(m/z)}/_{\Delta(m/z)} = t'/2\Delta t' \approx L/\Delta x$$

where $\Delta t'$ and $\Delta x$ is the time span or length thickness of an ion packet approaching the detector.

The above equation shows that resolution of mass spectrometer is proportional to the total flight time and flight distance. One way to increase the resolution is to increase the length of the flight tube. However, too long flight tubes decrease the performance of TOF because of the loss of ions by scattering and dispersion. Another way is to increase the flight time by lowering the acceleration voltage. However, too low voltage reduces the peak resolution. This is because under quite a low acceleration voltage, the initial velocity of ions must be taken into account and all the ions with the same *m/z* reach the detector in a longer time span, which broadens the mass spectral peak. Also ions are more likely to be lost during the flight process when their velocity is not high enough. Thus, not all of the formed ions can reach the detector, resulting in a low detection sensitivity. Therefore, the only way to have both high resolution and high sensitivity is to equilibrate the two aspects.

Normally, a flight tube with a length of 1-2 m and an acceleration voltage of ~ 20 kV are used.

Along with the continuous development of TOF analysers, two techniques have been proposed to enhance the resolution, *i.e.* delayed pulse extraction and reflectron mode of TOF. The delayed pulse extraction allows the ions to fly for a certain period of time with their initial velocity before being accelerated. Ions with the same *m/z* can reach the same or quite similar velocity when they leave the acceleration region. In this way, those ions can reach the detector at the same time, resulting in sharp mass peaks and thus improved mass spectrum resolution.[45] The reflectron mode of TOF uses an electrostatic reflector also called a reflectron to improve the resolution.[46] The simplest reflectron consists of a series of equally spaced grid electrodes that are connected through a resistive network of equal-value resistors. The reflectron is placed at the end of flight tube and faced to the ion source. The reflectron functions as a "mirror" by deflecting the ions and sending them back to the flight tube. The detector is placed on the same side with the ion source to capture the reflected ions. For ions with the same *m/z*, those with more kinetic energy and thus higher velocity will penetrate the reflectron more deeply than those with lower velocity. Therefore, the faster ions have to pass longer distance before reaching the detector, while the slower ions fly through a shorter distance. In this way, they can reach the detector at (almost) the same time, and result in a sharp mass peak and hence higher resolution. A drawback of the reflectron mode of TOF is that it could lead to the loss of some ions during the flight process and thus a decreased detection sensitivity.

After passing through the TOF analyser, analyte ions are captured by a detector. The detector is able to generate an electric current from the incident ions, which is proportional to the ion abundance. The detector is often a microchannel plate, which relies on parallel cylindrical channels to multiply incident ions under a strong electric field.[47] Each channel acts as a continuous dynode electron multiplier. The electrical signal from the detector is then recorded by a time-to-digital converter or a fast analog-to-digital converter to generate a mass spectrum.

## 1.4. Choice of matrix and sample preparation

The choice of matrix is crucial for a successful mass spectrometry measurement. A matrix firstly functions to separate analyte molecules from one another during the formation of analyte/matrix co-crystals. Generally, a matrix should have low vapor pressure in order not to be volatized under the high level vacuum condition in the ion source. A matrix should also have a high ability to take up laser energy. The uptake of
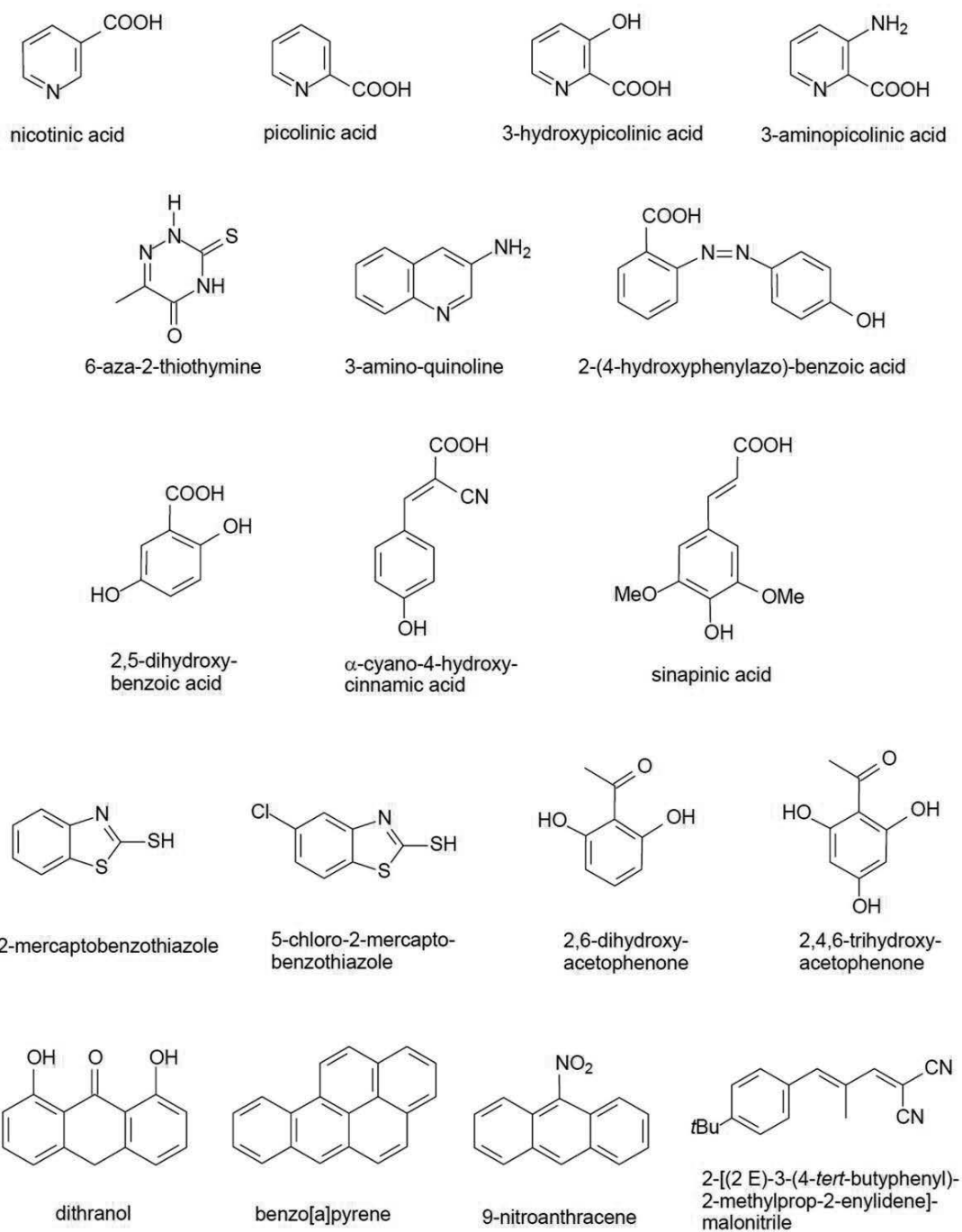
**Figure 1.5** Common MALDI matrices.[9] Copyright © 2004, 2011 Springer-Verlag Berlin Heidelberg.

energy is based on a strong absorption. Thus, the matrix molecule should have a suitable chromophore for the easy generation of excited state upon laser irradiation. When an ultraviolet laser is employed, the matrix often needs to possess an aromatic core in the molecular structure together with appropriate functional groups.[48] Under the condition of infrared lasers, the selection of matrix is more flexible, with fewer restrictions applying to the matrix molecular structure. Because infrared laser is easy to be adsorbed by the stretch vibration or bending vibration of O-H, N-H or C-O.[49] The matrix should have low enough mass for sublimation and a good solubility in solvents compatible with the analyte, and, of course, it should not chemically react with the analyte.

Nicotinic acid was the first matrix successfully used for the detection of peptides and proteins. Since then, more matrices have been introduced. **Figure 1.5** lists the MALDI matrices that are commonly used. Applications of these matrices are illustrated in detail in a text book of mass spectrometry written by Jürgen H. Gross.[9] Among them, picolinic acid, 3-hydroxypicolinic acid, 3-aminopicolinic acid and 6-aza-2-thiothymine are usually employed for the detection of oligonucleotides, which are short DNA or RNA molecules or oligomers. 3-amino-quinoline is a suitable matrix for oligosaccharides. The measurement of synthetic polymers and lipids are achievable with the matrices 2-mercaptobenzothiazole, 5-chloro-2-mercaptobenzothiazole, dithranol or 9-nitroanthracene. The most widely used matrices for biological analysis are 2,5-dihydroxybenzoic acid (DHB), α-cyano-4-hydroxycinnamic acid (CHCA) and sinapinic acid (SA). They are well-suited for the detection of biological macromolecules like oligosaccharides, peptides, proteins, as well as biological entities like intact bacterial cells, fungi, virus and mammalian cells. DHB and CHCA generate high quality spectra in the mass range of 2,000-15,000 *m/z*, while SA often works well over a wider mass range, *e.g.* 5,000-80,000 *m/z*. Generally, the selection of a matrix should be based on the type of the analyte and the laser wavelength used in the mass spectrometer.

Together with the selection of a suitable matrix, sample preparation is another important factor affecting the mass spectrometry measurement. Parameters such as matrix solution composition, target plate surface, sample deposition method, as well as relative humidity, temperature, air flow, *etc.*, can substantially influence the analyte/matrix crystallization, the desorption/ionisation process and ultimately the quality of the mass spectra.[50] When choosing a matrix solution, several factors should be taken into consideration, including the ability to form a homogenous analyte/matrix mixture, a suitable liquid solvent evaporation speed, a proper solvent pH value in favour of the ionisation process. For instance, the optimized solvent for the matrix of DHB, CHCA or SA for the detection of proteins is 49.9/50/0.1% (volume percentage) of water/acetonitrile/trifluoroacetic acid. A MALDI target plate must be electrically conductive to ensure a free flow of electrons. Otherwise, a static charge will build up on

the surface of the analyte/matrix condensed phase, which will disrupt the formation of the ion plume and result in lower spectrum quality. The target plate spot size defines the final sample spot size, and thus influences the detection limit. A normal target plate defines the sample spot size as ~ 3 mm in diameter, allowing the measurement of 0.5-2.5 µL of sample solution. The sample spot size can be reduced to 0.8 mm if an AnchorChip[TM] target (Bruker Daltonik, Germany) is employed. Such a target bears small hydrophilic spot regions on a hydrophobic surface. It can confine the sample solution within the small spot region to increase surface density of the analyte and thus to improve the detection limit.[51] This kind of AnchorChip[TM] target can facilitate the detection of bacteria, as illustrated in Chapter II of this thesis. As for sample deposition, a number of procedures have been proposed for different measurement purposes. The most widely used procedure is the *dried-droplet*. Specifically, 0.5-2.5 µL of droplet containing the mixture of analyte and matrix is placed on a spot of the target plate. The droplet is dried at room temperature, allowing the total evaporation of liquid solvent and the formation of analyte/matrix co-crystals before loading the target plate into a mass spectrometer for measurement. One disadvantage of this droplet deposition procedure is the possible presence of "sweet spots" coming from deposit heterogeneity, which leads to low laser shot-to-shot reproducibility and causes shot-to-shot spectrum variation. Such kind of negative influence can be overcome by accumulating multiple single-shot spectra (*e.g.* 200 laser shots) from an individual spot to create the final sample spectrum. The deposit heterogeneity can also be avoided or reduced by using (nano)electrospray deposition procedure, which is especially necessary for precise quantitative analysis.[52]

## 2. Current standards for bacterial infection diagnosis

### 2.1. Overview of bacterial infections

Bacterial infections, especially those occurring in the bloodstream (*i.e.* bloodstream infections), are associated with significant mortality and morbidity worldwide. They are one type of growing public health concern. According to the report from M. Goto and N. Ai Hasan in 2013, an estimation of 575,000-677,000 bloodstream infection episodes occur every year in North American, including 536,000-628,000 in the USA and 40,000-49,000 in Canada. The resulting deaths are around 79,000-94,000 per year, including 72,000-85,000 in the USA and 7,000-9,000 in Canada.[53] The situation is not better in Europe, with an estimation of 1,200,000 infection episodes and 157,000 deaths per year. In Switzerland, for instance, a total of 40,378 infection cases were reported from the year of 2008 to 2014. During this time span, the incidence rate increased by 14%, from 211 to 240 per 100,000 population (**Figure 1.6**).[54] Bloodstream infections rank among the top seven causes of death in North America and Europe.
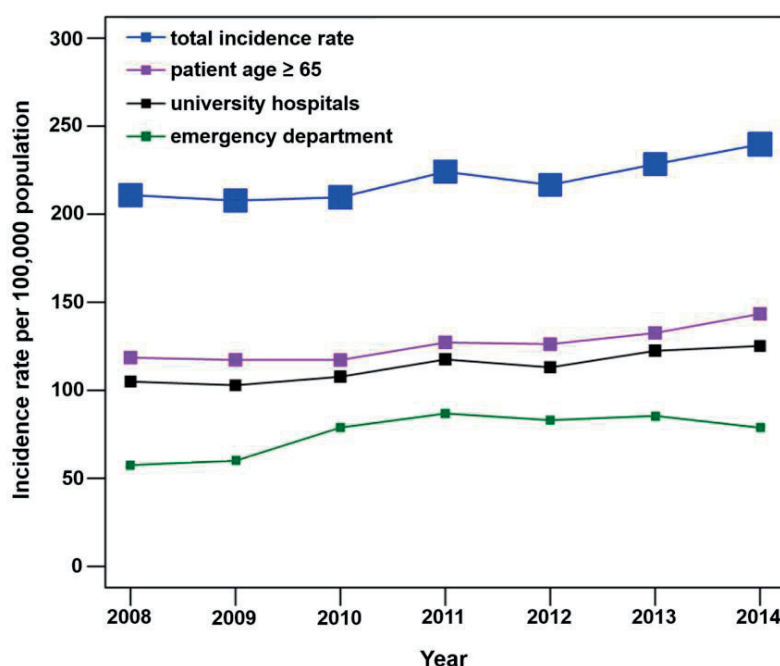
**Figure 1.6** Incidence rate of bloodstream infections (per 100,000 population) in Switzerland from the year 2008 to 2014.[54] Copyright © 2017 BMJ Publishing Group Ltd.

The infections are mainly caused by bacterial pathogens like *Staphylococcus aureus*, coagulase-negative *Staphylococci*, *Streptococcus pneumoniae*, *Escherichia coli*, *Klebsiella spp.*, *Acinetobacter baumannii*, *Enterobacter cloacae* and *Enterococcus spp.* A survey conducted in Switzerland showed that *Escherichia coli* has been the most frequently detected pathogen between the year of 2008 to 2014, while *Enterococcus spp.* shows a continuously increase trend.[54] The infections could also be caused by fungal pathogens like *Candida glabrata*, *Candida tropicalis* and *Candida albicans*. In many cases, the infections are of polymicrobial origins.[55]

During the past decades, antimicrobial-resistant bacteria have spread rapidly throughout the world, leading to a serious antibiotic resistance crisis. C. Lee Ventola reviewed that the crisis is mainly attributed to four factors, *i*) overuse of antibiotics due to the lack of medicine regulation, *ii*) inappropriate prescription of antibiotic therapies, *iii*) extensive use of antibiotics in agriculture, which affects human beings through food supply, *iv*) slow development of new antibiotics in the pharmaceutical industry.[56] Antimicrobial resistance threatens the effective prevention and treatment of bacterial infections, and causes increased physical pain and heavy financial burden to the patients.[57] The US Center for Disease Control and Prevention gives the estimation that

more than two million people per year are suffering from antibiotic-resistant infections, and a counterpart survey conducted in Europe shows that the number of infections caused by the most frequent multidrug-resistant bacteria is around 400,000 every year.[58,59] Common resistant bacterial pathogens include methicillin-resistant *Staphylococcus aureus*, vancomycin-resistant *enterococci*, drug-resistant *Streptococcus pneumoniae*, multidrug-resistant *Pseudomonas aeruginosa*, carbapenem-resistant *Enterobacteriaceae*, extended-spectrum beta-lactamase-producing *Enterobacteriaceae* (notably *Escherichia coli* and *Klebsiella pneumoniae*), and so on.[56]

Development of microbiological science and chemical techniques in the last century contributes to the emerging of many methods for the diagnosis of bloodstream infections. Among them, blood cultures remain the current gold standard. They not only allow the confirmation of an individual infection disease, but also provide enough amount of recovered pathogens for the purpose of genus or species identification and antimicrobial susceptibility testing. The blood culture strategies, as well as the approaches for the following pathogen identification and antimicrobial susceptibility testing, are introduced below.

## 2.2. Blood cultures

Normally, blood cultures are conducted when patients have fever, chills leukocytosis, septic shock or suspected endocarditis. Before blood collection, proper skin antisepsis is required to reduce the risk of contamination.[60] On the basis of published reports, tincture of iodine, chlorine peroxide and alcoholic chlorhexidine gluconate are good candidate for skin antisepsis. Among them, alcoholic chlorhexidine gluconate is recommended by the *Clinical and Laboratory Standards Institute* guidelines for blood collection from adults, children and infants older than 2 months of age.[61] According to several studies, peripheral venipuncture is the preferred method for blood collection. Arterial blood sampling is not necessary, as they will not increase the rate of a successful diagnosis. Blood sampling from intravascular lines should be avoided, because it brings high possibility of contamination.[62] The volume of collected blood directly affects the blood culture yield. The bacterial concentration is quite low in most patients, and their recovery rate can be higher if more blood is collected. Data from modeling and clinical studies display that the bacterial concentration is in the range of 0.01-1 colony-forming unit per mL of blood for around 50% of the infection episodes. And the Washington's empirical data published in 1975 showed that at least 30 mL of blood is required for detecting 99% of bloodstream infections in adult patients. Currently, it is recommended to collect blood from 2 or 3 sets of an individual patient. From each set, 10-20 mL of blood should be drawn and afterwards distributed into two bottles for continuous culture (one aerobic bottle and one anaerobic bottle). In each bottle, 5-10 mL of blood is

injected for culture. [63] The volume of blood drawn from infants and children is not well prescribed, but should be dependent on the patient age and the estimated total body blood volume of the patient. Basically, the drawn blood should not exceed 1% of the total body blood volume.[64] Once optimal blood samples are collected, they should be incubated in blood culture bottles in a continuous-monitoring blood culture instrument as soon as possible. Before the incubation, they should not be kept at room temperature for more than a few hours, and should not be refrigerated or frozen. A delayed incubation could result in delayed or impeded bacterial detection.

The instruments used for continuous monitoring of blood cultures are provided by several manufacturers. Examples include the BACTEC[TM] system series from Becton Dickinson in the USA, and the BACT/ALERT® system series from bioMérieux in France. Their performance characteristics are similar, both comprising the continuous incubation of blood sample-containing bottles for a certain period of time and a dynamic monitoring of the bacterial growth. In the blood culture bottles, carbohydrate substrates are included in the culture broth, which will produce $CO_2$ during the growth of bacteria and will result in the change of pH value. The pH value is monitored by a colorimetric or a fluorescent sensor installed on the bottom of the bottle, as shown in **Figure 1.7**.[65] The culture broth is often a mixture of nutritional culture medium to promote bacterial proliferation, an anticoagulant and resins or charcoal mixtures to reduce the negative influence on bacterial growth from toxic compounds.[66] The blood culture time is normally set to 5 to 7 days. Most bacterial pathogens can be recovered within this culture period. Longer time of incubation does not significantly improve the overall sensitivity of blood culture, but increases the recovery rate of unwanted contaminants.



**Figure 1.7** BACT/ALERT® blood culture bottles from bioMérieux (Marcy-l'Étoile, France). The bottles contain a colorimetric sensor on the bottom to detect the $CO_2$ level change resulting from bacterial growth. The positive bottle is indicated with color change on the bottom, indicating the presence and growth of bacteria in the blood culture. Copyright © 2017 bioMérieux Inc.

However, longer incubation time could be needed if the infections are predicted to be caused by slowly growing pathogen like *Legionella*, *Brucella*, *Bartonella*, or *Nocardia spp*. For fastidious pathogens like *Mycobacterium spp.,* the incubation time might be extended to as long as four weeks.[64] Blood culture bottles with recovered bacterial pathogens are the so-called positive bottles, which confirm the occurrence of bloodstream infections.

## 2.3. Identification of bacterial pathogen

Once blood cultures become positive, gram stain is performed, which further confirms the presence of bacterial pathogens and can classify the pathogens as gram-positive or gram-negative. The gram stain procedure was developed in 1884 by Hans Christian Gram. It allows one to distinguish gram-positive bacteria and gram-negative bacteria based on the differential staining using a crystal violet-iodine complex and a safranin counterstain. Gram-positive bacteria have a thick mesh-like cell wall with high abundance of peptidoglycan, which can retain the crystal violet-iodine complex after alcohol treatment and be stained purple. While, gram-negative bacteria contain a much thinner cell wall, which is composed of only a single layer of peptidoglycan. They will not retain the purple complex after alcohol treatment, and a following counterstaining with safranin will give them the new pink colour.[67] After gram stain, the positive blood cultures are used in colony plating to prepare pure cultures of the recovered bacterial pathogens for genus or species identification (**Figure 1.8**).[68] This step of subculture normally takes 12-24 h to obtain enough bacterial colonies. There are generally three types of methods for bacterial identification, including *i*) conventional biochemical and phenotypic characterization, *ii*) nucleic acid-based molecular detection of bacteria and *iii*) bacterial protein fingerprinting by MALDI-TOF mass spectrometry.

Over the first half of the 20th century, microbiologists mainly relied on morphological and biochemical characterization to classify bacterial strains. Important morphological information can be easily obtained by direct optical microcopy observation. And the biochemical properties can be obtained by conducting a series of biochemical tests. Examples include β-glucuronidase (MUG) test to identify *Escherichia coli*, bacitracin sensitivity test to distinguish *Streptococcus pyogenes* from other β-hemolytic *Streptococci*, bile solubility test to tell apart *Streptococcus pneumoniae* from other α-hemolytic *Streptococci*, CAMP test to identify group B β-hemolytic *Streptococci* such as *Streptococcus agalactiae*, catalase test to differentiate *Staphylococci* from *Streptococci*, citrate utilization test to tell apart *Enterobacteriaceae* family members, coagulase test to identify *Staphylococcus aureus* from coagulase-negative *Staphylococci*, DNase test to identify *Staphylococcus aureus*. They also include oxidase test to tell apart oxidase-positive bacteria (*e.g. Pseudomonadaceae*) from oxidase-negative bacteria (*e.g.*
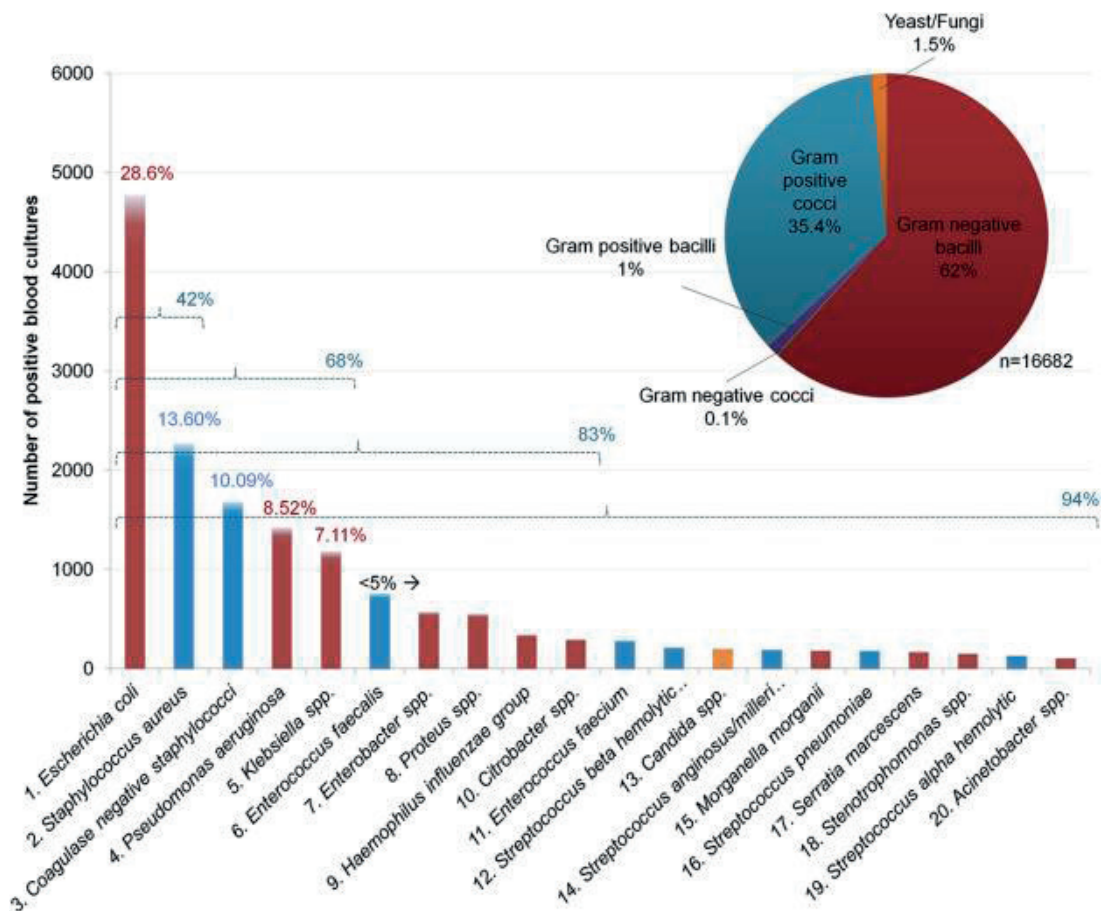
**Figure 1.8** Top 20 bacterial pathogens identified from 16,682 positive blood cultures during the year of 2013 in the University Hospital Centre in Lausanne, Switzerland.[68] Copyright © 2015 Elsevier.

*Enterobacteriaceae*), indole test to classify bacteria into indole-positive (*e.g. Escherichia coli*) and indole-negative bacteria (*e.g. Salmonella spp.*), lysine decarboxylase test to identify *Salmonella spp.* and *Shigella spp.*, litmus milk test to identify *Enterococci* and some *Clostridium spp.*, urease test to identify *Helicobacter pylori*, and so on.[69] In the later 1900s, the development of commercial kits (*e.g.* nine-test Enterotube from Roche, Basel, Switzerland) and automatic testing systems (*e.g.* Vitek® AutoMicro System from bioMérieux, Marcy-l'Étoile, France) have greatly speed up the testing.

Since 1960s, nucleic acid-based molecular methods were gradually introduced for bacterial identification. The methods mainly rely on profiling the genetic material (primarily DNA) in bacterial cells. D. J. Brenner pioneered the molecular identification procedure by DNA hybridization in 1977.[70] The rapid development of molecular biology in the 1980s greatly pushed forward the molecular identification procedure. Nowadays,

the two most widely used technologies are polymerase chain reaction (PCR) and small subunit ribosomal RNA (16S rRNA) gene sequencing. The most common PCR approach employs primers to recognize conserved DNA sequences of bacterial genes that encode ribosomal RNA. The DNA sequences are firstly extracted from bacterial cells, and then specific PCR primers are used to confirm the presence or absence of target DNA.[71] Strategies like real-time PCR and multiplex PCR have been frequently used for fast identification of bacteria.[72,73] The 16S rRNA gene sequencing procedure, as explained by the name, relies on the detection of specific 16s rRNA gene sequence to identify bacterial genus or species. 16S rRNA genes are present in almost all bacteria with almost the same function and sufficiently conserved sequence. They are large enough (1,500 base pairs) to provide sufficient information for bacterial identification.[74] In addition to the above two approaches, bacteria can also be identified by detecting the hybridization in DNA microarrays through fluorescence and infrared imaging, or by applying fluorescence *in situ* hybridization with 16S rRNA targeted oligonucleotide probes.[75,76] Nucleic acid-based molecular methods greatly reduce the turnaround time for pathogen identification. However, routine application of these methods in clinical laboratories requires more efforts to be made to reduce the cost and to simplify the detection process.

In 1990s, MALDI-TOF mass spectrometry technique was introduced for the identification of bacteria, which afterwards brought a breakthrough to clinical microbiology. In 1994, T. C. Cain *et al.*, reported that MALDI-TOF MS could be used for the differentiation of bacteria based on their water-soluble protein profiles. They extracted proteins from bacteria by sonication, precipitated the extracted proteins using organic solvent and dissolved the proteins in water. The water-soluble protein extracts generated MALDI-TOF mass spectra by using Nafion film as the substrate.[77] In 1996, X. Liang and colleagues extracted proteins from bacterial cells, and the proteins were separated by capillary liquid chromatography and detected on-line by a UV absorption detector. The eluent were then collected for off-line analysis by MALDI-TOF mass spectrometry. They found bacteria could be discriminated from each other to the species level based on the extracted protein profiles. Only picomolar level of extracted proteins were required for the measurement.[78] At almost the same time, T. Krishnamurthy and colleagues reported that proteins extracted from bacterial cells could be directly measured by MALDI-TOF mass spectrometry without the need of previous separation, and the obtained spectra revealed specific biomarkers for individual bacterial strains. The observed biomarkers enabled them to detect pathogenic bacteria and to distinguish pathogenic bacteria from the corresponding non-pathogenic species.[79] Immediately after, R. D. Holland and colleagues found that gram-negative enterobacteria could be detected by MALDI-TOF mass spectrometry directly in their intact whole state without the need to perform protein extraction. They collected bacterial cells from colonies on agar plates,

mixed the bacteria with MALDI matrix, air-dried the mixture on MALDI target plate and then conducted mass spectrometry measurement. The measurement results revealed that each bacterial strain showed a few characteristic high-mass ion peaks which were thought to be derived from bacterial proteins. With the characteristic peaks, unknown bacterial strains were identified correctly by matching their peaks with the peaks generated from previously-known bacterial strains. The detection time for each strain was only a few minutes.[80] Encouraged by this work, M. A. Claydon and colleagues demonstrated in the same year that MALDI-TOF mass spectrometry could generate characteristic spectra, or fingerprints, from both gram-negative bacteria and gram-positive bacteria in their intact whole state within minutes. Bacteria could be identified at the genus, species and even the strain levels by comparing the corresponding fingerprints.[81] Although at that time the spectrum quality was much lower than now, this type of fast identification approach based on whole cell fingerprinting and pattern matching analysis brought great interest worldwide. Later studies reveal that the fingerprint peaks mainly come from bacterial cellular proteins (representing 60-70% of the dry weight of bacteria), half of which are the highly abundant alkaline ribosomal proteins.[82] After around twenty years of improvement, the bacterial fingerprinting method has been incorporated into commercial systems like Vitek® MS (bioMérieux, France) and MALDI Biotyper® (Bruker, Germany), which have been installed in hospitals for routine diagnosis of bacterial infections.

## 2.4. Antimicrobial susceptibility testing

Once the identity of a bacterial pathogen is clarified, antimicrobial susceptibility testing is conducted to help the determination of efficient antibiotic therapies. Normally, pure and fresh subcultures of the bacteria derived from the positive blood cultures are used for the testing. Although many novel methods have been proposed for susceptibility testing, the current standard remains as the antimicrobial agent culture-based approach. The selection of antimicrobial agents for the testing is quite important. Usually, antimicrobial agents most appropriate for treating the target bacterial infection, including antibiotics and other substances that kill (bactericidal) or inhibit the growth (bacteriostatic) of bacteria, must be tested. National organizations such as the *Clinical and Laboratory Standards Institute* (CLSI) in the USA and the European Committee on Antimicrobial Susceptibility Testing (EUCAST) provide the lists of antimicrobial agents appropriate for different bacterial families.[83,84] These guidelines are reviewed and updated frequently, usually once per year, to provide the most current criteria for the testing.
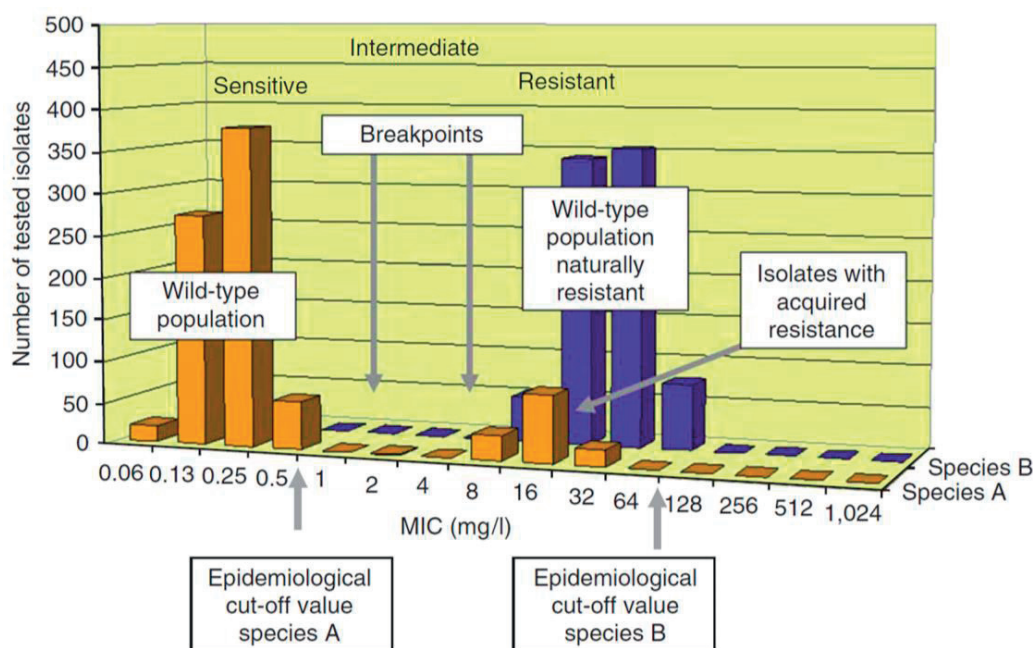
**Figure 1.9** Distribution of MIC values for different isolates of given bacterial species.[86] Copyright © 2008 Springer Nature Limited.

Commonly used approaches for antimicrobial susceptibility testing include agar or broth dilution tests, antimicrobial gradient method, disk diffusion test, as well as automate instrument systems that are developed based on these methods, such as MicroScan WalkAway® system (Beckman Coulter, USA), BD Phoenix[TM] system (Becton Dickinson, USA), Vitek® 2 system (bioMérieux, France) and Sensititre[TM] ARIS[TM] 2X system (Thermo Fisher Scientific, USA).[85] Among them, the agar or broth dilution tests are the fundamental procedures to quantitatively determine the minimal inhibitory concentration (MIC) of an antimicrobial agent, which means the lowest concentration of the tested antimicrobial agent that, under defined test conditions, inhibits the visible growth of the bacteria. Taking the broth dilution as an example, the procedure comprises preparing a series of two-fold dilutions of each tested antimicrobial agent, *e.g.* 0.5, 1, 2, 4, 8, 16, 32, 64, 128, 256 $\mu g \cdot mL^{-1}$, in liquid culture medium. The investigated bacteria, with defined concentration of $\sim 5 \cdot 10^5$ $CFU \cdot mL^{-1}$, are cultured in the antimicrobial agent-containing medium. After overnight incubation at 35 °C, the suspensions are examined for visible bacterial growth, which is indicated by the medium turbidity. The lowest concentration of the antimicrobial agent that prevents bacterial growth is defined as the MIC. The testing results are interpreted according to the MIC values by referring to an expert guideline such as the CLSI. For each tested antimicrobial agent, the investigated bacteria can be interpreted as *susceptible*,

*intermediate* or *resistant* to the agent (**Figure 1.9**).[86] The *susceptible* result indicates that the infection can be treated by that antimicrobial agent with the normally recommended dosage. On the contrary, the *resistance* result is associated with a high likelihood of the therapeutic failure. That antimicrobial agent should not be prescribed. An *intermediate* result indicates an uncertain therapeutic effect of the tested antimicrobial agent, and its prescription should be considered carefully.[87] The MIC determination can also be used to monitor the acquirement of an antimicrobial resistance, or employed as the first step to investigate the therapy potential of a new antimicrobial drug. The precision of this broth dilution test is considered to be plus or minus 1 the two-fold concentration, due to deviation from the manual preparation of dilution series of the antimicrobial agents. This method is the current reference to evaluate the performance of other newly proposed methods for *in vitro* susceptibility testing, as illustrated in CHAPTER IV of this thesis.

## 3. Cancer analysis by MALDI-TOF mass spectrometry

As a convenient analytical tool, MALDI-TOF mass spectrometry can also be applied for cancer analysis. Due to the complexity of the cancer microenvironment, or tumour microenvironment, the prevalence of MALDI-TOF mass spectrometry in cancer diagnosis is not as significant as in bacterial infection diagnosis. Nevertheless, it is a promising tool and numerous scientific works are being conducted to explore its application potentials. Currently, the applications are mainly focused on three aspects, *i.e.* typing or classification of cancer cell lines, discovery or detection of cancer biomarkers and imaging of cancer tissues.

Similar to bacterial identification, cancer cells can also be typed or classified by the approach of MALDI-TOF mass spectrometry fingerprinting. The cells can be measured after cell lysis and protein extraction.[88] Alternatively, cells grown in Petri dishes can be harvested by trypsinization (for adherent cells) and the obtained cells can be directly measured in their intact whole state.[89] Recently, A. Bondarenko reported a novel sample preparation method by directly growing the cells on disposable alumina foil pieces. The foil pieces bearing appropriate amount of cells were transferred onto the MALDI target plate for mass spectrometry measurement. In order to improve the spectrum quality, the cells were chemically fixed using methanol and acetone before the measurement.[90] After mass spectrometry measurement, the cancer cells are classified by pattern matching and statistical analysis of the generated mass spectra. With this fingerprinting approach, the cells derived from different species and different cancer types can be distinguished. It also offers the possibility to predict the metastatic potential of the cells.[91]

MALDI-TOF mass spectrometry is powerful for the discovery of new cancer biomarkers by combining with tandem mass spectrometry analysis, or for the detection

of established biomarkers according to the estimated molecular weight. The biomarkers are often proteins, or possibly lipids or metabolites. They have been measured from various types of sample origin, including *in vitro* grown cancer cells, materials extracted from solid tumour, tumour tissues or patient blood.[92] The biomarkers can be read directly from the mass spectra according to the *m/z* value and/or can be founded by comparing the spectra with the healthy counterparts. Identify of the suspected biomarker peaks are able to be clarified through on-line tandem mass spectrometry or off-line top-down or bottom-up proteomic analysis. This approach has allowed the detection of numerous markers for different cancer types. Examples include the serum degAla-FPA (fibrinipeptide-A with alanine truncation at the N-terminal) for patients suffering from gastric cancer with lymph node metastases, oxidative stress regulatory proteins for the respiratory system-related cancers like lung cancer, hyaluronan-hexa binding protein for breast cancer, TGFBIp (transforming growth factor-beta-induced protein) for ovarian cancer, and so on.[93-96] By using suitable external or internal standard, the mass spectrum is useful for semi-quantification of biomarkers, which provides an easy way for the investigation of cancer evolvement.[97]

MALDI-TOF mass spectrometry imaging of tumour tissue is an evolving technique in cancer diagnosis. Tumour tissues are valuable sources of biomaterial for cancer analysis. They contain numerous molecules like metabolites, lipids, glycans, peptides and proteins.[98] Mass spectrometry imaging is able to simultaneously record the spatial distribution of hundreds of biomolecules without the needed of any previous labelling and tagging. Thereby it allows unbiased visualization of the arrangement of biomolecules in the tumour environment, which contains not only cancer cells but also stromal tissue (including immune system cells, fibroblasts, vasculature, lymphatics, *etc*.), as well as the extracellular matrix.[99] This imaging approach requires minimal sample preparation, and provides a spatial resolution of 20-50 μm, which is promising to be further improved up to 5 μm with the assistance of special techniques.[100] The imaging allows the demonstration of tumour heterogeneity, definition of tumour margins and assessment of tumour grade.[101] Additionally, it has been used to characterize the distribution of drugs in the tumour microenvironment and thus useful for the evaluation of treatment efficacy.[102] The combination of tissue imaging and biomarker detection could open a new window for cancer diagnosis and prognosis.

## 4. Thesis outline

This thesis has been carried out with the initial goal of developing mass spectrometry-based methods for the detection of bacteria. After comparing with another soft ionisation technique, *i.e.* electrospray ionisation, MALDI is found to be more

efficient for the analysis of intact bacteria. Thus, the thesis is focused on MALDI-TOF mass spectrometry.

CHAPTER II presents a fast method to identify bacteria from human blood through the combination of immuno-affinity separation and MALDI-TOF mass spectrometry fingerprinting. This method provides a fast way for bloodstream infection diagnosis.

Beside of bacterial identification, another important concern of bacterial infection diagnosis is the determination of antimicrobial resistance/susceptibility. Thus, it comes the CHAPTER III, which shows that MALDI-TOF mass spectrometry is able to detect antimicrobial resistance marker proteins at the same time with bacterial identification.

MALDI-TOF mass spectrometry is well-suited for qualitative research, but less powerful for analyte quantification. Our research group is experienced in the fabrication of electrochemical sensors, which allows sensitive quantification analysis. Thus, an electrochemical quantification platform was developed for the purpose of both bacterial infection detection and antimicrobial resistance/susceptibility analysis, as illustrated in CHAPTER IV.

Going back to MALDI-TOF mass spectrometry, it also enables the analysis of other types of biological entities beside of bacteria. Examples include mammalian cells and the cell-secreted exosomes. CHAPTER V demonstrates MALDI-TOF mass spectrometry is useful for cancer monitoring through the detection of cancer-derived exosomes. Moreover, it is a promising tool for rapid detection of skin cancers or other skin diseases through the combination with tape stripping sampling procedure to recover skin cells, as included in the CHAPTER VI for future perspective.

# Reference

1.  Jannetto, P.J. & Fitzerald, R.L. Effective Use of Mass Spectrometry in the Clinical Laboratory. *Clin Chem* 62, 92-98 (2016).
2.  Grebe, S.K. & Singh, R.J. LC-MS/MS in the clinical laboratory–where to from here? *Clin Biochem Rev* 32, 5 (2011).
3.  Ho, C.S.*, et al.* Electrospray ionisation mass spectrometry: principles and clinical applications. *Clin Biochem Rev* 24, 3 (2003).
4.  Croxatto, A., Prod'hom, G. & Greub, G. Applications of MALDI-TOF mass spectrometry in clinical diagnostic microbiology. *FEMS Microbiol Rev* 36, 380-407 (2012).
5.  Patel, R. MALDI-TOF MS for the Diagnosis of Infectious Diseases. *Clin Chem* 61, 100-111 (2015).
6.  Hodis, E.*, et al.* A landscape of driver mutations in melanoma. *Cell* 150, 251-263 (2012).
7.  Budzikiewicz, H. H. Kienitz, Herausgeber: Massenspektrometrie. Verfaßt von F. Aulinger, G. Franke, K. Habfast, H. Kienitz und G. Spiteller. Verlag Chemie, GmbH, Weinheim/Bergstr. 1968. XV+ 883 Seiten mit 342 Abbildungen und 52 Tabellen im Text und einem Tabellenteil. Preis: DM 195 *Ber Bunsenges Physik Chem* 73, 114-115 (1969).
8.  Hoffman, E. & Stroobant, V. *Mass Spectrometry Principles and Applications*. John Wiley & Sons (2007).
9.  Gross, J.H. *Mass spectrometry: a textbook*. Springer Science & Business Media (2006).
10. Fenner, N.C. & Daly, N.R. Laser Used for Mass Analysis. *Rev Sci Instrum* 37, 1068-1070 (1966).
11. Vastola, F. & Pirone, A. Ionization of organic solids by laser irradiation. *Adv Mass Spectrom* 4, 107-111 (1968).
12. Mumma, R.-O. & Vastola, F. Analysis of organic salts by laser ionization mass spectrometry. Sulfonates, sulfates and thiosulfates. *J Org Chem* 6, 1373-1376 (1972).
13. Karas, M. & Hillenkamp, F. Laser Desorption Ionization of Proteins with Molecular Masses Exceeding 10000 Daltons. *Anal Chem* 60, 2299-2301 (1988).
14. Hillenkamp, F., Karas, M., Ingendoh, A. & Stahl, B. Matrix assisted UV-laser desorption/ionization: A new approach to mass spectrometry of large biomolecules. *Biol Mass Spectrom*, 49-60 (1990).
15. Siuzdak, G. *The expanding role of mass spectrometry in biotechnology*. Mcc Press San Diego (2003).
16. Murgasova, R. & Hercules, D.M. MALDI of synthetic polymers—an update. *Int J Mass Spectrom* 226, 151-162 (2003).
17. Dreisewerd, K. The desorption process in MALDI. *Chem Rev* 103, 395-426 (2003).
18. Abonnenc, M., Qiao, L.A., Liu, B.H. & Girault, H.H. Electrochemical Aspects of Electrospray and Laser Desorption/Ionization for Mass Spectrometry. *Annu Rev Anal Chem* 3, 231-254 (2010).
19. Zenobi, R. & Knochenmuss, R. Ion formation in MALDI mass spectrometry. *Mass Spectrom Rev* 17, 337-366 (1998).
20. Moon, J.H., Shin, Y.S., Bae, Y.J. & Kim, M.S. Ion Yields for Some Salts in MALDI: Mechanism for the Gas-Phase Ion Formation from Preformed Ions. *J Am Soc Mass Spectrom* 23, 162-170 (2012).
21. Glückmann, M.*, et al.* Mechanisms in MALDI analysis: surface interaction or incorporation of analytes? *Int J Mass Spectrom* 210, 121-132 (2001).
22. Liao, P.C. & Allison, J. Ionization processes in matrix-assisted laser desorption/ionization mass spectrometry: Matrix-dependent formation of [M+ H]+ vs [M+ Na]+ ions of small peptides and some mechanistic comments. *J Mass Spectrom* 30, 408-423 (1995).
23. Wang, B.H., Dreisewerd, K., Bahr, U., Karas, M. & Hillenkamp, F. Gas-phase cationization and protonation of neutrals generated by matrix-assisted laser desorption. *J Am Soc Mass Spectrom* 4, 393-398 (1993).

24. Gimon, M., Preston, L., Solouki, T., White, M. & Russell, D. Are proton transfer reactions of excited states involved in UV laser desorption ionization? *J Org Chem* 27, 827-830 (1992).

25. Harrison, A.G. *Chemical ionization mass spectrometry*. Routledge (2018).

26. Jaskolla, T.W. & Karas, M. Compelling Evidence for Lucky Survivor and Gas Phase Protonation: The Unified MALDI Analyte Protonation Mechanism. *J Am Soc Mass Spectrom* 22, 976-988 (2011).

27. Karas, M., Glückmann, M. & Schäfer, J. Ionization in matrix-assisted laser desorption/ionization: singly charged molecular ions are the lucky survivors. *J Mass Spectrom* 35, 1-12 (2000).

28. Pan, Y. & Cotter, R.J. Measurement of initial translational energies of peptide ions in laser desorption/ionization mass spectrometry. *J Org Chem* 27, 3-8 (1992).

29. Glückmann, M. & Karas, M. The initial ion velocity and its dependence on matrix, analyte and preparation method in ultraviolet matrix-assisted laser desorption/ionization. *J Mass Spectrom* 34, 467-477 (1999).

30. Berkenkamp, S., Menzel, C., Hillenkamp, F. & Dreisewerd, K. Measurements of mean initial velocities of analyte and matrix ions in infrared matrix-assisted laser desorption ionization mass spectrometry. *J Am Soc Mass Spectrom* 13, 209-220 (2002).

31. Karas, M., Bahr, U., Fournier, I., Glückmann, M. & Pfenninger, A. The initial-ion velocity as a marker for different desorption-ionization mechanisms in MALDI. *Int J Mass Spectrom* 226, 239-248 (2003).

32. Westmacott, G., Ens, W., Hillenkamp, F., Dreisewerd, K. & Schürenberg, M. The influence of laser fluence on ion yield in matrix-assisted laser desorption ionization mass spectrometry. *Int J Mass Spectrom* 221, 67-81 (2002).

33. Medina, N., Huth-Fehre, T., Westman, A. & Sundqvist, B. Matrix-assisted laser desorption: Dependence of the threshold fluence on analyte concentration. *J Org Chem* 29, 207-209 (1994).

34. Ingendoh, A., Karas, M., Hillenkamp, F. & Giessmann, U. Factors affecting the resolution in matrix-assisted laser desorption—ionization mass spectrometry. in *Time-of-Flight Mass Spectrometry and its Applications,* 345-354, Elsevier (1994).

35. Holle, A., Haase, A., Kayser, M. & Hoehndorf, J. Optimizing UV laser focus profiles for improved MALDI performance. *J Mass Spectrom* 41, 705-716 (2006).

36. Niehaus, M., Schnapp, A., Koch, A., Soltwisch, J. & Dreisewerd, K. New Insights into the Wavelength Dependence of MALDI Mass Spectrometry. *Anal Chem* 89, 7734-7741 (2017).

37. Cramer, R. & Dreisewerd, K. UV matrix-assisted laser desorption ionization: principles instrumentation and applications. in *The Encyclopedia of Mass Spectrometry*, Elsevier (2007).

38. Menzel, C., Dreisewerd, K., Berkenkamp, S. & Hillenkamp, F. The role of the laser pulse duration in infrared matrix-assisted laser desorption/ionization mass spectrometry. *J Am Soc Mass Spectrom* 13, 975-984 (2002).

39. Vertes, A., Luo, G.H., Ye, L., Chen, Y. & Marginean, I. Laser pulse length dependence of internal energy transfer in UV-MALDI-MS. *Appl Phys a-Mater* 79, 823-825 (2004).

40. Wolff, M. & Stephens, W. A pulsed mass spectrometer with time dispersion. *Rev Sci Instrum* 24, 616-617 (1953).

41. Wiley, W. & McLaren, I.H. Time-of-flight mass spectrometer with improved resolution. *Rev Sci Instrum* 26, 1150-1157 (1955).

42. Gohlke, R.S. & McLafferty, F.W. Early gas chromatography/mass spectrometry. *J Am Soc Mass Spectrom* 4, 367-371 (1993).

43. Weickhardt, C., Moritz, F. & Grotemeyer, J. Time-of-flight mass spectrometry: State-of the-art in chemical analysis and molecular science. *Mass Spectrom Rev* 15, 139-162 (1996).

44. Imrie, D., Pentney, J. & Cottrell, J. A Faraday cup detector for high-mass ions in matrix-assisted laser desorption/ionization time-of-flight mass spectrometry. *Rapid Commun Mass*

*Spectrom* 9, 1293-1296 (1995).

45. Brown, R.S. & Lennon, J.J. Mass resolution improvement by incorporation of pulsed ion extraction in a matrix-assisted laser desorption/ionization linear time-of-flight mass spectrometer. *Anal Chem* 67, 1998-2003 (1995).

46. Doroshenko, V.M. & Cotter, R.J. Ideal velocity focusing in a reflectron time-of-flight mass spectrometer. *J Am Soc Mass Spectrom* 10, 992-999 (1999).

47. Wiza, J.L. Microchannel plate detectors. *Nucl. Instrum. Methods* 162, 587-601 (1979).

48. Krause, J., Stoeckli, M. & Schlunegger, U.P. Studies on the selection of new matrices for ultraviolet matrix-assisted laser desorption/ionization time-of-flight mass spectrometry. *Rapid Commun Mass Spectrom* 10, 1927-1933 (1996).

49. Dreisewerd, K., Berkenkamp, S., Leisner, A., Rohlfing, A. & Menzel, C. Fundamentals of matrix-assisted laser desorption/ionization mass spectrometry with pulsed infrared lasers. *Int J Mass Spectrom* 226, 189-209 (2003).

50. Wiangnon, K. & Cramer, R. Sample Preparation: A Crucial Factor for the Analytical Performance of Rationally Designed MALDI Matrices. *Anal Chem* 87, 1485-1488 (2015).

51. Zhang, X.*, et al.* An improved method of sample preparation on AnchorChip™ targets for MALDI-MS and MS/MS and its application in the liver proteome project. *Proteomics* 7, 2340-2349 (2007).

52. Horneffer, V.*, et al.* Matrix–analyte-interaction in MALDI-MS: Pellet and nano-electrospray preparations. *Int J Mass Spectrom* 249, 426-432 (2006).

53. Goto, M. & Al-Hasan, M.N. Overall burden of bloodstream infection and nosocomial bloodstream infection in North America and Europe. *Clin Microbiol Infec* 19, 501-509 (2013).

54. Buetti, N., Atkinson, A., Marschall, J., Kronenberg, A. & AN, S.C.A.R. Incidence of bloodstream infections: a nationwide surveillance of acute care hospitals in Switzerland 2008-2014. *Bmj Open* 7 (2017).

55. Orsini, J.*, et al.* Microbiological profile of organisms causing bloodstream infection in critically ill patients. *J Clin Med Res* 4, 371-377 (2012).

56. Ventola, C.L. The antibiotic resistance crisis: part 1: causes and threats. *P T* 40, 277 (2015).

57. Prestinaci, F., Pezzotti, P. & Pantosti, A. Antimicrobial resistance: a global multifaceted phenomenon. *Pathog Glob Health* 109, 309-318 (2015).

58. Prevention, C.f.D.C.a. Antibiotic resistance threats in the United States. Health UDo & Services H (2013).

59. Norrby, R.*, et al.* The bacterial challenge: time to react-a call to narrow the gap between multidrug-resistant bacteria in the EU and the development of new antibacterial agents. European Center for Disease Prevention and Control (ECDC) & European Medicines Agency (EMA) (2009).

60. Garcia, R.A.*, et al.* Multidisciplinary team review of best practices for collection and handling of blood cultures to determine effective interventions for increasing the yield of true-positive bacteremias, reducing contamination, and eliminating false-positive central line–associated bloodstream infections. *Am J Infect Control* 43, 1222-1237 (2015).

61. Wilson, M.L.*, et al.* Principles and procedures for blood cultures; approved guideline. *CLSI document M47-A. Clinical and Laboratory Standards Institute, Wayne, PA* (2007).

62. Snyder, S.R.*, et al.* Effectiveness of practices to reduce blood culture contamination: a Laboratory Medicine Best Practices systematic review and meta-analysis. *Clin Biochem* 45, 999-1011 (2012).

63. Lamy, B. & Seifert, H. Microbial diagnosis: septicemia. *European Manual of Clinical Microbiology (SFM/ESCMID)*, 101-110 (2012).

64. Kirn, T. & Weinstein, M. Update on blood cultures: how to obtain, process, report, and interpret. *Clin Microbiol Infec* 19, 513-520 (2013).

65. Lamy, B., Dargere, S., Arendrup, M.C., Parienti, J.J. & Tattevin, P. How to Optimize the Use of Blood Cultures for the Diagnosis of Bloodstream Infections? A State-of-the Art.

*Front Microbiol* 7 (2016).

66. Mirrett, S*., et al.* Controlled clinical comparison of the BacT/ALERT FN and the standard anaerobic SN blood culture medium. *J Clin Microbiol* 42, 4581-4585 (2004).

67. Coico, R. Gram staining. *Curr Protoc Microbiol*, A. 3C. 1-A. 3C. 2 (2006).

68. Opota, O., Croxatto, A., Prod'hom, G. & Greub, G. Blood culture-based diagnosis of bacteraemia: state of the art. *Clin Microbiol Infec* 21, 313-322 (2015).

69. Hemraj, V., Diksha, S. & Avneet, G. A review on commonly used biochemical test for bacteria. *Innovare J Life Sci* 1, 1-7 (2013).

70. Brenner, D. Characterization and clinical identification of Enterobacteriaceae by DNA hybridization. *Prog Clin Pathol* 7, 71 (1978).

71. Fouad, A.F*., et al.* PCR-based identification of bacteria associated with endodontic infections. *J Clin Microbiol* 40, 3223-3231 (2002).

72. Ellerbrok, H*., et al.* Rapid and sensitive identification of pathogenic and apathogenic Bacillus anthracis by real-time PCR. *FEMS Microbiol Lett* 214, 51-59 (2002).

73. Oliveira, D.C. & de Lencastre, H. Multiplex PCR strategy for rapid identification of structural types and variants of the mec element in methicillin-resistant Staphylococcus aureus. *Antimicrob Agents Chemother* 46, 2155-2161 (2002).

74. Janda, J.M. & Abbott, S.L. 16S rRNA gene sequencing for bacterial identification in the diagnostic laboratory: Pluses, perils, and pitfalls. *J Clin Microbiol* 45, 2761-2764 (2007).

75. Al-Khaldi, S.F., Mossoba, M.M., Allard, M.M., Lienau, E.K. & Brown, E.D. Bacterial identification and subtyping using DNA microarray and DNA sequencing. in *Microbial Systems Biology,* 73-95, Springer (2012).

76. Kempf, V.A.J., Trebesius, K. & Autenrieth, I.B. Fluorescent in situ hybridization allows rapid identification of microorganisms in blood cultures. *J Clin Microbiol* 38, 830-838 (2000).

77. Cain, T.C., Lubman, D.M. & Weber, W.J. Differentiation of Bacteria Using Protein Profiles from Matrix-Assisted Laser-Desorption Ionization Time-of-Flight Mass-Spectrometry. *Rapid Commun Mass Spectrom* 8, 1026-1030 (1994).

78. Liang, X., Zheng, K., Qian, M.G. & Lubman, D.M. Determination of bacterial protein profiles by matrix-assisted laser desorption/ionization mass spectrometry with high-performance liquid chromatography. *Rapid Commun Mass Spectrom* 10, 1219-1226 (1996).

79. Krishnamurthy, T., Rajamani, U. & Ross, P. Detection of pathogenic and non-pathogenic bacteria by matrix-assisted laser desorption/ionization time-of-flight mass spectrometry. *Rapid Commun Mass Spectrom* 10, 883-888 (1996).

80. Holland, R*., et al.* Rapid identification of intact whole bacteria based on spectral patterns using matrix-assisted laser desorption/ionization with time-of-flight mass spectrometry. *Rapid Commun Mass Spectrom* 10, 1227-1232 (1996).

81. Claydon, M.A., Davey, S.N., EdwardsJones, V. & Gordon, D.B. The rapid identification of intact microorganisms using mass spectrometry. *Nat Biotechnol* 14, 1584-1586 (1996).

82. Ryzhov, V. & Fenselau, C. Characterization of the protein subset desorbed by MALDI from whole bacterial cells. *Anal Chem* 73, 746-750 (2001).

83. Patel, J.B. *Performance standards for antimicrobial susceptibility testing*, Clinical and Laboratory Standards Institute (2017).

84. Breakpoint tables for interpretation of MICs and zone diameters 2018. Version 8.0. *Breakpoint tables for interpretation of MICs and zone diameters*. European Committee on Antimicrobial Susceptibility Testing (2018).

85. Jorgensen, J.H. & Ferraro, M.J. Antimicrobial susceptibility testing: a review of general principles and contemporary practices. *Clin Infect Dis* 49, 1749-1755 (2009).

86. Wiegand, I., Hilpert, K. & Hancock, R.E.W. Agar and broth dilution methods to determine the minimal inhibitory concentration (MIC) of antimicrobial substances. *Nat Protoc* 3, 163-175 (2008).

87. Rodloff, A., Bauer, T., Ewig, S., Kujath, P. & Müller, E. Susceptible, intermediate, and

resistant–the intensity of antibiotic action. *Dtsch Arztebl Int* 105, 657 (2008).

88. Zhang, X., Scalf, M., Berggren, T.W., Westphall, M.S. & Smith, L.M. Identification of mammalian cell lines using MALDI-TOF and LC-ESI-MS/MS mass spectrometry. *J Am Soc Mass Spectrom* 17, 490-499 (2006).

89. Munteanu, B. & Hopf, C. Emergence of whole-cell MALDI-MS biotyping for high-throughput bioanalysis of mammalian cells? *Bioanalysis* 5, 885-893 (2013).

90. Bondarenko, A*., et al.* Aluminium foil as a single-use substrate for MALDI-MS fingerprinting of different melanoma cell lines. *Analyst* 141, 3403-3410 (2016).

91. Serafim, V*., et al.* Classification of cancer cell lines using matrix-assisted laser desorption/ionization time-of-flight mass spectrometry and statistical analysis. *Int J Mol Med* 40, 1096-1104 (2017).

92. Rodrigo, M.A.M*., et al.* MALDI-TOF MS as evolving cancer diagnostic tool: a review. *J Pharmaceut Biomed* 95, 245-255 (2014).

93. Zhang, M.H*., et al.* A prognostic biomarker for gastric cancer with lymph node metastases. *Anat Rec* 296, 590-594 (2013).

94. Pastor, M.D*., et al.* Identification of oxidative stress related proteins as biomarkers for lung cancer and chronic obstructive pulmonary disease in bronchoalveolar lavage. *Int J Mol Sci* 14, 3440-3455 (2013).

95. Srinivas, P., Kollapalli, S.P. & Thomas, A. Bioactive hyaluronan fragment (hexasaccharide) detects specific hexa-binding proteins in human breast and stomach cancer: Possible role in tumorogenesis (2012).

96. Ween, M.P*., et al.* Transforming growth factor-beta-induced protein secreted by peritoneal cells increases the metastatic potential of ovarian cancer cells. *Int J Cancer* 128, 1570-1584 (2011).

97. Szájli, E., Fehér, T. & Medzihradszky, K.F. Investigating the quantitative nature of MALDI-TOF MS. *Mol Cell Proteomics* 7, 2410-2418 (2008).

98. Kononen, J*., et al.* Tissue microarrays for high-throughput molecular profiling of tumor specimens. *Nat Med* 4, 844-847 (1998).

99. Weber, C.E. & Kuo, P.C. The tumor microenvironment. *Surg Oncol* 21, 172-177 (2012).

100. Zavalin, A., Yang, J. & Caprioli, R. Laser beam filtration for high spatial resolution MALDI imaging mass spectrometry. *J Am Soc Mass Spectrom* 24, 1153-1156 (2013).

101. Kriegsmann, J., Kriegsmann, M. & Casadonte, R. MALDI TOF imaging mass spectrometry in clinical pathology: a valuable tool for cancer diagnostics. *Int J Oncol* 46, 893-906 (2015).

102. Buck, A. & Walch, A. In situ drug and metabolite analysis in biological and clinical research by MALDI MS imaging. *Bioanalysis* 6, 1241-1253 (2014).

# CHAPTER II. Rapid identification of bacteria from blood by immuno-affinity mass spectrometry

## Abstract

Bloodstream infections rank among the most serious causes of morbidity and mortality in hospitalized patients, partly due to the long time period required for clinical diagnosis. In this work, we developed a sensitive method to quickly and accurately identify bacteria in human blood samples by combining MALDI-TOF mass spectrometry and immune-affinity enrichment/separation. A bacterial reference library was firstly built by collecting mass spectra from different numbers of bacterial cells. Due to reduced sample spot size, the reference spectra were obtained from as few as 10-100 intact bacterial cells. Then, bacteria were isolated from human blood by antibodies-modified magnetic beads for mass spectrometry fingerprinting. By comparing the sample spectra with the reference spectra based on cosine correlation, bacteria with concentrations as low as 500 cells·mL$^{-1}$ in blood serum and 8,000 cells·mL$^{-1}$ in whole blood were identified. The proposed method was further applied to clinical positive blood cultures provided by a local hospital, where *Escherichia coli* and *Staphylococcus aureus* were successfully identified. Because of the highly sensitive measurement, the blood culture time required for diagnosis can be significantly reduced. As a proof of concept, whole blood spiked with low initial concentrations ($10^2$-$10^3$ cells·mL$^{-1}$) of bacteria was used for blood culture and analysed by the proposed method after different culture times. The results showed the identification was successfully conducted after 4 hours of culture. Therefore, an entire diagnostic process could be accomplished within several hours, which will facilitate timely treatment of bacterial infections and decrease the risk of mortality.

# Chemical Science

www.rsc.org/chemicalscience

ROYAL SOCIETY
OF CHEMISTRY
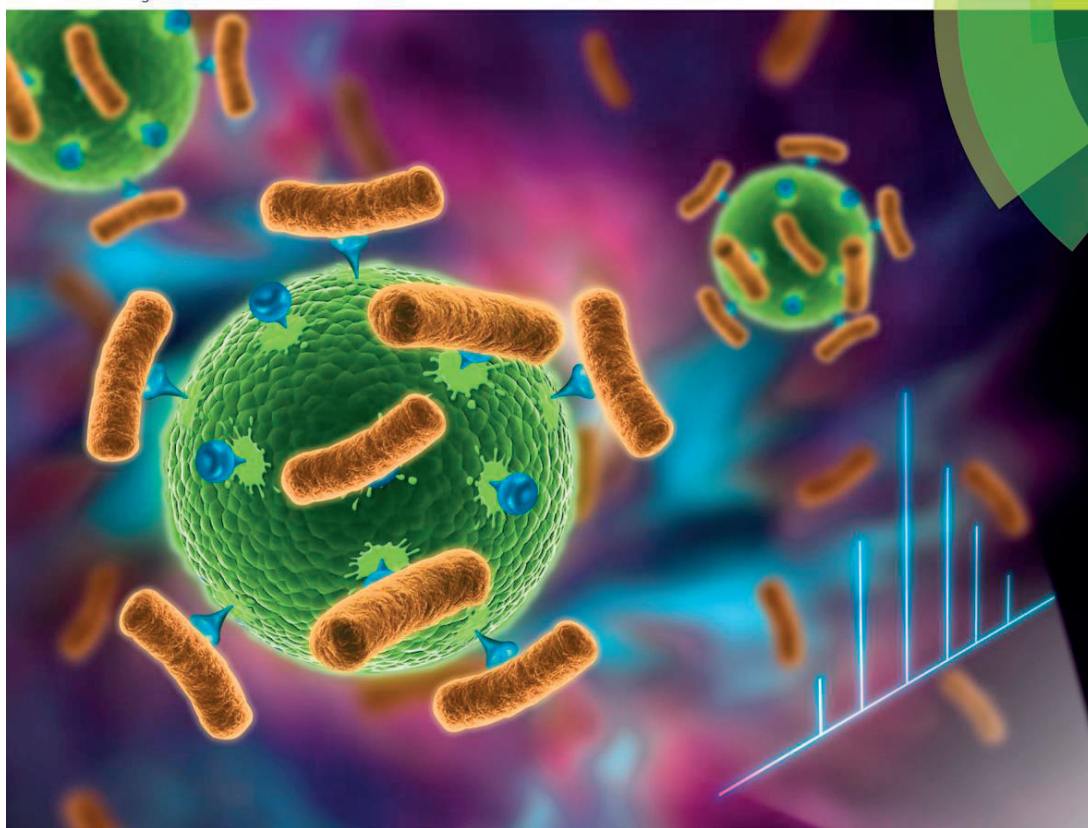
**EDGE ARTICLE**
Hubert H. Girault *et al.*
Sensitive and fast identification of bacteria in blood samples by
immunoaffinity mass spectrometry for quick BSI diagnosis

**175** YEARS

# 1. Introduction

Bloodstream infections (BSI), caused by the presence of bacteria or fungi in bloodstream, rank among the most serious causes of morbidity and mortality in hospitalized patients.[1] A systematic review has estimated that every year about 600,000 BSI episodes occur in North America, and about 1,200,000 BSI episodes attack Europe, resulting in roughly 86,000 and 157,000 deaths, respectively.[2] Timely diagnosis and treatment of the infections are of great importance.

Currently, the method of blood culture is regarded as the gold standard for BSI diagnosis and has been widely used in clinical microbiology laboratories. Traditionally, large volumes of blood samples were collected from patients (~ 30 mL for an adult, and 1–20 mL for a child) and are incubated in dedicated blood culture bottles for up to 5 days or even longer, followed by hours to days of subculture and microorganism phenotypic identification.[3] The whole identification process takes a long time and is highly dependent on the personal experience of the analysts, which forfeits diagnosis at early stages and increases the risk of mortality.

Rapid and accurate identification of bacteria from blood is crucial for effective therapy and reduction of cost and stay-time in hospital. At present, genotypic methods, such as real-time polymerase chain reaction, fluorescence *in situ* hybridization, and 16S ribosomal RNA gene sequencing, have been developed as alternative approaches for BSI diagnosis.[4,5] However, the stability and reproducibility of these methods can hardly reach the requirement of clinical diagnosis. Very recently, an integrated comprehensive droplet digital detection method integrating droplet microfluidics, DNAzyme-based sensors, and a high-throughput particle counter system was developed and could detect low abundant bacteria from *Escherichia coli*-spiked blood samples.[6]

Comparing to other methods for bacterial identification, mass spectrometry provides sensitive and accurate label-free detection with high-throughput. Since the pioneering works in 1990s, MALDI-TOF mass spectrometry (MALDI-TOF MS) has been widely used for bacterial identification at the genus, species and even strain levels.[7-9] With this concept, commercial systems, including Vitek® MS (bioMérieux, France) and MALDI Biotyper® (Bruker, Germany), have been adopted for the identification of a variety of bacteria from blood samples, and received the clearance from US Food and Drug Administration.[10,11] However, the typical MALDI-TOF MS identification works only for a high abundance of bacteria and is unable to identify bacteria directly from patient blood, where the initial bacterial concentration is normally low, often lower than 100 colony forming unit per milliliter (CFU·mL$^{-1}$) for adult patients.[12,13] Thereby, large volume of blood samples and longtime of blood culture are still needed.

Further improvement in the identification sensitivity is crucial for fast infection diagnosis. It can be realized by two approaches, *i.e.* more efficient bacterial enrichment/separation and more sensitive MALDI-TOF MS measurements. With respect to the first approach, affinity probes have been used for bacterial separation. For instance, Wu *et al.* used $Fe_3O_4$ NPs-graphene nanosheets decorated with chitosan to capture pathogenic bacteria from aqueous suspension, and as low as 500 $CFU·mL^{-1}$ *Pseudomonas aeruginosa* and 450 $CFU·mL^{-1}$ *Staphylococcus aureus* were detected from 1 mL of water.[13] Similarly, commercial anti-*Salmonella* Dynabeads® (Lake Success, NY, USA) were used to selectively isolate *Salmonella choleraesuis* for MALDI-TOF MS analysis, where the limit of detection was demonstrated as $10^7$ $cells·mL^{-1}$ in water, and $10^9$ $cells·mL^{-1}$ in human urine or chicken blood (1 mL of sample).[14] As for the second approach, Zenobi *et al.* has recently developed functional high-density micro-arrays for ultrasensitive analysis of single cells by MALDI-TOF MS.[15] The micro-arrays were fabricated by laser ablation on a hydrophobic and organo-phobic layer to focus sample spots within 100 μm in diameter. In such a way, cell position can be easily located, and a higher sample surface concentration can be achieved, leading to enhanced signal-to-noise ratio (*S/N*) during analysis.

In the present work, highly efficient immuno-affinity enrichment/separation of bacteria by antibodies-modified magnetic beads (Abs-MBs) was combined with sensitive MALDI-TOF MS for bacterial identification from blood samples. A library of bacterial reference spectra was firstly built by collecting mass spectral fingerprints of different bacterial species at different cell numbers. By reducing the sample spot size to 800 μm, reference spectra could be obtained from as few as 10-100 bacterial cells. With this library, bacteria were identified from blood samples by spectrum pattern matching. A frequently used cosine correlation algorithm was used to calculate spectral similarity score.[16] The identification was reached based on the highest similarity score, and validated with statistical confidence.

The immuno-affinity MALDI-TOF MS method was tested with three bacterial species, *i.e. Escherichia coli* (*E. coli*), *Bacillus subtilis* (*B. subtilis*) and *Staphylococcus aureus* (*S. aureus*). Both *E. coli* and *S. aureus* are among the most common pathogens causing BSI worldwide.[17,18] The detection limits achieved were ~ 500 $cells·mL^{-1}$ in human blood serum and ~ 8,000 $cells·mL^{-1}$ in human whole blood (1 mL of sample) for all of the three bacterial species. To the best of my knowledge, these are the lowest reported detection limits for bacterial identification from blood samples by MALDI-TOF MS. The accuracy of the method was determined with 20 positive and 20 negative control experiments using bacteria-spiked whole blood samples. Specificity was evaluated with multispecies-spiked whole blood samples. With high sensitivity, accuracy, and specificity, the present method is promising for BSI diagnosis. To demonstrate this

concept, the method was tested with clinical *E. coli* or *S. aureus* positive blood cultures provided by a local hospital (Hôpital du Valais, Sion, Switzerland), where the bacteria were successfully identified. Owing to the high sensitivity, the blood culture time needed for clinical diagnosis can be reduced. As a proof of concept, human whole blood spiked with low initial concentration ($10^2$ or $10^3$ cells·mL$^{-1}$) of *E. coli* was cultured in commercial blood culture bottles and analysed by the present method after different culture time. And the *E. coli* was successfully identified after 4 hours of culture.

## 2. Materials and methods

### 2.1 Materials

Goat polyclonal IgG isotype Abs against *E. coli*, rabbit polyclonal IgG isotype Abs against *B. subtilis* and rabbit polyclonal IgG isotype Abs against *S. aureus* were purchased from Abcam plc (Cambridge, UK). Pierce$^{TM}$ protein A/G-coated MBs were purchased from Thermo Fisher Scientific Inc. (Waltham, Massachusetts, USA). Human blood serum was purchased from Bioreclamation LLC (New York, USA). Human whole blood was donated by a healthy female at her age of 20s, collected by the Transfusion Interrégional CRS, Lausanne, Switzerland. Positive BC bottles with clinical BSI patients' blood and un-used BacT/Alert® FA Plus blood culture bottles were provided by Hôpital du Valais (Sion, Switzerland). Acetonitrile (HPLC grade) was purchased from Aventor Performance Materials (Center Valley, PA, USA). Trifluoroacetic acid (99.0%) was obtained from Acros Organics (New Jersey, USA). 2,5-dihydroxycinnamic acid (DHB), tween-20, albumin from bovine serum (BSA), disodium hydrogen phosphate dodecahydrate ($\geq$ 99.0%), sodium phosphate monobasic dihydrate ($\geq$ 99.0%), and sodium chloride (NaCl) ($\geq$ 99.5%) were all purchased from Sigma-Aldrich (St. Gallen, Switzerland). Deionized water (18.2 M$\Omega$ cm) was purified by an alpha Q Millipore system (Zug, Switzerland), and used in all aqueous solutions.

### 2.2 Culture of bacteria

*E. coli* strain DH5$\alpha$ (Life Technologies) was grown as a pre-culture in 2 mL of lysogeny broth (Sigma-Aldrich) at 37 °C for 6 h with continuous shaking at 250 rpm. 100 μL of the *E. coli* DH5$\alpha$ pre-culture was added into 3 mL of lysogeny broth and incubated overnight at 37 °C with continuous shaking. *B. subtilis* strain ATCC6633 (American Type Culture Collection) and *S. aureus* strain Col (Lausanne University) were grown in 20 mL of lysogeny broth in a 100 mL Erlenmeyer flask. Incubation was carried out at 37 °C for 16 h with continuous shaking at 180 rpm. Concentrations of bacterial cells in their fresh cultures were determined by measuring the optical density at 600 nm (OD$_{600nm}$), with 1.0 OD$_{600nm}$ corresponding to $\sim 8 \cdot 10^8$ cells·mL$^{-1}$.

All practical activities with pathogenic bacterial strains were conducted in a biosafety level 2 (P2) laboratory. Laboratory coats and gloves were worn during the entire activity process and they were never worn outside the laboratory. All bacterial wastes were disposed properly according to the safety guidelines. When activities were finished, instruments, facilities and benches were wiped with 70% ethanol. Hands were washed with soap and water before leaving the laboratory.

All blood samples used in this thesis were collected under the sign consent of the donors. No research on genetic material was carried out. Therefore, these samples were in agreement with "Loi fédérale relative à la recherche sur l'être humain, LRH – RS 810.30" and "Ordonnance relative à la recherche sur l'être humain, ORH – RS 810.301".

## 2.3 Bacterial identification from human blood samples

50 µg of protein A/G ($\sim$ 50.5 kDa)-coated MBs (1 µm in diameter) were washed twice with PBST buffer and dispersed in 50 µL of PBST buffer (10 mM phosphate buffered saline, pH 7.4, containing 0.05% tween-20). Excess of Abs (2 µL, 2 mg·mL$^{-1}$) were added to bind with the beads. The mixture was incubated for 30 min at room temperature with continuous shaking. The obtained Abs-MBs were collected using a magnetic stand and blocked with PBST buffer containing 1% bovine serum albumin (BSA). BSA was used to minimize nonspecific adsorption during the following immunoassay.

Blood serum samples or whole blood samples spiked with different concentration of bacteria were prepared. To reduce the interference from blood serum or whole blood, sample pre-treatment was conducted. As for the spiked serum samples, 0.1 mL of each sample was diluted with PBST buffer to 1 mL before the addition of Abs-MBs. As for the spiked whole blood samples, 1 mL of each sample was diluted 6 times with pure water and centrifuged at 140 $g$ for 10 min to sediment blood cells. The supernatant was recovered and mixed with 2 mL of water to lyse residual erythrocytes. After centrifugation at 2000 $g$ for 5 min, bacterial pellet was obtained, washed with 1 mL of water and finally resuspended in 300 µL of PBST buffer. As for the test with clinical positive blood cultures, 1 mL of culture liquid was employed for testing after the same sample pre-treatment.

Afterwards, 50 µg of Abs-MBs was added to capture bacterial cells. After incubation at 37 ºC for 30 min with continuous shaking, the beads were collected and washed twice with PBST buffer containing 0.1% BSA and once with pure water. Then, they were completely deposited on a normal MALDI target plate with the droplet-by-droplet protocol or deposited on an AnchorChip$^{TM}$ target plate. After drying at room temperature, the sample spot was overlaid with matrix for MALDI-TOF MS measurement.

## 2.4 Time-step test during blood culture

5 mL of human whole blood was spiked with *E. coli* cells with initial concentration of $10^2$ or $10^3$ cells·mL$^{-1}$. The spiked blood was injected into a BacT/Alert® FA Plus blood culture bottle (bioMérieux, Marcy-l'Étoile, France) and incubated at 37 °C with continuous shaking. For each concentration, four BC bottles were prepared in parallel. For two of them, during the culture process, 1 mL of culture liquid was taken out and analysed with the proposed immuno-affinity MALDI-TOF MS method. The test was conducted every two hours, *i.e.* 0 h, 2 h, 4 h, 6 h, 8 h, 10 h. The rest two bottles were kept un-touched and were checked regularly until they turned positive, indicated by automatic color change from grey-green to bright yellow on the bottom of the bottle.

## 2.5 Direct MALDI-TOF MS fingerprinting of intact bacteria

Bacterial cells were separated from the culture media by centrifugation at 13,000 rpm for 3 min, and washed three times with pure water. Finally, the cellular pellet was resuspended in water with the concentration of $10^8$ cells·mL$^{-1}$. The solutions with different concentrations of bacterial cells were obtained by a series of 10-fold dilution. 1 μL of each solution was deposited on a MALDI target plate, and dried at room temperature. For sample deposition, three different protocols were conducted. In the first one (the routine procedure), all of the 1 μL solution was deposited on a Bruker ground steel target plate, and the dried sample spot size was about 3 mm in diameter. In the second one, the 1 μL solution was deposited on the target plate by three repetitions (0.3-0.4 μL in each repetition), namely droplet-by-droplet, to keep the sample spot as small as possible (smaller than 0.8 mm in diameter). In the third one, a Bruker MTP AnchorChip$^{TM}$ target plate was employed, where the dried sample spot from 1 μL of bacterial solution could be confined within a well with 0.8 mm diameter. DHB matrix (10 mg·mL$^{-1}$ dissolved in the mixture of 50/49.9/0.1% (volume percentage) acetonitrile/pure water/trifluoroacetic acid) was added to cover the dried sample spots (1 μL on each spot) with the corresponding protocol for MALDI-TOF MS analysis. Each test was repeated 3-5 times. A library of bacterial reference mass spectra was built with the spectra obtained with the reduced sample spot size.

## 2.4 Mass spectrometry measurement and data analysis

MALDI-TOF MS measurements were performed on a Bruker microflex$^{TM}$ LRF instrument under linear positive mode. Instrumental parameters were set as laser intensity 70%, laser attenuator with 30% offset and 40% range, 500 laser shots accumulation for each spot, 20.0 Hz laser frequency, 20× detector gain, suppress up to 1000 Da, 350 ns pulsed ion extraction. Mass calibration was conducted with a calibration sample containing 1 mg·mL$^{-1}$ of cytochrome c ($m/z$[M+2H]$^{2+}$=6181.05000,

$m/z[\text{M+H}]^+=12360.97000$), 1 mg·mL$^{-1}$ of myoglobin ($m/z[\text{M+2H}]^{2+}=$ 8476.66000, $m/z[\text{M+H}]^+=16952.31000$) and 1 mg·mL$^{-1}$ of protein A ($m/z[\text{M+2H}]^{2+}=22307.00000$, $m/z[\text{M+H}]^+=44613.00000$). Mass spectra peak picking was performed with mMass open source mass spectrometry tool. Mass spectra were mathematically compared using a public bacteria identification service platform BacteriaMS (http://bacteriams.com/), with spectral similarity score calculated by the cosine correlation algorithm. Only peaks with $S/N \geq 3$ were considered for the comparison, with mass tolerance of 1000 ppm.

## 3. Results and discussion

### 3.1 Collection of bacterial reference mass spectra

The MALDI-TOF MS detection sensitivity for intact bacteria was firstly investigated by using a routine sample preparation procedure. 1 µL of bacterial aqueous solution was directly deposited on a MALDI target plate and overlaid with matrix for MS analysis. *E. coli* (gram-negative), *B. subtilis* (gram-positive) and *S. aureus* (gram-positive) were chosen as model bacteria. Notably, each test in this work was repeated 3-5 times to guarantee reproducibility and one of the mass spectra was chosen as the representative and displayed. Results showed that at least $10^3$ of bacterial cells were required to generate detectable MS signals (**Figure 2.1**). In this test, the average diameter of sample spots was 3 mm, while the size of bacterial cells is typically 0.5 to 10 µm and the diameter of laser beam used in the MALDI-TOF MS instrument is about 100 µm. As a result, the measurement of low number of bacterial cells was accomplished with many "blind" laser shots, leading to noise accumulation and limited detection sensitivity.
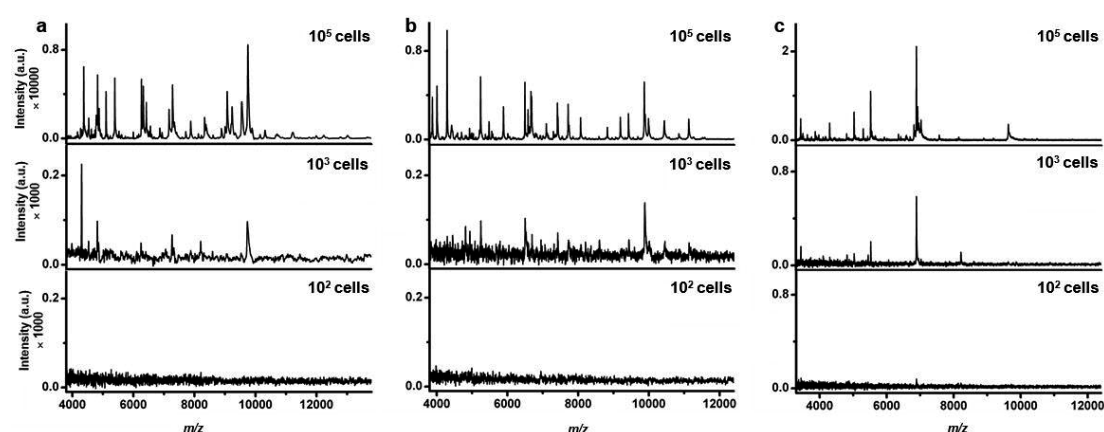


**Figure 2.1** MALDI-TOF MS fingerprinting of intact bacteria, *i.e.* (**a**) *E. coli*, (**b**) *B. subtilis* and (**c**) *S. aureus* by routine sample deposition procedure. The spectra were generated from different bacterial cell numbers.

In order to improve the sensitivity, it is necessary to decrease the size of sample spots, thereby to increase sample surface density and the chance of efficient laser shot. Recently, high-density micro-arrays were developed for ultrasensitive MALDI-TOF MS analysis of single bacterial cells, where each sample spot was only 100 μm in diameter.[15] In the present work, we tried to confine the sample spot size within 800 μm. This mediate sample spot size was optimized with the consideration of magnetic bead utilization in later experiments. If the sample spot size is too small, surface density of the beads will be too high, which could reduce ionisation efficiency of the bacterial components. The confined sample spot size was easily achievable in two ways. The first one consisted of depositing the samples on the target plate with droplet-by-droplet protocol, and the second one was based on the utilization of a Bruker MSP AnchorChip[TM] target.
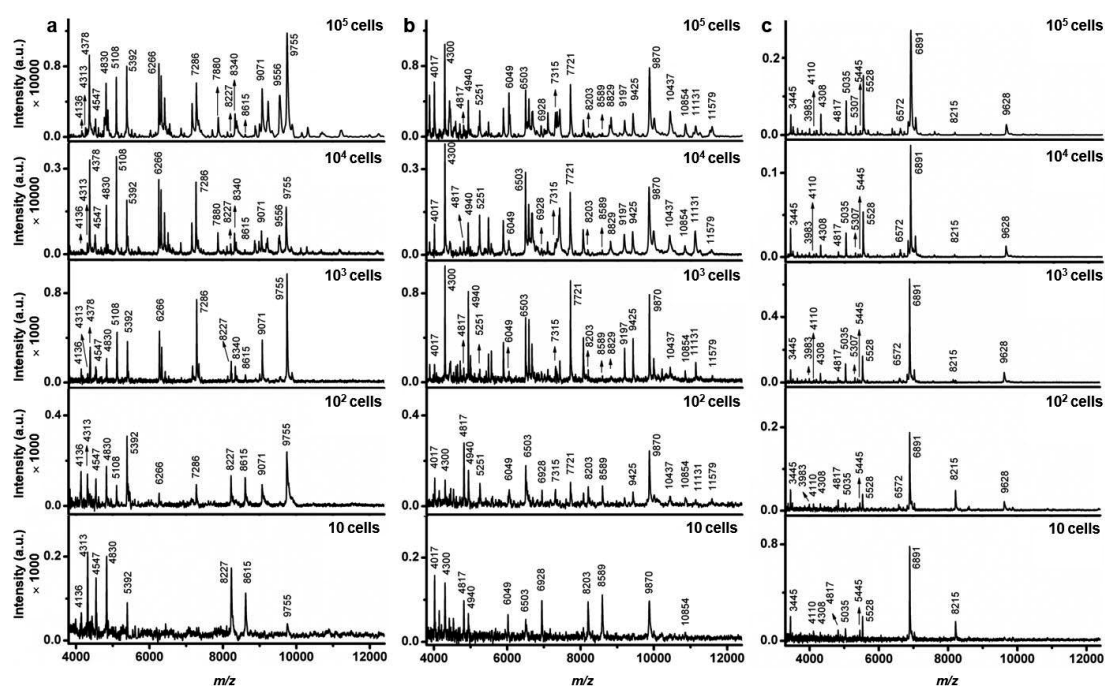


**Figure 2.2** MALDI-TOF MS fingerprinting of intact bacteria, *i.e.* (**a**) *E. coli*, (**b**) *B. subtilis* and (**c**) *S. aureus* with reduced sample spot size. The spectra were generated from different bacterial cell numbers.

Taking advantage of small sample spot sizes, the sensitivity of MALDI-TOF MS was significantly enhanced. Fingerprints of *E. coli* was successfully obtained from as low as 10 to $10^2$ cells (**Figure 2.2a**). To be noted, the cell numbers presented here is not the

exact cell numbers, but estimated numbers calculated through multiplying sample volume by cell concentration. Although the peak number decreased with the decrease of *E. coli* cell number, peaks at 4136, 4313, 4547, 4830, 5392, 8227, 8615, and 9755 *m/z* appeared reproducibly. Results for *B. subtilis* and *S. aureus* were similar (**Figure 2.2 b**, **c**), with characteristic peaks at 4017, 4300, 4817, 4940, 6049, 6503, 6928, 8203, 8589, 9870, 10854 *m/z* appearing reproducibly for *B. subtilis*, and peaks at 3445, 4110, 4308, 4817, 5035, 5445, 5528, 6891, 8215 *m/z* appearing reproducibly for *S. aureus*. These peaks corresponded to different intracellular proteins (mainly ribosomal proteins), which could serve as biomarkers to characterize bacterial species.[19,20]

A library of bacterial reference mass spectra was built with the current data, *i.e.* three species (*E. coli*, *B. subtilis*, *S. aureus*) at five different cells numbers (10, $10^2$, $10^3$, $10^4$, $10^5$) with three to five repetitions for each case. It is worth to notice that existing commercial databases for bacterial identification are normally built by collecting reference spectra from large cells number, which can provide fruitful peak information for highly confident identification.[21] However, in such a case, samples with high bacterial abundance are needed to provide spectra with good similarity to the reference for successful identification. Therefore, large sample volume or long bacterial culture time is required. In this work, reference spectra from small numbers of cells were collected as well and were demonstrated to be sufficient for bacterial identification.

## 3.2 Bacterial identification based on pattern matching

Bacterial species identification result was obtained through pattern matching, *i.e.* comparing the spectra obtained from a blood sample with spectra in the reference library with spectral similarity scores calculated. Higher score represents higher possibility of a correct identification. The similarity score between two mass spectra (*i* and *j*) was calculated by the often-used cosine correlation method, defined as:

$$\cos = \frac{\overrightarrow{y_i} \cdot \overrightarrow{y_j}}{\left|\overrightarrow{Y_i}\right| \cdot \left|\overrightarrow{Y_j}\right|} = \frac{\sum_{k=1}^{l} y_{ik} y_{jk}}{\sqrt{\sum_{t=1}^{n_i} Y_{it}^2} \cdot \sqrt{\sum_{t=1}^{n_j} Y_{jt}^2}}$$

where *y* is the normalized intensity of a peak appearing in both spectrum *i* and spectrum *j* (identical peak), *l* is the number of identical peaks in the two spectra, *Y* is the normalized intensity of a peak appearing in a spectrum, *n* the number of peaks in a spectrum.[16] Only peaks with *S/N* ≥ 3 were considered. Peaks appearing in different spectra with Δ(*m/z*)/(*m/z*) ≤ 1000 ppm were considered as identical peaks. The tolerance of 1000 ppm was set according to the resolving power of linear mode TOF analysis.

The cosine correlation algorithm was firstly adopted to calculate the similarity among

the previously collected reference mass spectra (not only those shown in **Figure 2.2** but also their repetitions). The similarity scores were calculated for three groups, including *i)* reference spectra obtained from different bacterial species (867 scores obtained), *ii)* reference spectra obtained from the same bacterial species (the same strain) but at different cell numbers (342 scores obtained) and *iii)* reference spectra obtained from different repetitions of the same bacterial strains at the same cell numbers (66 scores obtained). The frequency distribution of similarity scores in each group is shown in **Figure 2.3**. The reference spectra collected different bacterial species were quite different, with all similarity scores lower than 0.1 (**Figure 2.3 a**). As for the same bacterial species at different cell numbers, the similarity scores range from 0 to 1 (**Figure 2.3 b**). Meanwhile the reference spectra obtained from different repetitions of the same bacterial species at the same cell number were quite similar, with almost all similarity scores higher than 0.8 (**Figure 2.3 c**). Therefore, when the similarity score between a sample spectrum and a reference spectrum is higher than 0.8, we can believe that the species identity of the tested bacteria is the same as the reference bacteria.
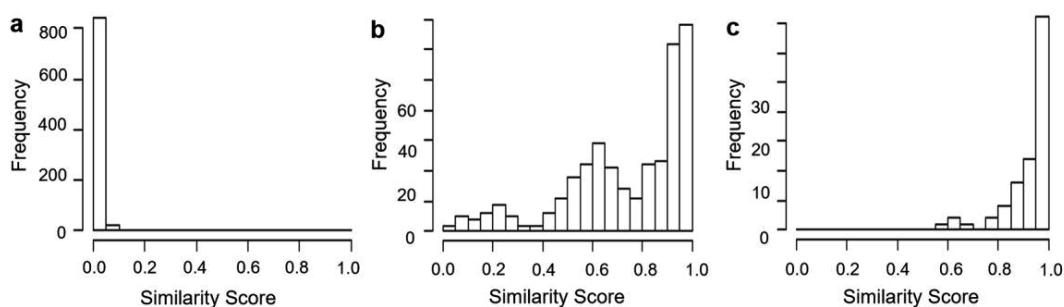


**Figure 2.3** The frequency distribution of similarity scores among bacterial reference mass spectra. The similarity scores were calculated for three groups, including (**a**) spectra obtained from different bacterial species, (**b**) spectra obtained from the same bacterial species (the same strain) but at different cell numbers, (**c**) spectra obtained from different repetitions of the same bacteria strains at the same cell numbers.

## 3.3 Bacterial identification from spiked blood serum and whole blood samples

When bacteria are present in a complex medium, *i.e.* human blood serum or whole blood, it is hard to perform direct MALDI-TOF MS identification due to the background interference from the blood, which usually contains a large number of proteins. Thereby, it is necessary to conduct bacterial isolation and purification before mass spectrometry measurement. Due to the high specificity of immunoassays and the convenience of

magnetic separation, magnetic beads modified with bacterial species-specific antibodies were chosen for the isolation and enrichment of target bacteria. This immuno-affinity MALDI-TOF MS approach is shown in **Figure 2.4**. At first, protein A/G-coated beads were mixed with an excess of antibodies to form bacterial affinity probes Abs-MBs. The recombinant protein A/G on the surface of beads contains six binding domains (four from protein A, two from protein G) to the Fc regions of IgG isotype antibodies.[22] Prior to bacterial isolation, the blood samples were pre-treated to reduce potential interference from blood proteins.[23] Neither the protein A/G-beads nor the antibodies generate any signal in the mass range for bacterial identification, *i.e.* 2,000-20,000 *m/z* (**Figure 2.5**). After immune-affinity isolation, all the obtained conjugations of beads, antibodies and bacterial cells were transferred onto a target plate for mass spectrometry measurement, followed by the identification based on pattern matching.
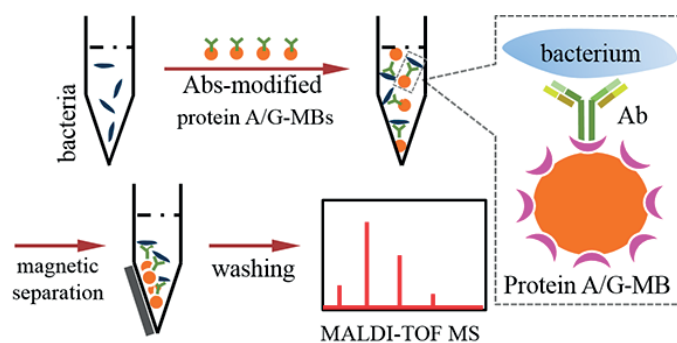


**Figure 2.4** Scheme of the immuno-affinity MALDI-TOF MS procedure.
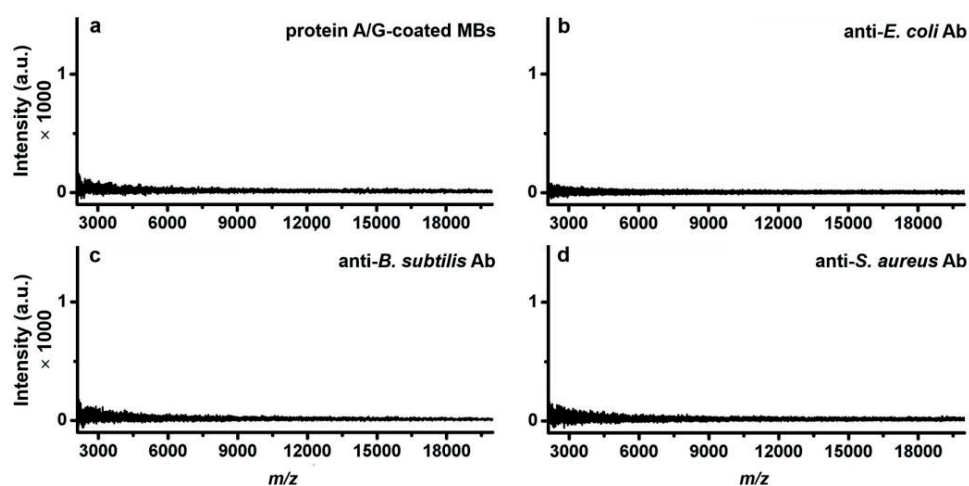


**Figure 2.5** MALDI-TOF mass spectra of (**a**) protein A/G-MBs, (**b**) anti-*E. coli* antibody, (**c**) anti-*B. subtilis* antibody, (**d**) anti-*S. aureus* antibody in 2,000-20,000 *m/z* mass range.
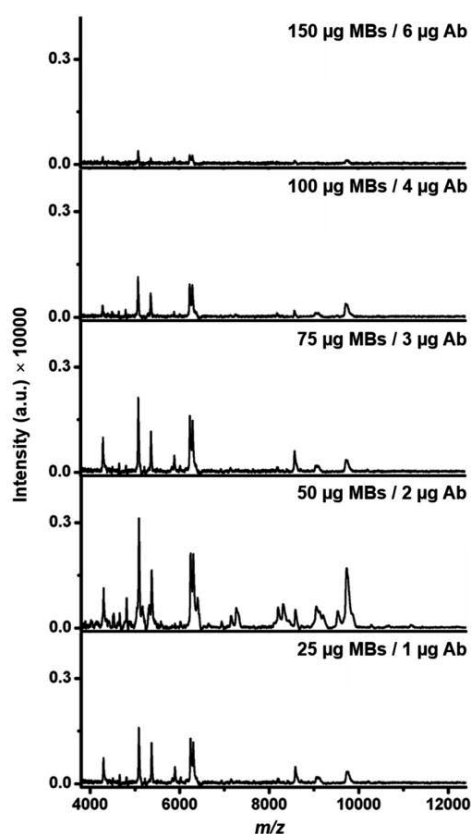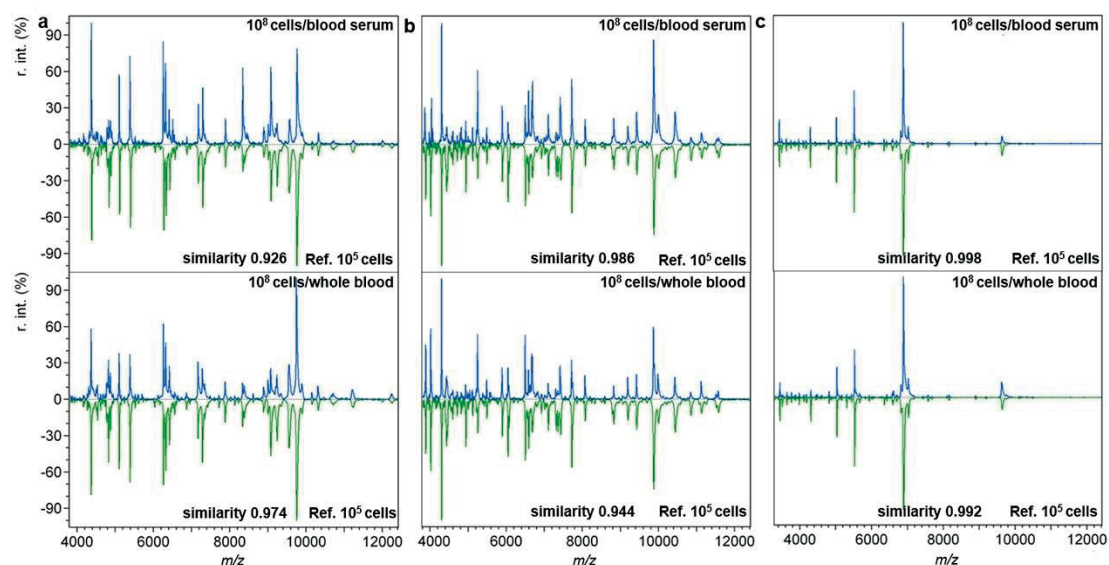
**Figure 2.6** Mass spectra obtained from the immuno-affinity isolation product by applying different amounts of Abs-MBs to 1 mL of PBST buffer containing $10^4$ cells·mL$^{-1}$ *E. coli*.

To maximize the efficiency of bacterial isolation and enrichment, experimental conditions were optimized by adjusting the amount of Abs-MBs. 1 mL of PBST buffer spiked with $10^4$ cells·mL$^{-1}$ *E.coli* was used as the testing sample. When the Abs-MBs amount was too low, few bacterial cells were captured and the obtained spectrum was of bad quality. In contrast, when the Abs-MBs amount was too high, high surface density of beads reduced the ionisation efficiency of the bacteria. Therefore, 50 μg of beads was employed for the following tests (**Figure 2.6**). Before the analysis of bacteria-spiked samples, pure blood serum and whole blood without bacteria were tested as negative control. And no peaks were observed in the mass range of 2,000-20,000 *m/z* (**Figure 2.7**), demonstrating a good specificity of the immuno-affinity isolation procedure. Then, blood serum and whole blood spiked with high concentration ($10^8$ cells·mL$^{-1}$) of *E. coli*, *B. subtilis* or *S. aureus* were analysed. After pattern matching it was found that the resulting mass spectra showed the highest similarity to the reference spectra collected from $10^5$ cells of the corresponding bacterial species. The similarity scores for blood serum samples and whole blood samples were $0.953 \pm 0.025$ and $0.966 \pm 0.020$ for *E. coli*, $0.976 \pm 0.009$

and $0.959 \pm 0.020$ for *B. subtilis*, $0.993 \pm 0.005$ and $0.986 \pm 0.006$ for *S. aureus*, respectively, as listed in **Appendix, No. 1-18**. Representative spectrum comparison is shown in **Figure 2.8**.
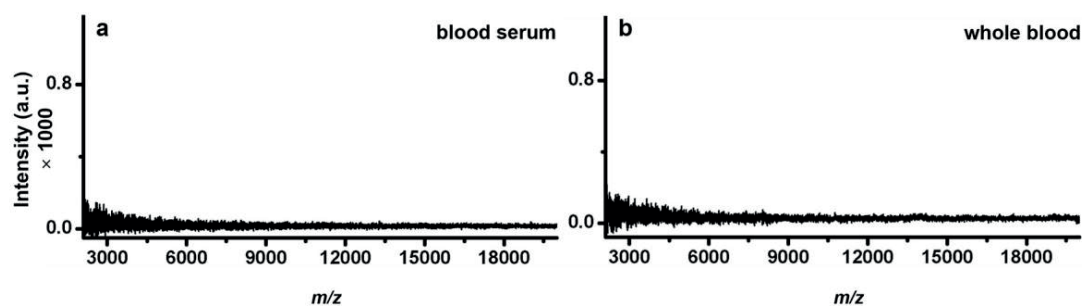


**Figure 2.7** Mass spectra of immuno-affinity isolation product from (**a**) pure blood serum and (**b**) pure whole blood by using anti-*E. coli* Abs-MBs as the affinity probe.



**Figure 2.8** Mass spectra of the immuno-affinity isolation product obtained from 1 mL of blood serum or whole blood spiked with $10^8$ cells·mL$^{-1}$ of (**a**) *E. coli,* (**b**) *B. subtilis* and (**c**) *S. aureus*. The spectra were compared with reference spectra of corresponding bacterial species ($10^5$ cells) with similarity score calculated. r.int: relative intensity.

By decreasing the bacterial concentration gradually, it was found that the detection limit was 500 cells·mL$^{-1}$ in blood serum and 8000 cells·mL$^{-1}$ in whole blood, with the

resulting mass spectra displaying highest similarity to the reference spectra from 10 cells (similarities were listed in **Appendix, No. 19-36**). Representative spectrum comparison is shown in **Figure 2.9**. For blood serum samples with 500 cells·mL$^{-1}$ bacteria, the concentration was only 50 cells·mL$^{-1}$ after dilution. Considering that only 1 mL of sample was used, it is reasonable that the obtained sample spectra matched the reference spectra of 10 cells. The detection limit for whole blood sample was not as good as that for blood serum sample, due to the loss of bacterial cells during the sample pre-treatment process.
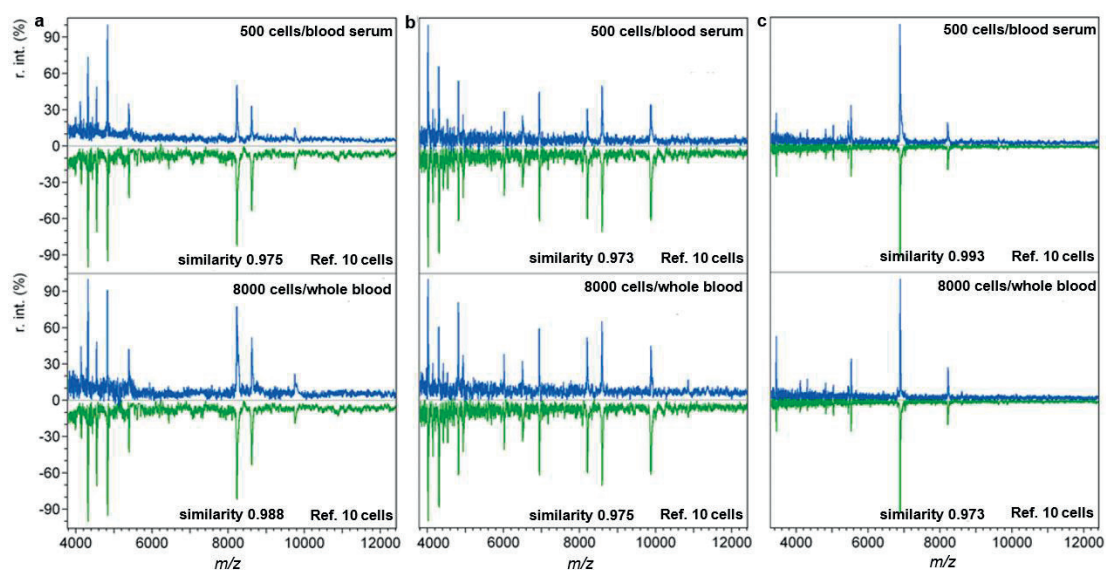


**Figure 2.9** Mass spectra of the immuno-affinity isolation product obtained from 1 mL of blood serum or whole blood spiked with 500 cells·mL$^{-1}$ or 8000 cells·mL$^{-1}$ of **(a)** *E.coli*, **(b)** *B. subtilis* and **(c)** *S. aureus*. The spectra were compared with reference spectra from 10 cells with similarity scores calculated.

The accuracy of the immuno-affinity MALDI-TOF MS identification procedure was evaluated by performing the tests with 20 whole blood samples spiked with random concentration of *S. aureus* (higher than 8000 cells·mL$^{-1}$). Anti-*S. aureus* Abs-MBs was used as affinity probe. The results showed *S. aureus* was correctly identified from 19 of the samples, with the spectral similarity scores listed in **Appendix, No. 37-56**. Another 20 whole blood samples spiked with random concentration (higher than 8000 cells·mL$^{-1}$) of *E. coli* or *B. subtilis* were tested as the negative controls, still using anti-*S. aureus* Abs-MBs as the affinity probes. The testing results shows none of the samples generated detectable mass spectral signals within the mass range of 2,000-20,000 *m/z*. Thence, the present method enables accurate bacterial identification from blood samples.

In many cases, the bloodstream infections are caused by more than one bacterial species.[29] Direct MALDI-TOF MS fingerprinting of a sample containing several bacterial species is inefficient for the identification of each bacterial species. Proteins or membrane lipids from different species would make the resulting mass spectra too complicated to be analysed. Therefore, subculture, taking hours to days, is often conducted to provide pure bacterial strains for the purpose of identification. The immuno-affinity isolation procedure using bacterial species-specific antibodies should allow the identification of target bacteria from multi-species infected blood samples without the need of subculture. To prove this concept, three groups of whole blood samples spiked simultaneously with *S. aureus, E.coli* and *B. subtilis* were analyzed by using anti-*S. aureus* Abs-MBs as the affinity probes. The sample composition was $10^5$ cells·mL$^{-1}$ *S. aureus*, $10^4$ cells·mL$^{-1}$ *E. coli* and $10^4$ cells·mL$^{-1}$ *B. subtilis* for group A, $10^5$ cells·mL$^{-1}$ *S. aureus*, $10^5$ cells·mL$^{-1}$ *E. coli* and $10^5$ cells·mL$^{-1}$ *B. subtilis* for group B, $10^5$ cells·mL$^{-1}$ *S. aureus*, $10^7$ cells·mL$^{-1}$ *E. coli* and $10^7$ cells·mL$^{-1}$ *B. subtilis* for group C. As shown in **Table 2.1**, *S. aureus* was correctly identified from all the samples. When the concentration of both *E. coli* and *B. subtilis* were 500 times higher than that of *S. aureus*, *S. aureus* could not be identified any more (data not shown), because extremely high concentrations of *E. coli* and *B. subtilis* decreased the binding chance of *S. aureus* to the immuno-affinity probes. Overall, the proposed procedure allows bacterial identification from multi-species infected blood samples, and shows potentials for the diagnosis of polymicrobial bloodstream infections.

**Table 2.1** Bacterial identification from multi-species spiked whole blood samples.

| Sample | Reference Spectra | Similarity Score |
|--------|-------------------|------------------|
| A-1 | 10 *S. aureus* cells | 0.99 |
| A-2 | $10^2$ *S. aureus* cells | 0.993 |
| A-3 | $10^2$ *S. aureus* cells | 0.991 |
| B-1 | 10 *S. aureus* cells | 0.991 |
| B-2 | 10 *S. aureus* cells | 0.985 |
| B-3 | 10 *S. aureus* cells | 0.992 |
| C-1 | $10^2$ *S. aureus* cells | 0.969 |
| C-2 | 10 *S. aureus* cells | 0.982 |
| C-3 | 10 *S. aureus* cells | 0.97 |

1-3: three independent repetitions

To sum up, a sensitive method has been demonstrated for accurate and specific identification of bacteria from human whole blood by combining immuno-affinity isolation/enrichment and optimized MALDI-TOF MS measurement. The method requires only 1 mL of blood with detection limit of 8,000 cells·mL$^{-1}$. This detection limit is higher than the bacterial concentration in most bloodstream infection patients, and thus direct bacterial identification from patient blood remains difficult. However, a much shorter blood culture period can be expected to magnify bacterial concentration to a detectable level. Moreover, this method is particularly suitable for child patients, as the infections in child patients are normally associated with higher pathogen concentration than adult patients (in many cases could be higher than 100 CFU·mL$^{-1}$).[23]

## 3.4 Bacterial identification from blood cultures

In clinical practice, blood samples collected from patients are incubated in blood culture bottles to investigate the presence or absence of bacterial pathogens. If bacteria are present, they can proliferate in the bottles during the culture process. When the cell abundance is high enough, the bottles turn positive automatically. For example, positive BacT/Alert® bottles indicate high bacterial abundance by colour change on the bottom. Before conducting the final definitive identification, isolates from the positive bottles undergo gram staining, plating, and subculture to provide pure bacterial cultures. Feasibility of the developed immuno-affinity mass spectrometry identification method was further examined with four positive blood cultures, which were provided by a local hospital. According to the identification conducted by the hospital, two of blood cultures (bottle I, II) were *E. coli*-positive, and the other two (bottle III, IV) were *S. aureus*-positive. During the examination, 1 mL of positive culture liquid was taken out from each bottle for bacterial isolation/enrichment using the affinity probes of anti-*E. coli* Abs-MBs and anti-*S. aureus* Abs-MBs, respective. Consequently, *E. coli* was correctly identified from bottle I and II, as the resulting mass spectra displayed highest similarity to the reference spectra of $10^5$ *E. coli* cells, with similarity score of 0.835 and 0.888, respectively. *S. aureus* was successfully identified from bottle III and IV, scoring 0.981 and 0.954, respectively. The mass spectra are compared in **Figure 2.10**. The result indicates that the present method can identify bacteria directly from positive blood cultures without the need of subculture. This can significantly shorten the diagnosis time. For all the four positive blood culture, the resulting mass spectra were comparable to reference spectra of $10^5$ cells of *E. coli* or *S. aureus*. It implies that the positive blood cultures contain a high concentration of bacteria. As the detection limit of the present method for whole blood samples is 8,000 cells·mL$^{-1}$, it should allow bacterial identification with shorter blood culture time. As a proof, a time-step test was conducted to investigate the influence of blood culture time on the identification result.
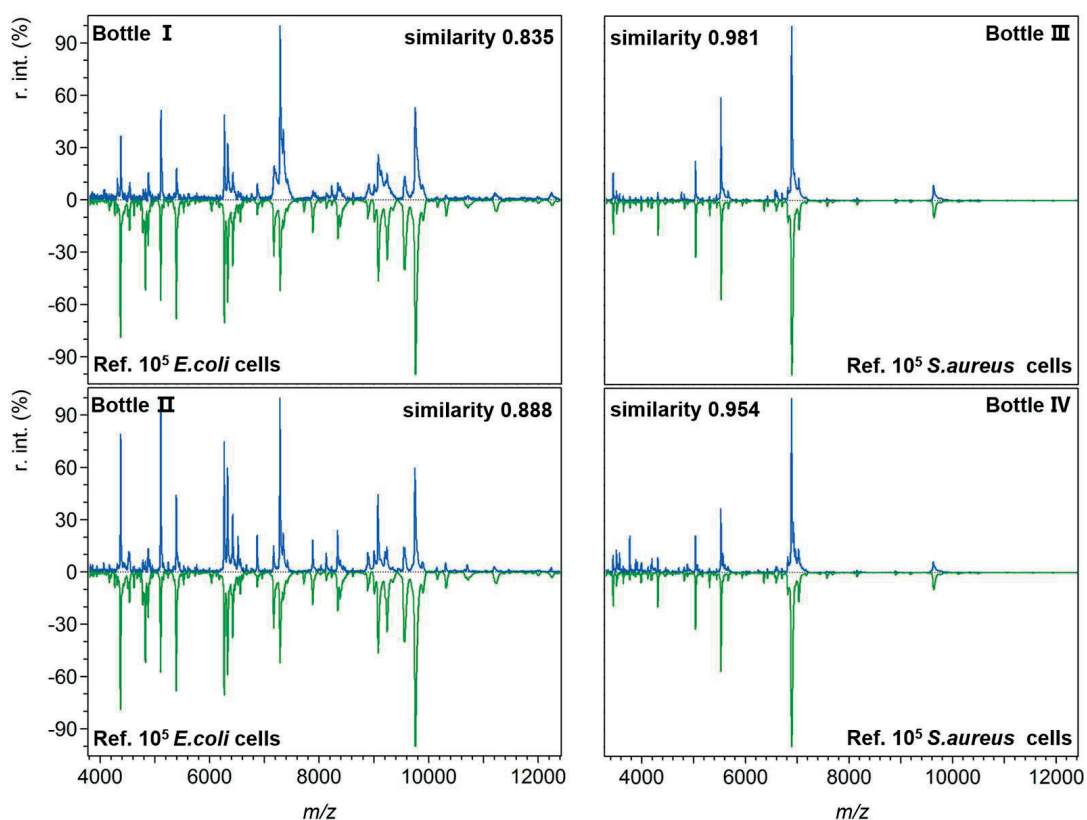
**Figure 2.10** Successful identification of bacteria from four positive blood cultures by using the proposed immuno-affinity mass spectrometry method.

During the time-step test, 5 mL of whole blood collected from a healthy adult was spiked with *E. coli* with initial concentration of $10^2$ or $10^3$ cells·mL$^{-1}$ and then incubated in BacT/Alert® blood culture bottles. The initial *E. coli* concentrations of $10^2$ and $10^3$ cells·mL$^{-1}$ were chosen in accordance with the normal bacterial concentration in bloodstream infection patients. For each concentration, four blood cultures were prepared in parallel. For two of them, 1 mL of culture liquid was taken out and analysed by the proposed method after every 2 hours of incubation. The rest two bottles were kept untouched and were checked regularly until they turned positive. Mass spectra obtained from two blood cultures with initial *E. coli* concentration of $10^2$ cells·mL$^{-1}$ after different time of incubation are shown in **Figure 2.11 a-I** and **a-II**. The best pattern matching results for the spectra are displayed in **Figure 2.12**. At the very beginning (0 h), no characteristic peaks were detected, as *E. coli* concentration was below the detection limit. At 2 h, the peak at 8226 *m/z* was detected for both cultures, and the peak also appeared on the reference spectrum of 10 *E. coli* cells (**Figure 2.12**, **I-2h**, **II-2h**). At 4 h, more peaks were detectable, with similarity of 0.927 and 0.867 to the reference spectrum

48

of 10 *E. coli* cells (**Figure 2.12**, **I-4h**, **II-4h**). Good quality mass spectra were obtained at 6 h, showing 0.959 and 0.876 similarity to the reference spectrum of $10^4$ and $10^3$ *E. coli* cells, respectively (**Figure 2.12**, **I-6h**, **II-6h**). At 8 h, the obtained spectra were comparable to the reference spectrum of $10^5$ *E. coli* cells, with the similarity of 0.913 and 0.897, respectively (**Figure 2.12**, **I-8h**, **II-8h**). The obtained spectra didn't change much when elongating the culture time (*e.g.* 10 h). Therefore, the bacterial abundance was high enough for species identification after 4-6 hours of blood culture. Meanwhile, it was observed that the two untouched bottles turned positive after 10.5 h of culture. Similarly, mass spectra obtained from the two parallel blood cultures with initial *E. coli* concentration of $10^3$ cells·mL$^{-1}$ are shown in **Figure 2.11 b-I** and **b-II**, with the best pattern matching results shown in **Figure 2.13**. It indicated that *E. coli* was successfully identified after 2-4 hours of blood culture. In comparison, the two untouched blood cultures turned positive after 9.5 hours of incubation.
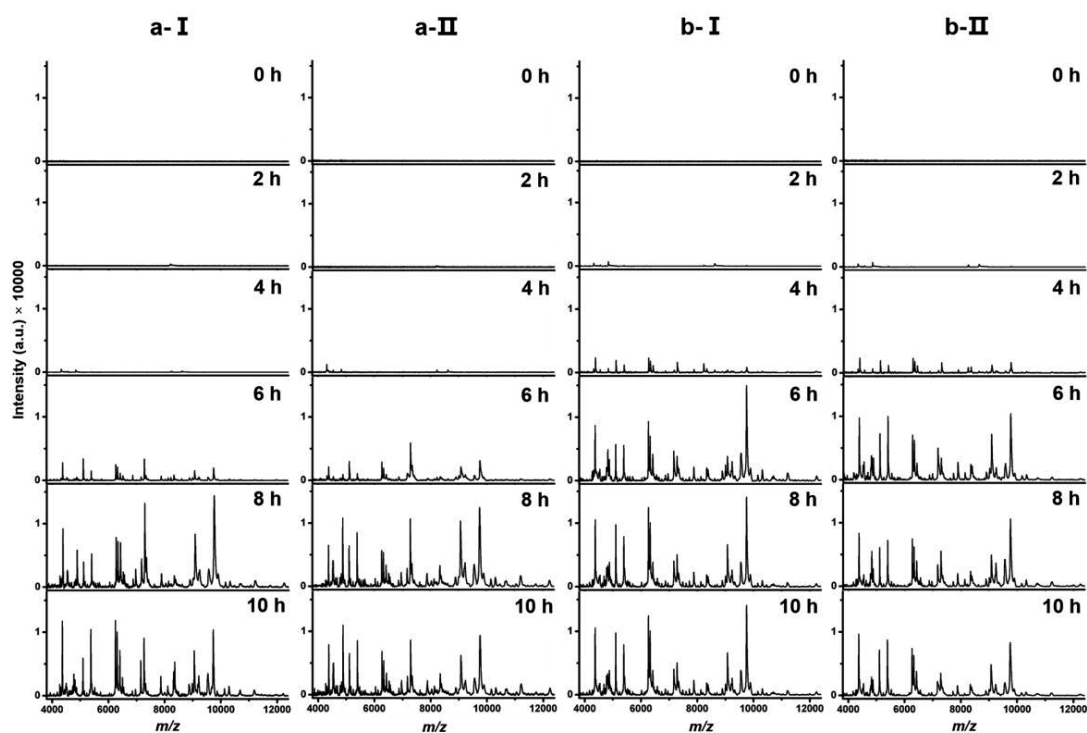


**Figure 2.11** Mass spectra obtained from four blood cultures with initial *E. coli* concentration of (**a-I**) $10^2$ cells·mL$^{-1}$ (bottle I), (**a-II**) $10^2$ cells·mL$^{-1}$ (bottle II), (**b-I**) $10^3$ cells·mL$^{-1}$ (bottle I), (**b-II**) $10^3$ cells·mL$^{-1}$ (bottle II) after different culture time, *i.e.* 0 h, 2 h, 4 h, 6 h, 8 h and 10 h.
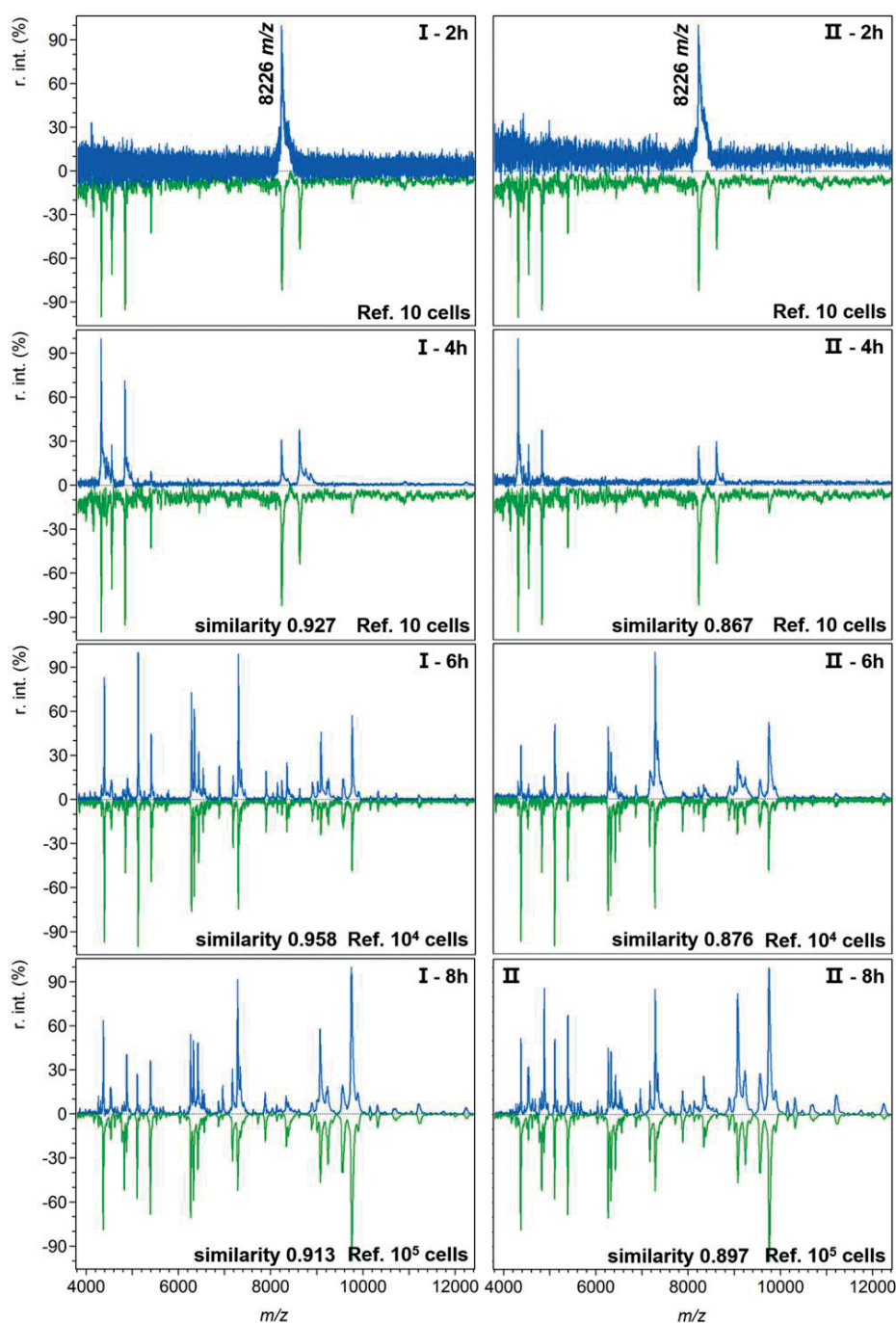
**Figure 2.12** Identification of *E. coli* from two blood cultures (bottle I and II, prepared in parallel) containing 5 mL of whole blood with initial *E. coli* concentration of $10^2$ cells·mL$^{-1}$ after different time of incubation by using the proposed immuno-affinity mass spectrometry method. The experimental spectra came from **Figure 2.11** (**a-I**) and (**a-II**). The reference spectra were collected from different numbers of *E. coli* DH5α cells. Similarity scores between each two spectra were calculated by the cosine correlation algorithm.
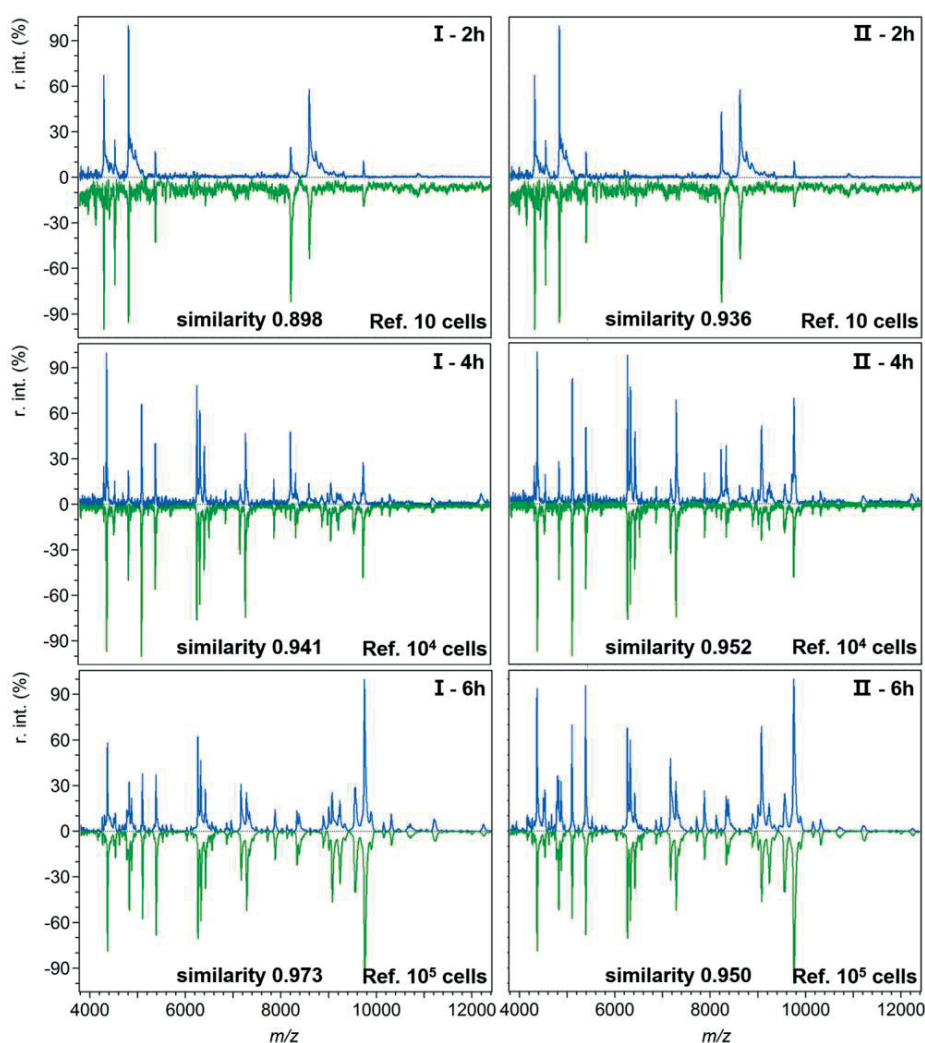
**Figure 2.13** Identification of *E. coli* from two blood cultures (bottle I and II) containing 5 mL of whole blood with initial *E. coli* concentration of $10^3$ cells·mL$^{-1}$ after different time of incubation by using the proposed immuno-affinity mass spectrometry method. The experimental spectra came from **Figure 2.11 (b-I)** and (**b-II**). The reference spectra were collected from different numbers of *E. coli* DH5α cells. Similarity scores between each two spectra were calculated by the cosine correlation algorithm.

These results demonstrate that the present method is able to identify bacteria before the blood cultures turn positive. Considering the time required for immuno-affinity bacterial isolation/enrichment and MALDI-TOF MS measurement (within 2 hours), the entire identification process, from blood collection to identification reports, could be completed within 4 to 6 hours, demonstrating its potential application for rapid diagnosis of bloodstream infections.

Utilization of appropriate bacterial affinity probes is critical for the success of the present method. In clinical practice, it is necessary to have a storage of antibodies specific to common bacterial pathogens, such as *Staphylococcus aureus*, *Staphylococcus epidermidis*, *Staphylococcus hominis*, *Escherichia coli*, *Enterococcus faecium*, *Streptococcus pneumoniae*, *Klebsiella pneumoniae*, *Acinetobacter baumannii* and *Enterobacter cloacae*.[24] To guide the selection of suitable antibodies, the pathogen species can be empirically pre-judged according to the infection symptoms of the patient, and then tested by the immuno-affinity mass spectrometry method. In worst cases, identification could always be carried out by scanning the blood cultures against the Abs-MBs affinity probe bank. Moreover, reference spectra of more bacterial species, especially common bacterial pathogens, should be collected from different cell numbers, which could be the future continuation of the current work. In addition to bacterial infection diagnosis, the method can also be used for quality control of blood products (*e.g.* whole blood, platelet and erythrocyte concentrates if not pathogen reduced) during their storage. For instance, bacterial strains involve in adverse transfusion reactions such as *Staphylococcus epidermis*, *Serratia marcescens* or *Serratia liquefaciens* could be tested in non-pathogen reduced blood products.[25,26]

## 4. Conclusions

In this work, an immuno-affinity MALDI-TOF mass spectrometry method has been developed for bacterial identification from human blood samples at the species level. By comparing the resulting sample spectra with reference ones in a self-built library, bacteria can be correctly identified from 1 mL of whole blood samples with a detection limit of 8000 cells·mL$^{-1}$. The method is able to identify bacteria from multi-bacterial blood samples, showing potential in polymicrobial infection diagnosis. It also shows success in bacterial identification directly from clinical positive blood cultures. A time-step test suggests that bacteria can actually be identified from blood cultures even before they turn positive. The culture time required for diagnosis is, then, significantly reduced. With this method, the entire diagnosis of bloodstream infections can be completed within several hours.

# Appendix

List of pattern-matching results. Sample name with 1-3 means three repetitions.

| No. | Sample Name | Reference Spectrum | Similarity Score |
|---|---|---|---|
| 1 | $10^8$ *E. coli* cells mL$^{-1}$ in blood serum-1 | $10^5$ *E. coli* cells | 0.926 |
| 2 | $10^8$ *E. coli* cells mL$^{-1}$ in blood serum-2 | $10^5$ *E. coli* cells | 0.976 |
| 3 | $10^8$ *E. coli* cells mL$^{-1}$ in blood serum-3 | $10^5$ *E. coli* cells | 0.956 |
| 4 | $10^8$ *E. coli* cells mL$^{-1}$ in whole blood-1 | $10^5$ *E. coli* cells | 0.974 |
| 5 | $10^8$ *E. coli* cells mL$^{-1}$ in whole blood-2 | $10^5$ *E. coli* cells | 0.981 |
| 6 | $10^8$ *E. coli* cells mL$^{-1}$ in whole blood-3 | $10^5$ *E. coli* cells | 0.943 |
| 7 | $10^8$ *B. subtilis* cells mL$^{-1}$ in blood serum-1 | $10^5$ *B. subtilis* cells | 0.986 |
| 8 | $10^8$ *B. subtilis* cells mL$^{-1}$ in blood serum-2 | $10^5$ *B. subtilis* cells | 0.972 |
| 9 | $10^8$ *B. subtilis* cells mL$^{-1}$ in blood serum-3 | $10^5$ *B. subtilis* cells | 0.970 |
| 10 | $10^8$ *B. subtilis* cells mL$^{-1}$ in whole blood-1 | $10^5$ *B. subtilis* cells | 0.944 |
| 11 | $10^8$ *B. subtilis* cells mL$^{-1}$ in whole blood-2 | $10^5$ *B. subtilis* cells | 0.979 |
| 12 | $10^8$ *B. subtilis* cells mL$^{-1}$ in whole blood-3 | $10^5$ *B. subtilis* cells | 0.951 |
| 13 | $10^8$ *S. aureus* cells mL$^{-1}$ in blood serum-1 | $10^5$ *S. aureus* cells | 0.998 |
| 14 | $10^8$ *S. aureus* cells mL$^{-1}$ in blood serum-2 | $10^5$ *S. aureus* cells | 0.993 |
| 15 | $10^8$ *S. aureus* cells mL$^{-1}$ in blood serum-3 | $10^5$ *S. aureus* cells | 0.988 |
| 16 | $10^8$ *S. aureus* cells mL$^{-1}$ in whole blood-1 | $10^5$ *S. aureus* cells | 0.992 |
| 17 | $10^8$ *S. aureus* cells mL$^{-1}$ in whole blood-2 | $10^5$ *S. aureus* cells | 0.986 |
| 18 | $10^8$ *S. aureus* cells mL$^{-1}$ in whole blood-3 | $10^5$ *S. aureus* cells | 0.980 |
| 19 | 500 *E. coli* cells mL$^{-1}$ in blood serum-1 | 10 *E. coli* cells | 0.975 |
| 20 | 500 *E. coli* cells mL$^{-1}$ in blood serum-2 | 10 *E. coli* cells | 0.954 |
| 21 | 500 *E. coli* cells mL$^{-1}$ in blood serum-3 | 10 *E. coli* cells | 0.980 |
| 22 | 8000 *E. coli* cells mL$^{-1}$ in whole blood-1 | 10 *E. coli* cells | 0.988 |
| 23 | 8000 *E. coli* cells mL$^{-1}$ in whole blood-2 | 10 *E. coli* cells | 0.971 |
| 24 | 8000 *E. coli* cells mL$^{-1}$ in whole blood-3 | 10 *E. coli* cells | 0.957 |
| 25 | 500 *B. subtilis* cells mL$^{-1}$ in blood serum-1 | 10 *B. subtilis* cells | 0.973 |
| 26 | 500 *B. subtilis* cells mL$^{-1}$ in blood serum-2 | 10 *B. subtilis* cells | 0.978 |
| 27 | 500 *B. subtilis* cells mL$^{-1}$ in blood serum-3 | 10 *B. subtilis* cells | 0.959 |

| 28 | 8000 *B. subtilis* cells mL$^{-1}$ in whole blood-1 | 10 *B. subtilis* cells | 0.975 |
| 29 | 8000 *B. subtilis* cells mL$^{-1}$ in whole blood-2 | 10 *B. subtilis* cells | 0.956 |
| 30 | 8000 *B. subtilis* cells mL$^{-1}$ in whole blood-3 | 10 *B. subtilis* cells | 0.954 |
| 31 | 500 *S. aureus* cells mL$^{-1}$ in blood serum-1 | 10 *S. aureus* cells | 0.993 |
| 32 | 500 *S. aureus* cells mL$^{-1}$ in blood serum-2 | 10 *S. aureus* cells | 0.984 |
| 33 | 500 *S. aureus* cells mL$^{-1}$ in blood serum-3 | 10 *S. aureus* cells | 0.979 |
| 34 | 8000 *S. aureus* cells mL$^{-1}$ in whole blood-1 | 10 *S. aureus* cells | 0.973 |
| 35 | 8000 *S. aureus* cells mL$^{-1}$ in whole blood-2 | 10 *S. aureus* cells | 0.963 |
| 36 | 8000 *S. aureus* cells mL$^{-1}$ in whole blood-3 | 10 *S. aureus* cells | 0.950 |
| 37 | *S. aureus*-spiked accuracy test sample-1 | 10$^5$ *S. aureus* cells | 0.991 |
| 38 | *S. aureus*-spiked accuracy test sample-2 | 10$^5$ *S. aureus* cells | 0.990 |
| 39 | *S. aureus*-spiked accuracy test sample-3 | 10$^4$ *S. aureus* cells | 0.997 |
| 40 | *S. aureus*-spiked accuracy test sample-4 | 10$^4$ *S. aureus* cells | 0.992 |
| 41 | *S. aureus*-spiked accuracy test sample-5 | 10$^4$ *S. aureus* cells | 0.991 |
| 42 | *S. aureus*-spiked accuracy test sample-6 | 10$^4$ *S. aureus* cells | 0.989 |
| 43 | *S. aureus*-spiked accuracy test sample-7 | 10$^4$ *S. aureus* cells | 0.994 |
| 44 | *S. aureus*-spiked accuracy test sample-8 | 10$^4$ *S. aureus* cells | 0.996 |
| 45 | *S. aureus*-spiked accuracy test sample-9 | 10$^3$ *S. aureus* cells | 0.994 |
| 46 | *S. aureus*-spiked accuracy test sample-10 | 10$^3$ *S. aureus* cells | 0.993 |
| 47 | *S. aureus*-spiked accuracy test sample-11 | 10$^3$ *S. aureus* cells | 0.993 |
| 48 | *S. aureus*-spiked accuracy test sample-12 | 10$^3$ *S. aureus* cells | 0.994 |
| 49 | *S. aureus*-spiked accuracy test sample-13 | 10$^3$ *S. aureus* cells | 0.987 |
| 50 | *S. aureus*-spiked accuracy test sample-14 | 10$^2$ *S. aureus* cells | 0.985 |
| 51 | *S. aureus*-spiked accuracy test sample-15 | 10$^2$ *S. aureus* cells | 0.983 |
| 52 | *S. aureus*-spiked accuracy test sample-16 | 10$^2$ *S. aureus* cells | 0.949 |
| 53 | *S. aureus*-spiked accuracy test sample-17 | 10 *S. aureus* cells | 0.989 |
| 54 | *S. aureus*-spiked accuracy test sample-18 | 10 *S. aureus* cells | 0.982 |
| 55 | *S. aureus*-spiked accuracy test sample-19 | 10 *S. aureus* cells | 0.978 |
| 56 | *S. aureus*-spiked accuracy test sample-20 | 10 *S. aureus* cells | 0.714 |

# Reference

1. Son, J.S.*, et al.* Bloodstream Infections and Clinical Significance of Healthcare-associated Bacteremia: A Multicenter Surveillance Study in Korean Hospitals. *J Korean Med Sci* 25, 992-998 (2010).
2. Goto, M. & Al-Hasan, M. Overall burden of bloodstream infection and nosocomial bloodstream infection in North America and Europe. *Clin Microbiol Infec* 19, 501-509 (2013).
3. Lamy, B., Dargere, S., Arendrup, M.C., Parienti, J.J. & Tattevin, P. How to Optimize the Use of Blood Cultures for the Diagnosis of Bloodstream Infections? A State-of-the Art. *Front Microbiol* 7 (2016).
4. Peters, R.P., van Agtmael, M.A., Danner, S.A., Savelkoul, P.H. & Vandenbroucke-Grauls, C.M. New developments in the diagnosis of bloodstream infections. *Lancet Infect Dis* 4, 751-760 (2004).
5. Emerson, D., Agulto, L., Liu, H. & Liu, L. Identifying and characterizing bacteria in an era of genomics and proteomics. *Bioscience* 58, 925-936 (2008).
6. Kang, D.-K.*, et al.* Rapid detection of single bacteria in unprocessed blood using Integrated Comprehensive Droplet Digital Detection. *Nat Commun* 5:5427 (2014).
7. Holland, R.*, et al.* Rapid identification of intact whole bacteria based on spectral patterns using matrix‐assisted laser desorption/ionization with time‐of‐flight mass spectrometry. *Rapid Commun Mass Spectrom* 10, 1227-1232 (1996).
8. Claydon, M.A., Davey, S.N., Edwards-Jones, V. & Gordon, D.B. The rapid identification of intact microorganisms using mass spectrometry. *Nat Biotechnol* 14, 1584-1586 (1996).
9. Croxatto, A., Prod'hom, G. & Greub, G. Applications of MALDI-TOF mass spectrometry in clinical diagnostic microbiology. *FEMS Microbiol Rev* 36, 380-407 (2012).
10. Dixon, P., Davies, P., Hollingworth, W., Stoddart, M. & MacGowan, A. A systematic review of matrix-assisted laser desorption/ionisation time-of-flight mass spectrometry compared to routine microbiological methods for the time taken to identify microbial organisms from positive blood cultures. *Eur J Clin Microbiol* 34, 863-876 (2015).
11. Chen, J.H.*, et al.* Direct bacterial identification in positive blood cultures by use of two commercial matrix-assisted laser desorption ionization–time of flight mass spectrometry systems. *J Clin Microbiol* 51, 1733-1739 (2013).
12. Mermel, L.A. & Maki, D.G. Detection of bacteremia in adults: consequences of culturing an inadequate volume of blood. *Ann Intern Med* 119, 270-272 (1993).
13. Yagupsky, P. & Nolte, F. Quantitative aspects of septicemia. *Clin Microbiol Rev* 3, 269-279 (1990).
14. Madonna, A.J., Basile, F., Furlong, E. & Voorhees, K.J. Detection of bacteria from biological mixtures using immunomagnetic separation combined with matrix‐assisted laser desorption/ionization time‐of‐flight mass spectrometry. *Rapid Commun Mass Spectrom* 15, 1068-1074 (2001).
15. Urban, P.L.*, et al.* High-density micro-arrays for mass spectrometry. *Lab Chip* 10, 3206-3209 (2010).
16. Wan, K.X., Vidavsky, I. & Gross, M.L. Comparing similar spectra: from similarity index to spectral contrast angle. *J Am Soc Mass Spectrom* 13, 85-88 (2002).
17. Javaloyas, M., Garcia-Somoza, D. & Gudiol, F. Epidemiology and prognosis of bacteremia: a 10-y study in a community hospital. *Scand J Infect Dis* 34, 436-441 (2002).
18. Corey, G.R. Staphylococcus aureus bloodstream infections: definitions and treatment. *Clin Infect Dis* 48, S254-S259 (2009).
19. Ryzhov, V. & Fenselau, C. Characterization of the protein subset desorbed by MALDI from whole bacterial cells. *Anal Chem* 73, 746-750 (2001).
20. Sohail, Z. Bruker Daltonics MALDI Theory Mass Spectrometry. *Information brochure* (2004).

21. Santos, A.F., Cayô, R., Schandert, L. & Gales, A.C. Evaluation of MALDI-TOF MS in the microbiology laboratory. *Jornal Brasileiro de Patologia e Medicina Laboratorial* 49, 191-197 (2013).

22. Schubert, S. & Freitag, R. Comparison of ceramic hydroxy-and fluoroapatite versus Protein A/G-based resins in the isolation of a recombinant human antibody from cell culture supernatant. *J Chromatogr A* 1142, 106-113 (2007).

23. Christner, M*., et al.* Rapid identification of bacteria from positive blood culture bottles by use of matrix-assisted laser desorption-ionization time of flight mass spectrometry fingerprinting. *J Clin Microbiol* 48, 1584-1591 (2010).

24. Orsini, J*., et al.* Microbiological profile of organisms causing bloodstream infection in critically ill patients. *J Clin Med Res* 4, 371-377 (2012).

25. Brecher, M.E. & Hay, S.N. Bacterial contamination of blood components. *Clin Microbiol Rev* 18, 195-204 (2005).

26. Walther-Wenke, G. Incidence of bacterial transmission and transfusion reactions by blood components. *Clin Chem Lab Med* 46, 919-925 (2008).

# CHAPTER III. Mass spectrometry detection of antimicrobial resistance marker proteins from intact bacteria

## Abstract

Titanium dioxide nanoparticle-modified target plates were developed to enhance the analysis of intact bacteria by MALDI-TOF mass spectrometry. The plates were designed to improve the ionisation efficiency of intracellular components, thereby promoting the measurable mass range and the achievable detection sensitivity. Accordingly, a method for rapid detection of antimicrobial resistance marker proteins, which confer bacterial resistance against antimicrobial drugs, was established by mass spectrometric fingerprinting of intact bacteria without the need of any sample pre-treatment. With this method, the variations in resistance protein expression levels within bacteria were quickly measured by following up the relative peak intensities. This resistance marker protein detection approach is useful for the fast discrimination of antimicrobial-resistant bacteria from their non-resistant counterparts whilst performing species identification. Also, it could be used as a rapid and convenient way for initial determination of the underlying resistance mechanisms.

## 1. Introduction

Infectious diseases caused by pathogenic bacteria are serious threats to human health. Misuse and overuse of antimicrobial drugs over many years have led to the emergence of antimicrobial resistance among microbes worldwide.[1] For the purpose of fast diagnosis and efficient treatment, it is crucial to perform rapid pathogen identification

and antimicrobial resistance/susceptibility determination. With the ability to generate characteristic mass spectral fingerprints directly from intact bacteria, MALDI-TOF mass spectrometry provides a quick way for bacterial identification, *e.g.* ~ 30 min for 48 samples using Vitek® MS system (bioMérieux, France).[2,3] Meanwhile, antimicrobial resistance detection in hospitals still mainly relies on antimicrobial drug culture approaches like broth (or agar) microdilution method and disk diffusion method, which need several hours or even several days.[4] Therefore, performing a complete clinical diagnosis remains a lengthy process. In addition to the classical culture-based methods, several new strategies have been proposed for antimicrobial resistance detection. Examples include nucleic acid-based resistance genes detection,[5] single-cell morphological analysis,[6] surface-enhanced Raman spectroscopic biomarker detection,[7] atomic force microscope cantilevers-based nano-mechanical sensors,[8] *etc*.

Recently, continuous efforts have been made to explore the potential of MALDI-TOF mass spectrometry for rapid antimicrobial resistance analysis. Related studies were mainly carried out with three approaches. The first one is an indirect evaluation by detection of resistance enzyme activity, such as the degradation of β-lactam antibiotics through hydrolysis (mass increased by 18 Da) by β-lactamases and the alternation of rRNA through methylation (mass increased by 14 Da) by rRNA methyltransferase.[9,10] This is a fast way for resistance mechanisms investigation, but is limited to enzymes-related resistance types. The second approach is isotope labelling-bacteria culture method, with the appearance of peak mass shifts in bacterial fingerprinting patterns if a resistant strain is incubated with a culture medium supplemented with stable (non-radioactive) isotope labelled amino acids and corresponding antibiotics.[11,12] Based on the machinery of protein biosynthesis, this approach is applicable to determine bacterial resistance or susceptibility to wide types of antibiotics, but limited at the need of special isotope labelled culture medium. The third one is also a culture-based method, in which semi-quantitative MALDI-TOF mass spectrometry using an internal standard is employed to investigate bacterial growth status with the presence or absence of antibiotics by measuring the biomass quantity on a mass spectrum.[13,14] This method has been demonstrated feasible for different combinations of antibiotic classes/bacterial species. In addition to the above three approaches, bacterial subtyping assays have also been conducted to study the correlation between antibiotic-susceptible and antibiotic-resistant strains by comparing their fingerprint patterns. For example, it has shown success in the discrimination of major methicillin-resistant *Staphylococcus aureus* lineages[15] and the identification of vancomycin-resistant *Enterococcus spp*.[16]

Proteins encoded by antimicrobial resistance genes are directly involved in bacterial resistance process against antimicrobial drugs.[17] Antimicrobial resistance can thus be analysed by tracing these resistance-associated proteins within bacterial cells. Ideally,

they could be read directly from MALDI-TOF mass spectral fingerprints of intact bacteria, a useful procedure that would be comparable to fast bacterial identification. But many of those proteins are large ones (more than 15,000 Da), and possibly expressed in low abundance. They are difficult to be detected directly from intact cells by classic mass spectrometry measurements, which typically focus on smaller proteins (less than 15,000 Da) expressed in high abundance.[18] Until now, to the best of my knowledge, no studies have reported the success of this procedure, as pointed out in a review by Walkova *et al.*[19] In order to detect those resistance-associated proteins, preparatory extraction/enrichment processes are required prior to their identification by top-down or bottom-up proteomics, which are labour-intensive and time-consuming.[20-22] Very recently, a surrogate marker around 11 kDa was detected from carbapenem-resistant bacteria containing *bla*$_{KPC}$-harbouring plasmids by directly measuring the bacterial protein extracts. But it is a particularly small protein and an additional step of protein extraction was required prior to the mass spectrometry measurement.[23]

Herein, a MALDI-TOF mass spectrometry approach has been developed for the detection of antimicrobial resistance-associated proteins from intact bacterial cells. Photo-reactive titanium dioxide (TiO$_2$)-modified target plates were employed to assist the measurement to provide access to the high mass range with enhanced detection sensitivity. TiO$_2$-modified target plate or more generally metal oxides-modified plates have been used for many different mass spectrometric applications.[24,25] In this work, the rationale of the proposed approach is to take advantage of the photo-reactivity of TiO$_2$ to facilitate the desorption/ionisation of bacterial components. Such experimental improvement makes feasible a fast read out of resistance-associated proteins from intact bacterial cells without any sample pre-treatment (**Scheme 3.1**).
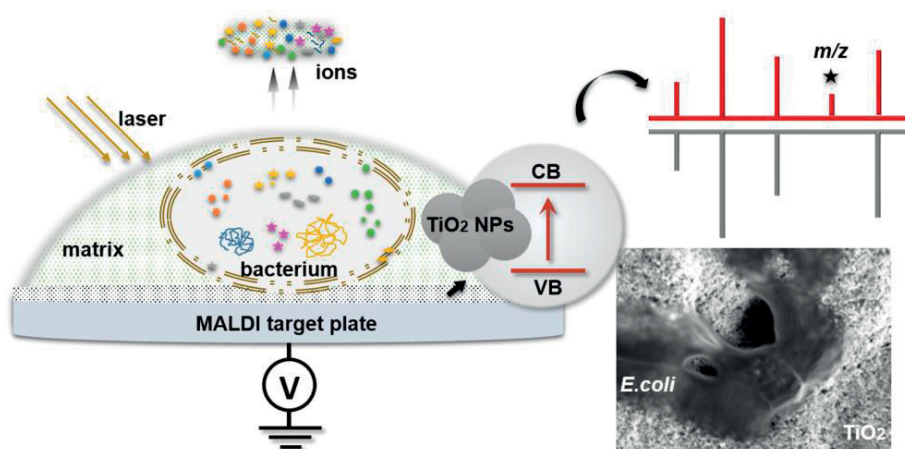


**Scheme 3.1** TiO$_2$-facilitated MALDI-TOF MS detection of intact bacteria.

## 2. Materials and methods

### 2.1 Materials and reagents

$TiO_2$ nanopowder (Aeroxide® P25, 21 nm primary particle size, $\geq$ 99.5% trace metals basis), α-cyano-4-hydroxycinnamic acid (CHCA) (matrix substance for MALDI-MS, $\geq$ 99.0%), 2,5-dihydroxybenzoic acid (DHB) (matrix substance for MALDI-MS, $\geq$ 99.0%), sinapinic acid (SA) (matrix substance for MALDI-MS, $\geq$ 99.0%), *trans*-ferulic acid (FA) (matrix substance for MALDI-MS, $\geq$ 99.0%), ethanol ($\geq$ 99.8%) and formic acid (ACS reagent, $\geq$ 96.0%) were bought from Sigma-Aldrich (St. Gallen, Switzerland). Acetic acid (glacial, 100%, EMSURE® ACS) was bought from Merck Millipore (Darmstadt, Germany). Acetonitrile (HPLC grade) was purchased from Aventor Performance Materials (Center Valley, PA, USA). Trifluoroacetic acid (99.0%, extra pure) was obtained from Acros Organics (New Jersey, USA). Deionized water (18.2 MΩ cm) was purified by an alpha Q Millipore system (Zug, Switzerland), and used in all aqueous solutions. Lysogeny broth microbial growth medium, 2xYT microbial growth medium, ampicillin (anhydrous basis, 96.0-100.5%), kanamycin sulfate salt (USP grade), gentamycin sulfate (USP grade) and chloramphenicol (USP grade) were purchased from Sigma-Aldrich (St. Gallen, Switzerland).

### 2.2 Fabrication of TiO₂-modified MALDI target plates

$TiO_2$ NPs aqueous suspensions were prepared according to a previously reported method.[26] Briefly, 1 g of P25 $TiO_2$ nanopowder was beforehand heated at 300 °C for 2 h and then separated in a mortar for 3 h. During the separation process, 1 mL of 10% acetic acid aqueous solution was added drop by drop to keep the nanopowder wet. The separated nanoparticles were suspended in an aqueous solution of ethanol (89%, volume percentage) to reach a concentration of 100 mg·mL$^{-1}$, followed by ultra-sonication for 1 h. The suspension was then diluted 25 times with deionized water to reach a final concentration of 4 mg·mL$^{-1}$. Such obtained $TiO_2$ NPs suspension was stored at 4 °C and was stable for four to six months.

The $TiO_2$ NPs-modified MALDI target plates were prepared by depositing the $TiO_2$ suspension onto the spots of a classic bare stainless-steel target plate, *i.e.* commercial MSP 96 ground steel target from Bruker Daltonics, Germany. The suspension was deposited by drop casting or by dispenser in the following manner: 2 μL of the suspension was firstly dropped onto each spot and air-dried for $\sim$ 10 min; thereafter, another 2 μL of the suspension was dropped to cover the previous one and again air-dried for $\sim$ 10 min. Alternatively, the $TiO_2$ suspension could also be dropped as an array of spots onto a piece of stainless steel foil (20 μm thick), which was afterwards affixed onto a commercial bare target plate before MALDI-TOF mass spectrometry

measurement. The dried target plate or steel foil was heated at 400 °C to sinter the nanoparticles. The heating process was accomplished with a three-step automatic program: raising temperature from 25 to 400 °C within 1h, keeping the temperature at 400 °C for 1h, cooling down to 25 °C within 4 h. Alternatively, instead of thermal heating at 400 °C, the sintering process could also be completed by photonic curing, which takes only a few milliseconds. The photonic curing was conducted using high intensity light pulses from a xenon flash lamp provided by a PulseForge 1300 photonic curing station (NovaCentrix, USA). The curing parameters were set as: 5 pulses exposure, 450 V bank voltage, 1 ms pulse duration. Through sintering, a stable layer of $TiO_2$ NPs was formed and firmly attached on the steel surface. The sintering process did not change the crystalline phase of $TiO_2$, which was kept as the mixed rutile (110) and anatase (101) (mainly) phase. Before the usage, prepared $TiO_2$-modified target plate or steel foil pieces were stored in a clean and dry room temperature environment.

## 2.3 Bacterial strains

*Escherichia coli* (*E. coli*) strains DH5α, XL1-Blue, BL21 and *Bacillus subtilis* (*B. subtilis*) strain 168 were cultured according to the same procedure explained in CHAPTER II. Non-resistant *Enterobacter cloacae ssp. Cloacae* (*E. cloacae s. C.*), multidrug-resistant *E. cloacae s. C.* (carrying resistance gene *AmpC*), non-resistant *Enterobacter aerogenes* (*E. aerogenes*), multidrug-resistant *E. aerogenes* (carrying resistance gene *AmpC*), *E. coli* ATCC 25922, CTX-M type extended-spectrum β-lactamase-producing *E. coli*, *Pseudomonas aeruginosa* (*P. aeruginosa*) ATCC 27853, multidrug-resistant *P. aeruginosa*, *Staphylococcus aureus* (*S. aureus*) ATCC 29213 and methicillin-resistant *S. aureus*, as well as the detailed information about antimicrobial resistance in each resistant strain, were provided by a local hospital (Hôpital du Valais, Sion, Switzerland). Their detailed antimicrobial susceptibility profiles were measured using a bioMérieux VITEK® 2 automated AST system, based on antimicrobial drug culture method. Bacterial cell concentrations of fresh cultures were determined by measuring the optical density at 600 nm, as explained in CHAPTER II.

## 2.4 Transformation of resistance genes into bacteria

Plasmid DNAs carrying a specific antimicrobial resistance gene were transformed into *E. coli* strains DH5α, XL1-Blue or BL21, according to the protocol provided by Sambrook and Russel.[27] The plasmids utilized were: pBluescriptIISK(+) carrying resistance against ampicillin (Stratagene, California, USA), pEGFP-N1 carrying resistance against kanamycin (Clontech, California, USA), pEN_TmiRc3 carrying resistance against gentamycin (addgene, Massachusetts, USA) and pOFXT7-2 carrying resistance against chloramphenicol (donated as a gift from University of Lausanne,

Lausanne, Switzerland). Specifically, 1.5 mL of each *E. coli* pre-culture was overnight incubated in 50 mL of lysogeny broth at 37 °C with continuous shaking at 200 rpm. The culture was transferred into an ice-cold polypropylene tube and cooled on ice for 10 min. *E. coli* cells were separated from the growth medium by centrifugation at 2700 × *g* for 10 min at 4 °C. After thoroughly removing the growth medium, the cell pellet was suspended in 30 mL of ice-cold MgCl$_2$-CaCl$_2$ solution (80 mM MgCl$_2$, 20 mM CaCl$_2$) by gentle mixing. The cells were again collected by centrifugation at 2,700 × *g* for 10 min at 4 °C, and gently resuspended in 2 mL of ice-cold 0.1 M CaCl$_2$. The resulting competent *E. coli* were either directly used for transformation as described below or dispensed into aliquots and stored at –80 °C.

For the transformation of resistance genes, 200 μL of above obtained competent *E. coli* cells were mixed with 100 ng of purified plasmid DNAs that carried a specific resistance gene. The mixture was incubated on ice for 30 min, and then applied with a heat shock for exactly 90 s in a 42 °C water bath. Thereafter, the mixture was rapidly transferred into an ice bath and chilled for 2 min. After adding 800 μL of lysogeny broth, the mixture was incubated for 45 min in a 37 °C water bath to let the bacteria recover and express the antibiotic resistance marker encoded by the plasmid. The obtained bacteria were spread on selective agar plates containing 20 mM MgSO$_4$ and appropriate antibiotic. Single colonies were picked up and added into 2 mL of lysogeny broth for overnight incubation at 37 °C with continuously shaking at 200 rpm. The resulting ampicillin-resistant, kanamycin-resistant, gentamicin-resistant or chloramphenicol-resistant *E. coli* strains were either directly analysed with MALDI-TOF mass spectrometry or incubated with antibiotics to experimentally control the expression level of these resistance genes.

## 2.5 Experimentally controlling the resistance gene expression level within *E. coli*

In order to experimentally control the resistance gene expression level within bacteria, *E. coli* DH5α cells transformed with resistance genes (including ampicillin-resistance, kanamycin-resistance and chloramphenicol-resistance) were incubated with lysogeny broth containing gradually increased concentration of corresponding antibiotic, *i.e.* ampicillin, kanamycin and chloramphenicol, respectively. The cells will then acquire different levels of resistance under different selective pressure from the antibiotics. To investigate the influence of growth condition to the cellular synthesis of resistance proteins, *E. coli* DH5α cells transformed with ampicillin-resistant gene were incubated with different growth media (lysogeny broth, or 2xYT medium) containing 60 μg·mL$^{-1}$ of ampicillin. All of the above mixtures were incubated overnight at 37 °C with continuously shaking at 200 rpm. The obtained fresh cultures were afterwards analysed with MALDI-TOF mass spectrometry.

## 2.6 Mass spectrometry measurement and data analysis

For each bacterial strain, bacterial cells were harvested from the growth medium by centrifugation at 7,500 $g$ for 3 min, then washed with deionized water for twice. The cell pellet was finally suspended in water to reach the concentration of $\sim 5 \cdot 10^8$ cells·mL$^{-1}$. 1 µL of the bacterial suspension was deposited onto a sample spot of a TiO$_2$-modified target plate or a classic bare target plate for mass spectrometry measurement. Each test was performed in triplicates by depositing the bacteria solution on three spots. Details about the MALDI-TOF mass spectrometry measurements and mass spectrum similarity calculation were illustrated in CHAPTER II. The peak numbers of each mass spectrum were automatically countered by the mMass tool, with "peak picking" parameters set as $S/N$ threshold 3.0, relative intensity threshold 2.0% for 2,000-15,000 $m/z$ and 0.1% for 15,000-80,000 $m/z$, together with the applying of smoothing and shoulder peak removing.

Four different matrices were investigated for the analysis of intact bacteria, $i.e.$ CHCA (10 mg·mL$^{-1}$ prepared in 50/49.9/0.1% acetonitrile/water/trifluoroacetic acid), DHB (10 mg·mL$^{-1}$ prepared in 50/49.9/0.1% acetonitrile/water/trifluoroacetic acid), SA (20 mg·mL$^{-1}$ prepared in 50/49.9/0.1% acetonitrile/water/trifluoroacetic acid) and FA (12.5 mg·mL$^{-1}$ prepared in 17/33/50% formic acid/acetonitrile/ water). All the percentage values here represent volume percentage.

Throughout the present work, all measurements were conducted with intact whole bacteria, except that protein extracts from $E. coli$ DH5α was utilized for the characterization of TiO$_2$-modified target plates. The protein extracts were prepared according to the typical ethanol/formic acid/acetonitrile extraction protocol, which is described in the Bruker MALDI Biotyper® 3.0 user manual (year 2011). Briefly, $E. coli$ DH5α cells were harvested from 1 mL of fresh culture by centrifugation at 7,500 $g$ for 3 min and washed two times with deionized water. The cell pellet was suspended in 300 µL of water, followed by adding 900 µL of ethanol and mixing thoroughly. The mixture of water and ethanol was completely removed by centrifugation at 8,500 $g$ for twice (2 min for each time) and air-drying for $\sim$ 30 min. The obtained cell pellet was resuspended in 50 µL of 70/30% formic acid/water. The mixture was vortexed thoroughly and let stand for 5 min, followed by adding 50 µL of acetonitrile. The final mixture was vortexed thoroughly for another 5 min. Thus, intracellular proteins were extracted into the solvent. After centrifugation at 8,500 $g$ for 2 min, the supernatant containing the extracted proteins was harvested. The product was pipetted onto a TiO$_2$-modified target plate and a bare target plate (1 µL for each spot) for mass spectrometry measurement. Sinapinic acid, 20 mg·mL$^{-1}$ dissolved in 50/49.9/0.1% acetonitrile/water/trifluoroacetic acid, was used as the matrix.

# 3. Results and discussion

### 3.1 TiO₂ facilitating MALDI-TOF MS fingerprinting of intact bacteria

One important factor affecting MALDI-TOF MS measurements is the choice of matrix. Here, four different matrices, *i.e.* CHCA, DHB, SA, FA, were compared for the fingerprinting of intact *E. coli* (strain DH5α) cells. As shown in **Figure 3.1**, CHCA, DHB and SA exhibited high detection sensitivity in 2,000-15,000 *m/z*, which is the typical mass range for bacterial identification. They also provided satisfying reproducibility, with pattern similarity scores higher than 0.99 for three replicates. By using CHCA and DHB, the detected proteins were smaller than ~ 15,000 Da. By using SA, proteins between 2-30 kDa were detected. Meanwhile, FA matrix gave more peaks in the mass range of 15,000-80,000 *m/z*, but the sensitivity in 2,000-15,000 *m/z* was drastically decreased together with the loss of reproducibility. The spectral similarity scores were lower than 0.5 for three replicates. Overall, SA was used as the matrix throughout this work.
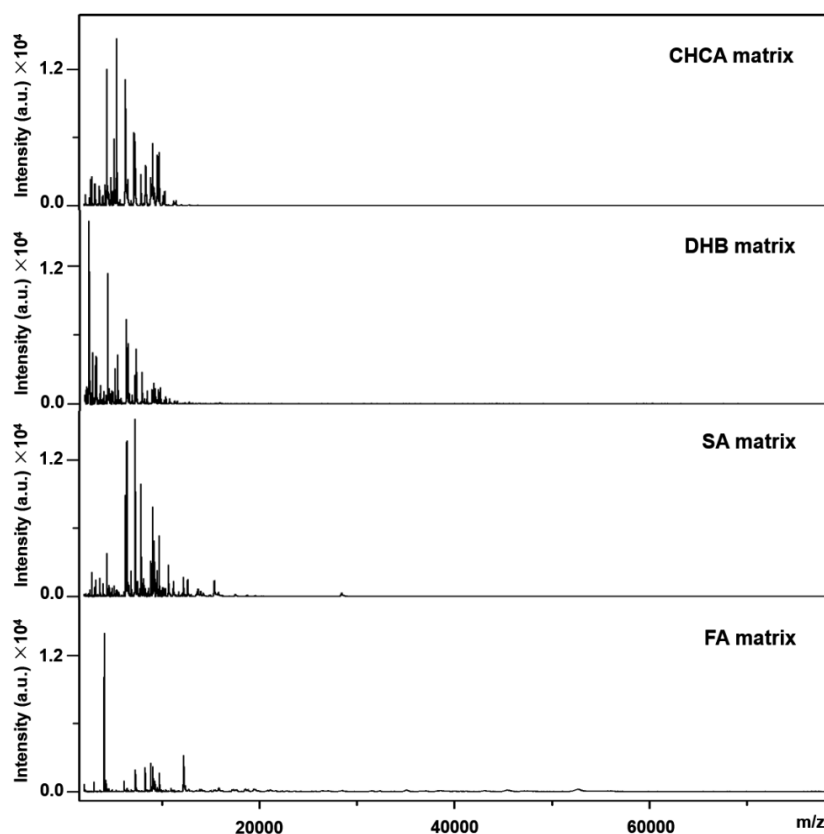


**Figure 3.1** Comparison of different matrices for intact bacteria MALDI-TOF MS fingerprinting. A classic bare stainless steel MALDI target plate was employed. Each spectrum was generated from ~ $5 \cdot 10^5$ bacterial cells.
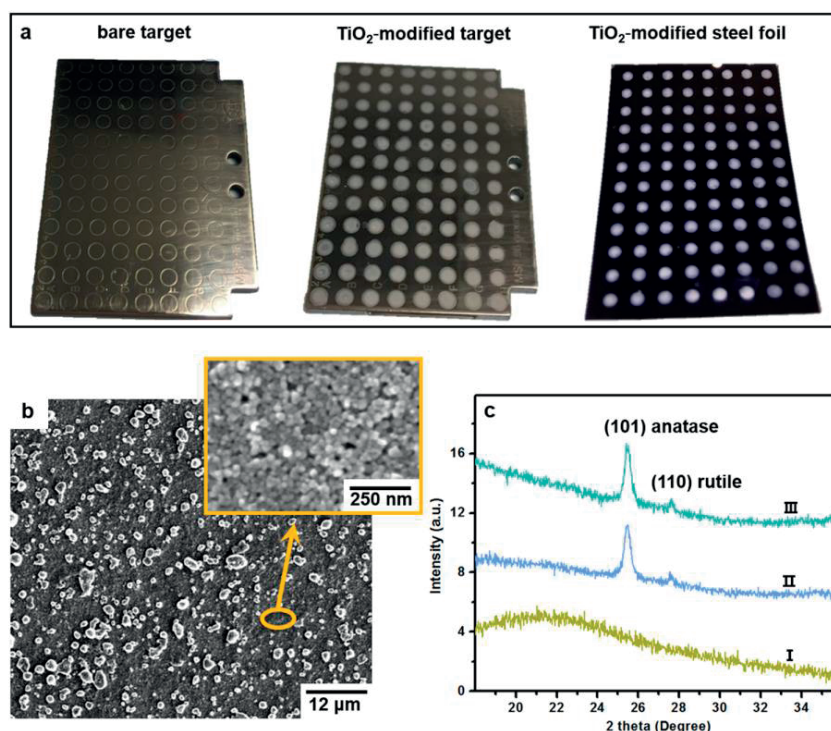
**Figure 3.2** (**a**) Photos of a classic bare stainless steel target (MSP 96 ground steel MALDI target, Bruker Daltonics), a TiO$_2$ NPs-modified target and a piece of TiO$_2$ NPs-modified stainless steel foil, which was affixed onto the bare target for mass spectrometry measurements; (**b**) scanning electron microscope image of the TiO$_2$ layer after sintering at 400°C; (**c**) X-ray powder diffraction patterns of (**I**) the steel substrate, (**II**) TiO$_2$ on steel surface before sintering at 400 °C and (**III**) TiO$_2$ on steel surface after sintering at 400 °C.

Based on the laboratory's experience in designing photo-reactive TiO$_2$-modified target plates for inducing in-source photochemical reactions, we have developed here a plate able to improve intact bacteria fingerprinting in a broad mass range, as demonstrated below.[28,29] This target plate was prepared by depositing an aqueous suspension of TiO$_2$ nanoparticles on the spots (3 mm diameter) of a classic bare stainless steel target plate, or by dropping TiO$_2$ suspension as an array of spots on a stainless steel foil (20 μm thick), which was afterwards affixed onto a bare target plate by an adhesive tape (**Figure 3.2 a**). The TiO$_2$ were subsequently thermally or photonically sintered. The sintered particles exhibited high adherence to the steel substrate and provided a stable support layer (~ 3 μm thick) for bacteria and matrix, with small particles (20-25 nm size) densely covering the bottom and large particles (0.5-3 μm size) observed on the top (**Figure 3.2 b**). The TiO$_2$ used is a commercial P25 nanopowder, a mixture of anatase (80%) and rutile (20%)

crystalline phases. The anatase is more photo-reactive than the rutile, but the latter is more thermodynamically stable. The crystalline phases of $TiO_2$ were not changed after sintering, with the corresponding X-ray powder diffraction patterns shown in **Figure 3.2 c**. Compared to the bare steel target, the $TiO_2$ nanoparticles provided a rough and mesoporous surface (**Figure 3.3 a, b**), with larger surface area and lower water contact angle (decreased from 70° to 38°, **Figure 3.3 c, d**). As the surface with $TiO_2$ is more hydrophilic than the steel substrate, this kind of $TiO_2$-modified target is a type of "AnchorChip" target. Upon the deposition, bacterial cells (mostly of 0.2-2 μm size) entered into the porous $TiO_2$ surface structure. Due to the high affinity between the bacterial membrane and $TiO_2$, the cells tended to be absorbed on the surface of $TiO_2$.[30] Matrix drop casting consequently led to the formation of fine and well dispersed bacteria/matrix co-crystals, highly favourable for an efficient desorption/ionisation process (**Figure 3.3 e**, **f**). MALDI-TOF MS detection of both the protein extracts of *E. coli* cells and the intact *E. coli* cells yielded much higher quality fingerprints by using a $TiO_2$-modified target plate in comparison to a bare target plate (**Figure 3.4**). Such an improvement, especially in the mass range higher than 15,000 *m/z*, could not be solely caused by the finer co-crystals of bacteria/matrix resulting from the mesoporous surface. It could also be explained by the well-known photo-reactivity of $TiO_2$ nanoparticles.[30,31]
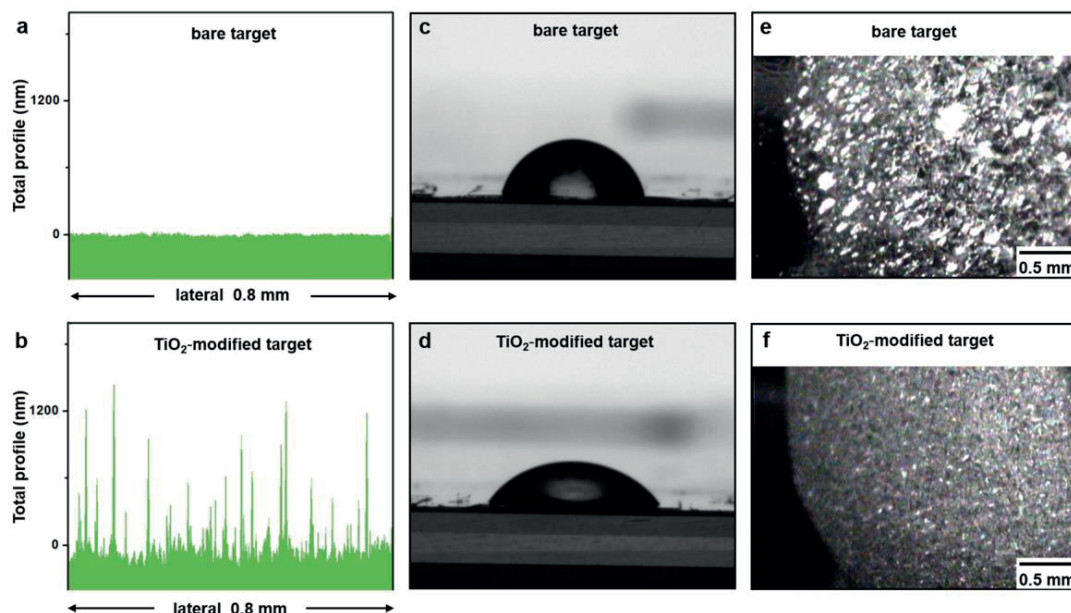


**Figure 3.3** Surface roughness profile of (**a**) a bare target and (**b**) a $TiO_2$-modified target. Contact angle of water on the surface of (**c**) a bare target (value 70°) and (**d**) a $TiO_2$-modified target (value 38°). Microscopy image of *E. coli*/sinapinic acid co-crystals on (**e**) a bare target and (**f**) a $TiO_2$-modified target.
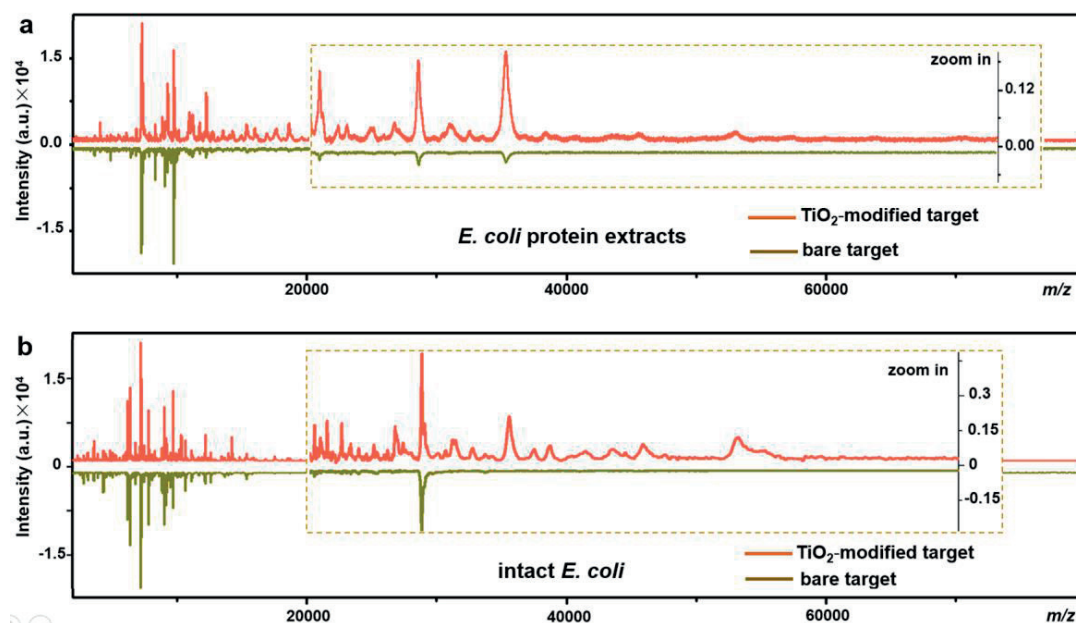
**Figure 3.4** Comparison of MALDI-TOF mass spectrometry detection of (**a**) protein extracts from *E. coli* (strain DH5α) or (**b**) intact *E. coli* cells (strain DH5α) in the mass range of 2,000-80,000 *m/z* by using a bare target and a TiO$_2$-modified target.

The morphological changes of *E. coli* cells were visualized by scanning electron microscopy (**Figure 3.5**). Intact *E. coli* cells showed a straight, rod-like shape when they were deposited on a bare and a TiO$_2$-modified target without matrix covering and without MALDI laser irradiation (**Figure 3.5 a**, **b**). The *E. coli* were then covered with matrix and underwent the running of a typical mass spectrometry measurement (500 nitrogen laser shots on each sample spot, 20 Hz laser frequency). On the bare target, most *E.coli* cells generally maintained their rod-like shape (**Figure 3.5 c**). Diameter of the laser beam employed by the mass spectrometer is about 100 µm, 30-fold smaller than the sample spot size (3 mm diameter). Thus, a typical mass spectrometry measurement is accomplished with many "blind shots", and only the cells exactly shot by the laser could be lysed. However, the situation was different with the presence of TiO$_2$. Many cells were seriously damaged with apparent deformation and membrane rupture, and the "melted" cells were embedded into the mesoporous surface (**Figure 3.5 d**). Interestingly, it was found that the crystal shape of matrix on TiO$_2$ surface was quite different from that on bare steel surface (**Figure 3.5 c**, **d**), consistent with the previous observation shown in **Figure 3.3 e, f**. TiO$_2$ has a unique electronic structure, which is characterized by a filled valence band and an empty conduction band. With the band gap of 3.0-3.2 eV (3.0 eV for rutile phase and 3.2 eV for anatase phase), it has a strong absorption in the UV range (wave length shorter than
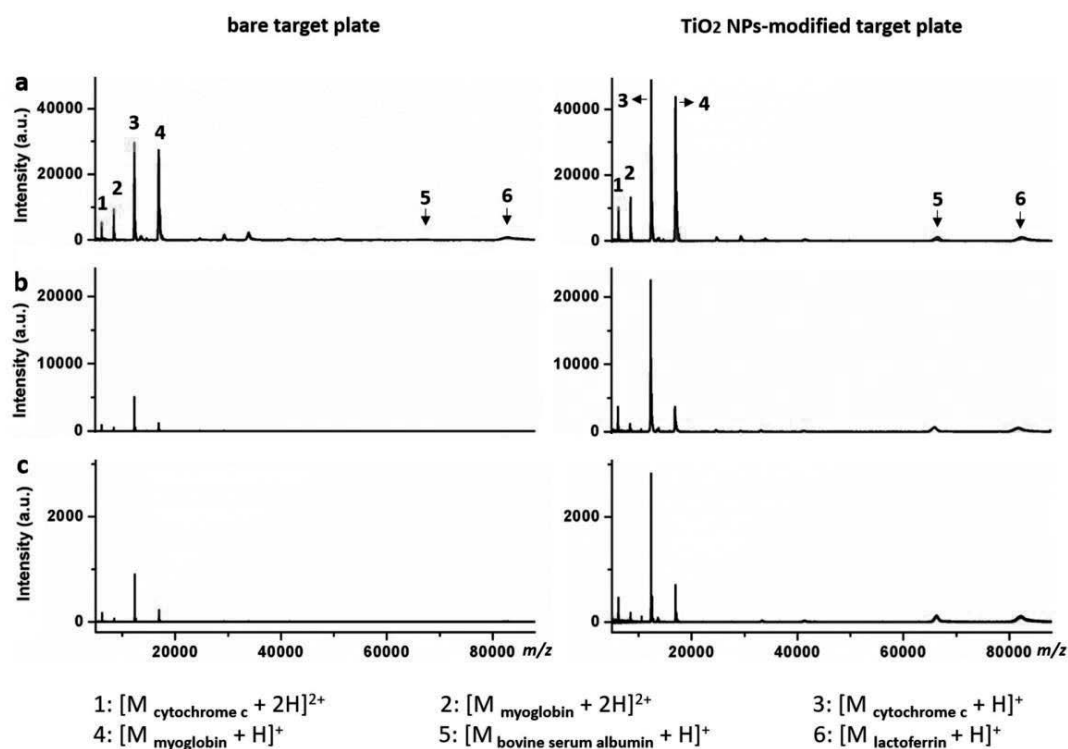
400 nm).[32] MALDI techniques typically use UV lasers such as nitrogen lasers (337.1 nm) and frequency-tripled and quadrupled Nd:YAG lasers (355 nm and 266 nm, respectively). Thus, $TiO_2$ nanoparticles on the surface of MALDI target can absorb energy from the laser source during mass spectrometry measurements. The energy absorption could lead to the generation of electron-hole pairs, and trigger electron-transfer and radical reactions.[31] The generated reactive oxygen species like positive hole $h^+$, hydroxyl radical $^{\bullet}OH$ and peroxide $H_2O_2$ on the $TiO_2$ surface might cause oxidative disruption of the bacterial envelope, as previously reported.[33,34] The disruption of more bacterial cells can promote the ionisation of cellular components.
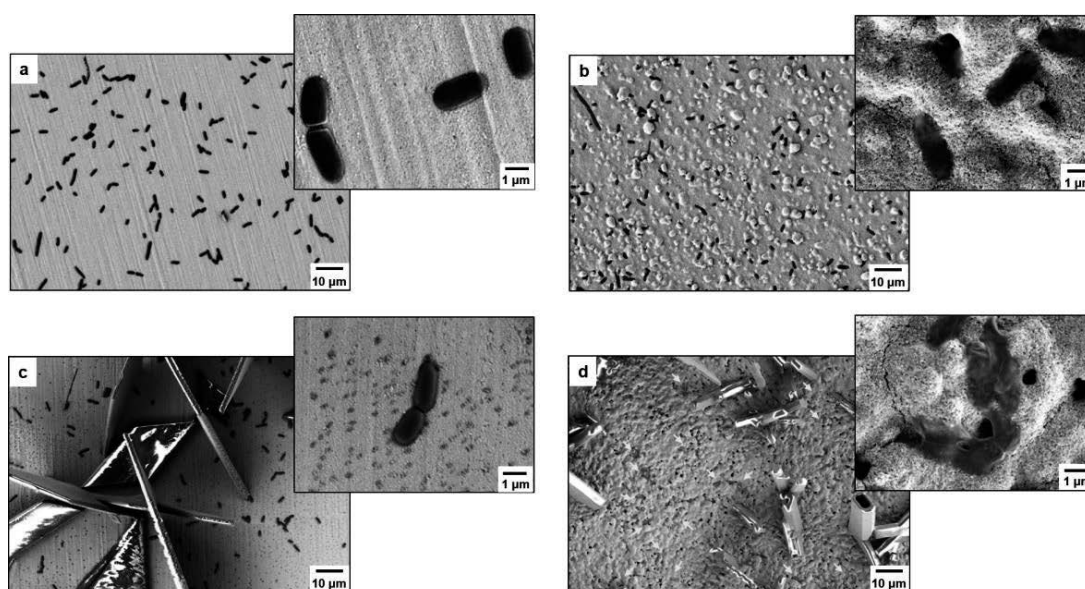


**Figure 3.5** Scanning electron microscope images of *E. coli* under following conditions: (**a**) deposited on a bare target with no matrix covering and no MALDI laser irradiation, (**b**) deposited on a spot of $TiO_2$-modified target with no matrix covering and no MALDI laser irradiation, (**c**) deposited on a bare target after matrix covering and MALDI-TOF MS measurement, (**d**) deposited on a $TiO_2$ target plate after matrix covering and MALDI-TOF MS measurement, with the yellow arrows pointed to some of the *E.coli* cells.
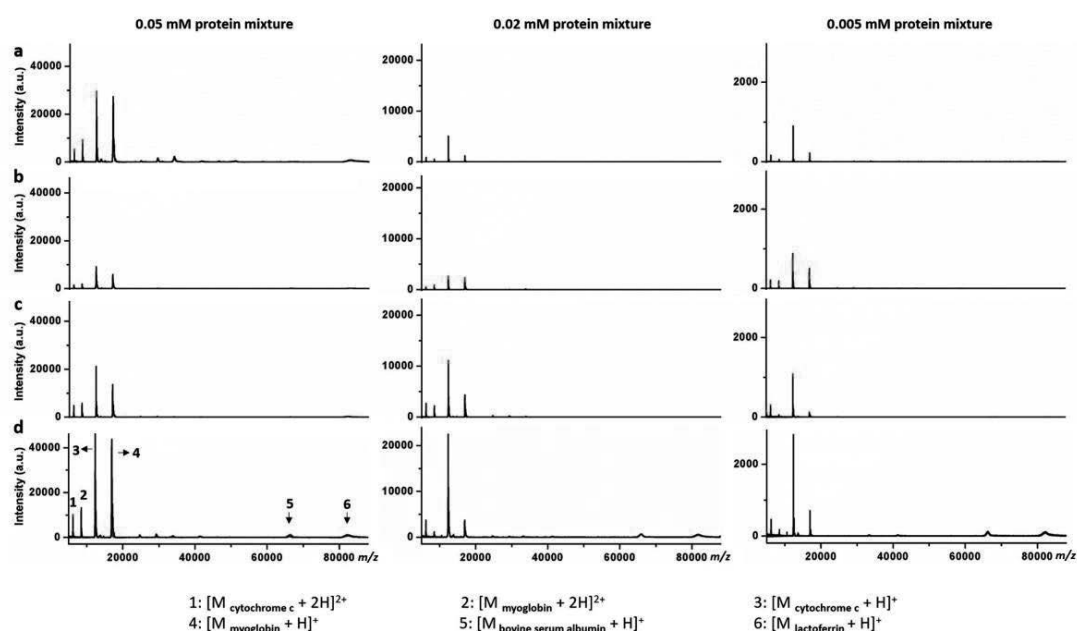
Additionally, the high photo-reactivity of $TiO_2$ favours the transfer of energy from the laser source to the matrix/analyte mixture, which facilitates desorption/ionisation of the analyte and thus increases the detection sensitivity. [35] To further characterize this phenomenon, the $TiO_2$-modified target was used for the detection of a protein mixture containing cytochrome c (~ 12 kDa), myoglobin (~ 17 kDa), bovine serum albumin (BSA,

~ 66 kDa) and lactoferrin (~ 82 kDa) (**Figure 3.6)**. The mixture was comprised of the same molar concentration of the four proteins. The detection was conducted for three such kind of samples, in which the concentration of each protein was gradually decreased, *i.e.* decreased from 0.05 mM (**Figure 3.6 a**) to 0.02 mM (**Figure 3.6 b**) and further to 0.005 mM (**Figure 3.6 c**). Compared to a bare target, the use of TiO$_2$-modified target increased the peak intensity of each protein at all the three concentrations. When the protein concentration was decreased to 0.005 mM (**Figure 3.6 c**), the bare target allowed the .detection of only cytochrome c and myoglobin, while all the four proteins were still detectable with the presence of TiO$_2$. The results showed that TiO$_2$ indeed improved the detection sensitivity, especially for the two hardly-ionized large proteins BSA and lactoferrin.



1: $[M_{cytochrome\ c} + 2H]^{2+}$    2: $[M_{myoglobin} + 2H]^{2+}$    3: $[M_{cytochrome\ c} + H]^{+}$
4: $[M_{myoglobin} + H]^{+}$    5: $[M_{bovine\ serum\ albumin} + H]^{+}$    6: $[M_{lactoferrin} + H]^{+}$

**Figure 3.6** MALDI-TOF MS detection of protein mixture samples using a bare and a TiO$_2$-modified target. The samples contained four proteins, *i.e.* cytochrome c, myoglobin, bovine serum albumin and lactoferrin. The concentration of each protein was (**a**) 0.05 mM, (**b**) 0.02 mM and (**c**) 0.005 mM. All of the measurements were conducted with the exactly same instrumental parameters. Each sample spot contained 1 µL of protein mixture and 1 µL of matrix. Each sample was measured three time, and the generated three mass spectra were overlaid on each panel (in red, blue and black, respectively).

As a comparison, we also have investigated the performance of non-photo-reactive nanomaterials like $SiO_2$ nanoparticles (200 nm in particle size) and $Al_2O_3$ nanoparticles (smaller than 50 nm in particle size). Target plate modified with these two nanoparticles were used for the detection of the above three protein mixture samples as well as intact *E. coli* cells, and the generated mass spectra were compared with those from bare target and $TiO_2$-modified target, as shown in **Figure 3.7** and **Figure 3.8**, respectively. The comparison results showed that $SiO_2$ (**Figure 3.7 b**, **Figure 3.8 b**) and $Al_2O_3$ (**Figure 3.7 c**, **Figure 3.8 c**) are inferior to $TiO_2$ (**Figure 3.7 d**, **Figure 3.8 d**) for MALDI process improving, demonstrating the importance of the $TiO_2$ photo-reactivity.



1: $[M_{cytochrome\ c} + 2H]^{2+}$
4: $[M_{myoglobin} + H]^+$

2: $[M_{myoglobin} + 2H]^{2+}$
5: $[M_{bovine\ serum\ albumin} + H]^+$

3: $[M_{cytochrome\ c} + H]^+$
6: $[M_{lactoferrin} + H]^+$

**Figure 3.7** MALDI-TOF MS detection of three protein mixture samples using a target plate modified with different nanomaterials, *i.e.* (**a**) bare target plate, (**b**) target plate modified with $SiO_2$ nanoparticles (mesoporous structure, 200 nm particle size, Sigma-Aldrich), (**c**) target plate modified with $Al_2O_3$ nanoparticles ($\leq$ 50 nm primary particle size, Sigma-Aldrich) and (**d**) target plate modified with $TiO_2$ nanoparticles. The $SiO_2$ and $Al_2O_3$-modified target plates were prepared in the same way as $TiO_2$-modified ones. The samples contained four different proteins, *i.e.* cytochrome c (~ 12 kDa), myoglobin (~ 17 kDa), bovine serum albumin (BSA, ~ 66 kDa) and lactoferrin (~ 82 kDa). In each sample, the concentration of each protein was decreased from 0.05 mM to 0.02 mM and further to 0.005 mM. Each sample spot contained 1 μL of protein mixture and 1 μL of matrix. Each test was repeated three times, and the generated three mass spectra were overlaid on each panel (in red, blue and black colour, respectively).
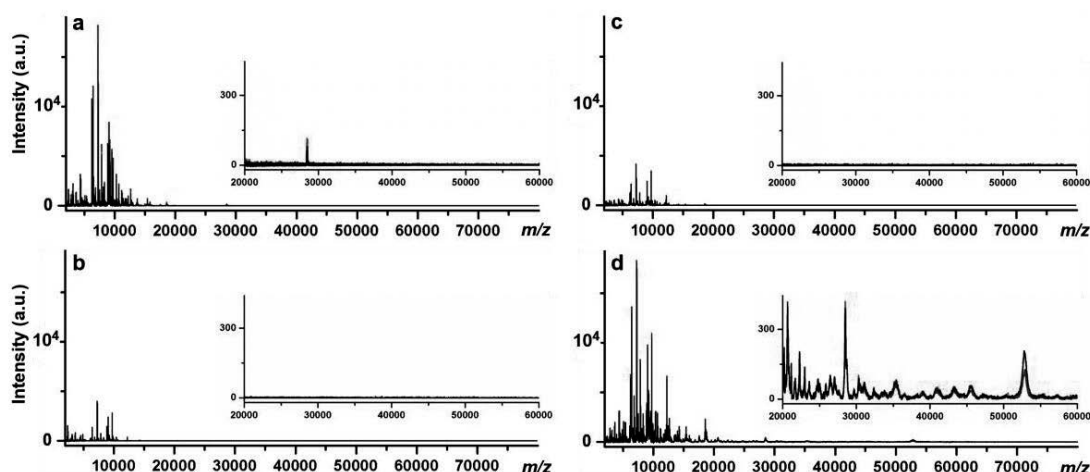
**Figure 3.8** MALDI-TOF MS detection of intact *E. coli* cells (strain DH5α) using target plate modified with different nanomaterials, *i.e.* (**a**) bare target plate, (**b**) target plate modified with $SiO_2$ nanoparticles, (**c**) target plate modified with $Al_2O_3$ nanoparticles and (**d**) target plate modified with $TiO_2$ nanoparticles. Each spectrum was generated from ~ $5 \cdot 10^5$ *E. coli* cells. Each test was repeated three times, and the generated three mass spectra were overlaid on each panel (in red, blue and black color, respectively).

The $TiO_2$-modified target was further tested with more bacterial species. In addition to *E. coli*, two more species, *i.e. P. aeruginosa* (strain ATCC 27853) and *B. subtilis* (strain 168), were chosen as model analytes. All bacteria were measured in their intact whole state without any preparatory protein extraction. Corresponding fingerprint patterns generated with a bare target and a $TiO_2$-modified target with exactly the same measurement parameters are compared in **Figure 3.9 a-c**. To facilitate data interpretation, the patterns were compared in three separate sections, *i.e.*, 2,000-15,000 *m/z* (**Figure 3.9 a/b/c-I**), 15,000-29,000 *m/z* (**Figure 3.9 a/b/c-II**) and 29,000-80,000 *m/z* (**Figure 3.9 a/b/c-III**). Substantial improvements of spectrum quality, especially visible in the high mass range ($\geq$ 15,000 *m/z*), was observed for all the three bacterial samples when a $TiO_2$-modified target was utilized. The total mass spectral peak numbers ($S/N \geq 3$) were increased by 50-70%, *i.e.* from $103 \pm 1$ to $174 \pm 1$ for *E. coli*, $87 \pm 1$ to $139 \pm 2$ for *P. aeruginosa* and $52 \pm 1$ to $88 \pm 1$ for *B. subtilis*, respectively (**Figure 3.9 a/b/c-IV**). The newly detected peaks, completely absent in case of a bare target, are mostly low intensity ones, corresponding to low-abundant or hardly-ionized bacterial components. Notably, each test was repeated three times. In each replicate, a fresh bacterial culture was measured, and the generated mass spectra demonstrated high reproducibility (see examples in **Figure 3.10**).
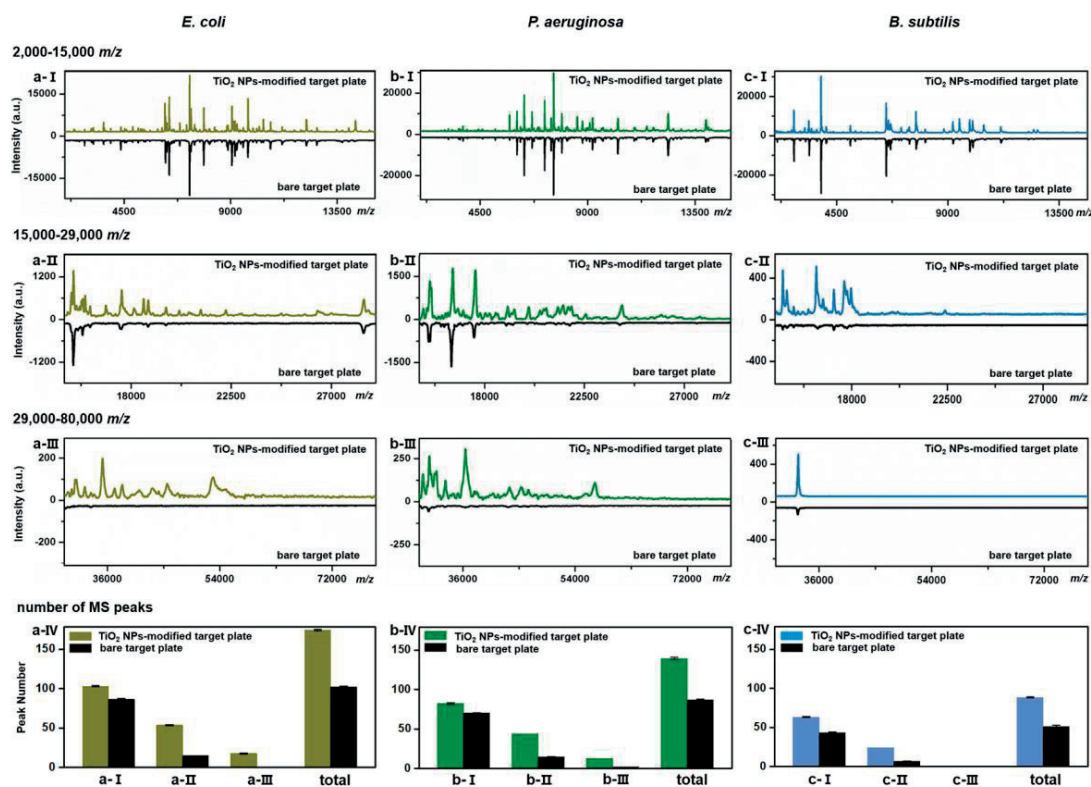
**Figure 3.9** Comparison of a bare and a TiO₂-modified target for MALDI-TOF MS fingerprinting of intact bacteria. The mass spectra were generated from (**a**) *E. coli*, (**b**) *P. aeruginosa* and (**c**) *B. subtilis* in the mass range of (**a/b/c-I**) 2,000-15,000 *m/z*, (**a/b/c-II**) 15,000-29,000 *m/z* and (**a/b/c-III**) 29,000-80,000 *m/z*, with peak numbers counted in **a/b/c-IV**. Each spectrum was generated from $\sim 5 \cdot 10^5$ bacterial cells.
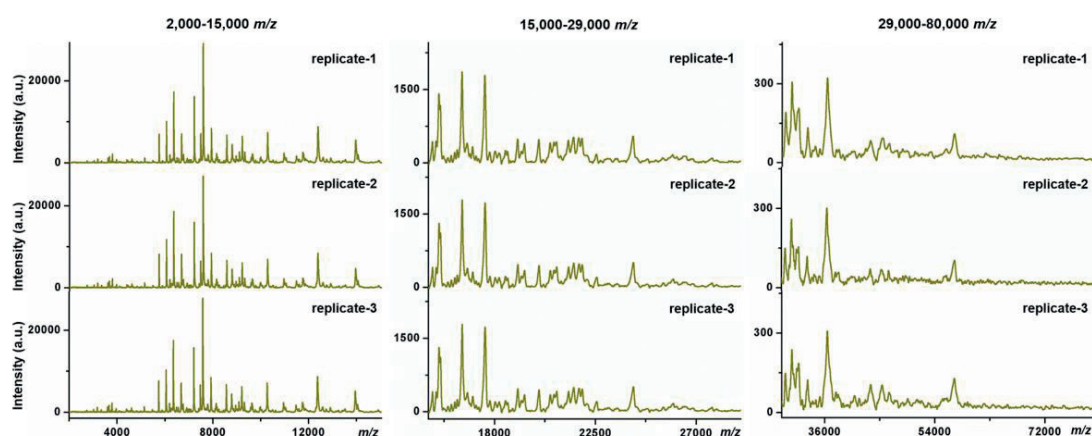


**Figure 3.10** Mass spectra of *P. aeruginosa* ($\sim 5 \cdot 10^5$ cells) from three independent measurements, in the mass range of 2,000-15,000, 15,000-29,000 and 29,000-80,000 *m/z*.

Overall, MALDI-TOF MS analysis of bacteria was promoted by TiO$_2$, with significant improvement in both peak numbers and peak intensities of bacterial fingerprints within a broad mass range. The TiO$_2$-modified target could greatly boost the reliability of bacterial identification. More importantly, it facilitates the extraction of more bacterial cellular information, and enables the detection of large molecular weight and low abundant bacterial components, especially those related with antimicrobial drug resistance, as shown further.

**3.2 Detection of antimicrobial resistance marker proteins from intact bacteria**

The TiO$_2$-modified target plate was used to detect antimicrobial resistance marker proteins from intact bacteria. The detection was firstly conducted with bacteria that were transfected with antimicrobial resistance genes. Corresponding plasmid DNAs, carrying specific resistance genes, were artificially transformed into recipient bacteria using recombinant techniques.[36] Following this strategy, defined non-resistant (antibiotic-susceptible) *E. coli* strains were equipped with desired antimicrobial resistance, *i.e.* resistance against ampicillin, kanamycin, gentamicin and chloramphenicol, respectively. MALDI-TOF MS fingerprint patterns of the resistant strains were measured within the mass range of 2,000-80,000 *m/z* and compared with those of non-resistant strains. To ensure result reliability, each type of resistance was repeatedly developed in two *E. coli* strains, *i.e.*, two of DH5α, XL1-Blue or BL21. The mass spectrometry measurements results showed that resistance-associated proteins were successfully detected from all of those resistant strains (**Figure 3.11**), as explained in further detail below.

Gene *bla*TEM-1, encoding a TEM-1 β-lactamase, conferred the resistance against β-lactam antibiotics including ampicillin. With molecular weight around 29 kDa, TEM-1 β-lactamase inactivates ampicillin by hydrolysis of the β-lactam ring in the ampicillin molecule.[37] Compared to ampicillin-susceptible *E. coli*, the ampicillin-resistant ones exhibited almost the same fingerprints except of an additional peak at 28,972 *m/z* (averaged value, allowing 1000 ppm tolerance) for both strain DH5α and strain XL1-Blue (**Figure 3.11 a**). This result coincides with a previous study, in which a special preparatory protein extraction was conducted before mass spectrometry measurement.[37] The resistance against kanamycin resulted from the expression of neomycin-kanamycin phosphotransferase type II (29,048 Da, UniProtKB-P00552), which inactivates kanamycin by phosphoryl transfer at its 3'-hydroxyl group.[38] Using TiO$_2$-modified target plates, this phosphotransferase was successfully detected from two kanamycin-resistant *E. coli* strains (at 29,046 *m/z* for strain DH5α, 29,047 *m/z* for strain BL21), but not from their non-resistant counterparts (**Figure 3.11 b**). The resistance against gentamicin was conferred by gene *aacC1*, encoding gentamicin acetyltransferase

I (19,442 Da, UniProtKB-P23181), which inactivates gentamicin by acetylating its 3-amino deoxystreptamine moiety.[39] This protein was detected exclusively from the gentamicin-resistant *E. coli* at 19,442 *m/z* for both strain DH5α and XL1-Blue (**Figure 3.11 c**). The resistance against chloramphenicol was caused by the synthesis of chloramphenicol acetyltransferase (CAT, 24-26 kDa), which catalyses the transfer of acetyl moiety from bacterial coenzyme A to chloramphenicol molecules, and, therefore, results in the antibiotic inactivation.[40] Here, in contrast with non-resistant *E. coli*, a peak around 24,820 *m/z* was clearly detected from the chloramphenicol-resistant *E. coli* for both strain DH5α and strain XL1-Blue, confirming the expression of protein CAT (**Figure 3.11 d**). For all of the above measurements, each resistance marker protein was measured with high-reproducibility for both tested *E. coli* strains, indicating the reliability of the detection.
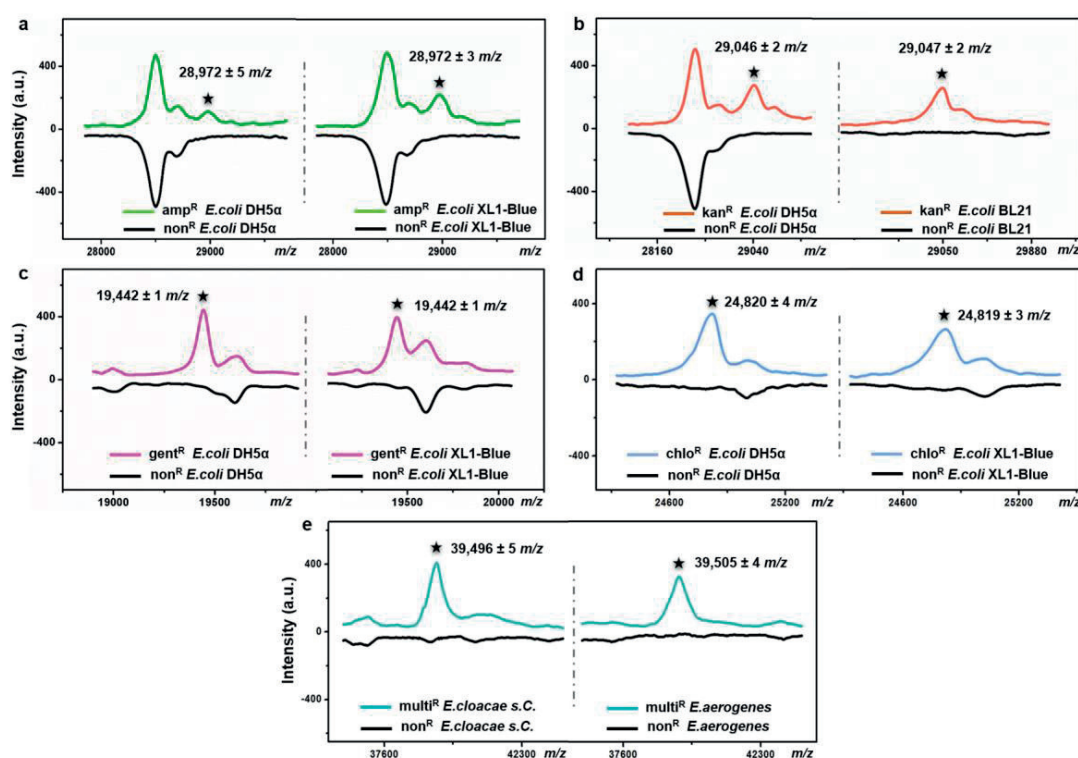


**Figure 3.11** MALDI-TOF MS detection of antimicrobial resistance-associated proteins from (**a**) ampicillin-resistant (amp[R]), (**b**) kanamycin-resistant (kan[R]), (**c**) gentamicin-resistant (gent[R]), (**d**) chloramphenicol-resistant (chlo[R]) *E. coli* strains (two strains in each case), as well as (**e**) *ampC* gene-encoded multidrug-resistant (multi[R]) *E. cloacae s. C.* and *E. aerogenes*. The measurements were conducted with TiO$_2$-modified target plates. Each spectrum was generated from ~ $5 \cdot 10^5$ intact bacterial cells.

To investigate the expression of the same resistance gene in different bacterial species, *E. cloacae s. C.* and *E. aerogenes* were artificially transformed with an *ampC* gene encoding AmpC type β-lactamase (~ 39.5 kDa), and were measured with MALDI-TOF MS by using TiO$_2$-modified target.[41,42] After the gene transfer, both *E. cloacae s. C.* and *E. aerogenes* acquired resistance against 10 different β-lactam antibiotics, becoming multidrug resistant. Their detailed antimicrobial susceptibility profiles (measured with bioMérieux VITEK™ 2 automated AST system) before and after the gene transfer are shown in **Appendix II Table 1-4**, respectively. For the multidrug-resistant *E. cloacae s. C.* and *E. aerogenes*, the minimum inhibitory concentrations (MIC) of the 10 antibiotics varied from 16 to 128 μg·mL$^{-1}$. Compared to their non-resistant counterparts, the two resistant strains both exhibited an additional peak around 39,500 *m/z* (**Figure 3.11 e**), confirming the expression of AmpC type β-lactamase. To be mentioned, none of the above resistance-associated proteins were detectable when a bare target plate was used (**Figure 3.12**), showing the superiority of TiO$_2$-modified target plate.
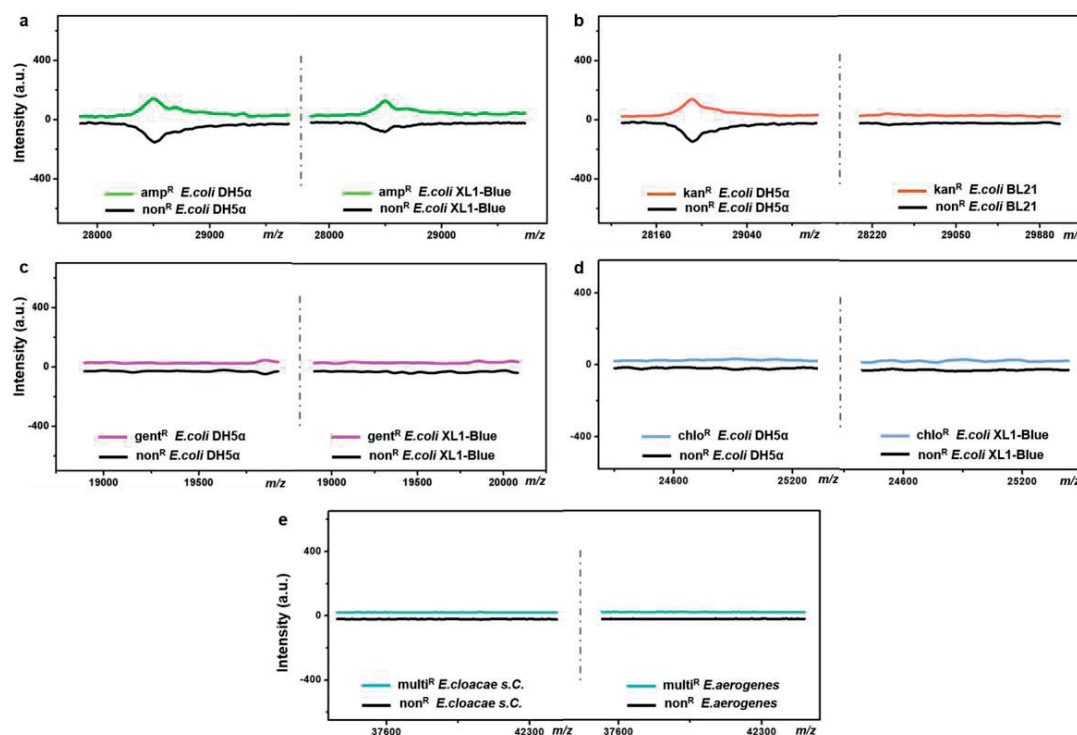


**Figure 3.12** Bare target plate was used to detect antimicrobial resistance-associated proteins from (**a**) ampicillin-resistant (amp$^R$), (**b**) kanamycin-resistant (kan$^R$), (**c**) gentamicin-resistant (gent$^R$), (**d**) chloramphenicol-resistant (chlo$^R$) *E. coli* strains and (**e**) multidrug-resistant (multi$^R$) *E. cloacae s. C.* and *E. aerogenes*. Each spectrum was generated from ~ 5·10$^5$ intact bacterial cells.
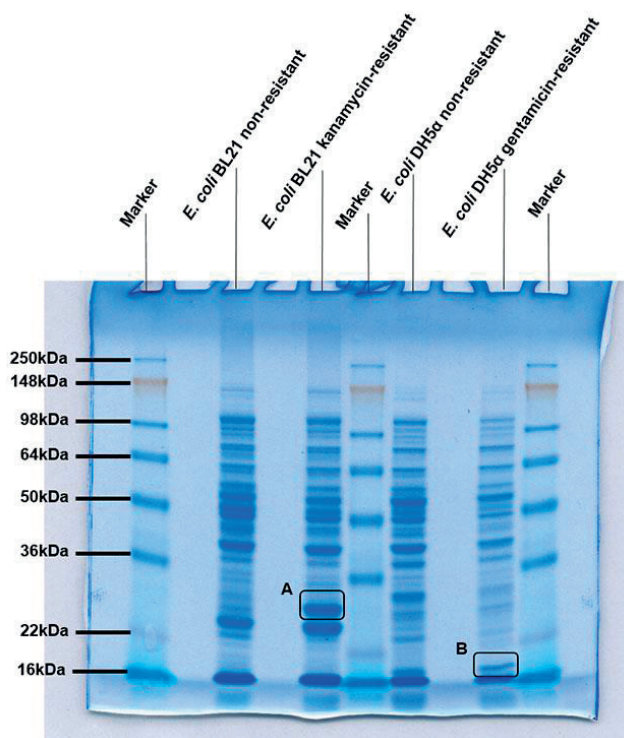
**Figure 3.13** Coomassie blue stained sodium dodecyl sulfate polyacrylamide gel electrophoresis gel of kanamycin-resistant *E. coli* BL21, non-resistant *E. coli* BL21, gentamicin-resistant *E. coli* DH5α and non-resistant *E. coli* DH5α. The bands around 29 kDa (A) and around 19 kDa (B) were clearly observed on the kanamycin-resistant *E. coli* BL21 lane and the gentamicin-resistant *E. coli* DH5α lane, respectively.

To further confirm the identity of the detected resistance-associated proteins, those antibiotic-resistant or non-resistant strains were analysed with a widely used bottom-up proteomic approach. Bacterial cells were lysed in sodium dodecyl sulphate loading buffer, and the extracted proteins were separated by sodium dodecyl sulphate-polyacrylamide gel electrophoresis (SDS-PAGE) and subsequently identified by liquid chromatography-tandem mass spectrometry (LC-MS/MS). Take gentamicin-resistant *E. coli* DH5α and kanamycin-resistant *E. coli* BL21 as examples, a protein band around 19 kDa or 29 kDa was clearly observed on their corresponding SDS-PAGE gel running lane, but not observed from their non-resistant counterparts (**Figure 3.13**). Excision of the ~ 19 kDa band from both gentamicin-resistant and non-resistant *E. coli* DH5α (as control) lanes, followed by digestion in trypsin, revealed the presence of 60 gentamicin acetyltransferase I exclusive unique peptides in the gentamicin-resistant strain, with 100% protein identification probability and 93% (164/177) amino acids coverage (**Appendix I, Note 1**). The ~ 29 kDa bands from

kanamycin-resistant and non-resistant *E. coli* BL21 (as control) lanes were analysed in the same way, revealing the presence of 72 neomycin-kanamycin phosphotransferase type II exclusive unique peptides in the kanamycin-resistant strain, with 100% protein identification probability and 93% (246/264) amino acids coverage (**Appendix I, Note 2**). The above results coincides with the MALDI-TOF MS results presented in **Figure 3.11**, confirming the expression of antibiotic resistance proteins in the gene-transferred bacterial strains.

The described TiO$_2$-facilitated MALDI-TOF MS approach can also measure the variations in the expression level of resistance genes in bacterial cells in a quick manner. As a demonstration, resistance gene-transferred bacterial cells were incubated with lysogeny broth that contained different concentrations of corresponding antibiotics. A gradual increase of a given antibiotic concentration brings a proportionally higher selection pressure to the bacterial cells. As a response, bacterial cells modulate the resistance gene expression level to increase the synthesis of the resistance proteins for survival.[43] Such kind of change was measured for ampicillin-, kanamycin- and chloramphenicol-resistant *E. coli* DH5α, by comparing the relative peak intensities (r.t.) of corresponding resistance proteins in the MALDI-TOF MS fingerprints (**Figure 3.14 a-c**). The relative intensity of resistance proteins (*i.e.* TEM-1 β-lactamase at 28,972 m/z, neomycin-kanamycin phosphotransferase type II at 29,046 m/z and CAT at 24,820 m/z) were calculated by using *E. coli* DH5α D-ribose-binding periplasmic protein (RbsB, ~ 28.5 kDa) as the internal standard (r.t.RbsB = 1)[44]. For all three proteins, their relative intensities increased with the increase of corresponding antibiotic concentration. These data confirm that higher level of antibiotic-resistance would result in higher expression level of resistance proteins and consequently higher mass spectral peak intensities. For the chloramphenicol-resistant strain, however, the intensity of protein CAT decreased when chloramphenicol concentration reached 120 μg·mL$^{-1}$ (**Figure 3.14 c**). Probably, this concentration was already too high and started to negatively affect the bacterial physiological state. In addition to the presence of antibiotics, the type of culture medium can also affect the expression level of resistance proteins. Synthesis of resistance proteins to fight against antibiotics is an energy-consuming process, which can be positively influenced by the use of nutritionally rich growth medium.[45] To observe this effect, ampicillin-resistance gene transferred-*E. coli* DH5α cells were incubated with different growth media (lysogeny broth and 2xYT medium, respectively) containing a fixed concentration (60 μg·mL$^{-1}$) of ampicillin. The corresponding MALDI-TOF MS fingerprints indicated that 2xYT medium, specifically rich in amino acids and peptides, favoured the up-regulation of gene *bla*TEM-1 expression. Specifically, when the growth medium was changed from lysogeny broth to 2xYT, the averaged relative peak intensity of TEM-1 β-lactamase increased from 0.60 to 6.66 (**Figure 3.14 d**).
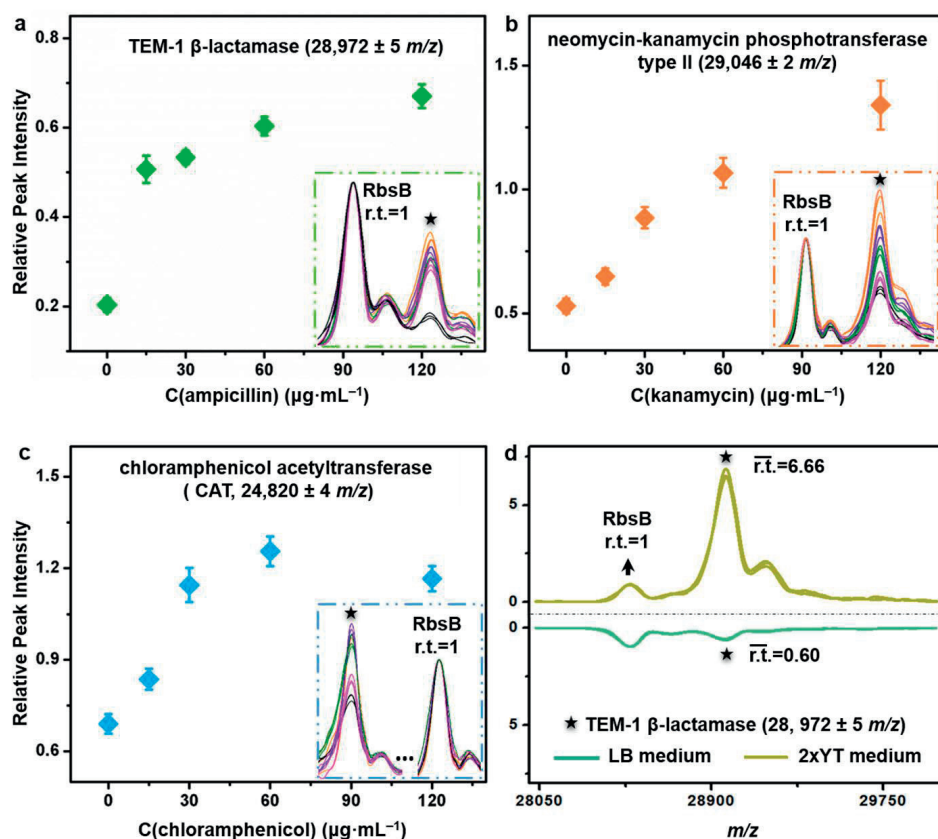
**Figure 3.14** Monitoring the variations of resistance protein expression level in bacteria. Relative mass spectral peak intensities of (**a**) TEM-1 β-lactamase, (**b**) neomycin-kanamycin phosphotransferase type II and (**c**) CAT when the resistance-gene transferred *E. coli* DH5α cells were incubated with lysogeny broth containing 0, 15, 30, 60, 120 μg·mL$^{-1}$ of ampicillin, kanamycin and chloramphenicol, respectively. Corresponding MALDI-TOF MS patterns of related peaks (overlapping of three replicates for each test) were shown in the insert graphs. (**d**) MALDI-TOF MS patterns in 28,000-30,000 *m/z* mass range (overlapping of three replicates) of ampicillin resistance gene-transferred *E. coli* DH5α that were incubated with lysogeny broth or 2xYT medium containing 60 μg·mL$^{-1}$ of ampicillin. Relative intensities (r.t.) of all peaks were calculated using signal from protein RbsB as an internal intensity standard (r.t.$_{RbsB}$ = 1). Data were obtained by MALDI-TOF MS bacterial fingerprinting using TiO$_2$-modified target. Each spectrum was generated from ~ $5·10^5$ intact bacterial cells.

## 3.3 Demonstration with clinical pathogens

The proposed method can be used for antimicrobial resistance proteins detection

whilst performing bacterial species identification. The feasibility was explored with three clinical pathogens, *i.e.* extended-spectrum β-lactamase-producing *E. coli* (ESBL-*E. coli*), multidrug-resistant *P. aeruginosa* (MDR-*P. aeruginosa*) and methicillin-resistant *S. aureus* (MRSA).

ESBL, firstly reported in Germany in 1983, confers resistance to a broad spectrum of β-lactam antibiotics.[46] Worldwide emergency of ESBL-*E. coli* raises serious therapeutic problems. Resistance in the ESBL-*E. coli* tested here was conferred by the expression of CTX-M type β-lactamase (~ 28 kDa).[47] *E. coli* ATCC25922, a strain without such kind of resistance, was used as the reference for species identification and resistance proteins detection of the testing strain (ESBL-*E. coli*). Detailed antimicrobial susceptibility profiles of the two strains, measured with bioMérieux VITEK™ 2 automated AST system, are shown in **Appendix II**, **Table 5**, **6**. The profiles showed the MIC of corresponding antibiotics were 4-320 μg·mL$^{-1}$. The MALDI-TOF MS fingerprints of the two strains are displayed in **Figure 3.15 a**. With the spectrum cosine similarity as high as 0.9427, the testing strain was identified to be the same species as the reference one, *i.e. E. coli*. The two strains shared almost all mass spectral peaks in the mass range of 10,000-80,000 *m/z*, except of a peak at 28,074 *m/z* only detected from the testing strain (**Figure 3.15 a**, **zoom-in**). The appearance of this peak most probably results from the expression of CTX-M type β-lactamase.

Similarly, the MDR-*P. aeruginosa* and MRSA were also identified at the species level by comparison of their fingerprint patterns with those of corresponding reference strains (*i.e. P. aeruginosa* ATCC 27853 and *S. aureus* ATCC 29213), resulting in pattern similarity scores of 0.8546 and 0.9578, respectively (**Figure 3.15 b**, **c**). Simultaneously, two mass spectral peaks, at 38,080 and 40,900 *m/z*, were exclusively observed from the MDR-*P. aeruginosa* (**Figure 3.15 b**, **zoom-in**). They most likely come from efflux pump proteins MexA (~ 38 kDa) and MexX (40.9 kDa, UniProtKB-Q9ZNG9), which confer multidrug resistance of the MDR-*P. aeruginosa*.[48,49] These two proteins are involved in the extrusion of β-lactam antibiotics (*e.g.* tazobactam, ceftazidime, cefepime) and aminoglycosides (*e.g.* amikacin, gentamicin, netilmicin, tobramycin) from within bacterial cells into external environment.[50] Meanwhile, antimicrobial resistance in MRSA, one of the most common multidrug resistant pathogens, arises from the expression of gene *mecA*, which renders alteration of penicillin binding protein (PBP) and triggers the expression of its alternative, *i.e.* PBP 2a (~ 78 kDa). PBP 2a has a low affinity for most β-lactam antibiotics including methicillin, thereby making bacteria resistant against them.[51] According to previous studies, a characteristic fragment of PBP 2a (~ 13 kDa) can be detected from MRSA by proteomics-based method.[52-54] In the present work, a peak at 13,080 *m/z* was exclusively detected from the MRSA strain (**Figure 3.15 c**, **zoom-in**), which could come from the PBP 2a fragment. To confirm this

assumption, two more MRSA strains were tested and the peak around 13 kDa (at 13,083 and 13,081 *m/z*, respectively) were repeatedly detected, as shown in **Figure 3.16**. The detailed antimicrobial susceptibility profiles of MDR-*P. aeruginosa*, MRSA and their reference strains are shown in **Appendix II**, **Table 7-12**.
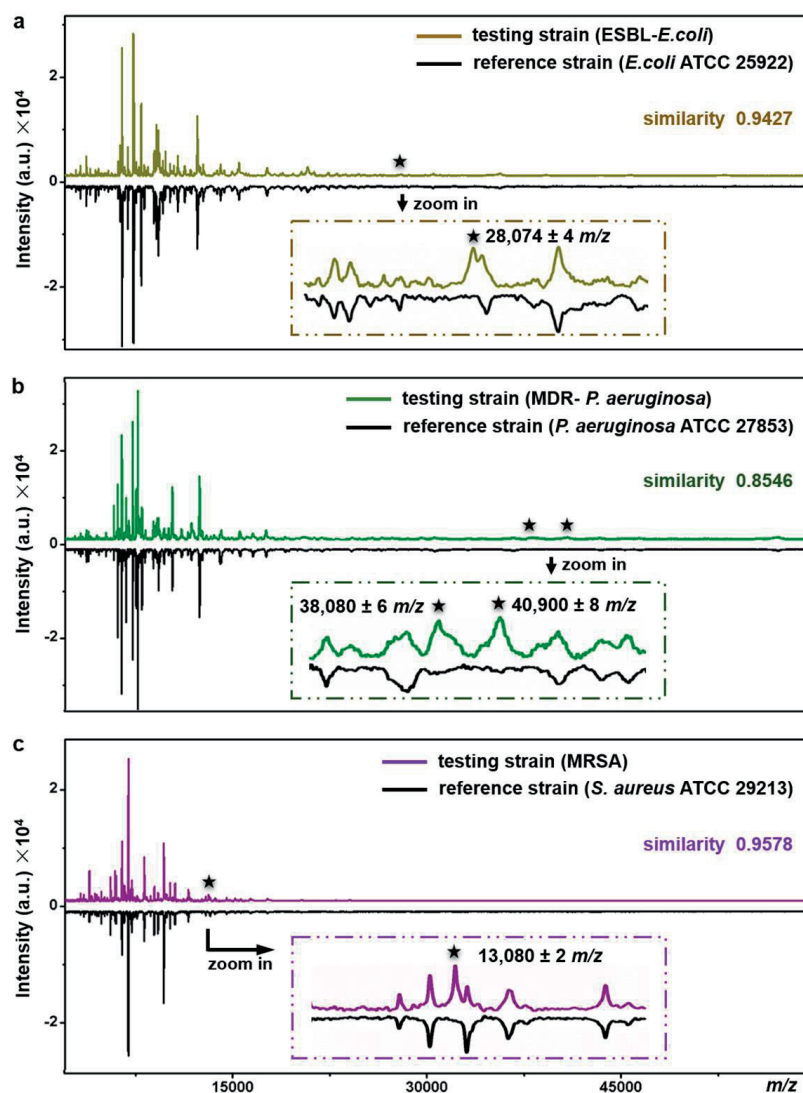


**Figure 3.15** Simultaneously species identification and antimicrobial resistance protein detection for three clinical pathogens, *i.e.* (**a**) ESBL-*E. coli*, (**b**) MDR-*P. aeruginosa* and (**c**) MRSA, by comparing their MS fingerprint patterns with those of reference strains (*i.e. E. coli* ATCC25922, *P. aeruginosa* ATCC 27853 and *S. aureus* ATCC29213). Data were obtained by MALDI-TOF MS bacterial fingerprinting using TiO$_2$-modified target plate. Each spectrum was generated from $\sim 5 \cdot 10^5$ intact bacterial cells.
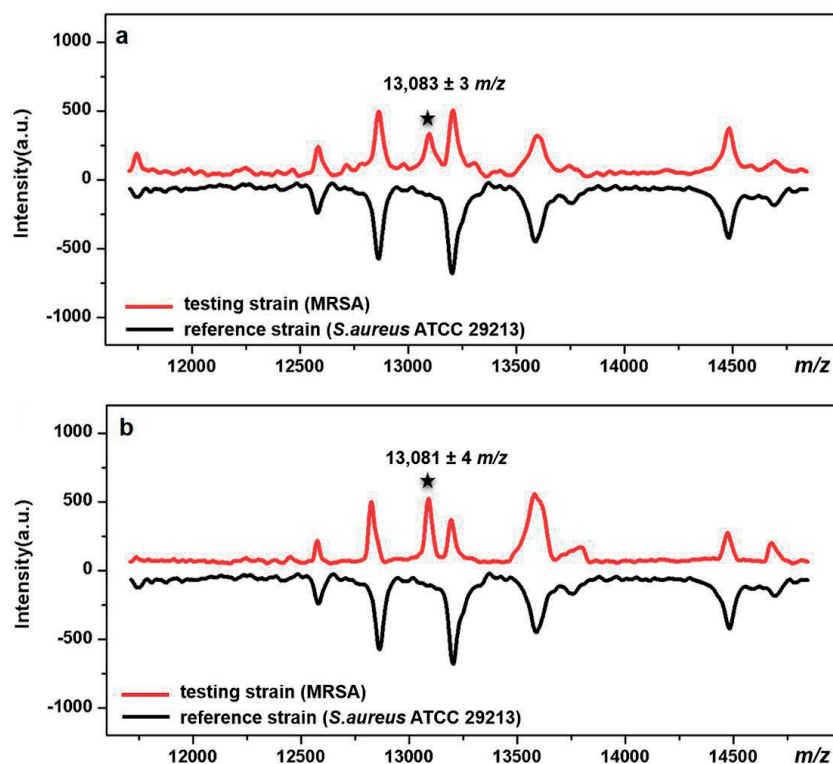
**Figure 3.16** Detection of antimicrobial-resistance proteins from two more methicillin-resistant *S. aureus* (MRSA) strains by comparing their MALDI-TOF MS fingerprints with reference strain *S. aureus* ATCC 29213.

Herein, antimicrobial resistance marker proteins were successfully detected directly from intact bacteria without any sample pre-treatment by $TiO_2$-facilitated MALDI-TOF MS. The present approach showed feasibility for both gram-negative and gram-positive bacterial species bearing different types of antimicrobial resistance. Each of the resistance proteins was specifically detected from the corresponding antibiotic-resistant strains, not from the non-resistant reference strains or the strains resistant against other antibiotics. For certain resistance types tested in this work, it was also shown that higher level of antibiotic resistance could accompany with higher expression level of the resistance proteins. A measurement of the expression level variations was proven possible through direct readout of relative intensities of the corresponding mass spectrum peaks.

The described method performed resistance proteins recognition according to their *m/z* values. Due to the limited resolving power of current MALDI-TOF MS instruments, it would be difficult to distinguish closely-related protein isoforms with quite similar molecular weight like TEM-1, TEM-2 and TEM-3 β-lactamases, which differ only in a

few amino acid substitutions. This is a drawback for MALDI-TOF MS-based analysis of proteins in comparison with nucleic acids-based molecular detection of related genes or proteomics-based approaches. In this work, it has been confirmed that the expression level of resistance proteins directly determines their mass spectrum peak intensities. As intact bacteria are analysed directly without preparatory extraction, enrichment or selective separation of the proteins, the proposed method could lack sensitivity when the resistance proteins are expressed at a very low level. Here, the method was shown sensitive enough for resistant strains with antibiotic MICs as low as a few microgram per millilitre.

Nonetheless, compared to existing methods for the detection of resistance genes or proteins, such as nucleic acids-based molecular techniques or proteomics-based approaches, the proposed mass spectrometry method has clear advantages of simplicity and rapidity in sample preparation, measurement protocol and data analysis. It is a useful procedure for quick discrimination of antimicrobial-resistant bacteria strains from their non-resistant counterparts, as well as a fast way for the determination of resistance mechanisms and prediction of antibiotic classes the strains could be resistant to.

## 4. Conclusions

In this work, MALDI-TOF mass spectrometry detection of intact bacteria was improved by $TiO_2$ nanoparticles. A clear improvement in detection sensitivity and working mass range was achieved, pushing the current limits of the bacterial MALDI-TOF mass spectrometry fingerprinting approach. Accordingly, antimicrobial resistance marker proteins, especially those larger than 15 kDa, were successfully detected from intact bacterial cells by direct readout of corresponding mass spectral peaks from the fingerprint patterns, together with a rapid monitoring of their expression levels. With the potential of simultaneous species identification and antimicrobial resistance analysis, the $TiO_2$-facilitated MALDI-TOF mass spectrometry opens new avenues for bacterial analysis.

# Appendix I

**Note 1** Gentamicin acetyltransferase I was detected from the ~ 19 kDa band of the gentamicin-resistant *E. coli* DH5α by in-gel digest and LC-MS/MS.

Gentamicin acetyltransferase I; UniProt access P23181; 100% protein identification probability; 19,442.7 Da; 60 exclusive unique peptides; 114 exclusive unique spectrum; 295 total spectra; 164/177 amino acids (93% coverage), with recovered protein sequence highlighted with underline:

```
MLRSSNDVTQ  QGSRPKTKLG  GSSMGIIRTC  RLGPDQVKSM  RAALDLFGRE  FGDVATYSQH
QPDSDYLGNL  LRSKTFIALA  AFDQEAVVGA  LAAYVLPRFE  QPRSEIYIYD  LAVSGEHRRQ
GIATALINLL  KHEANALGAY  VIYVQADYGD  DPAVALYTKL  GIREEVMHFD  IDPSTAT
```

**Note 2** Neomycin-kanamycin phosphotransferase type II was detected from the ~ 29 kDa band of the kanamycin-resistant *E. coli* BL21 by in-gel digest and LC-MS/MS.

Neomycin-kanamycin phosphotransferase type II; UniProt access P00552; 100% protein identification probability; 29,048.4 Da; 72 exclusive unique peptides; 116 exclusive unique spectrum; 206 total spectra; 246/264 amino acids (93% coverage), with recovered protein sequence highlighted with underline:

```
MIEQDGLHAG  SPAAWVERLF  GYDWAQQTIG  CSDAAVFRLS  AQGRPVLFVK  TDLSGALNEL
QDEAARLSWL  ATTGVPCAAV  LDVVTEAGRD  WLLLGEVPGQ  DLLSSHLAPA  EKVSIMADAM
RRLHTLDPAT  CPFDHQAKHR  IERARTRMEA  GLVDQDDLDE  EHQGLAPAEL  FARLKARMPD
GEDLVVTHGD  ACLPNIMVEN  GRFSGFIDCG  RLGVADRYQD  IALATRDIAE  ELGGEWADRF
LVLYGIAAPD  SQRIAFYRLL  DEFF
```

# Appendix II

**Table 3.1** Antimicrobial susceptibility profile of *Enterobacter cloacae ssp. cloacae* before the transfer of gene *AmpC* (test duration 9.00 h)

| Antibiotic | MIC* μg·mL$^{-1}$ | Interpretation* | Antibiotic | MIC* μg·mL$^{-1}$ | Interpretation* |
|---|---|---|---|---|---|
| Amoxicillin | -- | R | Ertapenem | $\leq 0.5$ | S |
| Ampicillin | 16 | R | Imipenem | $\leq 0.25$ | S |
| Amoxicillin/ clavulanic acid | $\geq 32$ | R | Meropenem | -- | S |
| Cefuroxime | -- | I | Gentamicin | $\leq 1$ | S |
| Cefuroxime Axetil | -- | I | Ciprofloxacin | $\leq 0.25$ | S |
| Cefoxitine | -- | I | Norfloxacin | $\leq 0.5$ | S |
| Cefpodoxime | -- | I | Tetracycline | $\leq 1$ | S |
| Ceftazidime | $\leq 1$ | S | Fosfomycin | $\leq 16$ | S |
| Ceftriaxone | $\leq 1$ | S | Nitrofurantoin | $\leq 16$ | S |
| Cefepime | $\leq 1$ | S | Trimethopri/ Sulfamethoxazole | $\leq 20$ | S |
| Piperacillin/ tazobactam | $\leq 4$ | S | | | |

**Table 3.2** Antimicrobial susceptibility profile of Enterobacter cloacae ssp. cloacae after the transfer of gene AmpC (test duration 9.50 h)

| Antibiotic | MIC* μg·mL$^{-1}$ | Interpretation* | Antibiotic | MIC* μg·mL$^{-1}$ | Interpretation* |
|---|---|---|---|---|---|
| Amoxicillin | -- | R | Ertapenem | 1 | I |
| Ampicillin | $\geq 32$ | R | Imipenem | $\leq 0.25$ | S |
| Amoxicillin/ clavulanic acid | $\geq 32$ | R | Meropenem | -- | S |
| Cefuroxime | $\geq 64$ | R | Gentamicin | $\leq 1$ | S |
| Cefuroxime Axetil | $\geq 64$ | R | Ciprofloxacin | $\leq 0.25$ | S |
| Cefoxitine | $\geq 64$ | R | Norfloxacin | $\leq 0.5$ | S |
| Cefpodoxime | $\geq 8$ | R | Tetracycline | 2 | S |
| Ceftazidime | $\geq 64$ | R | Fosfomycin | $\leq 16$ | S |
| Ceftriaxone | $\geq 64$ | R | Nitrofurantoin | 32 | S |
| Cefepime | 2 | I | Trimethoprim/ Sulfamethoxazole | $\leq 20$ | S |
| Piperacillin/ tazobactam | $\geq 128$ | R | | | |

**Table 3.3** Antimicrobial susceptibility profile of *Enterobacter aerogenes* before the transfer of gene *AmpC* (test duration 9.25 h)

| Antibiotic | MIC* μg·mL$^{-1}$ | Interpretation* | Antibiotic | MIC* μg·mL$^{-1}$ | Interpretation* |
|---|---|---|---|---|---|
| Amoxicillin | -- | R | Ertapenem | ≤ 0.5 | S |
| Ampicillin | 8 | R | Imipenem | ≤ 0.5 | S |
| Amoxicillin/ clavulanic acid | 16 | R | Meropenem | -- | S |
| Cefuroxime | 4 | S | Gentamicin | ≤ 1 | S |
| Cefuroxime Axetil | 4 | S | Ciprofloxacin | ≤ 0.25 | S |
| Cefoxitine | -- | I | Norfloxacin | ≤ 0.5 | S |
| Cefpodoxime | ≤ 0.05 | S | Tetracycline | ≤ 1 | S |
| Ceftazidime | ≤ 1 | S | Fosfomycin | ≤ 16 | S |
| Ceftriaxone | ≤ 1 | S | Nitrofurantoin | ≤ 16 | S |
| Cefepime | ≤ 1 | S | Trimethoprim/ Sulfamethoxazole | ≤ 20 | S |
| Piperacillin/ tazobactam | ≤ 4 | S | | | |

**Table 3.4** Antimicrobial susceptibility profile of *Enterobacter aerogenes* after the transfer of gene *AmpC* (test duration 9.25 h)

| Antibiotic | MIC* μg·mL$^{-1}$ | Interpretation* | Antibiotic | MIC* μg·mL$^{-1}$ | Interpretation* |
|---|---|---|---|---|---|
| Amoxicillin | -- | R | Ertapenem | ≤ 0.5 | S |
| Ampicillin | ≥ 32 | R | Imipenem | ≤ 0.25 | S |
| Amoxicillin/ clavulanic acid | ≥ 32 | R | Meropenem | -- | S |
| Cefuroxime | ≥ 64 | R | Gentamicin | ≤ 1 | S |
| Cefuroxime Axetil | ≥ 64 | R | Ciprofloxacin | ≤ 0.25 | S |
| Cefoxitine | ≥ 64 | R | Norfloxacin | ≤ 0.5 | S |
| Cefpodoxime | ≥ 8 | R | Tetracycline | ≤ 1 | S |
| Ceftazidime | ≥ 64 | R | Fosfomycin | ≤ 16 | S |
| Ceftriaxone | 16 | R | Nitrofurantoin | 32 | S |
| Cefepime | 2 | I | Trimethoprim/ Sulfamethoxazole | ≤ 20 | S |
| Piperacillin/ tazobactam | ≥ 128 | R | | | |

**Table 3.5** Antimicrobial susceptibility profile of *Escherichia coli* ATCC25922 (test duration 10.25 h)

| Antibiotic | MIC* $\mu g \cdot mL^{-1}$ | Interpretation* | Antibiotic | MIC* $\mu g \cdot mL^{-1}$ | Interpretation* |
|---|---|---|---|---|---|
| Amoxicillin | -- | R | Ertapenem | ≤ 0.5 | S |
| Ampicillin | 4 | S | Imipenem | ≤ 0.25 | S |
| Amoxicillin/ clavulanic acid | 4 | S | Meropenem | -- | S |
| Cefuroxime | 4 | S | Gentamicin | ≤ 1 | S |
| Cefuroxime Axetil | 4 | S | Ciprofloxacin | ≤ 0.25 | S |
| Cefoxitine | ≤ 4 | S | Norfloxacin | ≤ 0.5 | S |
| Cefpodoxime | ≤ 0.25 | S | Tetracycline | ≤ 1 | S |
| Ceftazidime | ≤ 1 | S | Fosfomycin | ≤ 16 | S |
| Ceftriaxone | ≤ 1 | S | Nitrofurantoin | ≤ 16 | S |
| Cefepime | ≤ 1 | S | Trimethoprim/ Sulfamethoxazole | ≤ 20 | S |
| Piperacillin/ tazobactam | ≤ 4 | S | | | |

**Table 3.6** Antimicrobial susceptibility profile of CTX-M type extended-spectrum β-lactamase-producing *Escherichia coli* (test duration 8.75 h)

| Antibiotic | MIC* $\mu g \cdot mL^{-1}$ | Interpretation* | Antibiotic | MIC* $\mu g \cdot mL^{-1}$ | Interpretation* |
|---|---|---|---|---|---|
| Amoxicillin | -- | R | Ertapenem | ≤ 0.5 | S |
| Ampicillin | ≥ 32 | R | Imipenem | ≤ 0.25 | S |
| Amoxicillin/ clavulanic acid | 16 | R | Meropenem | -- | S |
| Cefuroxime | ≥ 64 | R | Gentamicin | ≥ 64 | R |
| Cefuroxime Axetil | ≥ 64 | R | Ciprofloxacin | ≥ 4 | R |
| Cefoxitine | 32 | I | Norfloxacin | ≥ 16 | R |
| Cefpodoxime | ≥ 8 | S | Tetracycline | ≥ 16 | R |
| Ceftazidime | 16 | R | Fosfomycin | ≤ 16 | S |
| Ceftriaxone | ≥ 64 | R | Nitrofurantoin | ≤ 16 | S |
| Cefepime | 8 | R | Trimethoprim/ Sulfamethoxazole | ≥ 320 | R |
| Piperacillin/ tazobactam | 8 | S | | | |

**Table3.7** Antimicrobial susceptibility profile of *Pseudomonas aeruginosa* ATCC 27853 (test duration 17 h)

| Antibiotic | MIC* µg·mL⁻¹ | Interpretation* | Antibiotic | MIC* µg·mL⁻¹ | Interpretation* |
|---|---|---|---|---|---|
| Ticarcillin | ≤ 8 | S | Amikacin | ≤ 2 | S |
| Ticarcillin/ clavulanic acid | 16 | S | Gentamicin | ≤ 1 | S |
| Piperacillin | ≤ 4 | S | Netilmicin | -- | S |
| Piperacillin/ tazobactam | ≤ 4 | S | Tobramycin | ≤ 1 | S |
| Ceftazidime | ≤ 1 | S | Ciprofloxacin | ≤ 0.25 | S |
| Cefepime | ≤ 1 | S | Levofloxacin | ≤ 0.12 | S |
| Aztreonam | 2 | I | Colistin | ≤ 0.5 | S |
| Imipenem | 1 | S | Rifampicin | -- | -- |
| Meropenem | ≤ 0.25 | S | Trimethoprim/ Sulfamethoxazole | ≥ 320 | R |

**Table 3.8** Antimicrobial susceptibility profile of multidrug-resistant *Pseudomonas aeruginosa* (test duration 10.75 h)

| Antibiotic | MIC* µg·mL⁻¹ | Interpretation* | Antibiotic | MIC* µg·mL⁻¹ | Interpretation* |
|---|---|---|---|---|---|
| Ticarcillin | -- | -- | Amikacin | -- | R |
| Ticarcillin/ clavulanic acid | -- | -- | Gentamicin | -- | R |
| Piperacillin | -- | -- | Netilmicin | -- | R |
| Tazobacam | -- | R | Tobramycin | -- | R |
| Ceftazidime | -- | R | Ciprofloxacin | -- | -- |
| Cefepime | -- | R | Levofloxacin | -- | -- |
| Aztreonam | -- | -- | Colistin | -- | S |
| Imipenem | -- | -- | Rifampicin | -- | -- |
| Meropenem | -- | S | Trimethoprim/ Sulfamethoxazole | -- | -- |

**Table 3.9** Antimicrobial susceptibility profile of *Staphylococcus aureus* ATCC 29213 (test duration 9.75 h)

| Antibiotic | MIC* µg·mL$^{-1}$ | Interpretation* | Antibiotic | MIC* µg·mL$^{-1}$ | Interpretation* |
|---|---|---|---|---|---|
| Test Cefoxitine Screen | -- | Negative | Erythromycin | -- | S |
| Benzylpenicillin | 0.06 | S | Clindamycin | -- | S |
| Amoxicillin/ clavulanic acid | -- | S | Linezolid | 2 | S |
| Oxacillin | ≤ 0.25 | S | Teicoplanin | ≤ 0.5 | S |
| Cephalotin | -- | S | Vancomycin | ≤ 0.5 | S |
| Ceftriaxone | -- | S | Doxycycline | -- | S |
| Meropenem | -- | S | Tetracycline | ≤ 1 | S |
| Gentamicin | ≤ 0.5 | S | Fosfomycin | ≤ 8 | S |
| Kanamycin | ≤ 4 | S | Fusidic acid | ≤ 0.5 | S |
| Tobramycin | ≤ 1 | S | Mupirocin | ≤ 2 | S |
| Ciprofloxacin | ≤ 0.5 | S | Chloramphenicol | 8 | S |
| Levofloxacin | -- | S | Rifampicin | ≤ 0.03 | S |
| Resistance inductile to clindamycin | -- | Negative | Trimethoprim/ Sulfamethoxazole | ≤ 10 | S |

**Table 3.10** Antimicrobial susceptibility profile of methicillin-resistant *Staphylococcus aureus* tested in Figure 3.15 c, main article (test duration 10.25 h)

| Antibiotic | MIC* µg·mL$^{-1}$ | Interpretation* | Antibiotic | MIC* µg·mL$^{-1}$ | Interpretation* |
|---|---|---|---|---|---|
| Test Cefoxitine Screen | -- | Positive | Erythromycin | 1 | S |
| Benzylpenicillin | ≥ 0.5 | R | Clindamycin | 0.25 | S |
| Amoxicillin/ clavulanic acid | -- | R | Linezolid | 2 | S |
| Oxacillin | ≥ 4 | R | Teicoplanin | ≤ 0.5 | S |
| Cephalotin | -- | R | Vancomycin | ≤ 0.5 | S |
| Ceftriaxone | -- | R | Doxycycline | -- | S |
| Meropenem | -- | R | Tetracycline | ≤ 1 | S |
| Gentamicin | ≤ 0.5 | S | Fosfomycin | ≤ 8 | S |
| Kanamycin | ≤ 4 | S | Fusidic acid | ≤ 0.5 | S |
| Tobramycin | ≤ 1 | S | Mupirocin | ≤ 2 | S |
| Ciprofloxacin | ≥ 8 | R | Chloramphenicol | 8 | S |
| Levofloxacin | -- | R | Rifampicin | ≤ 0.03 | S |
| Resistance inductile to clindamycin | -- | Negative | Trimethoprim/ Sulfamethoxazole | ≤ 10 | S |

**Table 3.11** Antimicrobial susceptibility profile of methicillin-resistant *Staphylococcus aureus* tested in Figure 3.16 a (test duration 10.25 h)

| Antibiotic | MIC* μg·mL⁻¹ | Interpretation* | Antibiotic | MIC* μg·mL⁻¹ | Interpretation* |
|---|---|---|---|---|---|
| Test Cefoxitine Screen | -- | Positive | Erythromycin | 1 | S |
| Benzylpenicillin | ≥ 0.5 | R | Clindamycin | 0.25 | S |
| Amoxicillin/ clavulanic acid | -- | R | Linezolid | 2 | S |
| Oxacillin | ≥ 4 | R | Teicoplanin | 1 | S |
| Cephalotin | -- | R | Vancomycin | 1 | S |
| Ceftriaxone | -- | R | Doxycycline | -- | S |
| Meropenem | -- | R | Tetracycline | ≤ 1 | S |
| Gentamicin | ≤ 0.5 | S | Fosfomycin | ≤ 8 | S |
| Kanamycin | 8 | R | Fusidic acid | ≤ 0.5 | S |
| Tobramycin | ≥ 8 | R | Mupirocin | ≤ 2 | S |
| Ciprofloxacin | -- | I | Chloramphenicol | 8 | S |
| Levofloxacin | -- | I | Rifampicin | ≤ 0.03 | S |
| Resistance inductile to clindamycin | -- | Negative | Trimethoprim/ Sulfamethoxazole | ≤ 10 | S |

**Table 3.12** Antimicrobial susceptibility profile of methicillin-resistant *Staphylococcus aureus* tested in Figure 3.16 b (test duration 10.25 h)

| Antibiotic | MIC* μg·mL⁻¹ | Interpretation* | Antibiotic | MIC* μg·mL⁻¹ | Interpretation* |
|---|---|---|---|---|---|
| Test Cefoxitine Screen | -- | Positive | Erythromycin | ≥ 8 | R |
| Benzylpenicillin | ≥ 0.5 | R | Clindamycin | 0.25 | S |
| Amoxicillin/ clavulanic acid | -- | R | Linezolid | 2 | S |
| Oxacillin | ≥ 4 | R | Teicoplanin | ≤ 0.5 | S |
| Cephalotin | -- | R | Vancomycin | ≤ 0.5 | S |
| Ceftriaxone | -- | R | Doxycycline | -- | S |
| Meropenem | -- | R | Tetracycline | ≤ 1 | S |
| Gentamicin | ≤ 0.5 | S | Fosfomycin | ≤ 8 | S |
| Kanamycin | ≤ 4 | S | Fusidic acid | ≤ 0.5 | S |
| Tobramycin | ≤ 1 | S | Mupirocin | ≤ 2 | S |
| Ciprofloxacin | ≥ 8 | R | Chloramphenicol | 8 | S |
| Levofloxacin | -- | R | Rifampicin | ≤ 0.03 | S |
| Resistance inductile to clindamycin | -- | Negative | Trimethoprim/ Sulfamethoxazole | ≤ 10 | S |

**\*MIC**: minimum inhibitory concentration, the lowest concentration of an antimicrobial drug that will inhibit the visible growth of a microorganism after overnight incubation

**\*Interpretation**: R: Resistant    S:Susceptible    I:Intermediate

# Reference

1. Sharland, M., Saroey, P. & Berezin, E.N. The global threat of antimicrobial resistance - The need for standardized surveillance tools to define burden and develop interventions. *J Pediat-Brazil* 91, 410-412 (2015).

2. Seng, P.*, et al.* Ongoing Revolution in Bacteriology: Routine Identification of Bacteria by Matrix-Assisted Laser Desorption Ionization Time-of-Flight Mass Spectrometry. *Clin Infect Dis* 49, 543-551 (2009).

3. Matsuda, N.*, et al.* Evaluation of a Simple Protein Extraction Method for Species Identification of Clinically Relevant Staphylococci by Matrix-Assisted Laser Desorption Ionization-Time of Flight Mass Spectrometry. *J Clin Microbiol* 50, 3862-3866 (2012).

4. Jorgensen, J.H. & Ferraro, M.J. Antimicrobial Susceptibility Testing: A Review of General Principles and Contemporary Practices. *Clin Infect Dis* 49, 1749-1755 (2009).

5. Fluit, A.C., Visser, M.R. & Schmitz, F.J. Molecular detection of antimicrobial resistance. *Clin Microbiol Rev* 14, 836-871 (2001).

6. Choi, J.*, et al.* A rapid antimicrobial susceptibility test based on single-cell morphological analysis. *Sci Transl Med* 6 (2014).

7. Liu, C.Y.*, et al.* Rapid bacterial antibiotic susceptibility test based on simple surface-enhanced Raman spectroscopic biomarkers. *Sci Rep-Uk* 6 (2016).

8. Longo, G.*, et al.* Rapid detection of bacterial resistance to antibiotics using AFM cantilevers as nanomechanical sensors. *Nat Nanotechnol* 8, 522-526 (2013).

9. Sparbier, K., Schubert, S., Weller, U., Boogen, C. & Kostrzewa, M. Matrix-Assisted Laser Desorption Ionization-Time of Flight Mass Spectrometry-Based Functional Assay for Rapid Detection of Resistance against beta-Lactam Antibiotics. *J Clin Microbiol* 50, 927-937 (2012).

10. Savic, M., Lovric, J., Tomic, T.I., Vasiljevic, B. & Conn, G.L. Determination of the target nucleosides for members of two families of 16S rRNA methyltransferases that confer resistance to partially overlapping groups of aminoglycoside antibiotics. *Nucleic Acids Res* 37, 5420-5431 (2009).

11. Sparbier, K.*, et al.* MALDI Biotyper-Based Rapid Resistance Detection by Stable-Isotope Labeling. *J Clin Microbiol* 51, 3741-3748 (2013).

12. Jung, J.S.*, et al.* Rapid detection of antibiotic resistance based on mass spectrometry and stable isotopes. *Eur J Clin Microbiol* 33, 949-955 (2014).

13. Lange, C., Schubert, S., Jung, J., Kostrzewa, M. & Sparbier, K. Quantitative Matrix-Assisted Laser Desorption Ionization-Time of Flight Mass Spectrometry for Rapid Resistance Detection. *J Clin Microbiol* 52, 4155-4162 (2014).

14. Sparbier, K., Schubert, S. & Kostrzewa, M. MBT-ASTRA: A suitable tool for fast antibiotic susceptibility testing? *Methods* 104, 48-54 (2016).

15. Wolters, M.*, et al.* MALDI-TOF MS fingerprinting allows for discrimination of major methicillin-resistant Staphylococcus aureus lineages. *Int J Med Microbiol* 301, 64-68 (2011).

16. Griffin, P.M.*, et al.* Use of Matrix-Assisted Laser Desorption Ionization-Time of Flight Mass Spectrometry To Identify Vancomycin-Resistant Enterococci and Investigate the Epidemiology of an Outbreak. *J Clin Microbiol* 50, 2918-2931 (2012).

17. Blair, J.M.A., Webber, M.A., Baylay, A.J., Ogbolu, D.O. & Piddock, L.J.V. Molecular mechanisms of antibiotic resistance. *Nat Rev Microbiol* 13, 42-51 (2015).

18. Sauer, S. & Kliem, M. Mass spectrometry tools for the classification and identification of bacteria. *Nat Rev Microbiol* 8, 74-82 (2010).

19. Hrabak, J., Chudackova, E. & Walkova, R. Matrix-Assisted Laser Desorption Ionization-Time of Flight (MALDI-TOF) Mass Spectrometry for Detection of Antibiotic Resistance Mechanisms: from Research to Routine Diagnosis. *Clin Microbiol Rev* 26, 103-114 (2013).

20. Pinto, L., *et al.* Genomic and proteomic evaluation of antibiotic resistance in Salmonella strains. *J Proteomics* 73, 1535-1541 (2010).
21. dos Santos, K.V., *et al.* Proteomic analysis of Escherichia coli with experimentally induced resistance to piperacillin/tazobactam. *Res Microbiol* 161, 268-275 (2010).
22. Boulund, F., *et al.* Typing and Characterization of Bacteria Using Bottom-up Tandem Mass Spectrometry Proteomics. *Mol Cell Proteomics* 16, 1052-1063 (2017).
23. Youn, J.H., *et al.* Clinical Performance of a Matrix-Assisted Laser Desorption Ionization-Time of Flight Mass Spectrometry Method for Detection of Certain bla(KPC)-Containing Plasmids. *J Clin Microbiol* 54, 35-42 (2016).
24. Bi, H.Y., *et al.* TiO2 Printed Aluminum Foil: Single-Use Film for a Laser Desorption/Ionization Target Plate. *Anal Chem* 81, 1177-1183 (2009).
25. Cox, C.R., Jensen, K.R., Saichek, N.R. & Voorhees, K.J. Strain-level bacterial identification by CeO2-catalyzed MALDI-TOF MS fatty acid analysis and comparison to commercial protein-based methods. *Sci Rep-Uk* 5(2015).
26. Qiao, L., *et al.* Specific on-plate enrichment of phosphorylated peptides for direct MALDI-TOF MS analysis. *J Proteome Res* 6, 4763-4769 (2007).
27. Sambrook, J. & Russell, D.W. Preparation and Transformation of Competent E. coli Using Calcium Chloride. *CSH protocols* 2006(2006).
28. Qiao, L., *et al.* MALDI in-source photooxidation reactions for online peptide tagging. *Angew Chem Int Edit* 47, 2646-2648 (2008).
29. Qiao, L., *et al.* Photocatalytic Redox Reactions for In-Source Peptide Fragmentation. *Chem-Eur J* 15, 6711-6717 (2009).
30. Gogniat, G., Thyssen, M., Denis, M., Pulgarin, C. & Dukan, S. The bactericidal effect of TiO2 photocatalysis involves adsorption onto catalyst and the loss of membrane integrity. *Fems Microbiol Lett* 258, 18-24 (2006).
31. Nakano, R., *et al.* Broad Spectrum Microbicidal Activity of Photocatalysis by TiO2. *Catalysts* 3, 310-323 (2013).
32. Zhai, H.J. & Wang, L.S. Probing the electronic structure and band gap evolution of titanium oxide clusters (TiO2)(n)(-) (n=1-10) using photoelectron spectroscopy. *J Am Chem Soc* 129, 3022-3026 (2007).
33. Kubacka, A., *et al.* Understanding the antimicrobial mechanism of TiO2-based nanocomposite films in a pathogenic bacterium. *Sci Rep-Uk* 4 (2014).
34. Ma, S.L., Zhan, S.H., Jia, Y.N. & Zhou, Q.X. Superior Antibacterial Activity of Fe3O4-TiO2 Nanosheets under Solar Light. *Acs Appl Mater Inter* 7, 21875-21883 (2015).
35. Ansari, S.A. & Cho, M.H. Highly Visible Light Responsive, Narrow Band gap TiO2 Nanoparticles Modified by Elemental Red Phosphorus for Photocatalysis and Photoelectrochemical Applications. *Sci Rep-Uk* 6 (2016).
36. Bennett, P.M. Plasmid encoded antibiotic resistance: acquisition and transfer of antibiotic resistance genes in bacteria. *Brit J Pharmacol* 153, S347-S357 (2008).
37. Camara, J.E. & Hays, F.A. Discrimination between wild-type and ampicillin-resistant Escherichia coli by matrix-assisted laser desorption/ionization time-of-flight mass spectrometry. *Anal Bioanal Chem* 389, 1633-1638 (2007).
38. Daigle, D.M., McKay, G.A., Thompson, P.R. & Wright, G.D. Aminoglycoside antibiotic phosphotransferases are also serine protein kinases. *Chem Biol* 6, 11-18 (1999).
39. Schwocho, L.R., Schaffner, C.P., Miller, G.H., Hare, R.S. & Shaw, K.J. Cloning and characterization of a 3-N-aminoglycoside acetyltransferase gene, aac (3)-Ib, from Pseudomonas aeruginosa. *Antimicrob Agents Chemother* 39, 1790-1796 (1995).
40. Murray, I.A. & Shaw, W.V. O-Acetyltransferases for chloramphenicol and other natural products. *Antimicrob Agents Chemother* 41, 1-6 (1997).
41. Preston, K.E., Radomski, C.C. & Venezia, R.A. Nucleotide Sequence of the ChromosomalampC Gene of Enterobacter aerogenes. *Antimicrob Agents Chemother* 44, 3158-3162 (2000).

42. Jacoby, G.A. AmpC β-lactamases. *Clin Microbiol Rev* 22, 161-182 (2009).

43. Depardieu, F., Podglajen, I., Leclercq, R., Collatz, E. & Courvalin, P. Modes and modulations of antibiotic resistance gene expression. *Clin Microbiol Rev* 20, 79-114 (2007).

44. Xia, X.X., Qian, Z.G. & Lee, S.Y. Comparative proteomic and genetic analyses reveal unidentified mutations in Escherichia coli XL1-Blue and DH5 alpha. *Fems Microbiol Lett* 314, 119-124 (2011).

45. Carling, D. The AMP-activated protein kinase cascade–a unifying system for energy control. *Trends Biochem Sci* 29, 18-24 (2004).

46. Knothe, H., Shah, P., Krcmery, V., Antal, M. & Mitsuhashi, S. Transferable Resistance to Cefotaxime, Cefoxitin, Cefamandole and Cefuroxime in Clinical Isolates of Klebsiella-Pneumoniae and Serratia-Marcescens. *Infection* 11, 315-317 (1983).

47. Bonnet, R. Growing group of extended-spectrum β-lactamases: the CTX-M enzymes. *Antimicrob Agents Chemother* 48, 1-14 (2004).

48. Ferrandez, Y*., et al.* Stoichiometry of the MexA-OprM binding, as investigated by blue native gel electrophoresis. *Electrophoresis* 33, 1282-1287 (2012).

49. Mikolosko, J., Bobyk, K., Zgurskaya, H.I. & Ghosh, P. Conformational flexibility in the multidrug efflux system protein AcrA. *Structure* 14, 577-587 (2006).

50. Llanes, C*., et al.* Clinical strains of Pseudomonas aeruginosa overproducing MexAB-OprM and MexXY efflux pumps simultaneously. *Antimicrob Agents Chemother* 48, 1797-1802 (2004).

51. Fuda, C., Suvorov, M., Vakulenko, S.B. & Mobashery, S. The basis for resistance to beta-lactam antibiotics by penicillin-binding protein 2a of methicillin-resistant Staphylococcus aureus. *J Biol Chem* 279, 40802-40806 (2004).

52. Haghighat, S., Siadat, S.D., Sorkhabadi, S.M.R., Sepahi, A.A. & Mahdavi, M. Cloning, Expression and Purification of Penicillin Binding Protein2a (PBP2a) from Methicillin Resistant Staphylococcus aureus: A Study on Immunoreactivity in Balb/C Mouse. *Avicenna J Med Biotechnol* 5, 204 (2013).

53. Keserű, J.S., Gál, Z., Barabás, G., Benkő, I. & Szabó, I. Investigation of β-lactamases in clinical isolates of Staphylococcus aureus for further explanation of borderline methicillin resistance. *Chemotherapy* 51, 300-304 (2005).

54. Di Guilmi, A.M., Dessen, A., Dideberg, O. & Vernet, T. Functional characterization of penicillin-binding protein 1b from Streptococcus pneumoniae. *J Bacteriol* 185, 1650-1658 (2003).

# CHAPTER IV. Immuno-affinity amperometric detection of bacterial infections

## Abstract

A combination of immuno-affinity enrichment strategy and sensitive amperometric read-out was implemented in a point-of-care platform, intended for bacterial infection analysis. Bacterial cells, selectively captured and enriched from complex matrices *via* immuno-affinity, were detected by amperometric monitoring of the redox state of metabolic activity indicators, providing species identification and living cell quantification. The methodology was successfully employed for the diagnosis of bacterial infections and antimicrobial susceptibility testing with only several hours of total working time.
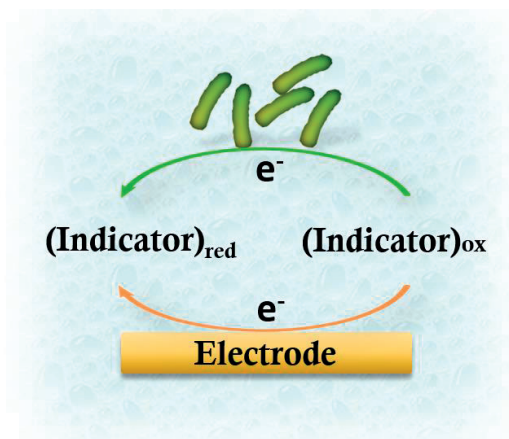
# 1. Introduction

Bacterial infections, in particular bloodstream infections, seriously threaten human health worldwide.[1] Due to the misuse and overuse of antimicrobial drugs over years, many bacterial pathogens are found to be drug-resistant and often multidrug-resistant,[2] leading to increased medical costs and high risks of infection recurrence and patient mortality.[3] Timely infection diagnosis and early, appropriate antimicrobial treatment is greatly important. Current standard for bloodstream infection diagnosis comprises blood culture, gram-staining, subculture, pathogen genus or species identification, and antimicrobial susceptibility determination.[4,5] The emerging of genotypic techniques and mass spectrometry methods greatly speeds up the pathogen identification process.[6] In the meantime, the antimicrobial susceptibility assay still mainly relies on the time-consuming antimicrobial drug culture-based methods, and the whole diagnosis often takes several days or even weeks.[7-9]

Herein, a sensitive immuno-affinity amperometric method is proposed to accomplish the whole diagnosis within several hours. **Scheme 4.1** illustrates the general workflow, composed of three steps: *i*) bacterial pathogen (*Bac*) capture and enrichment from complex matrices using superparamagnetic beads (MB) coated with bacterial species-specific antibodies (Ab); *ii*) chemical reduction of metabolic activity indicators ($I_{ox}$ to $I_{red}$) by bead-captured bacteria in a multi-well microchip, with the reduction happening mainly in the respiratory electron transport chain (ETC) on the plasma membrane of metabolically active cells (or *via* trans-plasma membrane electron transport in the presence of electron mediator); *iii*) amperometric read-out directly from the reaction mixture *via* a portable M-POT device (*i.e.* multiplexed potentiostat with integrated microchip holder and magnets) by electrochemically reducing the non-chemically reacted indicators. The method allows fast and high-throughput species identification, living cell quantification and antimicrobial susceptibility testing.
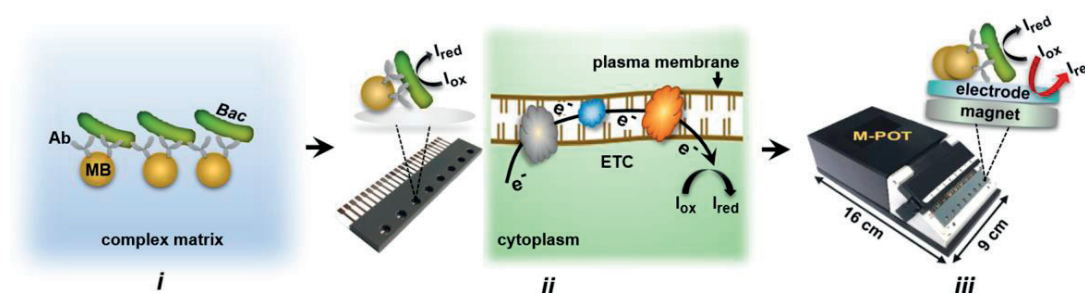


**Scheme 4.1** Workflow of the immuno-affinity amperometric method.

## 2. Materials and methods

### 2.1 Materials

Goat polyclonal IgG isotype antibody against *Escherichia coli* (anti-*E. coli* Ab), rabbit polyclonal IgG isotype antibody against *Bacillus subtilis* (anti-*B. Subtilis* Ab) and rabbit polyclonal IgG isotype antibody against *Staphylococcus aureus* (anti-*S. aureus* Ab) were purchased from Abcam plc (Cambridge, UK). Pierce[TM] protein A/G-coated superparamagnetic beads were purchased from Thermo Fisher Scientific Inc. (Waltham, Massachusetts, USA). Human whole blood was donated by a healthy female at her age of 20s, collected by the Transfusion Interrégional CRS in Lausanne, Switzerland. BacT/Alert® FA Plus aerobic bottle and BacT/Alert® FN Plus anaerobic bottle for blood culture were purchased from bioMérieux, Inc. Marcy-l'Étoile, France. Lysogeny broth and all antibiotics, including imipenem (Imi), tetracyclin (Tet), nitrofurantoin (Nit), fosfomycin (Fos), ampicillin (Amp), cefpodoxime (Cefp), ceftriaxone (Ceft), gentamicin (Gent) and ciprofloxacin (Cip), were bought from Sigma-Aldrich (St. Gallen, Switzerland). All the antibiotics were USP grade. Ferrocenemethanol (97%) and all metabolic activity indicators, including 5-cyano-2,3-di-(p-tolyl) tetrazolium chloride, 2-(4-iodophenyl)-3-(4-nitrophenyl)-5-(phenyl) tetrazolium chloride, 2,3,5-triphenyl tetrazolium chloride, resazurin, WST-1 (cell proliferation reagent, Roche), WST-8 (cell counting kit-8), were bought from Sigma-Aldrich (St. Gallen, Switzerland).

### 2.2 Microchip fabrication

The 8-well microchips were inkjet-printed on a 250 μm-thick transparent polyethylene terephthalate substrate (Goodfellow, Huntingdon, England) using an X-Serie CeraPrinter (Ceradrop, Limoges, France). The inkjet-printing method was developed in our laboratory and reported previously.[10,11] The X-Serie CeraPrinter comprised permanently three parallel piezoelectric drop-on-demand printheads, *i.e.*, two Q-Class Sapphire QS-256 each with 256 individually addressable nozzles for either 10, 30 or 80 pL nominal droplet volumes and one disposable DMC-11610 cartridge containing 16 individually addressable nozzles with 10 pL nominal droplet volume. All printheads were bought from Dimatix Fujifilm, NY, USA. The microchip design was created with the CeraSlice software from Ceradrop. Custom waveforms were developed for all inks to gain optimal droplet formation. Several print parameters were optimized, including the horizontal drop distance on the substrate, substrate temperature and the printhead height. In brief, the substrate temperature was increased to 60 °C for the printing of both silver and carbon nanotube inks to accelerate ink solvent evaporation and ensure highly resolved patterns. The silver ink (Silverjet DGP-40LT-15C, 30-35 wt.%, Sigma Aldrich, Buchs, Switzerland) was printed with a Q-Class Sapphire QS-256

printhead. The printed patterns were then dried and cured "in-line" in the CeraPrinter post-processing chamber using a high intensity light pulse from a xenon flash lamp. The flash lamp was provided by the PulseForge 1300 photonic curing station (NovaCentrix, Austin TX, USA). The carbon nanotube ink (CNTRENE® 3024 A3-R, Brewer Science, Rolla, USA) and UV curable dielectric ink (jettable insulator EMD 6201, Sun Chemical, Carlstadt, USA) were printed using disposable cartridges. The UV curable dielectric ink was simultaneously printed and photo-polymerized with a UV LED lamp (FireEdge FE300 380-420 nm, Pheseon Technology) integrated into the according printhead slot of the CeraPrinter. After photonic curing, each of the microchips, bearing eight parallel three-electrode systems, was ready for optical characterization. The optical characterization was performed with the fabrication analyser camera inside the CeraPrinter and an external Keyence VK 8700 laser scanning microscope (Keyence, Osaka, Japan), to check if all the patterns were well printed and if all the electrical tracks were well connected. For the fabrication of eight independent wells on the microchip, high-density polyethylene plastic pieces, in the dimension of 77 mm × 15 mm × 3 mm, were drilled with mechanically well-defined eight holes (4 mm in diameter). Afterwards, the plastic pieces with eight wells were glued directly on the printed microchips using double-sided strong adhesive tapes (Digi-Key 3M9726-ND). In this way, the fabrication of microchips containing eight sample wells on the top and eight three-electrode systems on the bottom were completed. The eight-channel microchips were fabricated in large quantities for the testing for a large number of bacteria samples.

## 2.3 Preparation of antibody-coated magnetic beads (MB-Ab affinity probes)

500 μg of Pierce$^{TM}$ protein A/G-coated magnetic beads were mixed with 20 μg of bacterial antibody, *e.g.* anti-*E. coli* Ab, anti-*B. subtilis* Ab and anti-*S. aureus* Ab, respectively, in 200 μL of PBST buffer (10 mM phosphate buffered saline, pH 7.4, containing 0.05% tween-20). The mixture was incubated at room temperature for 30 min with continuous shaking. The binding product was harvested by magnetic separation, *i.e.* using an external magnet to precipitate the magnetic beads and discarding all the supernatant. This magnetic separation process took ~ 1 min. The obtained bead-antibody conjugations, *e.g.* MB-Ab$_{E.coli}$, MB-Ab$_{B.subtilis}$, MB-Ab$_{S.aureus}$, were used as bacterial species-specific affinity probes. Each of probes was re-suspended in 100 μL of PBST buffer for immediate use, or stored at 4 °C fridge for the usage within 4 weeks. To capture bacteria from every 1 mL of liquid sample, 5 μL of a MB-Ab probe was used.

## 2.4 Bacteria culture

*E. coli* strain DH5α, *B. subtilis* strain 168M, *E. coli* strain ATCC 25922 and extended-spectrum β-lactamase-producing *E. coli* (ESBL-*E. coli*) were grown as

pre-cultures in lysogeny broth at 37 °C for 6 h with continuous shaking at 200 rpm. 100 μL of each pre-culture was added into 3 mL of lysogeny broth and incubated overnight at 37 °C with continuous shaking at 200 rpm. The obtained fresh cultures were afterwards used for measurements. Concentrations of bacterial cells in their fresh cultures were determined by measuring the optical density at 600 nm ($OD_{600nm}$), with 1.0 $OD_{600nm}$ corresponding to $\sim 8 \cdot 10^8$ cells·mL$^{-1}$.

## 2.5 Capture and enrichment of bacteria *via* immuno-affinity

To capture and enrich bacterial cells from every 1 mL of liquid sample, 5 μL of a previously prepared MB-Ab affinity probe was added into the sample. The mixture was incubated at 37 °C for 30 min with continuous shaking, allowing the binding of antibodies to the surface of target bacterial cells. The bead-captured bacteria were harvested by magnetic separation, *i.e.* using an external magnet to collect the bead-captured bacteria and discarding all the supernatant.

## 2.6 Screening of antimicrobial drugs

Once the species identification of the pathogen was completed, the blood culture liquid, either from the aerobic bottle or anaerobic bottle (two bottles generated the similar result), was used for the screening of antimicrobial drugs. The volume of blood culture liquid used for each antibiotic testing was 0.5 mL. Here, nine antibiotics were tested, together with an antibiotic-free positive control assay. Therefore, 5 mL of the culture liquid was taken out from the blood culture bottle, and was centrifuged at 1,000 rpm for 3 min to precipitate blood cells. 3 mL of the supernatant containing pathogens was collected and mixed with 7 mL of lysogeny broth, followed by the addition of previously prepared MB-Ab$_{E.coli}$ probe (50 μL). The mixture was incubated at 37 °C for 30 min with continuous gentle shaking. The obtained bead-captured pathogens were harvested by magnetic separation, and then distributed evenly to ten aliquots. Nine of the aliquots were re-suspended respectively in 20 μL lysogeny broth containing certain concentration of an antibiotic. The mixtures were incubated at 37 °C for 90 min with continuous shaking. At the same time, the tenth aliquot was incubated with pure lysogeny broth (in the absence of antibiotics) as positive control. Then 5 μL of 625 μM resazurin was added into each of ten mixtures to reach a final resazurin concentration of 125 μM. The mixtures were incubated for 30 min in the microchip, allowing the reaction between the bacteria and the indicator. The mixtures were then analysed by differential pulse voltammetry using the M-POT device. The concentration of each antibiotic was set as the highest MIC (minimum inhibitory concentration) value for susceptible interpretation according to the *Clinical and Laboratory Standards Institute* (CLSI) guidelines. For example, the concentration of cefpodoxime was set as 2 μg·mL$^{-1}$, since

the highest MIC value for susceptible interpretation according to the CLSI guidelines (2017 version) is 2 µg·mL$^{-1}$. Details for setting the concentration of each antibiotic are explained in the **Appendix**.

## 2.7 Antimicrobial drugs MIC determination

A "quasi" antimicrobial drugs MIC determination assay was performed using a similar procedure as the above antimicrobial drug screening. Instead of treating the bead-captured pathogen with a single concentration of each antibiotic, the treatment was conducted with 2-fold increased concentrations of each antibiotic in parallel. The concentrations were set according to the tested antibiotic, and should at least include the MIC threshold values for susceptible, intermediate and resistant interpretation according to the CLSI guidelines. For example, the concentrations of cefpodoxime were set as 0 (positive control), 0.5, 1, 2, 4, 8, 16 and 32 µg·mL$^{-1}$, as the MIC threshold values provided by the CLSI guidelines (2017 version) were $\leq 2$ µg·mL$^{-1}$ for susceptible interpretation, 4 µg·mL$^{-1}$ for intermediate interpretation and $\geq 8$ µg·mL$^{-1}$ for resistant interpretation. Details for setting the concentration of each antibiotic are explained in the **Appendix**. The testing for different antibiotics were conducted in parallel, taking advantage of the high-throughput microchip/M-POT device.

## 2.8 Amperometric measurements

All amperometric measurements were conducted with the microchips and the home-made M-POT device, which contained an integrated microchip holder with implanted eight magnets and an OEM EmStat MUX8 multiplex potentiostat (PalmSens, Houten, Netherlands). The signal recording and calculation were operated using the PSTrace 4.8 software. The microchips containing the mixtures of indicators, bead-captured bacteria, lysogeny broth, and antibiotics in the case of antimicrobial susceptibility assay, were firstly incubated at 37 °C for 25 min, allowing the reaction between the indicators and bacterial cells. The microchips were then loaded into the microchip holder for 5 min of equilibration, to concentrate all the bead-captured bacteria on the surface of working electrodes. The reaction between indicators and bacteria continued during this 5 min equilibration. The mixtures were then analysed by cyclic voltammetry or differential pulse voltammetry. The parameters employed for cyclic voltammetry were 10 mV step potential, 100 mV/s scan rate, within the potential window between 0.0 V and –0.8 V, starting with the negative forward scan. And the parameters for differential pulse voltammetry were 10 mV step potential, 100 mV pulse potential, 0.05 s pulse time, with scanning starting from 0.0 V and ending at –0.8 V. All the samples in one microchip were measured simultaneously. The measurement time for each sample was ~ 1 min.

# 3. Results and discussion

## 3.1 Immuno-affinity isolation of bacteria from complex matrices

Bacterial species-specific antibodies, *e.g.* anti-*E. coli* antibody, anti-*B. subtilis* antibody, anti-*S. aureus* antibody, *etc.*, were bound to protein A/G-coated superparamagnetic beads (~ 1 μm diameter) to generate bacteria affinity probes MB-Ab.[12] The recombinant protein A/G on the bead surface contained six binding domains to IgG isotype antibody, providing a convenient and universal tool for antibody binding.[13] The MB-Ab probes showed high efficiency to selectively capture and enrich the target bacteria from complex matrices like human whole blood, which has already been demonstrated in CHAPTER II of this thesis by the technique of MALDI-TOF mass spectrometry. As a further confirmation, the test was conducted with multi-species contaminated human whole blood samples. Specifically, freshly collected human whole blood was spiked with $5 \cdot 10^8$ cells·mL$^{-1}$ *E. coli* (strain DH5α) and $5 \cdot 10^8$ cells·mL$^{-1}$ *B. subtilis* (strain 168M). The blood sample was centrifuged at 1,000 rpm for 3 min at room temperature to precipitate the blood cells, and the supernatant was harvested and two-fold diluted with PBST buffer (10 mM phosphate buffered saline, pH 7.4, containing 0.05% tween-20). MB-Ab$_{E.coli}$ or MB-Ab$_{B.subtilis}$ probe was added into the 1 mL of the above mixture, and incubated at 37 °C for 30 min, allowing the binding of antibodies to the target bacteria. The isolation product was harvested by magnetic separation with all the supernatant discarded. The obtained isolate was dissolved in 2 μL of pure water, and then transferred onto the MALDI target plate by pipetting. After drying at room temperature (~ 5 min), the sample spot was overlaid with 1 μL of sinapinic acid matrix (20 mg·mL$^{-1}$ in 50/49.9/0.1% acetonitrile/water/trifluoroacetic acid) for MALDI-TOF mass spectrometry measurement. The measurement was conducted at linear positive mode within the mass range of 2,000-20,000 *m/z*. The generated mass spectra were compared with the reference spectrum of *E. coli* or *B. subtilis* by calculating the spectral cosine similarity score. The reference spectra were generated from 2 μL of pure *E. coli* or *B. subtilis* cells that were suspended in pure water with the concentration of $5 \cdot 10^8$ cells·mL$^{-1}$. As shown in **Figure 4.1 a**, the MB-Ab$_{E.coli}$ isolation product showed very high spectrum cosine similarity (0.966) to the *E. coli* reference, while very low similarity (0.005) to *B. subtilis* reference. Similarly, the MB-Ab$_{B.subtilis}$ probe was efficient for selectively isolating *B. subtilis*, with the generated spectrum showing high similarity (0.987) to the *B. subtilis* reference spectrum (**Figure 4.1 b**), but quite low similarity (0.004) to the *E. coli* reference spectrum. As has been illustrated in CHAPTER II, a spectrum cosine similarity ≥ 0.8 ensures a reliable identification at the species level.[14] This indicates that the MB-Ab probes are highly able to selectively isolate and enrich bacterial pathogens from complex samples.
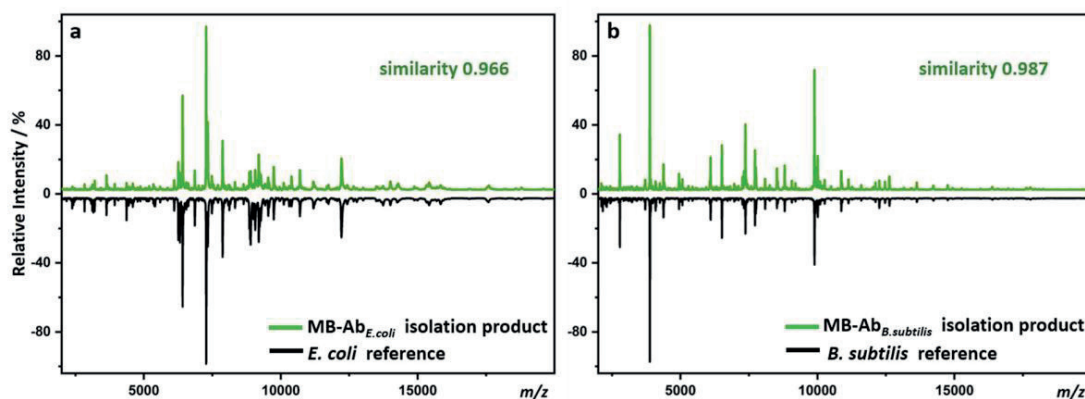
**Figure 4.1** (**a**) Comparison of MALDI-TOF mass spectra generated from pure *E. coli* (reference) and the isolation product obtained from multi-bacteria-contaminated human blood using the MB-Ab$_{E.coli}$ affinity probe; (**b**) comparison of MALDI-TOF mass spectra generated from pure *B. subtilis* (reference) and the isolation product obtained from multi-bacteria-contaminated human blood using MB-Ab$_{B.subtilis}$ affinity probe.

## 3.2 Inkjet-printed electrochemical sensors

Inkjet-printed microchips were used as microtiter plates for amperometric read-out *via* the portable, home-made M-POT device, providing stable and reproducible signal responses for point-of-care testing. Each of the microchips comprised eight independent wells (4 mm diameter), allowing eight tests in parallel. Each well contained on the bottom a carbon nanotube (CNT) working electrode (WE), a silver/silver chloride quasi-reference electrode (RE), a CNT counter electrode (CE) and silver tracks for electrical connection (**Figure 4.2 a**).

The eight independent three-electrode systems on each microchip were fabricated through a subsequent, highly reproducible inkjet printing process. The first step was printing the silver layer for electrical connection and the quasi-reference electrodes. The printed silver layer was converted into conductive traces by photonic flash sintering within second. Silver is not a suitable material for reference electrodes, as the facile chemical modification of the surface (*e.g.* by oxidation) could cause a drift of the potential during measurements. Due to that, silver/silver chloride (Ag/AgCl) quasi-reference electrodes were printed, by drop-casting 1 µL of bleach solution for 3 min on a small area of the silver layer. The electrodes were then washed with deionized water and dried with a stream of nitrogen. The obtained quasi-reference electrodes were ready-to-use and showed long-term stability during dry storage of more than 3 months.[15,16] Afterwards, carbon nanotube patterns were printed to form the working and

counter electrodes. According to the manufacturer, the carbon nanotube ink is composed of a network of carbon nanotubes, mostly of double-walled nanotubes with an unknown amount of single-walled nanotubes, with average length of $0.8 \pm 0.6$ µm and diameter below 2 nm. The electrodes were prepared with four inkjet-printed layers, containing randomly distributed and densely overlapping nanotubes. The UV curable dielectric ink was printed to generate a protection layer for the conductive traces and to precisely define the active area of the three electrodes. The fabrication process was finished by placing a plastic sheet, which has been drilled with eight mechanically well-defined wells, on the top of the inkjet-printed three-electrodes. Microtiter plates composed of eight independent electrochemical wells were thus generated. To be noted, the active electrode areas were defined by the highly reproducible inkjet printing process, being 0.72 mm$^2$ for each electrode. Meanwhile, the wells, in diameter slightly larger than the active electrode areas, defined the sample volume (20-50 µL).
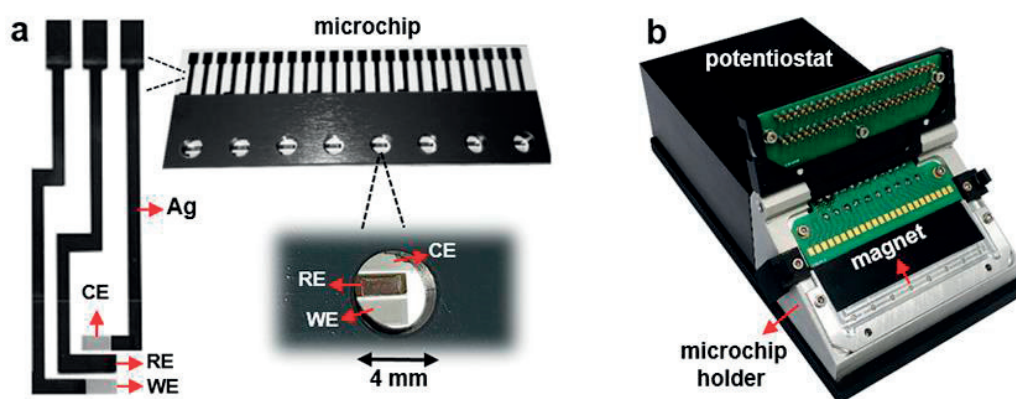


**Figure 4.2** Photos of (**a**) one inkjet-printed microchip and (**b**) the M-POT device.

According to our previous reports, the carbon nanotube working electrode showed superior electrochemical responses compared to other commercial carbonaceous electrodes, and each chip was reusable for at least 20 times.[10,11,17] By using the microchips, bacteria isolated from large-volume matrices (*e.g.* 1-10 mL) by MB-Ab probes could be enriched into the as low as 20 µL final working volume, highly concentrating the cells and thus elevating the detection sensitivity. The M-POT device (16 cm × 9 cm × 5 cm) comprised a multiplex potentiostat and a microchip holder with eight magnets (2 mm in diameter) implanted (**Figure 4.2 b**). The holder provided electric connection between the microchip and the potentiostat, thereby avoiding the use of cables and making the device user-friendly. The implanted magnets matched the

microchip working electrode positions to concentrate all the bead-captured bacteria on the working electrode area (0.72 mm$^2$), further improving the detection sensitivity, which will be demonstrated later in this chapter.

One of the eight-well microchips was electrochemically characterized by cyclic voltammetry using ferrocene methanol (FcMeOH) as the redox mediator. The measurement was conducted with the home-made M-POT device. The cyclic voltammetry measurement was accomplished with one electron oxidation of FcMeOH to FcMeOH$^+$ during the positive forward scan and the reduction of FcMeOH$^+$ to FcMeOH in the reverse negative scan. The cyclic voltammograms generated from the eight channels were shown in **Figure 4.3**. It was clear that the eight curves overlapped well with each other with almost the same scanning current and reduction/oxidation potential. This result demonstrated the amperometric response of the microchip was highly reproducible, which should be attributed to the precise working electrode area defined by the inkjet printing and the stability of the Ag/AgCl quasi-reference electrodes. The stable amperometric response from each channel also indicated that the microchip and the potentiostat were connected well with each other through the microchip holder. Observation of the cyclic voltammograms in **Figure 4.3** finds the cathodic and anodic peak-to-peak separation is around 85 mV, larger than the value of 59 mV for a reversible system. This increased peak distance is mainly caused by the uncompensated resistance drop of the printed electrodes.
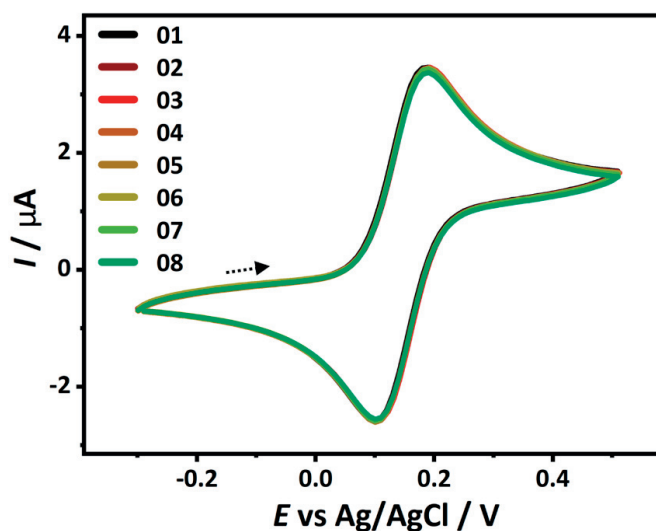


**Figure 4.3.** Cyclic voltammograms of FcMeOH (2 mM, dissolved in 0.1 M KNO$_3$) obtained from the eight wells of a single inkjet-printed microchip. The measurements were conducted with the M-POT device, with the scan rate of 100 mV·s$^{-1}$.

## 3.3 Redox indicators for measuring metabolic activity of bacteria

Tetrazolium salts and resazurin have been widely used as indicators for measuring metabolic activity of microorganisms.[18,19] Metabolically active bacteria chemically reduce these compounds due to the reducing cellular environment, with reactions happening mainly on the plasma membrane where the respiratory electron transport chain operates (or *via* trans-plasma membrane electron transport in the presence of electron mediator).[20-22] The reduction products have usually a characteristic colour and/or fluorescence emission, and various colorimetric and fluorometric cell viability assays have been reported.[23-25] Many indicators are proven to be stable, sensitive and minimally toxic to living cells, and available in ready-to-use commercial kits.[26] Recently, electrochemical properties of certain indicators were also explored.[27,28]
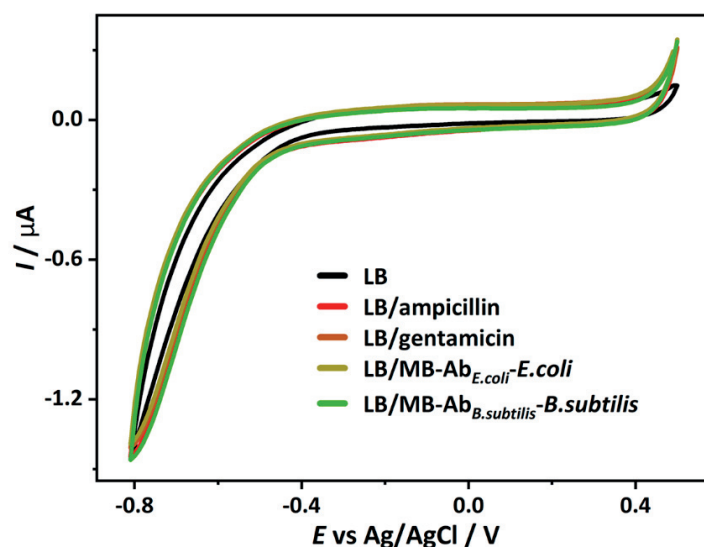


**Figure 4.4.** Cyclic voltammograms of lysogeny broth (LB), lysogeny broth containing antibiotics (*e.g.* ampicillin, gentamicin) and lysogeny broth containing MB-Ab affinity probes-captured bacteria (*e.g.* MB-Ab$_{E.coli}$-*E. coli,* MB-Ab$_{B.subtilis}$-*B. subtilis*). The volume of each sample was 20 μL. The measurements were conducted with microchip/M-POT device, with the scan rate of 100 mV·s$^{-1}$.

Here, viable bacteria were detected based on amperometric response of indicators. Bead-captured bacteria were mixed with indicators in lysogeny broth, together with antibiotics in case of antimicrobial susceptibility assay. The redox state of the indicators were monitored amperometrically directly from the mixture (20 μL) using the

microchip/M-POT device. The nutritionally rich lysogeny broth was favourable for maintaining the bacteria metabolic activity, and acted as supporting electrolyte. To investigate the amperometric response of these components other than the indicators, lysogeny broth, lysogeny broth containing antibiotics (*e.g.* ampicillin, gentamicin) and lysogeny broth containing bead-captured bacteria (*e.g.* MB-Ab$_{E.coli}$-*E. coli,* MB-Ab$_{B.subtilis}$-*B. subtilis*), were analysed with cyclic voltammetry using the microchip/M-POT device. The obtained cyclic voltammograms are displayed in **Figure 4.4**. The bead-captured bacteria were prepared by using MB-Ab$_{E.coli}$ or MB-Ab$_{B.subtilis}$ affinity probes to capture bacterial cells from 1 mL of a fresh culture of *E. coli* (strain DH5α) or *B. subtilis* (strain 168M) with cell concentration around $5 \cdot 10^8$ cells·mL$^{-1}$. **Figure 4.4** shows that lysogeny broth can be used as a suitable supporting electrolyte for amperometric measurement, and neither bead-captured bacteria (*e.g.* MB-Ab$_{E.coli}$-*E. coli,* MB-Ab$_{B.subtilis}$-*B. subtilis*) nor the antibiotics (*e.g.* ampicillin, gentamicin) generate any peak within the selected potential range (0.5 V to –0.8 V, *vs* Ag/AgCl). The results indicate that none of those components interfere with the amperometric read-out from the indicators.

The proposed application was generally feasible with a wide variety of indicators. Six indicators, which have been commonly used for colorimetric and/or fluorometric cell viability or proliferation assays, were selected as representatives to investigate their performance for bacteria detection *via* the present immuno-affinity amperometric method. They were prototype tetrazolium salt TTC (2,3,5-triphenyl tetrazolium chloride), the early tetrazolium derivatives such as INT (2-(4-iodophenyl) -3-(4-nitrophenyl)-5-(phenyl) tetrazolium chloride) and CTC (5-cyano-2,3-di-(p-tolyl) tetrazolium chloride), the new generation of water-soluble tetrazolium derivatives like WST-1 and WST-8, and the blue dye resazurin (RS). The WST-1 is a commercial ready-to-use reagent, containing at least 2-(4-Iodophenyl)-3-(4-nitrophenyl) -5-(2,4-disulfophenyl)-2*H* tetrazolium monosodium salt and an electron mediator mPMS (1-methoxy-5-methyl-phenazium methyl sulfate). The WST-8 is also a commercial reagent, containing at least 2-(2-methoxy-4-nitrophenyl)-3-(4-nitrophenyl)-5- (2,4-disulfophenyl)-2*H* tetrazolium monosodium salt and the electron mediator mPMS. During the investigation, a fresh culture of *E. coli* (strain DH5α), with cell concentration around $5 \cdot 10^8$ cells·mL$^{-1}$, was used as the model bacteria sample. *E. coli* cells were isolated from 1 mL of the fresh culture using previously prepared MB-Ab$_{E.coli}$ probe. After magnetic separation, the bead-captured *E. coli* (MB-Ab$_{E.coli}$-*E. coli*) was re-suspended in 20 µL of lysogeny broth containing one of the indicators. Each of the mixture was incubated for 30 min in the microchip well, allowing chemical reaction between the bacteria and the indicator. The resulting mixtures were analysed by cyclic voltammetry within the potential window between 0.0 V and –0.8 V (*vs* Ag/AgCl) using

cthe M-POT device. The concentration of each indicator in the lysogeny broth was tentatively set as 1 mM for TTC, INT, CTC, RS, and 10-fold dilution for the WST-1 and WST-8 commercial reagent. As a bacteria-free control, 20 µL of lysogeny broth containing each of the pure indicators underwent the same measurement. The results are shown in **Figure 4.5**. The potential was scanned negatively to electrochemically reduce the indicators.[29,30] Peak current declined clearly with the presence of bead-captured bacteria, owing to the competitive chemical reduction caused by cellular respiration of bacteria. These results showed that all these representative indicators could be used for the detection of bacteria.
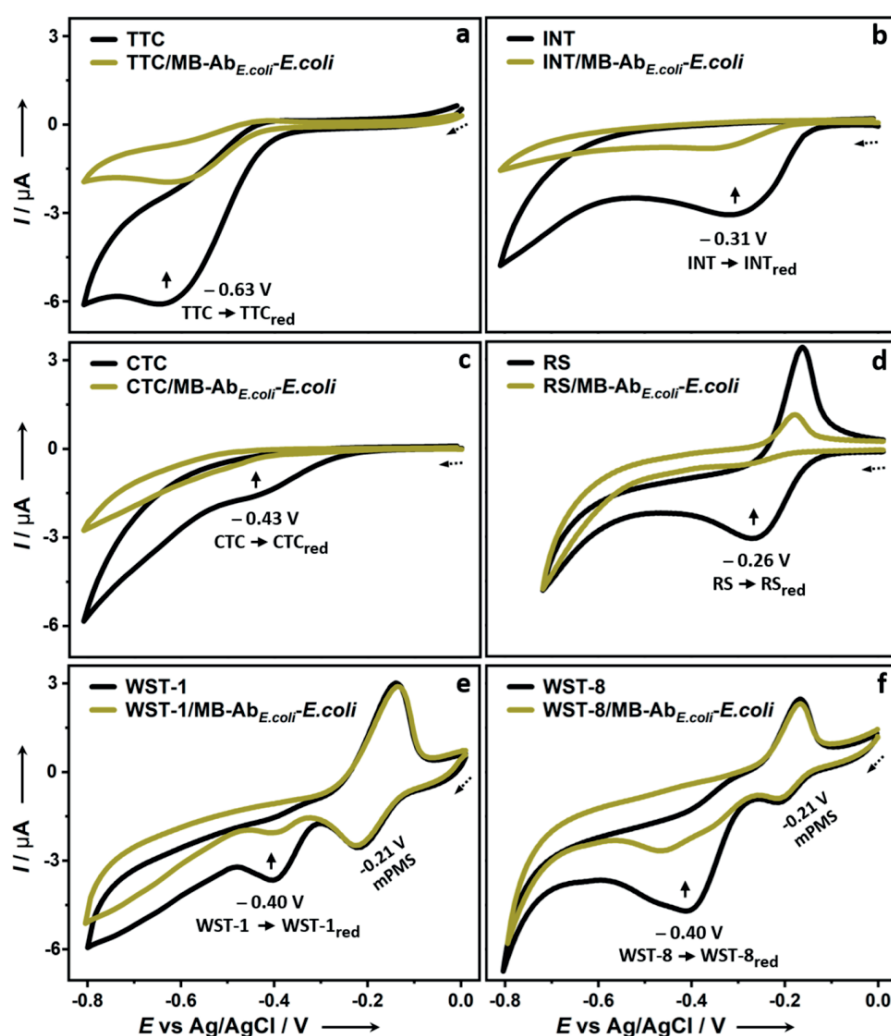


**Figure 4.5** Cyclic voltammograms of six indicators without and with the presence of MB-Ab$_{E.coli}$-*E. coli*. The indicators were (**a**) TTC, (**b**) INT, (**c**) CTC, (**d**) RS, (**e**) WST-1 and (**f**) WST-8.
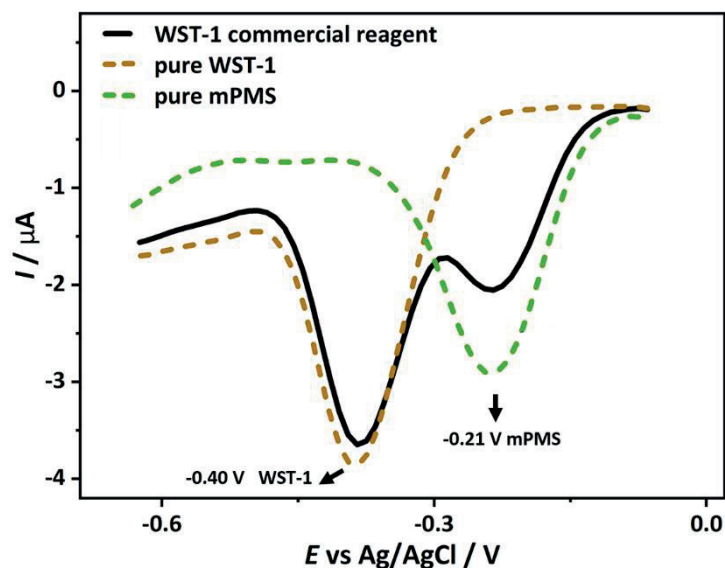
**Figure 4.6** Differential pulse voltammograms of WST-1 commercial ready-to-use reagent (10-fold dilution in lysogeny broth), pure WST-1 (500 µM in lysogeny broth) and pure mPMS (20 µM in lysogeny broth). The measurements were conducted with the microchip/M-POT device, with the scanning starting from 0.0 V and ending at –0.8 V (*vs* Ag/AgCl).

Tetrazolium salts contain at least one tetrazole ring in their molecular structure. The positive charge on the tetrazole ring facilitates the transfer of most tetrazolium salts across the plasma membrane of viable cells, since the membrane potential is –30 to –60 mV.[18] Therefore, most tetrazolium salts can be directly chemically reduced by metabolically active bacteria during cellular respiration. However, the new generation of water-soluble tetrazolium salts like WST-1 and WST-8 contain two sulfonate groups in their molecular structure, making the molecules negatively charged and excluded from bacterial cells. Reduction of this type of tetrazolium salts requires an intermediate electron acceptor (also called electron mediator). In the presence of an electron mediator, these tetrazolium salts are reduced through trans-plasma membrane electron transport.[18,22] The electron mediator commonly used in conjugation with WST-1 and WST-8 is mPMS, as contained in the commercial ready-to-use reagents used in this work. In **Figure 4.5**, an additional peak at –0.21 V was noticed for WST-1 and WST-8. It should come from mPMS. As a demonstration, pure WST-1, pure mPMS, and the WST-1 commercial ready-to-use reagent that contains both WST-1 and mPMS were analysed by differential pulse voltammetry. As shown in **Figure 4.6**. The peak at –0.21 V measured from the WST-1 commercial reagent matched the peak from pure mPMS,

confirming that this peak indeed came from the electrochemical reduction of mPMS. Meanwhile, the peak at –0.40 V measured from the WST-1 commercial reagent matched the peak from pure WST-1, confirming that this peak refers to electrochemical reduction of WST-1. To be noted, **Figure 4.5** showed generally broad and varying reduction waves for the six indicators. The electrochemical reductions of TTC, INT, CTC were irreversible, as demonstrated by the missing oxidation peak during the reverse scan (**Figure 4.5 a-c**). These three indicators are similar tetrazolium salt derivatives, but their reduction peaks (under the condition of identical initial concentration) were in different shapes and currents, suggesting different kinetics of the electrochemical reaction. In the case of RS, the peak at –0.26 V (*vs* Ag/AgCl) (**Figure 4.5 d**) corresponded to the irreversible reduction of RS to resorufin. Resorufin can be further reduced into dihydroresorufin. This second reduction generated quite low reduction current (hardly visible from **Figure 4.5d**), but it really happened, which will be explained later. This second reduction step was reversible, and the corresponding oxidation peak during the reverse scan was quite clear, shown as the sharp peak appearing at –0.16 V (*vs* Ag/AgCl) in **Figure 4.5 d**. This sharp peak with a higher peak current could be attributed to the adsorption of the electrochemical reduction product on the carbon nanotube electrode surface. Carbon nanotubes contain hexagonally arranged $sp^2$ carbons facilitating the adsorption of aromatic molecules. The reduction of WST-1 and WST-8 were also irreversible. The electron mediator mPMS itself is electroactive with its electrochemical reduction peak appearing at –0.21 V (*vs* Ag/AgCl), as explained in **Figure 4.6**, and the corresponding oxidation peak during the reverse scan appearing at –0.17 V (*vs* Ag/AgCl), as shown in **Figure 4.5 e**, **f**. Compared to the reduction peak, the oxidation peak is sharper in shape and higher in current, indicating the adsorption of (mPMS)$_{red}$ on the electrode surface. The postwave in the voltammograms of WST-8 (in **Figure 4.5 f**, around –0.45 V *vs* Ag/AgCl, next to the main reduction peak of WST-8 at –0.40 V *vs* Ag/AgCl) could give further indication of the adsorption phenomenon. The observed effects, including the adsorption and the reaction kinetics, have not been studied in detail in this work. It is important to point out that these effects do not limit the electrochemical analysis, as it is possible to clean the inkjet-printed electrodes or to use the electrodes disposably.

Under physiological pH condition (pH 7.4), for example in the lysogeny broth, tetrazolium salts are reduced into formazans, accompanied with the breakup of the four nitrogen atoms-contained five membered unsaturated tetrazole ring, which is positive charged.[31-33] The reduction, including chemical reduction caused by bacterial respiration and electrochemical reduction occurring on the carbon nanotube working electrode, of the five tetrazolium salts are shown as following:

*1)* reduction of TTC



TTC              TTC Formazan

*2)* reduction of INT



INT            INT Formazan

*3)* reduction of CTC



CTC           CTC Formazan

*4)* reduction of WST-1



WST-1          WST-1 Formazan

mPMS
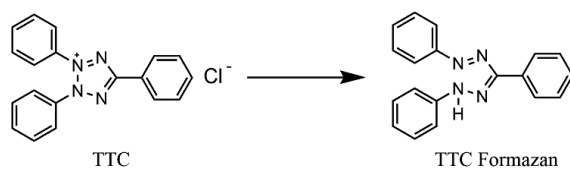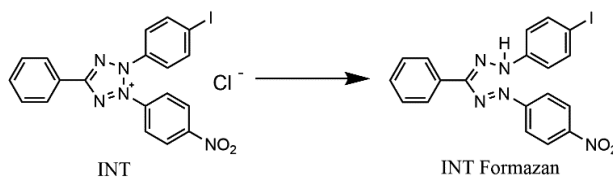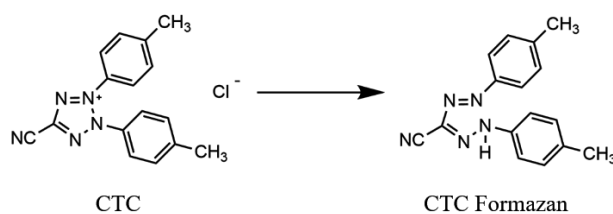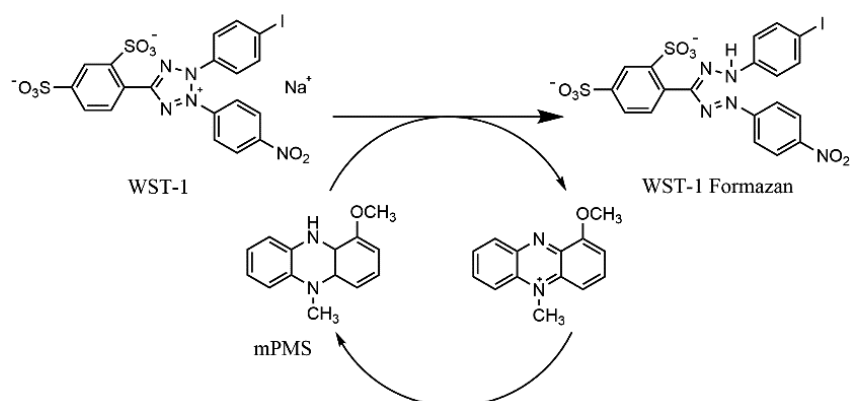
*5)* reduction of WST-8



WST-8          WST-8 Formazan

mPMS
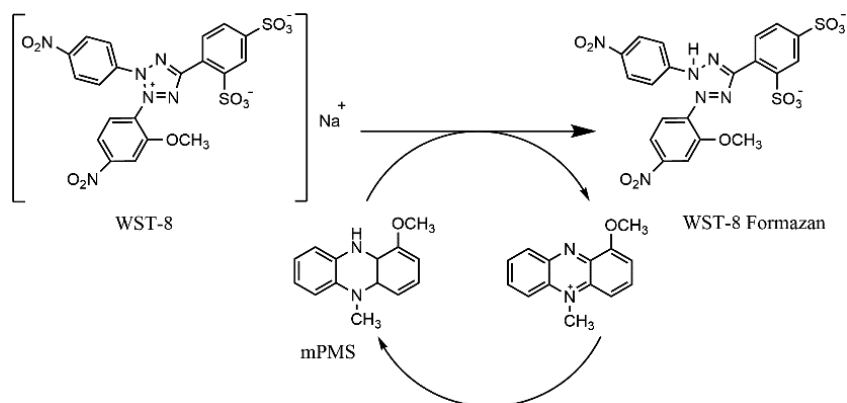
Different from the tetrazolium salts, the reduction of resazurin is due to the loss of an oxygen atom loosely bound to the nitrogen atom of the phenoxazine nucleus:



Resazurin (RS)          Resorufin          Dihydroresorufin

The reduction comprises two steps. During the first step, the weakly-fluorescent resazurin is irreversibly reduced into resorufin, which has fluorescence emission at 596 nm.[34] This step generated the main reduction current during amperometric scanning, shown as the peak appearing at –0.26 V (*vs* Ag/AgCl) in the cyclic voltammograms in **Figure 4.5 d** and in the differential pulse voltammograms in **Figure 4.7**. The resorufin can be further reduced into non-fluorescent dihydroresorufin. This second reduction step is reversible by atmospheric oxygen.[35] During amperometric scanning, the second-step reduction current was quite low, shown as the weak peak appearing at –0.43 V (*vs* Ag/AgCl) in the differential pulse voltammograms in **Figure 4.7**. As discussed previously, this second-step reduction was associated with the sharp oxidation peak during the positive forward scan shown in **Figure 4.5 d**, as the dihydroresorufin were absorbed on the carbon nanotube working electrode.
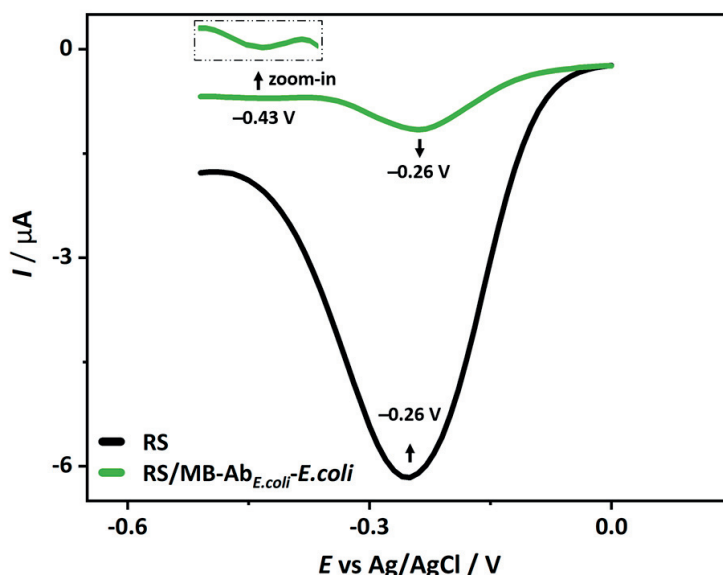


**Figure 4.7** Differential pulse voltammograms of pure RS (1 mM) with and without 30 min incubation with bead-captured *E. coli* (MB-Ab$_{E.coli}$-*E. coli*). The scan was negative forward, starting from 0.0 V and ending at –0.8 V (*vs* Ag/AgCl).
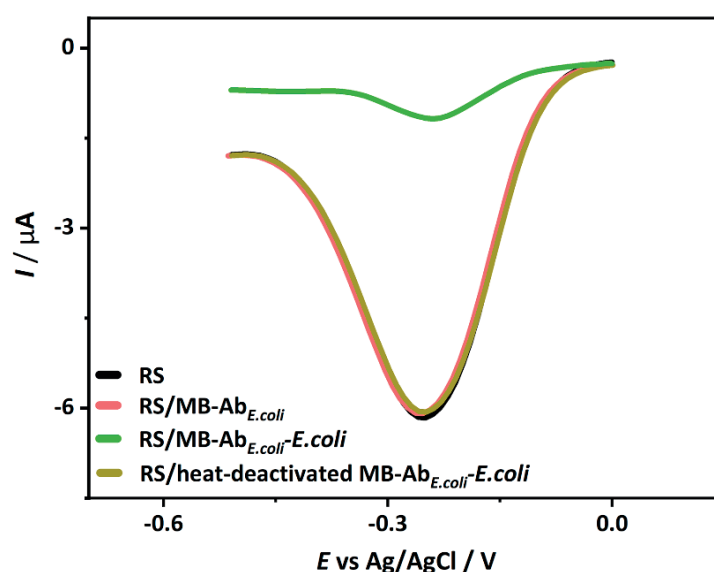
**Figure 4.8** Differential pulse voltammograms of pure RS (1 mM) and RS (1 mM) after 30 min of incubation with MB-Ab$_{E.coli}$, MB-Ab$_{E.coli}$-*E. coli*, or heat-deactivated MB-Ab$_{E.coli}$-*E. coli*, respectively.

Before using the indicators for the detection of living bacteria, we need to make sure that the indicators were chemically reduced by metabolically active bacteria only, neither by the MB-Ab affinity probes nor dead bacteria. As proof, 20 µL of lysogeny broth containing any one of the indicators (*e.g.* RS, 1mM) was incubated respectively with *i*) MB-Ab$_{E.coli}$ affinity probe, *ii*) bead-captured *E. coli*, *i.e. E. coli* captured from a fresh culture with cell concentration around $5 \cdot 10^8$ cells·mL$^{-1}$ by MB-Ab$_{E.coli}$ affinity probe, *iii*) heat-deactivate bead-captured *E. coli*, *i.e.* treating the above bead-captured *E. coli* at 120 °C for 20 min to kill the bacteria. After 30 min of incubation, the mixtures were conducted with differential pulse voltammetry scanning from 0.0 V to –0.8 V using the microchip/M-POT device. The obtained curves are shown in **Figure 4.8**. Compared to the case of pure RS, only the freshly prepared bead-captured *E. coli* led to the decline in scanning peak current. This confirmed that the MB-Ab probes alone and dead bacteria did not reduce indicators.

## 3.4 Quantification of bacterial cells

On the basis of all the above demonstrations, the immuno-affinity amperometric approach was employed for living bacteria detection with the utilization of one of indicators. For calculation convenience, differential pulse voltammetry was employed to monitor the indicator, and the reduction peak was integrated to get peak area decline percentage, defined as $\Delta A\% = (A_0 - A) / A_0 \times 100\%$. $A_0$ is the peak integration from the

pure indicator, being constant once the indicator concentration is fixed. *A* corresponds to the case with the presence of bead-captured bacteria.
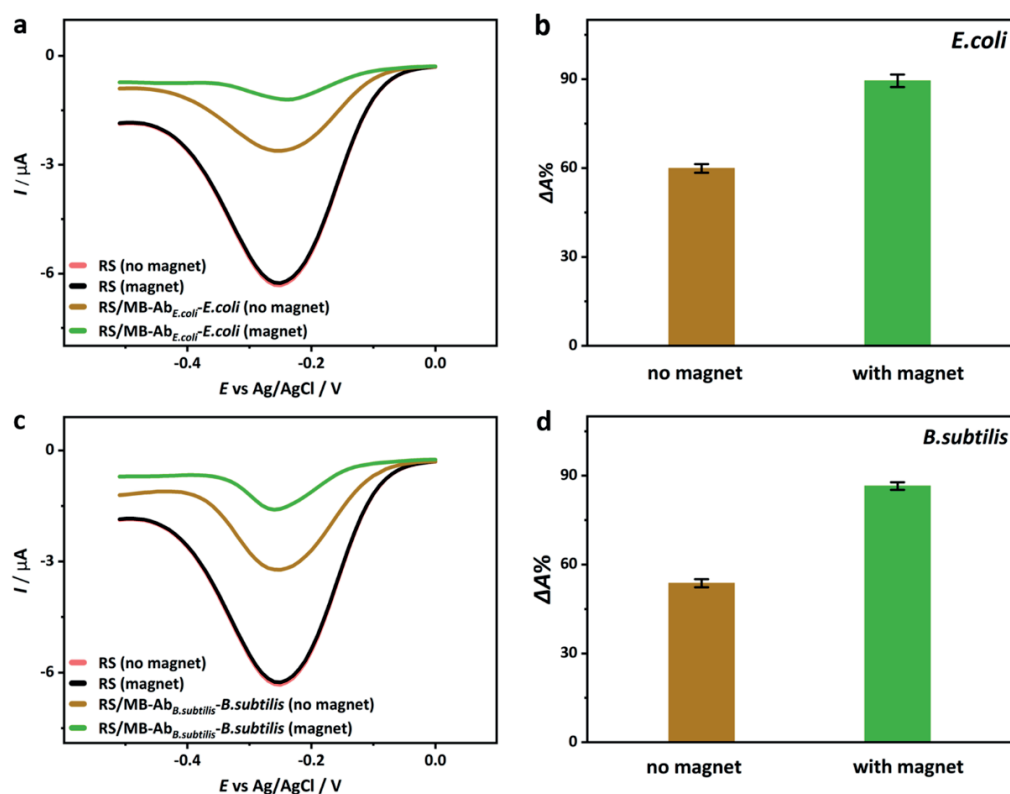


**Figure 4.9** (**a**) Representative differential pulse voltammograms of RS (1 mM) after 30 min reaction with MB-Ab$_{E.coli}$-*E. coli* with and without the installation of magnets in the microchip holder, with the corresponding peak current decline percentage shown in graph (**b**); (**c**) representative differential pulse voltammograms of RS (1 mM) after 30 min reaction with MB-Ab$_{B.subtilis}$-*B. subtilis* with and without the installation of magnets in the microchip holder, with the corresponding peak current decline percentage shown in graph (**d**).

As mentioned before, eight magnets were installed in the microchip holder to improve the detection sensitivity. Now we can prove it quantitatively. *E. coli* and *B. subtilis* were tested as the analyte models, and RS (1 mM) was used as the indicator. 20 µL of RS, prepared in lysogeny broth, was mixed with bead-captured *E. coli* or bead-captured *B. subtilis*. The mixtures were incubated for 30 min in the microchip, allowing the reaction between the bacterial cells and the indicator. Thereafter, the mixtures were analysed by differential pulse voltammetry from 0.0 V to –0.8 V (*vs* Ag/AgCl). Afterwards, the

magnets were removed from the microchip holder, and the same experiments were repeated. Each test was conducted with triplicates. The bead-captured bacteria were prepared by using MB-Ab$_{E.coli}$ or MB-Ab$_{B.subtilis}$ affinity probes to capture bacterial cells from 1 mL of a fresh culture of *E. coli* or *B. subtilis* with cell concentration around $5·10^8$ cells·mL$^{-1}$. During the differential pulse voltammetry scanning, the non-chemically reacted RS was electrochemically reduced on the working electrode. The generated electrochemical reduction peak was integrated to calculate the signal response, *i.e.* $\Delta A\%$, which was related to the proportion of RS chemically reduced by the bacteria. The generated voltammograms are shown in **Figure 4.9 a** for the *E. coli* sample and **Figure 4.9 c** for the *B. subtilis* sample. For each test, one representative voltammogram was displayed. Compared to the case without magnets, the presence of magnets increased the signal response, *i.e.* $\Delta A\%$, from $59.9 \pm 1.3\%$ to $89.4 \pm 2.1\%$ for the *E. coli* sample (**Figure 4.9 b**), and from $53.7 \pm 1.4\%$ to $86.5 \pm 1.3\%$ for the *B. subtilis* sample (**Figure 4.9 d**). The signal response was thus enhanced by $\sim 49\%$ and $\sim 61\%$ for the two samples, respectively, clearly improving the detection sensitivity. With the installation of magnets, all the bead-captured bacterial cells were concentrated on the working electrode area, which was 0.72 mm$^2$. This led to highly elevated cell concentration on that limited area, and thus more indicators were chemically reduced on that area.
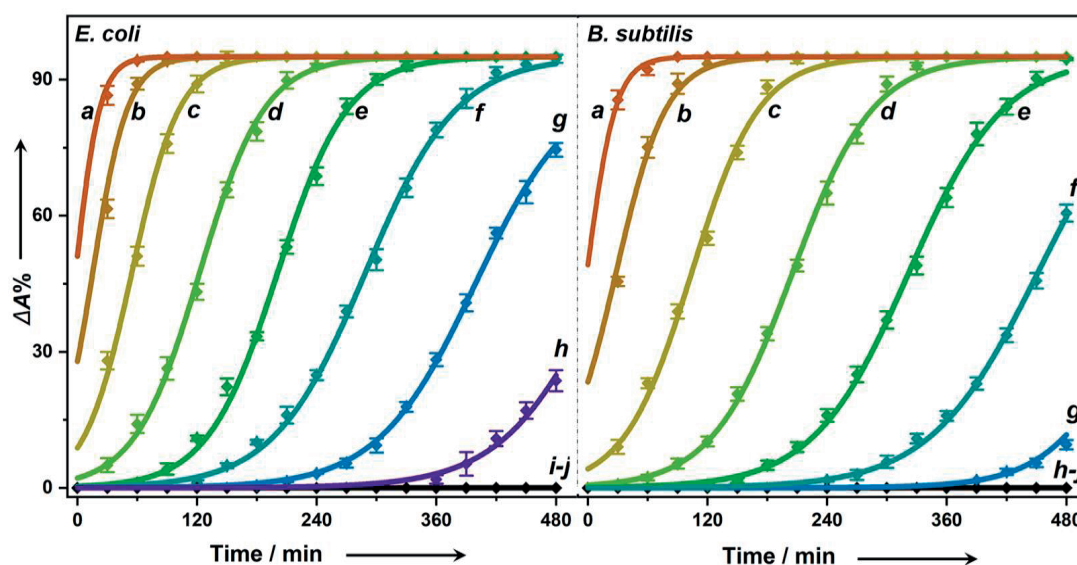


**Figure 4.10** Bacterial species-, cell number- and time-dependent chemical reduction of indicator (1 mM RS). The initial concentrations of *E. coli* and *B. subtilis* in lysogeny broth (1 mL) before immuno-affinity capture/enrichment were $5·10^8$ (*a*), $5·10^7$ (*b*), $5·10^6$ (*c*), $5·10^5$ (*d*), $5·10^4$ (*e*), $5·10^3$ (*f*), 500 (*g*), 50 (*h*), 5 (*i*), and 0 (*j*, negative control) cells·mL$^{-1}$.

*E. coli* and *B. subtilis* were further selected as models for gram-negative bacteria and gram-positive bacteria, respectively, to investigate the ability of the present immuno-affinity amperometric method for the quantification of bacterial cells. RS (1 mM) was still used as the indicator. To be noted, RS was just used as a model indicator, not meaning it was definitely better than all other indicators. MB-Ab$_{E.coli}$ probe was used to capture and enrich *E. coli* cells from 1 mL of lysogeny broth. The cell concentrations in the lysogeny broth were set as $5 \cdot 10^8$, $5 \cdot 10^7$, $5 \cdot 10^6$, $5 \cdot 10^5$, $5 \cdot 10^4$, $5 \cdot 10^3$, 500, 50, 5, 0 (negative control) cells·mL$^{-1}$, obtained by a series of 10-fold dilution of a fresh *E. coli* culture. After 30 min of immuno-affinity recognition between the antibody and the bacterial cells, the bead-captured *E. coli*, *i.e.* MB-Ab$_{E.coli}$-*E. coli*, were harvested by magnetic separation, and then re-suspended in 20 µL of RS (1 mM in lysogeny broth) for incubation at 37 °C. For each concentration, the sample was prepared in sixteen copies in parallel. After every 30 min of incubation, one sample for each concentration was analysed by differential pulse voltammetry from 0.0 V to –0.8 V (*vs* Ag/AgCl), using the microchip/M-POT device with the peak current decline percentage (Δ*A*%) recorded. The measurement was continuously conducted until 480 min. The same tests were performed with *B. subtilis* using MB-Ab$_{B.subtilis}$ as the affinity probe. The evolution of the signal response during the 480 min for both bacteria were shown in **Figure 4.10**. It showed that the reduction of the indicator caused by bead-captured bacteria was dependent on the bacterial cell number and bacterial presence time. This showed the capability of the present method in viable cell quantification. For instance, with
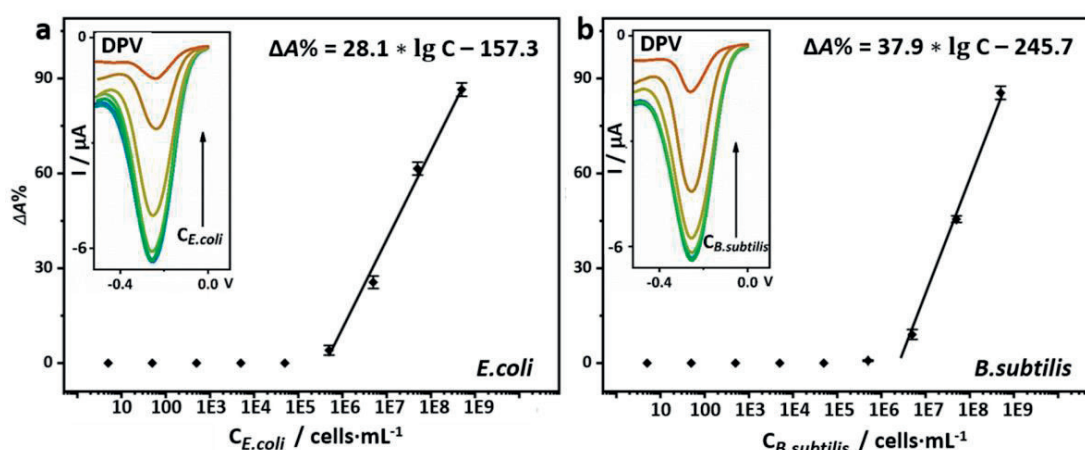


**Figure 4.11** Linear regression between the *ΔA%* of RS (1 mM) at 30 min and the logarithm to the base 10 of (**a**) *E. coli* or (**b**) *B. subtilis* initial concentration (lg C). The inserted curves were the corresponding differential pulse voltammograms recorded at 30 min for different initial cell concentrations.

30 min presence of bead-captured with *E. coli*, a linear regression was obtained between the $\Delta A\%$ value and the logarithm of the cell initial concentration in the range of $5 \cdot 10^8$ - $5 \cdot 10^5$ cells·mL$^{-1}$. The linear fitting equation was $\Delta A\% = 28.1 * \lg C - 157.3$, with statistics adjusted R-squared value of 0.9880 (**Figure 4.11 a**). Similarly, a linear regression was obtained at 30 min between the $\Delta A\%$ and the logarithm of the *B. subtilis* initial concentration in the range of $5 \cdot 10^8$ - $3 \cdot 10^6$ cells·mL$^{-1}$. The linear fitting equation was $\Delta A\% = 37.9 * \lg C - 245.7$, with statistics adjusted R-squared value of 0.9894 (**Figure 4.11 b**). Longer bacterial presence time increased the $\Delta A\%$ due to cell proliferation. Similar linear regressions were obtained for lower concentrations of bacteria when elongating the incubation time, not illustrated in detail here.
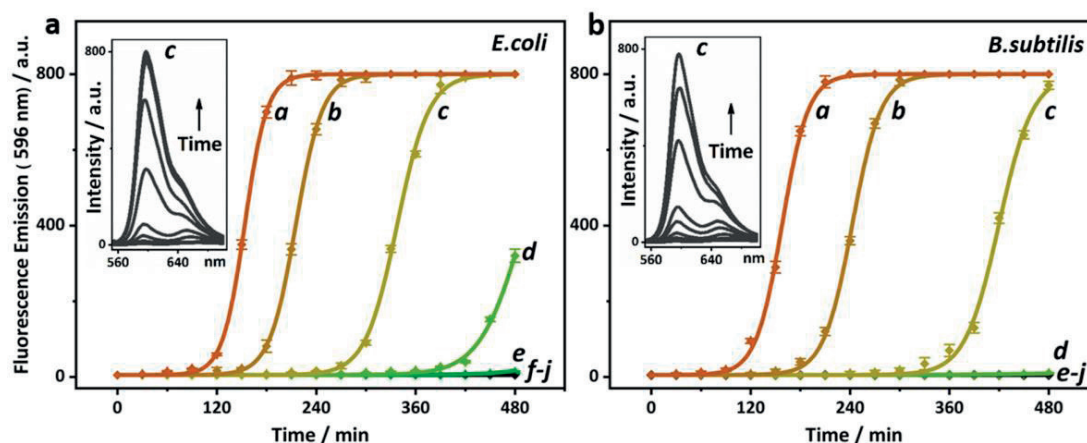


**Figure 4.12** Bacterial cell number- and presence time-dependent reduction of indicator (1 mM RS), measured with fluorometric method. (**a**) *E. coli* and (**b**) *B. subtilis* initial concentrations were $5 \cdot 10^8$ (*a*), $5 \cdot 10^7$ (*b*), $5 \cdot 10^6$ (*c*), $5 \cdot 10^5$ (*d*), $5 \cdot 10^4$ (*e*), $5 \cdot 10^3$ (*f*), 500 (*g*), 50 (*h*), 5 (*i*), 0 (*j*, negative control) cells·mL$^{-1}$ in lysogeny broth. The inserted graphs were the fluorescence emission spectra generated at very 30 min from the *E. coli* or *B. subtilis* sample with initial cell concentration of $5 \cdot 10^6$ cells·mL$^{-1}$ (line *c*).

In order to evaluate the detection sensitivity of the present immuno-affinity amperometric method, the same *E. coli* and *B. subtilis* samples were tested with an often-used fluorometric method, *i.e.* alamarBlue$^{TM}$ cell viability assay. Pure RS is weakly-fluorescent, but the reduced form of RS has strong fluorescence emission at 596 nm. The detection was conducted according to the Thermo Scientific alamarBlue$^{TM}$ assay protocol. Briefly, 1 mM of RS was incubated with *E. coli* or *B. subtilis* with different initial concentrations in 1 mL of lysogeny broth at 37 °C. The cell

concentrations were set as $5 \cdot 10^8$, $5 \cdot 10^7$, $5 \cdot 10^6$, $5 \cdot 10^5$, $5 \cdot 10^4$, $5 \cdot 10^3$, 500, 50, 5, 0 (negative control) cells·mL$^{-1}$, obtained by a series of 10-fold dilution of a fresh *E. coli* or *B. subtilis* culture. After every 30 min of incubation, fluorescence emission of the mixture at 596 nm was recorded using a fluorescence spectrometer (PerkinElmer, LS 55) with 540 nm excitation wavelength. The measurement was continuously conducted until 480 min. The obtained bacterial cell number- and bacteria presence time-dependent signal response from RS were shown in **Figure 4.12**. Representative fluorescence emission spectra generated from *E. coli* or *B. subtilis* sample with initial cell concentration of $5 \cdot 10^6$ cells·mL$^{-1}$ at very 30 min were shown in the inserted graphs.

As shown in **Figure 4.12**, clear fluorescence emission was measured from 1 mM RS after 120 min incubation with $5 \cdot 10^8$ cells·mL$^{-1}$ *E. coli* or *B. subtilis*. At 480 min, fluorescence emission was measured from the sample with initial cell concentration $\geq$ $5 \cdot 10^5$ cells·mL$^{-1}$ for *E. coli* or $\geq 5 \cdot 10^6$ cells·mL$^{-1}$ for *B. subtilis*. Meanwhile, the proposed immuno-affinity amperometric method gave clear signal response within only 30 min for $5 \cdot 10^8$ cells·mL$^{-1}$ bacteria and 480 min for as low as $\sim 10^2$ cells·mL$^{-1}$ bacteria, as previously shown in **Figure 4.10**. Clearly, the proposed method was much more sensitive than the standard alamarBlue$^{TM}$ cell viability assay. It should be due to the combination of immuno-affinity enrichment strategy and the magnet-facilitated amperometric read-out. To be noted, it was found from both methods that the increase of $\Delta A\%$ for *E. coli* was slightly faster than that for *B. subtilis*, most probably due to the different metabolic activity of the two bacterial species. Under ideal conditions, for example, *E. coli* cells divide every 20 min,[36] while the time for *B. subtilis* is 24-28 min.[37]

### 3.5 Detection of bacterial infections and antimicrobial susceptibility testing

The high sensitivity of the present method helped to discern small changes in bacterial cell concentration and metabolic state. The method was thereafter employed for bloodstream infection diagnosis. Concentration of the RS indicator was optimized before performing the diagnosis. The optimization was conducted with 1 mL of lysogeny broth containing intermediate concentration of *E. coli*, *i.e.* $5 \cdot 10^5$ and $5 \cdot 10^6$ cells·mL$^{-1}$. The *E. coli* cells were captured by MB-Ab$_{E.coli}$ probe, and then mixed with the RS indicator, which was prepared in 20 µL of lysogeny broth with different concentrations. The mixtures were incubated for 30 min in the microchip, allowing the reaction between bacterial cells and the indicator. The mixtures were then analysed by differential pulse voltammetry from 0.0 V to –0.8 V (*vs* Ag/AgCl) using the M-POT device. The RS concentrations were set as 1000, 500, 250, 125 and 62.5 µM. As shown in **Figure 4.13**, lower RS initial concentration resulted in higher $\Delta A\%$ for both concentrations of *E. coli*. It means the signal response for lower concentrations of

indicators progressed more rapidly, hence allowing earlier recognition of bacteria. Considering that the use of too low concentrations of indicators bring the risks of false positive, 125 μM of RS was used for infection detection and the following antimicrobial susceptibility assay.
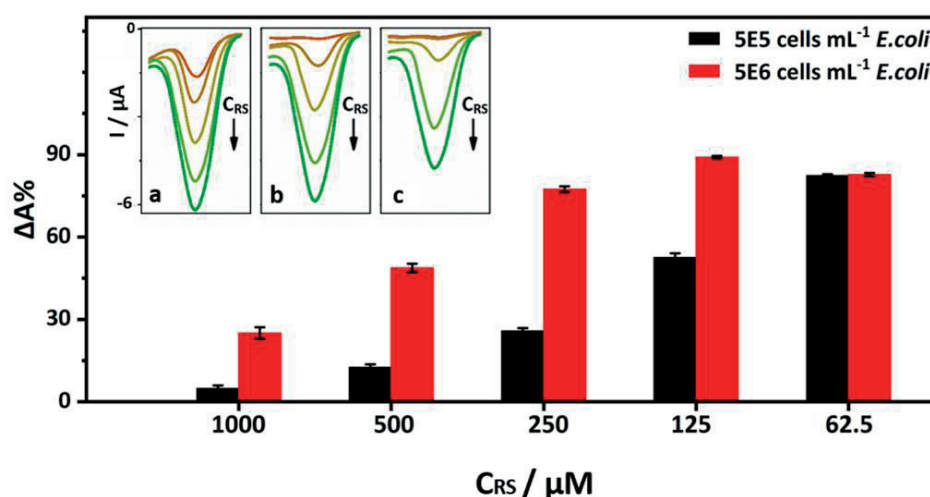


**Figure 4.13** Peak current decline percentage of different concentrations of RS after 30 min reaction with *E. coli*. The *E. coli* was captured from 1 mL lysogeny broth containing initially $5·10^5$ or $5·10^6$ cells·mL$^{-1}$ *E. coli* cells using MB-Ab$_{E.coli}$ probes. The inserted graphs were differential pulse voltammograms of RS in the case of (**a**) pure RS, (**b**) 30 min incubation with bead-captured *E. coli* isolated from lysogeny broth containing $5·10^5$ cells·mL$^{-1}$ *E. coli* or (**c**) $5·10^6$ cells·mL$^{-1}$ *E. coli*.

Pathogen concentration in infected patients is typically 0.1-100 colony forming unit per millimeter (CFU·mL$^{-1}$).[38,39] Blood culture is the current "gold standard" preparatory diagnosis step to increase the pathogen number for further testing. Here, the human blood was infected with extended-spectrum β-lactamase producing *E. coli* pathogen (ESBL-*E. coli*), 1 colony (~ 100 cells) per 8 mL blood. 8 mL of the infected human whole blood was incubated respectively in a BacT/Alert® FA Plus aerobic bottle (containing 30 mL of broth) and a BacT/Alert® FN Plus anaerobic bottle (containing 40 mL of broth) at 37 °C. The employment of both types of culture bottles was to ensure that the pathogen could grow no matter if it preferred an aerobic or an anaerobic culture environment.[40] Each blood culture bottle was prepared in two copies. One copy was used for the testing with the present method, and the other was kept untouched and were checked regularly until it turned positive. After every 2 h of incubation, 2 mL of the blood culture liquid was taken out respectively from the aerobic and anaerobic bottle,

and centrifuged at 1,000 rpm for 3 min to precipitate blood cells. Directly after, 1.5 mL of the supernatant containing pathogens were collected and evenly distributed into three 500 µL aliquots. The blood culture liquid was screened against three MB-Ab probes, *i.e.* MB-Ab$_{E.coli}$, MB-Ab$_{B.subtilis}$, MB-Ab$_{S.aureus}$, respectively, taking advantage of the high-throughput microchip/M-POT device. The bead-captured bacteria were harvested by magnetic separation, and then incubated with 20 µL of RS (125 µM in lysogeny broth) for 30 min in the microchip before differential pulse voltammetry measurement. The MB-Ab$_{E.coli}$ probe resulted in clear scanning peak current decline after 6 h of blood culture, with the $\Delta A\%$ value of 30.57% for the aerobic culture bottle and 25.79% for the anaerobic culture bottle. The $\Delta A\%$ increased with longer time of blood culture and reached the maximum value after 10 h of culture, as shown in **Figure 4.14**. Meanwhile, the MB-Ab$_{B.subtilis}$ and MB-Ab$_{S.aureus}$ probes didn't generated any peak current decline even after 24 h of blood culture. The pathogen was thus identified as *E. coli* species, with the requirement of only 6 h of blood culture. The identification itself took only 1 h, including 30 min for pathogen isolation from the blood culture liquid using MB-Ab affinity probes, 30 min for the reaction with indicator and then 1 min for amperometric measurement. The presence of pathogen was confirmed by the decline of electric current, and the pathogen species was recognized according to the MB-Ab probe type.
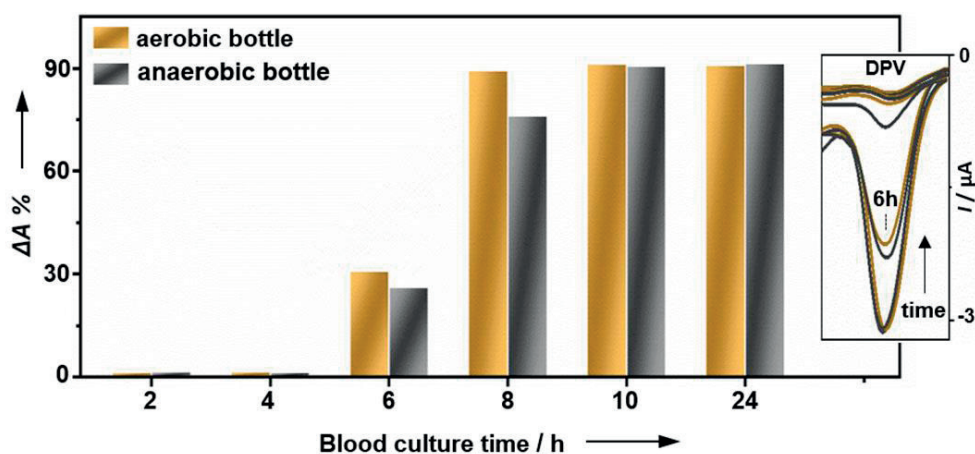


**Figure 4.14** Blood culture-based detection of the *ESBL-E. coli* bloodstream infection using MB-Ab$_{E.coli}$ probe. The infected blood was cultured in both aerobic and anaerobic bottles in parallel.

As a comparison, the two un-touched bottles (one aerobic, one anaerobic) turned positive after $\geq 24$ h of blood culture, indicated by automatically colour change on the bottle bottom, from green to bright yellow. In conventional diagnosis, the positive blood

cultures are used for pathogen subculture after colony plating, and the pure pathogen subculture is employed for pathogen species identification using either biochemical phenotypic method, genetic method or MALDI-TOF mass spectrometry method. The whole identification process, from blood collection to the identification result reporting, often takes several days or even longer time, dependent on the growth speed of the pathogen.[41] Here, in order to confirm the reliability of the identification result provided with the present amperometric method, a pure subculture of the pathogen, prepared from the positive blood culture in the aerobic culture bottle, was analysed by MALDI-TOF mass spectrometry. The generated mass spectrum was compared with the spectrum of *E. coli* ATCC 25922, which is a commonly used *E. coli* quality control strain. As shown in **Figure 4.15,** the pathogen subculture showed quite high spectrum similarity, *i.e.* 0.904, to the *E. coli* reference strain, indicating that the pathogen was indeed *E. coli* specie. Same identification result was obtained for the pathogen subculture prepared from the positive blood culture in the anaerobic culture bottle, not illustrated in detail here. The result confirmed that the pathogen species identification provided by the present immuno-affinity amperometric method was correct.
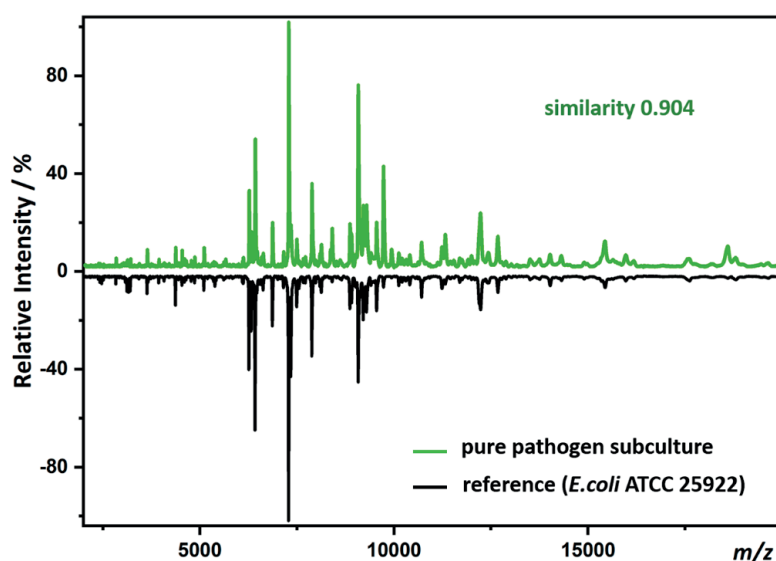


**Figure 4.15** MALDI-TOF mass spectra generated from an *E. coli* reference strain (*E. coli* ATCC 25922) and a pure subculture of the pathogen. Sinapinic acid, 20 mg·mL$^{-1}$ in 50/49.9/0.1% acetonitrile/water/trifluoroacetic acid, was used as the matrix.

ESBL-*E. coli* is a multidrug-resistant pathogen, whose worldwide emergency has raised serious therapeutic problems.[42] Once the pathogen was identified, a rapid

screening of antimicrobial drugs was conducted to help antimicrobial therapy determination. Pathogen isolated from the blood culture using MB-Ab$_{E.coli}$ probe was treated with different antibiotics for 90 min, followed by 30 min reaction with the RS indicator and amperometric measurement. The concentration of each antibiotic was set as the highest MIC value for susceptible interpretation according to the CLSI guidelines, as explained in the **Appendix**. In parallel, an antibiotic-free test was conducted as positive control. If an antibiotic was effective against the pathogen, metabolic state of the pathogen cells would be affected and viable cell number would decrease compared to the antibiotic-free positive control, and thus lower $\Delta A\%$ would be obtained. With this concept, the pathogen was determined as susceptible to imipenem, tetracyclin, nitrofurantoin and fosfomycin, as they resulted in clearly lower $\Delta A\%$ compared to the positive control (**Figure 4.16 a**). On the contrary, ampicillin, cefpodoxime, ceftriaxone, gentamicin and ciprofloxacin were determined as resistant or intermediate by the pathogen, since they generated about the same $\Delta A\%$ as the positive control.
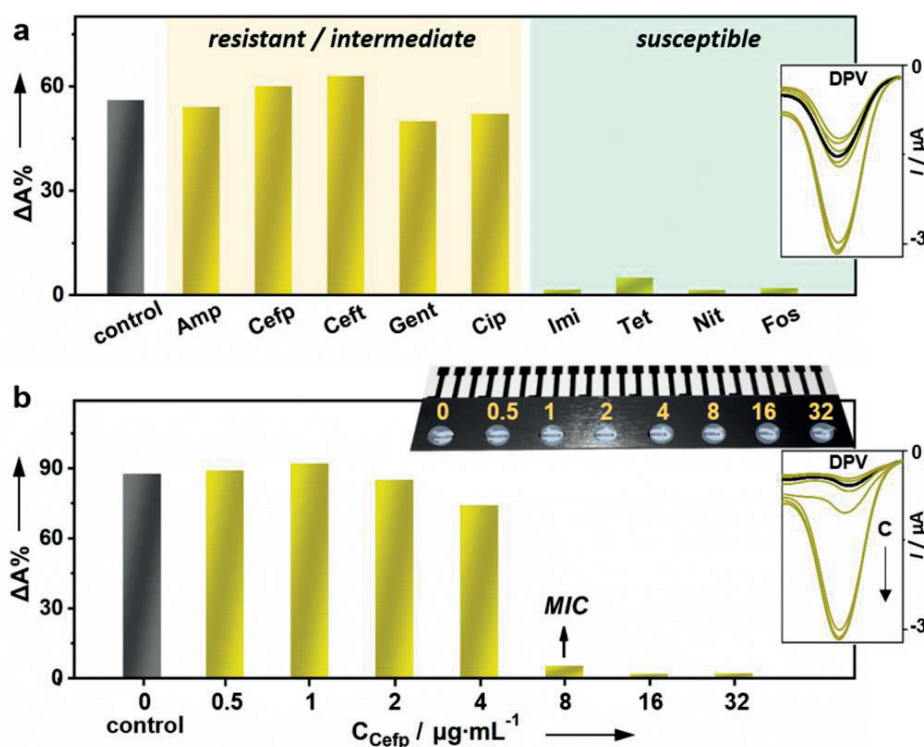


**Figure 4.16** Antimicrobial susceptibility testing using the present immuno-affinity amperometric method. (**a**) Quick antibiotic screening using the 6 h-blood culture liquid; (**b**) antibiotic MIC determination using the 6 h-blood culture liquid, taking cefpodoxime as an example antibiotic.

**Table 4.1** Antimicrobial susceptibility testing results of the ESBL-*E. coli* pathogen

| antibiotic | present method antibiotic screening interpretation | present method MIC determination | | bioMérieux VITEK 2 automate AST system | |
|---|---|---|---|---|---|
| | | MIC ($\mu g \cdot mL^{-1}$) | interpretation | MIC ($\mu g \cdot mL^{-1}$) | interpretation |
| ampicillin | R/I | 32 | R | 32 | R |
| cefpodoxime | R/I | 8 | R | 8 | R |
| ceftriaxone | R/I | ≥ 32 | R[a] | 64 | R |
| gentamicin | R/I | 16 | R | 16 | R |
| ciprofloxacin | R/I | 8 | R | 4 | R |
| imipenem | S | 0.25 | S | 0.25 | S |
| tetracyclin | S | 1 | S | 1 | S |
| nitrofurantoin | S | 8 | S | 16 | S |
| fosfomycin | S | 16 | S | 16 | S |

"R", "I", "S" means "resistant", "intermediate", "susceptible", respectively.

[a] The concentrations of ceftriaxone were set as 0, 0.5, 1, 2, 4, 8, 16, 32 $\mu g \cdot mL^{-1}$. After the testing with the present method, it was found that all the concentrations of ceftriaxone generated about the same $\Delta A\%$ as the positive control. It meant that even 32 $\mu g \cdot mL^{-1}$ of ceftriaxone didn't inhibit the growth of the ESBL-*E. coli* pathogen, and the MIC was thus determined as ≥ 32 $\mu g \cdot mL^{-1}$.

Alternatively, a "quasi" antibiotics MIC determination was performed based on the same working mechanism, to provide suggestion for proper antibiotic dose.[43] The above 2 h-procedure was slightly modified according to the widely used broth dilution standard protocol, by treating the pathogen with 2-fold increasing concentrations of antibiotics, with eight concentrations tested in a single microchip.[8] The MIC value was determined as the lowest concentration resulting in clearly lower $\Delta A\%$ compared to the positive control, meaning the lowest antibiotic concentration affected pathogen metabolic state and caused pathogen death or growth-inhibition (**Figure 4.16 b**). Antibiotics can cause obvious impact to bacteria metabolic activity within 30 min, [44] and here the pathogen was treated with antibiotics throughout the 2 h-procedure, which was enough for a reliable test. Compared with this fast susceptibility testing, current standard methods, *e.g.* broth dilution, typically require much longer time, including 24-48 h of bacteria pre-culture and 8-24 h of the testing itself.[7,8]

In order to confirm the reliability of these testing results, a pure subculture of the ESBL-*E. coli* pathogen was performed a standard antimicrobial susceptibility testing using the clinically-used bioMérieux VITEK® 2 automate AST system.[45] The test was conducted in a local hospital, Hôpital du Valais (Sion, Valais, Switzerland), where a

VITEK® 2 platform is installed. The subculture was prepared from the positive blood culture liquid in the aerobic culture bottle. The total working time was around 4 days, including 3 days of pathogen preparation (blood culture and sub-culture) and 9.15 h of the testing itself. All the interpretations were made according to the CLSI guidelines summarized in the **Appendix**. The susceptibility results provided by the clinically-used VITEK® 2 automate AST system, as well as the antibiotic screening and MIC determination results provided by the present immuno-affinity amperometric method, were summarized in **Table 4.1**. They matched well with each other.

## 4. Conclusions

The developed immuno-affinity amperometric method provides a fast and reliable bacterial infection diagnosis. It reduced the total time-to-report from several days or even weeks to only several hours, helping the early delivery of appropriate anti-infective therapy. The method is universally applicable to all types of culturable bacterial pathogens in various types of body fluids. In recent years, many chemical methods and techniques have emerged in bacterial infection analysis, for either cell quantification, or pathogen identification, or susceptibility/resistance determination. The present work proposed a simple methodology that merges all these individual steps onto a single platform, avoiding the need of multiple expensive instruments and saving the total working time. We envision that the present concept could be scalable from point-of-care assay to automated centralized testing where a large number of samples could be treated.

## Appendix

In standard antimicrobial susceptibility testing approaches, *e.g.* the broth dilution or agar dilution, the MIC (minimal inhibitor concentration) of an antimicrobial drug is defined as the lowest concentration (in $\mu g \cdot mL^{-1}$ or $g \cdot mL^{-1}$) of the drug that prevents the visible growth of a microorganism under defined conditions. In clinical practice, this *in vitro* MIC value is employed to determine the tested microorganism as either clinically susceptible, or intermediate, or resistant to the tested drug.[8] The interpretative standards for the susceptibility/resistance determination are provided by different national organizations, such as the *Clinical and Laboratory Standards Institute* (CLSI) in the USA and the *European Committee on Antimicrobial Susceptibility Testing* (EUCAST).[46,47] In the present work, all the susceptibility/resistance determination for the ESBL-*E. coli* pathogen was made according to the CLSI guidelines published in the year of 2017. The ESBL-*E. coli* pathogen is included in the family of

*Enterobacteriaceae* listed in the guidelines. The MIC interpretative standards of the nine antibiotics tested in this work are summarized as below.

| antibiotic | susceptible MIC ($\mu$g·mL$^{-1}$) | intermediate MIC ($\mu$g·mL$^{-1}$) | resistant MIC ($\mu$g·mL$^{-1}$) |
|---|---|---|---|
| ampicillin | $\leq 8$ | 16 | $\geq 32$ |
| cefpodoxime | $\leq 2$ | 4 | $\geq 8$ |
| ceftriaxone | $\leq 1$ | 2 | $\geq 4$ |
| gentamicin | $\leq 4$ | 8 | $\geq 16$ |
| ciprofloxacin | $\leq 1$ | 2 | $\geq 4$ |
| imipenem | $\leq 1$ | 2 | $\geq 4$ |
| tetracyclin | $\leq 4$ | 8 | $\geq 16$ |
| nitrofurantoin | $\leq 32$ | 64 | $\geq 128$ |
| fosfomycin | $\leq 64$ | 128 | $\geq 256$ |

The CLSI guidelines were used for the setting of antibiotic concentrations during antimicrobial susceptibility testing. For the antibiotic screening assay conducted in this work, the concentration of each antibiotic was set as the highest MIC value for susceptible interpretation according to the guidelines. Accordingly, the concentration of ampicillin (Amp), cefpodoxime (Cefp), ceftriaxone (Ceft), gentamicin (Gent), ciprofloxacin (Cip), imipenem (Imi), tetracyclin (Tet), nitrofurantoin (Nit) and fosfomycin (Fos) was set as 8, 2, 1, 4, 1, 1, 4, 32 and 64 $\mu$g·mL$^{-1}$, respectively.

As for the MIC determination assay, the 2-fold increasing concentrations should at least include the three MIC threshold values for susceptible, intermediate and resistant interpretation. For instance, the concentrations of cefpodoxime (Cefp) should include at least 2, 4, 8 $\mu$g·mL$^{-1}$. In the present work, the concentrations of cefpodoxime were set as 0 (positive control), 0.5, 1, 2, 4, 8, 16 and 32 $\mu$g·mL$^{-1}$. Based on the same principle, the concentrations of other antibiotics were set as 0, 0.5, 1, 2, 4, 8, 16, 32 $\mu$g·mL$^{-1}$ for ceftriaxone, gentamicin, ciprofloxacin, imipenem, tetracyclin, and 0, 4, 8, 16, 32, 64, 128 and 256 $\mu$g·mL$^{-1}$ for ampicillin, nitrofurantoin, fosfomycin.

# Reference

1. Wisplinghoff, H*., et al.* Nosocomial bloodstream infections in US hospitals: Analysis of 24,179 cases from a prospective nationwide surveillance study. *Clin Infect Dis* 39, 309-317 (2004).
2. Sharland, M., Saroey, P. & Berezin, E.N. The global threat of antimicrobial resistance - The need for standardized surveillance tools to define burden and develop interventions. *J Pediat-Brazil* 91, 410-412 (2015).
3. Wang, W.W*., et al.* Predictors of mortality in bloodstream infections caused by multidrug-resistant gram-negative bacteria: 4 years of collection. *Am J Infect Control* 45, 59-64 (2017).
4. Opota, O., Croxatto, A., Prod'hom, G. & Greub, G. Blood culture-based diagnosis of bacteraemia: state of the art. *Clin Microbiol Infec* 21, 313-322 (2015).
5. Lamy, B., Dargere, S., Arendrup, M.C., Parienti, J.J. & Tattevin, P. How to Optimize the Use of Blood Cultures for the Diagnosis of Bloodstream Infections? A State-of-the Art. *Front Microbiol* 7 (2016).
6. Klouche, M. & Schroder, U. Rapid methods for diagnosis of bloodstream infections. *Clin Chem Lab Med* 46, 888-908 (2008).
7. Jorgensen, J.H. & Ferraro, M.J. Antimicrobial Susceptibility Testing: A Review of General Principles and Contemporary Practices. *Clin Infect Dis* 49, 1749-1755 (2009).
8. Wiegand, I., Hilpert, K. & Hancock, R.E.W. Agar and broth dilution methods to determine the minimal inhibitory concentration (MIC) of antimicrobial substances. *Nat Protoc* 3, 163-175 (2008).
9. Murray, P.R. & Masur, H. Current approaches to the diagnosis of bacterial and fungal bloodstream infections for the ICU. *Crit Care Med* 40, 3277 (2012).
10. Jović, M*., et al.* Inkjet-printed microtiter plates for portable electrochemical immunoassays. *J Electroanal Chem* 786, 69-76 (2017).
11. Lesch, A*., et al.* Large scale inkjet-printing of carbon nanotubes electrodes for antioxidant assays in blood bags. *J Electroanal Chem* 717, 61-68 (2014).
12. Zhu, Y.D*., et al.* Sensitive and fast identification of bacteria in blood samples by immunoaffinity mass spectrometry for quick BSI diagnosis. *Chem Sci* 7, 2987-2995 (2016).
13. Singhal, N., Kumar, M., Kanaujia, P.K. & Virdi, J.S. MALDI-TOF mass spectrometry: an emerging technology for microbial identification and diagnosis. *Front Microbiol* 6 (2015).
14. Yang, Y*., et al.* Bacterial Whole Cell Typing by Mass Spectra Pattern Matching with Bootstrapping Assessment. *Anal Chem* 89, 12556-12561 (2017).
15. Jovic, M*., et al.* Electrochemical detection of free chlorine at inkjet printed silver electrodes. *J Electroanal Chem* 756, 171-178 (2015).
16. da Silva, E.T., Miserere, S., Kubota, L.T. & Merkoci, A. Simple on-plastic/paper inkjet-printed solid-state Ag/AgCl pseudoreference electrode. *Anal Chem* 86, 10531-10534 (2014).
17. Lesch, A., Cortés-Salazar, F., Amstutz, V., Tacchini, P. & Girault, H.H. Inkjet printed nanohydrogel coated carbon nanotubes electrodes for matrix independent sensing. *Anal Chem* 87, 1026-1033 (2015).
18. Berridge, M.V., Herst, P.M. & Tan, A.S. Tetrazolium dyes as tools in cell biology: new insights into their cellular reduction. *Biotechnol Annu Rev* 11, 127-152 (2005).
19. O'Brien, J., Wilson, I., Orton, T. & Pognan, F. Investigation of the Alamar Blue (resazurin) fluorescent dye for the assessment of mammalian cell cytotoxicity. *Eur J Biochem* 267, 5421-5426 (2000).
20. Bernas, T. & Dobrucki, J.W. The role of plasma membrane in bioreduction of two tetrazolium salts, MTT, and CTC. *Arch Biochem Biophys* 380, 108-116 (2000).
21. Chen, J.L., Steele, T.W.J. & Stuckey, D.C. Metabolic reduction of resazurin; location within the cell for cytotoxicity assays. *Biotechnol Bioeng* 115, 351-358 (2018).

22. Del Principe, D., Avigliano, L., Savini, I. & Catani, M.V. Trans-Plasma Membrane Electron Transport in Mammals: Functional Significance in Health and Disease. *Antioxid Redox Sign* 14, 2289-2318 (2011).

23. Hice, S.A., Santoscoy, M.C., Soupir, M.L. & Cademartiri, R. Distinguishing between metabolically active and dormant bacteria on paper. *Appl Microbiol Biotechnol* 102, 367-375 (2018).

24. Präbst, K., Engelhardt, H., Ringgeler, S. & Hübner, H. Basic colorimetric proliferation assays: MTT, WST, and Resazurin. *Cell Viability Assays: Methods and Protocols*, 1-17 (2017).

25. Avesar, J*., et al.* Rapid phenotypic antimicrobial susceptibility testing using nanoliter arrays. *P Natl Acad Sci USA* 114, E5787-E5795 (2017).

26. Pace, R.T. & Burg, K.J.L. Toxic effects of resazurin on cell cultures. *Cytotechnology* 67, 13-17 (2015).

27. Renault, C*., et al.* Observation of nanometer-sized electro-active defects in insulating layers by fluorescence microscopy and electrochemistry. *Anal Chem* 87, 5730-5737 (2015).

28. Besant, J.D., Sargent, E.H. & Kelley, S.O. Rapid electrochemical phenotypic profiling of antibiotic-resistant bacteria. *Lab Chip* 15, 2799-2807 (2015).

29. Umemoto, K.B. Electrochemical Studies of the Reduction-Mechanism of Tetrazolium Salts and Formazans. *B Chem Soc Jpn* 62, 3783-3789 (1989).

30. Xu, W.L*., et al.* Single-Molecule Electrocatalysis by Single-Walled Carbon Nanotubes. *Nano Lett* 9, 3968-3973 (2009).

31. Jambor, B. Reduction of Tetrazolium Salt. *Nature* 173, 774-775 (1954).

32. Jambor, B. Mechanism of the Reduction of Tetrazolium Salts. *Nature* 176, 603-603 (1955).

33. Nineham, A. The chemistry of formazans and tetrazolium salts. *Chem Rev* 55, 355-483 (1955).

34. Guerin, T.F., Mondido, M., McClenn, B. & Peasley, B. Application of resazurin for estimating abundance of contaminant-degrading micro-organisms. *Lett Appl Microbiol* 32, 340-345 (2001).

35. Twigg, R.S. Oxidation-Reduction Aspects of Resazurin. *Nature* 155, 401-402 (1945).

36. Fossum, S., Crooke, E. & Skarstad, K. Organization of sister origins and replisomes during multifork DNA replication in Escherichia coli. *Embo J* 26, 4514-4522 (2007).

37. Jensen, S.O., Thompson, L.S. & Harry, E.J. Cell division in bacillus subtilis: FtsZ and FtsA association is Z-ring independent, and FtsA is required for efficient midcell Z-ring assembly. *J Bacteriol* 187, 6536-6544 (2005).

38. Yagupsky, P. & Nolte, F.S. Quantitative Aspects of Septicemia. *Clin Microbiol Rev* 3, 269-279 (1990).

39. Puttaswamy, S., Lee, B.D. & Sengupta, S. Novel Electrical Method for Early Detection of Viable Bacteria in Blood Cultures. *J Clin Microbiol* 49, 2286-2289 (2011).

40. Lee, D.H., Kim, S.C., Bae, I.G., Koh, E.H. & Kim, S. Clinical Evaluation of BacT/Alert FA Plus and FN Plus Bottles Compared with Standard Bottles. *J Clin Microbiol* 51, 4150-4155 (2013).

41. Kirn, T.J. & Weinstein, M.P. Update on blood cultures: how to obtain, process, report, and interpret. *Clin Microbiol Infec* 19, 513-520 (2013).

42. Oteo, J., Perez-Vazquez, M. & Campos, J. Extended-spectrum [beta]-lactamase producing Escherichia coli: changing epidemiology and clinical impact. *Curr Opin Infect Dis* 23, 320-326 (2010).

43. Hasselmann, C. & Microbiology, E.S.C. Determination of minimum inhibitory concentrations (MICs) of antibacterial agents by broth dilution. *Clin Microbiol Infec* 9 (2003).

44. Baltekin, O., Boucharin, A., Tano, E., Andersson, D.I. & Elf, J. Antibiotic susceptibility testing in less than 30 min using direct single-cell imaging. *P Natl Acad Sci USA* 114, 9170-9175 (2017).

45. Eigner, U., Schmid, A., Wild, U., Bertsch, D. & Fahr, A.M. Analysis of the comparative workflow and performance characteristics of the VITEK 2 and Phoenix systems. *J Clin Microbiol* 43, 3829-3834 (2005).
46. Breakpoint tables for interpretation of MICs and zone diameters 2018. Version 8.0. *Breakpoint tables for interpretation of MICs and zone diameters*. European Committee on Antimicrobial Susceptibility Testing (2018).
47. Patel, J.B. *Performance standards for antimicrobial susceptibility testing*. Clinical and Laboratory Standards Institute (2017).

# CHAPTER V. Mass spectrometry detection of exosomes for cancer studies

*Adapted with permission from <u>Y. Zhu</u>, H. Pick, N. Gasilova, X. Li, T. Lin, H. P. Laeubli, A. Zippelius, P. C. Ho, H. H. Girault, MALDI detection of exosomes: a potential tool for cancer studies, a manuscript in submission.*

## Abstract

MALDI-TOF MS is used to detect exosomes, yielding exosomal fingerprints within minutes. This rapid exosome detection approach is proposed as a potential tool for cancer analysis. Melanoma, a dangerous form of skin cancer, is analysed as a cancer model. The approach allows classification of melanoma cells from the stage level, and enables the tracking of protein transfer from parental cells to the secreted exosomes. By correlation with proteomic analysis, the approach provides a direct read-out of melanoma biomarkers, and helps to explore melanoma progression *via* exosome-mediated intercellular communication. Targeting bloodstream-circulating exosomes, the proposed approach also promises fast detection of melanoma disease and dynamic monitoring of the disease status, with proof of concept in mouse and human.

## 1. Introduction

Exosomes, a type of nanosized extracellular vesicles, are secreted by almost all types of human cells and are circulating throughout the human body.[1] In living cells, multivesicular bodies containing intraluminal vesicles are fused with plasma membrane to release exosomes to the extracellular space and the body fluids. Enclosed by a lipid bilayer, exosomes contain bioactive compounds like lipids, metabolites, proteins, as well as genetic materials including DNA, messenger RNA (mRNA), microRNA (miRNA) and long non-coding RNA (**Figure 5.1**).[2] Proteomic studies showed that exosomes contain a certain subset of cellular proteins including those from cytosol, endosomes and plasma membrane, but proteins from nucleus, Golgi complex, endoplasmic reticulum and mitochondria are often excluded. Some of the present proteins depend on the parental cell types, while others are found in most exosomes regardless of their cell

origins. Physical features of exosomes to distinguish them from other subtypes of extracellular vesicles include their cup-shaped appearance, 30-150 nm size range and 1.13-1.19 g·mL$^{-1}$ density in sucrose.[2] With the initial function of cell waste disposal to maintain cellular homeostasis, together with the novel role in biological signal transport to facilitate cell-to-cell communication, exosomes have been associated with numerous physiological and pathological processes.[3,4] Compared to normal proliferating cells, cancer cells often release higher amounts of exosomes with elevated cargo levels.[5] The cancer-derived exosomes can promote cancer progression by stimulating angiogenesis, modulating host immune response, remodelling extracellular matrix, generating pre-metastatic niches, *etc.*[6,7] Evidence has shown that exosomes are useful targets for laboratory study of cancer biology and clinical management of cancer diseases.[8]
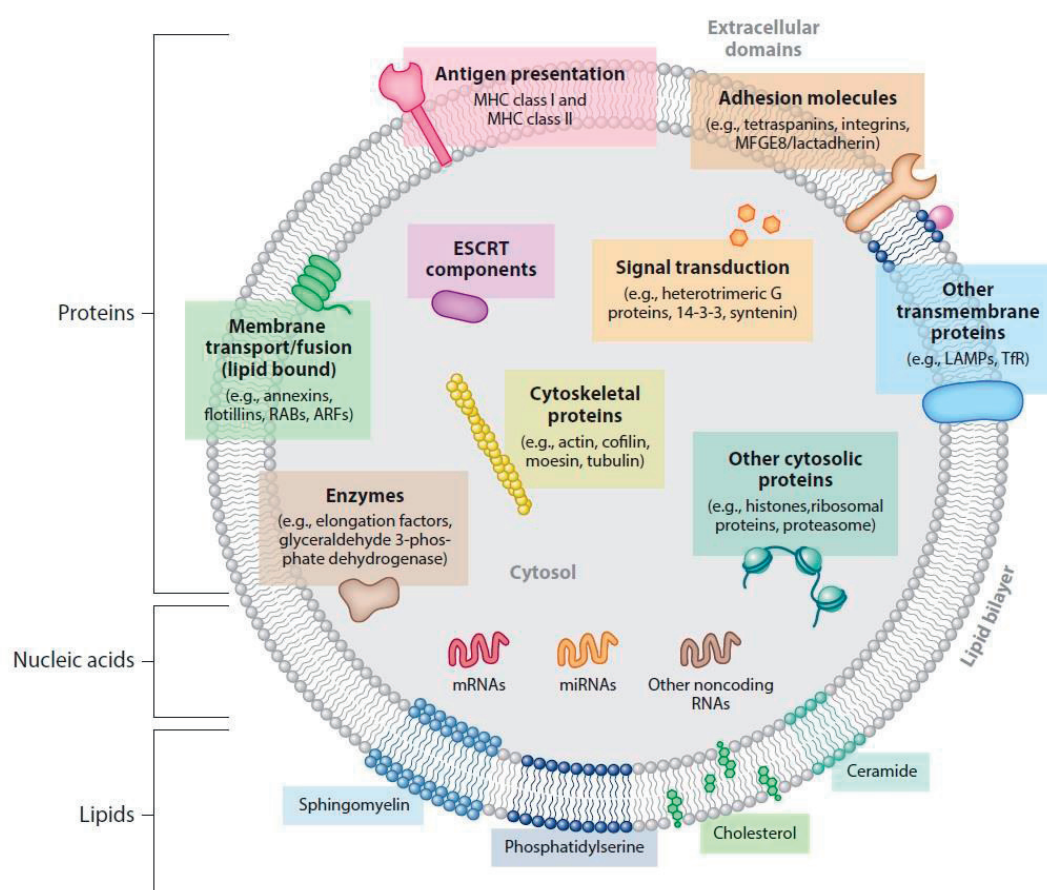


**Figure 5.1** Overall composition of exosomes.[2h] Abbreviations: ARF, ADP ribosylation factor; ESCRT, endosomal sorting complex required for transport; LAMP, lysosome-associated membrane protein; MHC, major histocompatibility complex; MFGE8, milk fat globule-epidermal growth factor-factor VIII; RAB, Ras-related proteins in brain; TfR, transferrin receptor. Copyright © 2014 Annual Reviews.

Laboratory studies often isolate exosomes from tissue culture supernatant, cell culture supernatant or different types of body fluids. The most widely used exosome isolation method is differential centrifugation, which comprises firstly low-speed centrifugation to remove debris and large vesicles and then ultracentrifugation (normally at 100,000 $g$) to precipitate exosome particles. Dependent on the analysis purpose, the products could be further purified by methods like density gradient separation.[9] Recently, some commercial kits have become available for fast and simple exosome isolation without the need of ultracentrifugation, greatly facilitating exosome-related research.[10] Currently, three types of methodologies are frequently used for exosome analysis, including *i)* the RNA and DNA detection approaches like next-generation sequencing, polymerase chain reaction and northern blotting, *ii)* the protein detection procedures like western blotting, enzyme-linked immunosorbent assay and proteomics based on liquid chromatography-tandem mass spectrometry, as well as *iii)* the fluorescence labelling methods for optical visualization of exosomes.[11] In this chapter, exosomes were analysed with MALDI-TOF MS technique. With the ability to detect a large number of samples within a short time, MALDI-TOF MS allows a rapid, high-throughput analysis and has been widely used in clinical laboratories.[12] This technique employs a pulsed laser to irradiate the solid mixture of exosomes and laser energy-absorbing matrices to produce protonated or deprotonated ions, mostly single charged, from the exosome particles for mass measurement. It enables the detection of exosomal components with minimal fragmentation, and generates characteristic fingerprints for the exosome entities. This exosome detection approach is proposed for cancer cell study and cancer disease monitoring.

## 2. Materials and methods

### 2.1. Cell culture and plasmid transfection.

Human melanoma cell lines SBCl2, WM115, WM239, human cervical cancer cell line HeLa and human embryonic kidney cell line HEK293, obtained from American Type Culture Condition (ATCC®, Virginia, USA), were cultured in Dulbecco's modified Eagle's medium (Gibco Life Technologies, Basel, Switzerland) supplemented with 10% (volume percentage) of newborn fetal calf serum (New Zealand origin, Gibco® Life Technologies, Basel, Switzerland) and 1% of 100× penicillin/streptomycin (Gibco Life Technologies, Basel, Switzerland) at 37 °C in a humidified atmosphere filled with 5% $CO_2$. The cells were passed every 3 or 4 days, when the cells reached 80% flask confluency. In order to obtain green fluorescence protein-expressed WM239 cells, the WM239 cells were transfected with EGFP-N1 plasmid DNA (Clontech, Basel, Switzerland) or pLV-ER GFP plasmid DNA (Addgene, Massachusetts, USA) by using

Lipofectamine® 2000 transfection reagent (Invitrogen, Basel, Switzerland). Before the transfection, WM239 cells were passed in a T-75 flask (Techno Plastic Products AG, Trasadingen, Switzerland) and were cultured 24 h until the cells reached ~ 80% confluency. The transfection mixture was prepared by mixing 24 µg of plasmid DNA (prepared in 1.5 mL of OptiMEM medium) (Gibco Life Technologies, Basel, Switzerland) and 60 µL of Lipofectamine® 2000 reagent (prepared in 1.5 mL of OptiMEM medium). The transfection mixture was equilibrated at room temperature for 20 min, and then co-incubated with the WM239 cells for 24-48 h. The transfection efficiency was checked by confocal fluorescence microscopy observation.

## 2.2. Isolation of exosomes from cell culture supernatant

Before the isolation of exosomes, all the cells were grown in cell culture medium until they reached 80-90% confluency. The cell culture supernatant was then removed from flasks, and the cells were continuously grown in fresh serum-free Dulbecco's modified Eagle's medium for 24 h. Thereafter, exosomes secreted by the cells were isolated from the serum-free cell culture supernatant by differential centrifugation. The employment of serum-free culture medium was to make sure that all the isolated exosomes were secreted by the cells, not from the newborn calf serum. The cell culture supernatant was transferred into sterile centrifuge tubes and centrifuged at 500 $g$ at 4 ℃ for 10 min to remove dead cells. The supernatant was quickly poured off into clean centrifuge tubes and centrifuged at 2,000 $g$ at 4 ℃ for 15 min to remove cell debris. The obtained supernatant was transferred into clean polycarbonate centrifuge tubes and centrifuged at 10,000 $g$ at 4 ℃ for 30 min (using Beckman Coulter ultracentrifuge and Type 70 Ti rotor) to remove the remaining cell debris and microvesicles. The obtained supernatant was poured off into new polycarbonate centrifuge tubes and centrifuged at 100,000 $g$ at 4 ℃ for 70 min (using Beckman Coulter ultracentrifuge and Type 70 Ti rotor) to precipitate exosomes. The exosome pellet was washed in phosphate-buffered saline (pH 7.4, 10 mM) and precipitated again by centrifugation at 100,000 $g$ at 4 ℃ for 70 min. The collected exosomes were finally suspended in 100 µL of phosphate-buffered saline or deionized water or Dulbecco's modified Eagle's medium, which were going to be characterized or measured or conducted with transfer assays immediately, or kept at – 80 ℃ for long time storage. Size and morphology of the collected exosomes were observed with a transmission electron microscope (Jeol JEM-1400, JEOL Inc, Tokyo, Japan). Exosome size distribution was analysed by dynamic light scattering using Zetasizer Nano ZS (Malvern Panalytical Ltd, Great Malvern, United Kingdom). Exosome particle concentration of the final exosome suspension was measured by nanoparticle tracking analysis using Malvern NanoSight NS300 (Malvern Panalytical Ltd, Great Malvern, United Kingdom).

## 2.3. Transfer of exosomes into recipient cells

Exosomes were collected from 150 mL of serum-free cell culture supernatant from the cultures of SBCl2, WM115 or WM239 cells, and were finally suspended in 100 μL of Dulbecco's modified Eagle's medium. Before conducting exosome transfer assays, SBCl2 cells were grown in 9.2 cm$^2$ Nunc$^{TM}$ petri dishes (Thermo Fisher Scientific, Basel, Switzerland) until the cells reached ~ 70% confluency. The cell culture supernatant was removed, and the cells were co-incubated with Dulbecco's modified Eagle's medium containing the previously collected exosomes. After 24 h of co-incubation, newborn calf serum was added into the culture supernatant for another 24 h of co-incubation. Newborn calf serum was supplied to provide sufficient nutrition and growth factors for the cells. After this 48 h of co-incubation with exosomes, the cells were harvested by trypsinization and centrifugation for MALDI-TOF MS measurement.

## 2.4. Mouse model of subcutaneous B16 melanoma

Wild-type C57BL/6 mice were purchased from Jackson Laboratory and maintained at the animal facility of Université de Lausanne, Switzerland. B16 melanoma cells in the logarithmic growth phase (grown *in vitro*) with ≤ 80% flask confluency were harvested by trypsinization and centrifugation, and counted in a hemocytometer to adjust cell concentration to $10^6$ cells·mL$^{-1}$ in ice cold Hanks' balanced salt solution. Five of 7 week old female C57BL/6 mice were injected with 100 μL of the B16 cell suspension by sliding needle 5-10 mm subcutaneously until the appearance of a clear "bleb". The mice were maintained and observed regularly to check tumour growth. After subcutaneous injection, a palpable tumour was formed in each of the mice on day 12, and the tumour grew to the average size of 1 cm$^3$ on day 19. Around 60 μL of blood was drawn from each mice by tail vein sampling on day 5, day 12 and day 19, respectively, for the isolation of circulating exosomes. Another group of five mice with the same age and same gender were maintained as healthy control, and blood was also drawn from these healthy mice on the same dates for the isolation of circulating exosomes. All experiments were performed in accordance with Swiss federal regulations and procedures approved by veterinary authority of Canton Vaud.

## 2.5. Isolation of bloodstream-circulating exosomes

Vacutainer tubes coated with K$_2$ EDTA were used for mouse blood drawing. The blood-containing tubes were kept upright at 37 °C for 30 min, followed by centrifugation at 1500 *g* at 4 °C for 12 min. After the centrifugation, blood plasma was present on the top layer of the tubes and was carefully transferred into new tubes for exosome isolation. Human blood plasma samples were directly provided by Universitätsspital Basel, Switzerland. Exosomes were isolated from mouse blood plasma or human blood plasma

with ExoQuick^TM Plasma prep and Exosome precipitation kit (Catalog # EXOQ5TM-1, System Bioscience, Palo Alto, Canada), which contains thrombin liquid suspension (611 U·mL$^{-1}$) and exosome precipitation reagent. Briefly, 2 µL of thrombin was added into 100 µL of blood plasma, and the mixture was incubated at room temperature for 5 min followed by centrifugation at 10,000 $g$ for 5 min and discarding the fibrin pellet on the tube bottom. The supernatant was transferred into a new Eppendorf tube, and 30 µL of exosome precipitation reagent was added and co-incubated with the plasma at 4 °C for 30 min. The mixture was then centrifuged at 1,500 $g$ at room temperature for 30 min to precipitate exosomes. The supernatant was discarded, and the residual solution was totally removed by centrifugation at 1,500 $g$ at room temperature for 5 min. The obtained exosomes were finally suspended in 25 µL of deionized water or phosphate-buffered saline for MALDI-TOF MS measurement or proteomic analysis. Blood samples were used under the signed assent of blood donors. No research on genetic material was carried out. Therefore, no specific ethical processing was required and these samples were used in agreement with the local legislation (Loi fédérale relative à la recherche sur l'être humain, LRH – RS 810.30" and "the "Ordonnance relative à la recherche sur l'être humain, ORH – RS 810.301").

## 2.6. Proteomic analysis and MALDI-TOF MS measurement

In order to clarify the protein identity of peaks appearing on the MALDI-TOF mass spectra, the exosomes or cells were subjected to top-down and bottom-up proteomic analysis. The MALDI-TOF mass spectral peaks were tentatively assigned by matching them with the protein profiles provided by the proteomic analysis. At the beginning of both proteomic analyses, proteins were extracted and denatured from the exosomes or the cells. Specifically, the exosomes and cells were diluted 2-fold in pre-chilled lysis buffer (Laemmli 2× buffer, pH 6.8), which contained 4% SDS, 20% glycerol, 10% 2-mercaptoethanol, 0.004% bromphenol blue and 0.125 M Tris HCl. The mixtures were pipetted thoroughly until sample viscosity was obviously increased, and then incubated at 95 °C for 10 min to denature proteins. The mixtures were thereafter centrifuged at 13,000 rpm at room temperature for 10 min to spin down lipids, and the supernatants were harvested. As for top-down proteomic analysis, proteins were precipitated from the supernatant using methanol and chloroform. Briefly, four volumes of optima-grade methanol were added into the supernatant, and the mixture was pipetted vigorously to mix the solution thoroughly, followed by adding one volume of HPLC-grade chloroform, three volumes of optima-grade water and a thorough mixing of the mixture. The resulting mixture was centrifuged at 13,000 rpm for 10 min at room temperature to spin down proteins. There were distinct layers visible within each fraction, *i.e.* an organic layer on the bottom, an aqueous layer on the top, and an interface in the middle. The

precipitated proteins were present as a single pellet floating on the interface. The top layer was pipetted off carefully without disturbing the pellet or the organic layer. After that, three volumes of optima-grade methanol were added to the organic layer carefully without breaking up the protein pellet. The mixture was centrifuged at 13,000 rpm for 10 min to remove the organic solution, and the protein pellet on tube bottom was air-dried at room temperature (~ 2 min). The pellet was finally dissolved in a buffer solution that contained 95% (volume percentage) optima-grade water, 5% optima-grade acetonitrile and 0.2% MS-grade formic acid. The protein solution was centrifuged at 13,000 rpm for 10 min to remove any remaining debris. The supernatant containing intact proteins was harvested, and subjected to top-down proteomic analysis. As for bottom-up proteomic analysis, the denatured proteins dissolved in the Laemmli buffer were separated by sodium dodecyl sulphate-polyacrylamide gel electrophoresis, and the protein band between 2-80 kDa was excised for protein digestion in trypsin. The protein digestion product was subsequently measured by liquid chromatography-tandem mass spectrometry. The top-down and bottom-up proteomic analyses were performed by Proteomics Core Facility and ISIC Mass Spectrometry Facility in École Polytechnique Fédérale de Lausanne, Switzerland. All the MALDI-TOF MS measurements were conducted under liner positive mode, using sinapinic acid (20 mg·mL$^{-1}$ in 50/49.9/0.1% acetonitrile/water/trifluoroacetic acid) as the matrix. Details about mass calibration, measurement parameters and data analysis are explained in CHAPTER II and CHAPTER III of this thesis.

## 3. Results and discussion

### 3.1. MALDI-TOF MS detection of exosomes

Exosomes secreted from human melanoma cell lines grown *in vitro* were used as analysis models. Melanoma is one of the most dangerous types of skin cancer, developed from transformed dermal melanocytes. It typically occurs in skin, but sometimes also in the mouth, the eyes or the intestines. It is a lethal neoplasm with the incidence increasing gradually during the past three decades, especially in America and Europe.[13] The cell lines used here were derived from different melanoma stages, *i.e.* a non-tumorigenic radial growth phase primary melanoma cell line SBCl2, a tumorigenic vertical growth phase primary melanoma cell line WM115 and a metastatic melanoma cell line WM239.[14,15] Exosomes were isolated from the serum-free cell culture supernatant through differential centrifugation. The isolated extracellular vesicles were confirmed as exosomes based on transmission electron microscopy observation, dynamic light scattering analysis and bottom-up proteomic analysis. As shown in **Figure 5.1,** the vesicles displayed the characteristic cup-shaped morphology with the typical

size of 30-150 nm. The vesicles also contained well-known exosome-associated proteins like the tetraspanins CD9, CD63, CD81, programmed cell death 6-interacting protein (ALIX) and tumor susceptibility gene 101 protein (TSG101), with the proteomic information shown in **Appendix Note I**.[16]
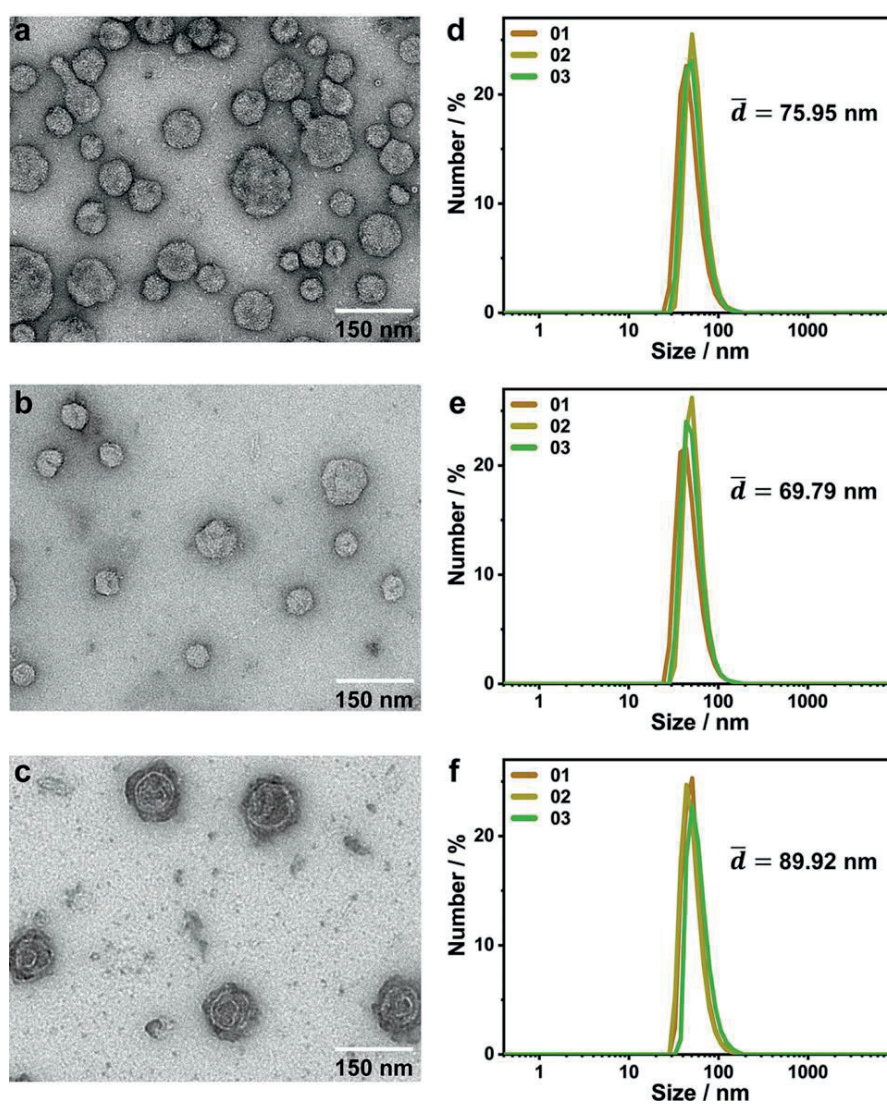


**Figure 5.1** Morphology and size characterization of exosomes. Transmission electron microscopy images of (**a**) exosomes derived from radial growth phase primary melanoma cell line SBCl2, (**b**) exosomes derived from vertical growth phase primary melanoma cell line WM115 and (**c**) exosomes derived from metastatic human melanoma cell line WM239. Dynamic light scattering analysis of (**d**) exosomes derived from SBCl2 cells, (**e**) exosomes derived from WM115 cells and (**f**) exosomes derived from WM239 cells, with average size of 75.95 nm, 69.79 nm and 89.92 nm, respectively.
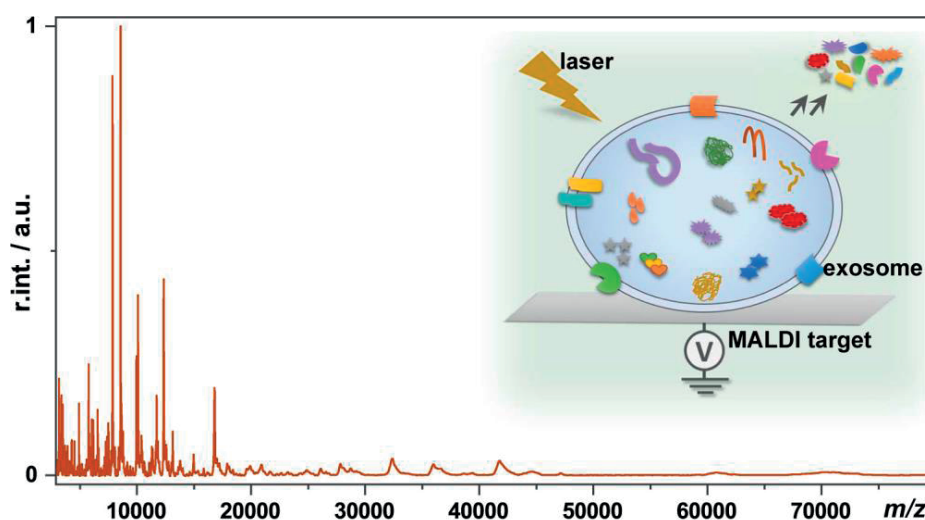
**Figure 5.2** A representative exosome MALDI-TOF mass spectrum. The exosomes were derived from WM115 cells. The spectrum was generated from $\sim 5 \cdot 10^7$ exosome particles. The insert graph shows the general working principle for exosome detection.

The obtained exosomes were subjected to MALDI-TOF MS measurements in their intact whole state. Mass spectral fingerprints were generated within minutes under pulsed laser irradiation with the assistance of a laser energy absorbing matrix. The choice of matrix is an important factor affecting the measurements, and sinapinic acid was utilized as the matrix throughout the present work as it provides satisfactory reproducibility for biological samples in a wide mass range.[17] Experimentally, it was found that 1 µL of an aqueous solution containing $\sim 5 \cdot 10^7$ exosome particles was able to produce a high quality mass spectrum. The exosome concentration was measured by nanoparticle tracking analysis. **Figure 5.2** displays a representative fingerprint of exosomes derived from WM115 cells in the mass range of 2,000-80,000 *m/z*. The observed fingerprint peaks mainly came from proteins and possibly peptides loaded in the exosomes. It is clear that peaks with high intensity (normalized relative intensity) mainly appeared in the 2,000-20,000 *m/z* range, because proteins within this mass range are more easily ionized compared to those with a higher mass. Spectrum quality in the higher mass range could be improved by enhancing the ionisation efficiency, for instance, by using a titanium dioxide nanoparticles-coated MALDI target, as illustrated in Chapter III of this thesis.[17] In order to investigate the detection reproducibility, WM115 cells were cultured for three passages, and mass spectra of the corresponding exosomes were compared. It turned out that the spectra were highly similar to each other, with an overlap of almost all the peaks. The same phenomenon was observed for SBCl2 and WM239 exosomes, as displayed in **Figure 5.3**. This result shows that exosomes

derived from the same cell line are consistent in their compositions, providing reproducible mass spectral fingerprints. The exosome cargo sorting in this case is shown to be a systematically controlled process, with the loading of particular cellular components into the vesicles.
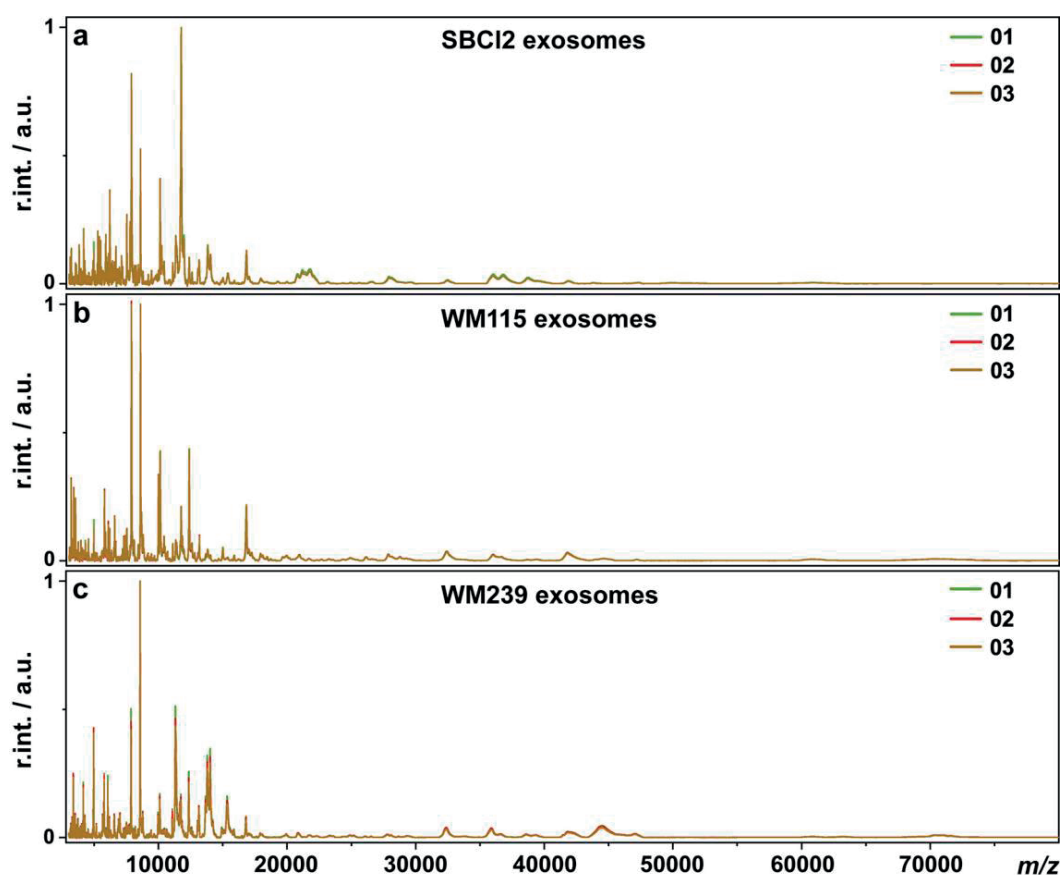


**Figure 5.3** MALDI-TOF mass spectra of (**a**) exosomes derived from SBCl2 cells, (**b**) exosomes derived from WM115 cells and (**c**) exosomes derived from WM239 cells. For each cell line, the cells were cultured for three passages, and exosomes were collected from the serum-free culture supernatant of each passage. Three mass spectra were displayed on each panel, labelled as '01', '02' and '03', corresponding to the three culture passages. Each spectrum was generated from $\sim 5 \cdot 10^7$ exosome particles.

## 3.2. Classification of parental cells by exosome fingerprinting

Classification of cell lines is often needed for cancer analysis. It helps the differentiation of cancer cells from normal cells, and facilitates the determination of cancer types and stages. For the purpose of cell line classification, two approaches based

on MALDI-TOF MS were investigated, *i.e.* fingerprinting of intact cells and fingerprinting of intact exosomes derived from the cells. Human embryonic kidney cell line HEK293, human cervical cancer cell line HeLa and the three different stage human melanoma cell lines SBCl2, WM115, WM239 were investigated with both approaches. The mass spectra generated from triplicate measurements (three culture passages for each cell line) are shown in **Figure 5.4** and **Figure 5.5**.
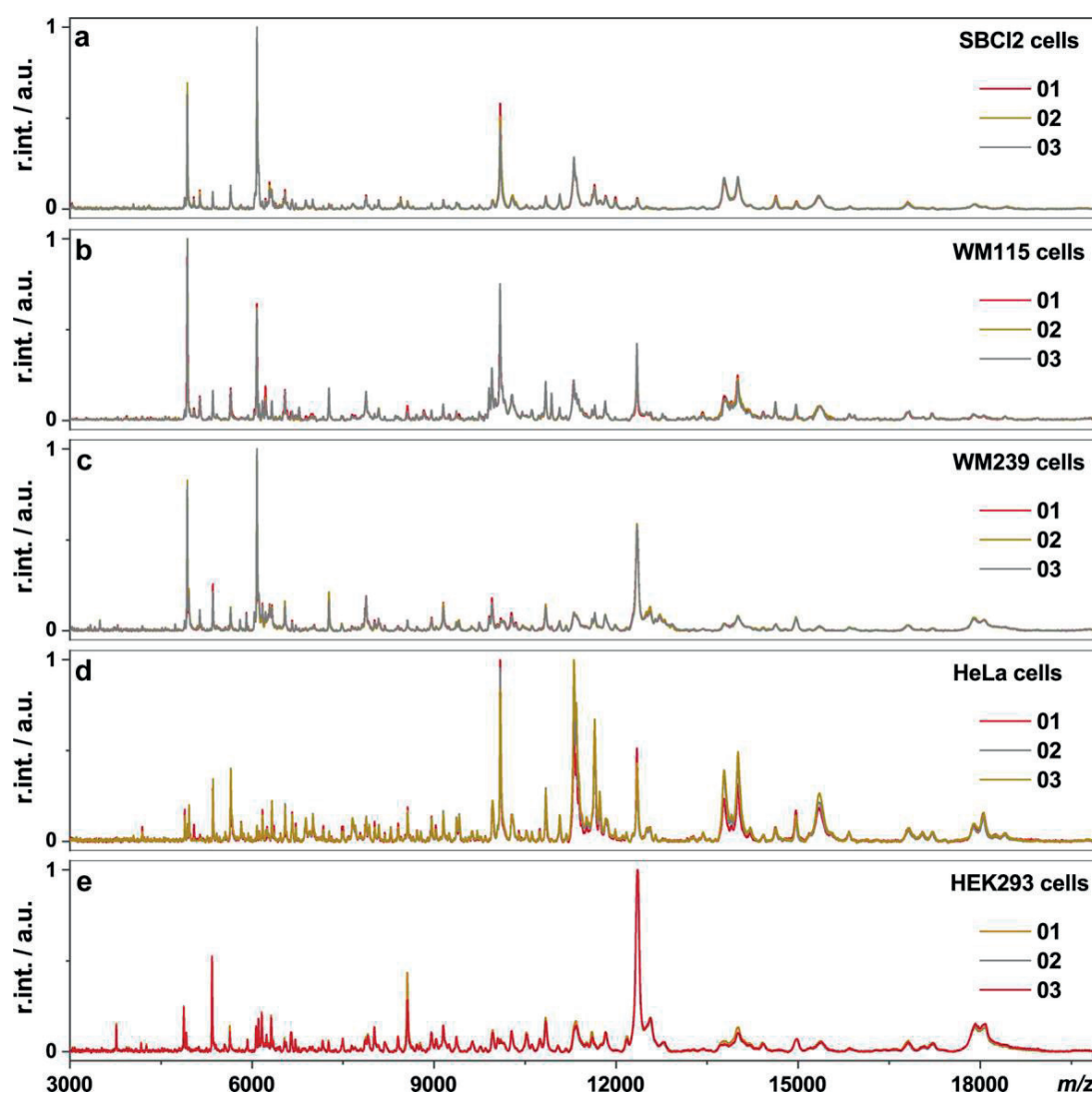


**Figure 5.4** MALDI-TOF mass spectra of (**a**) radial growth phase human primary melanoma cells SBCl2, (**b**) vertical growth phase human primary melanoma cells WM115, (**c**) metastatic human melanoma cells WM239, (**d**) human cervical cancer cells HeLa and (**e**) human embryonic kidney cell line HEK293. All the cells were cultured *in vitro* for three passages. Each spectrum was generated from ~$10^3$ cells.
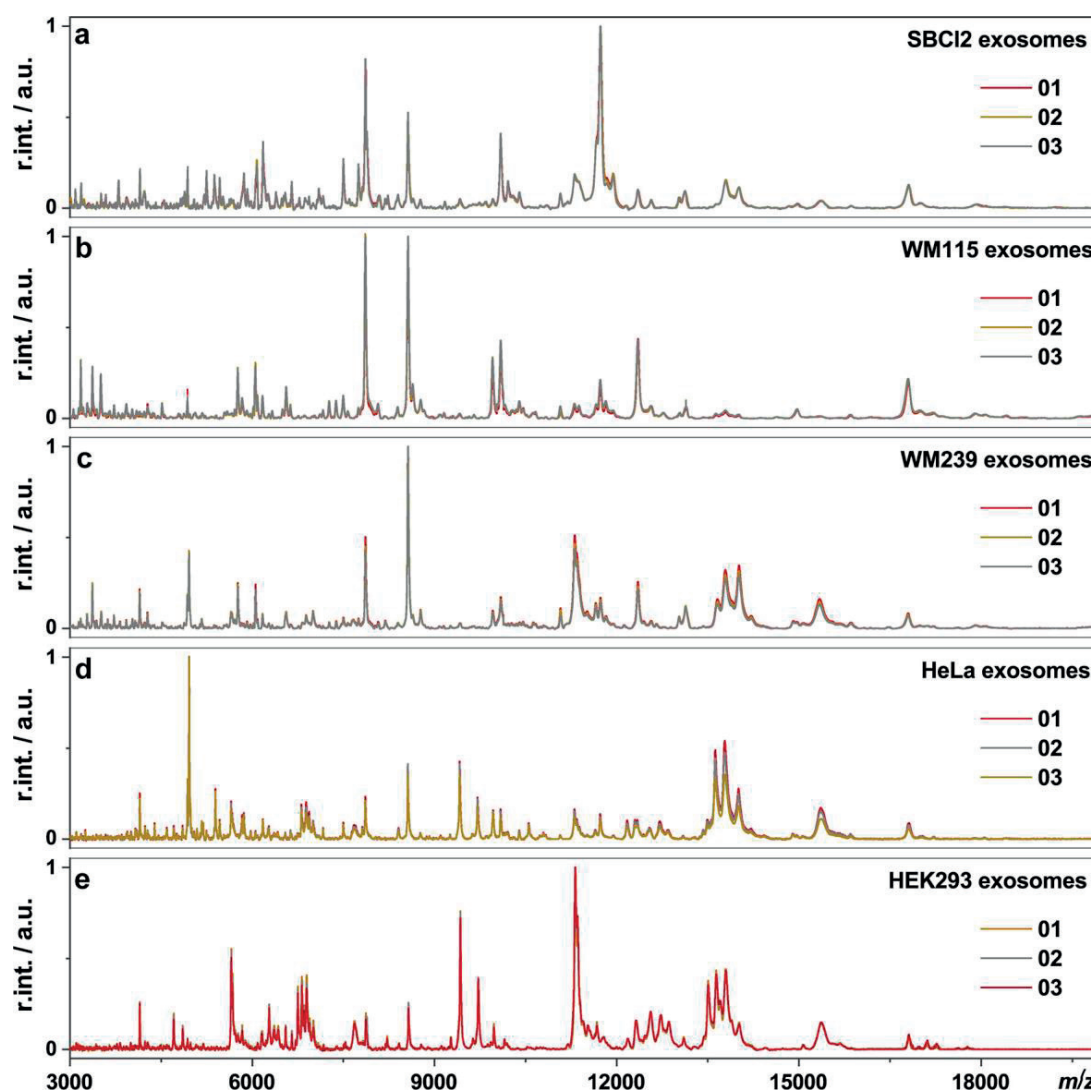
**Figure 5.5** MALDI-TOF mass spectra of (**a**) exosomes derived from SBCl2 cells, (**b**) exosomes derived from WM115 cells, (**c**) exosomes derived from WM239 cells, (**d**) exosomes derived from HeLa cells and (**e**) exosomes derived from HEK293 cells. All cells were cultured for three passages, and exosomes were collected from the serum-free cell culture supernatant. Each spectrum was generated from $\sim 5 \cdot 10^{7}$ exosome particles.

The mass spectra in **Figure 5.4** and **Figure 5.5**.underwent mathematical cluster analysis by calculating spectrum cosine similarity, with the algorithm described in CHAPTER II of this thesis. The resulting heatmaps are displayed in **Figure 5.6**, in which a darker colour represents a higher similarity score. **Figure 5.6 a** shows that the cell-fingerprinting approach was able to distinguish the melanoma cells from the cervical cancer cells (HeLa) and the non-cancerous cells (HEK293), with the spectrum
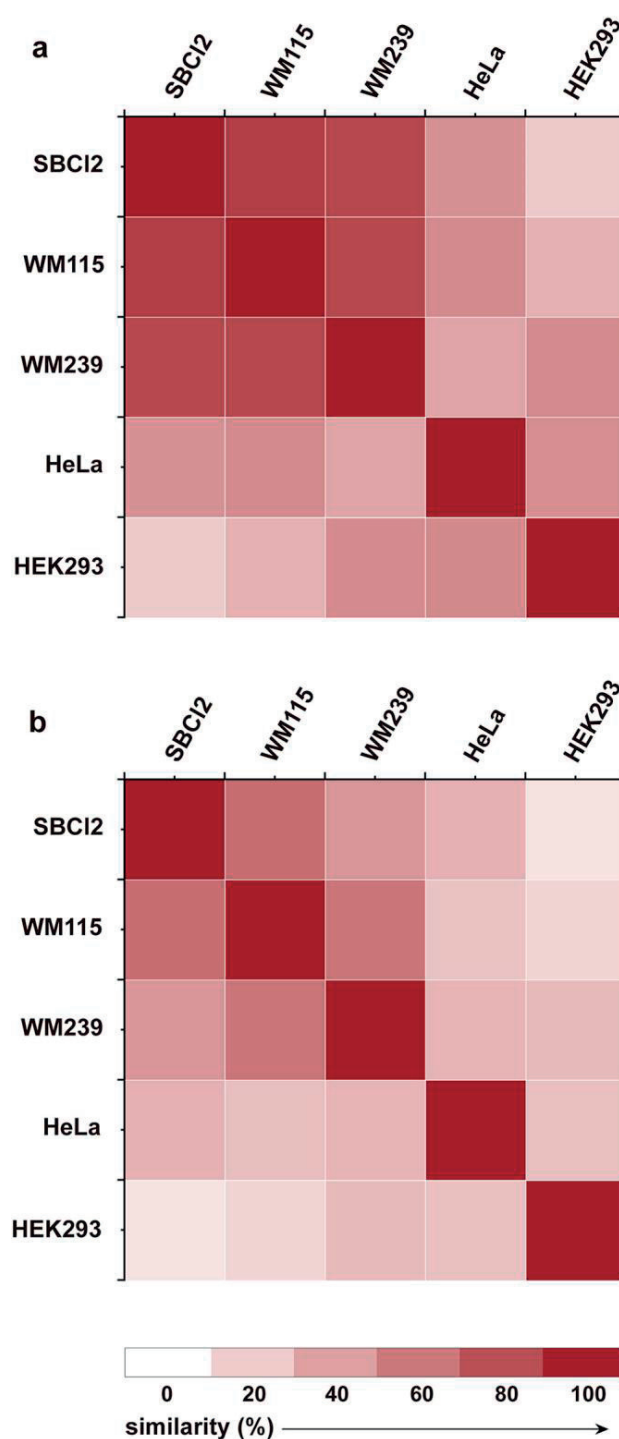
**Figure 5.6** Classification of five human cell lines. Two approaches were used for the classification, *i.e.* (**a**) MALDI-TOF MS fingerprinting of intact cells, (**b**) MALDI-TOF MS fingerprinting of intact exosomes derived from the cells. For each cell line, the mass spectra were generated from three culture passages. The colour darkness in the heatmaps represents the similarity score, with a darker colour corresponding to a higher similarity.

cosine similarities lower than 50%, *i.e.* 47.6% between HeLa and SBCl2, 49.9% between HeLa and WM115, 39.3% between HeLa and WM239, 21.2% between HEK293 and SBCl2, 32.5% between HEK293 and WM115, 49.6% between HEK293 and WM239, as well as 48.5% between HEK293 and HeLa. However, it was difficult to distinguish between the three melanoma cells, as their spectra shared more than 80% of similarity with each other, *i.e.* 86.9% between SBCl2 and WM115, 82.6% between SBCl2 and WM239, 82.2% between WM115 and WM239. As for the exosome-fingerprinting approach, it was not only able to separate the melanoma cluster from other cell types (spectrum similarities lower than 32%), but also allowed the differentiation among the three melanoma cells (spectrum similarities decreased to 42-65%) (**Figure 5.6 b**). The result indicates that each cancer cell line secretes specific exosomes, which could be used to distinguish cancer cells from normal cells and to differentiate between cancer types and cancer stages.

### 3.3. Tracing of protein transfer from cells to exosomes

Tracking the transfer of particular proteins from parental cells to the secreted exosomes is a common way to investigate mechanisms involved in exosome biogenesis or release. Fluorescence labelling method is often used to follow up the target proteins. Antibody-based methods like western blotting, enzyme-linked immunosorbent assay, immuno-electron microscopy, *etc.*, have also been used for target protein detection. Here, MALDI-TOF MS fingerprinting is shown to be a convenient supplement or alternative, as it allows a direct read-out of target proteins from both cells and exosomes based on the predicted molecular weight.
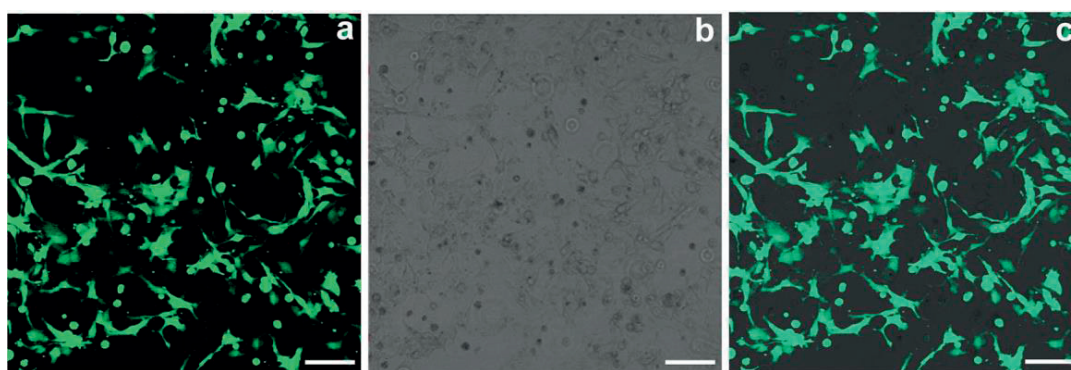


**Figure 5.7** Confocal microscopy images of WM239 cells that were transfected with GFP gene-containing plasmid (EGFP-N1 plasmid, Clontech, Basel, Switzerland). The images were taken in (**a**) fluorescence mode, (**b**) bright field mode, and (**c**) the merge mode. The images were taken at 20 h of post-transfection, with 488 nm excitation and 510 nm emission. Scale bar, 100 μm.
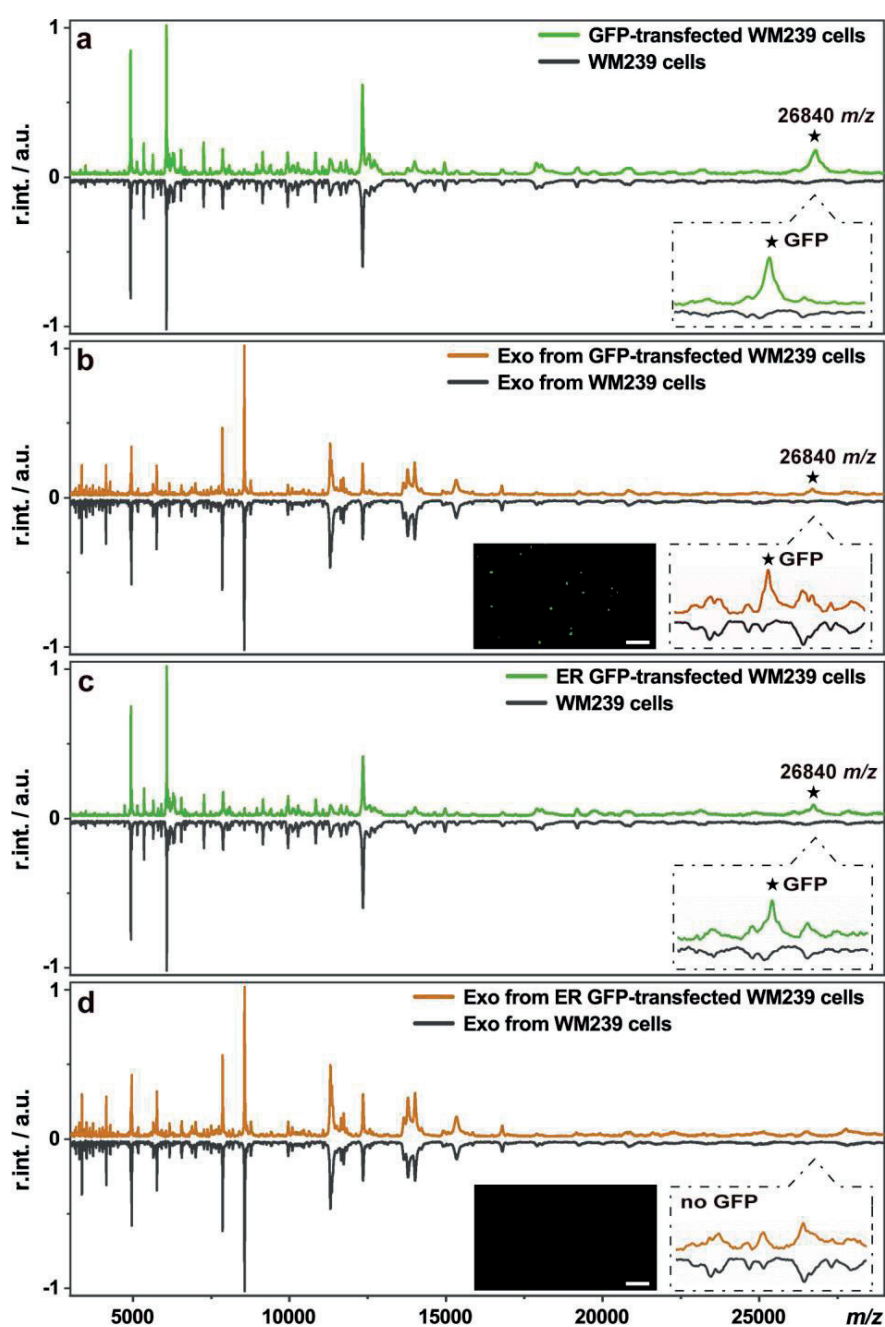
**Figure 5.8** Tracing protein transfer from parental cells to exosomes. (**a**) Mass spectra from GFP-transfected WM239 cells and non-transfected cells. (**b**) Mass spectra from exosomes secreted by GFP-transfected WM239 cells and the non-transfected control. (**c**) Mass spectra from ER-GFP-transfected WM239 cells and non-transfected cells. (**d**) Mass spectra from exosomes secreted by the ER-GFP-transfected WM239 cells and the non-transfected control. Each spectrum was obtained from $\sim 10^3$ intact cells or $\sim 5\cdot10^7$ intact exosomes. The insert graph on (**b**) and (**d**) were confocal fluorescence microscopy images of exosomes secreted from the plasmid transfected cells (scale bar, 5 μm).

As an example, green fluorescence protein (GFP) with different subcellular locations was monitored. WM239 cells were transfected with plasmid DNA to produce GFP in the cytoplasm. Expression of GFP in the transfected cells was confirmed by confocal fluorescence microscopy, with the observation of green fluorescence in the cells (**Figure 5.7**). The transfected cells and the secreted exosomes were measured by MALDI-TOF MS. As shown in **Figure 5.8 a**, compared to non-transfected cells, the transfected cells generated an additional mass spectral peak at 26,840 *m/z*. This peak is from GFP, which is composed of 238 amino acid residues with a theoretical molecular weight of ~26.9 kDa. The same peak was detected from the exosomes derived from the transfected cells, not from those derived from the non-transfected cells (**Figure 5.8 b**). It illustrates the sorting of the cytoplasm GFP into the exosomes, as was confirmed by the microscopy observation of green fluorescence in the exosomes (**Figure 5.8 b insert graph**). As a comparison, WM239 cells were transfected with a different plasmid DNA to synthesize GFP targeted to the endoplasmic reticulum (ER), a continuous membrane system that forms a series of flattened sacs within the cell cytoplasm. The ER-GFP was successfully expressed in the transfected cells, according to the appearance of a new peak at 26,840 *m/z* on the cell fingerprint compared to the case without transfection (**Figure 5.8 c**). The secreted exosomes, however, did not generate any additional peak compared to the non-transfected control (**Figure 5.8 d**), indicating that the ER-GFP was most probably not sorted into the exosomes. Confocal microscopy observation confirmed the lack of green fluorescence in the exosomes (**Figure 5.8 d insert graph**). It could be explained by the non-direct contact between the endoplasmic reticulum and the intracellular precursors of exosomes.[2,18] This MALDI-TOF MS based protein tracking method is universally feasible for all proteins, in principle, without the need of any labelling.

### 3.4. Read-out of cancer markers from exosome fingerprints

Proteins specifically produced or differentially expressed by cancer cells can be used as markers for clinical management of cancer diseases. They play crucial roles in cancer diagnosis, prognosis and therapeutic treatment efficacy prediction.[19] It would, of course, be an interesting analytical procedure if cancer marker proteins could be read directly from the fingerprints of the secreted exosomes. I tried to assign melanoma exosome fingerprint peaks by matching them with the exosome protein profiles that were obtained from top-down proteomic analysis. This proteomic analysis included protein extraction from exosomes, on-line liquid chromatography separation of the denatured intact proteins and detection of individual proteins using a high resolution Orbitrap mass spectrometer, which allowed accurate mass measurement and tandem mass spectrometry fragmentation analysis. The obtained raw data were processed with ProSight and TopPIC software to clarify protein identity.[20] This top-down proteomic procedure was

compatible with the MALDI-TOF MS fingerprinting approach, both of which detected the original proteins or protein fragments without protein digestion. The MALDI-TOF mass spectral peaks were thus tentatively assigned to particular proteins according to the detected mass values. The presence of the proteins in the exosomes was further confirmed by bottom-up proteomic analysis, which included SDS-PAGE separation of the denatured protein extracts, protein digestion and liquid chromatography-tandem mass spectrometric measurement of the protein digestion products.[21]
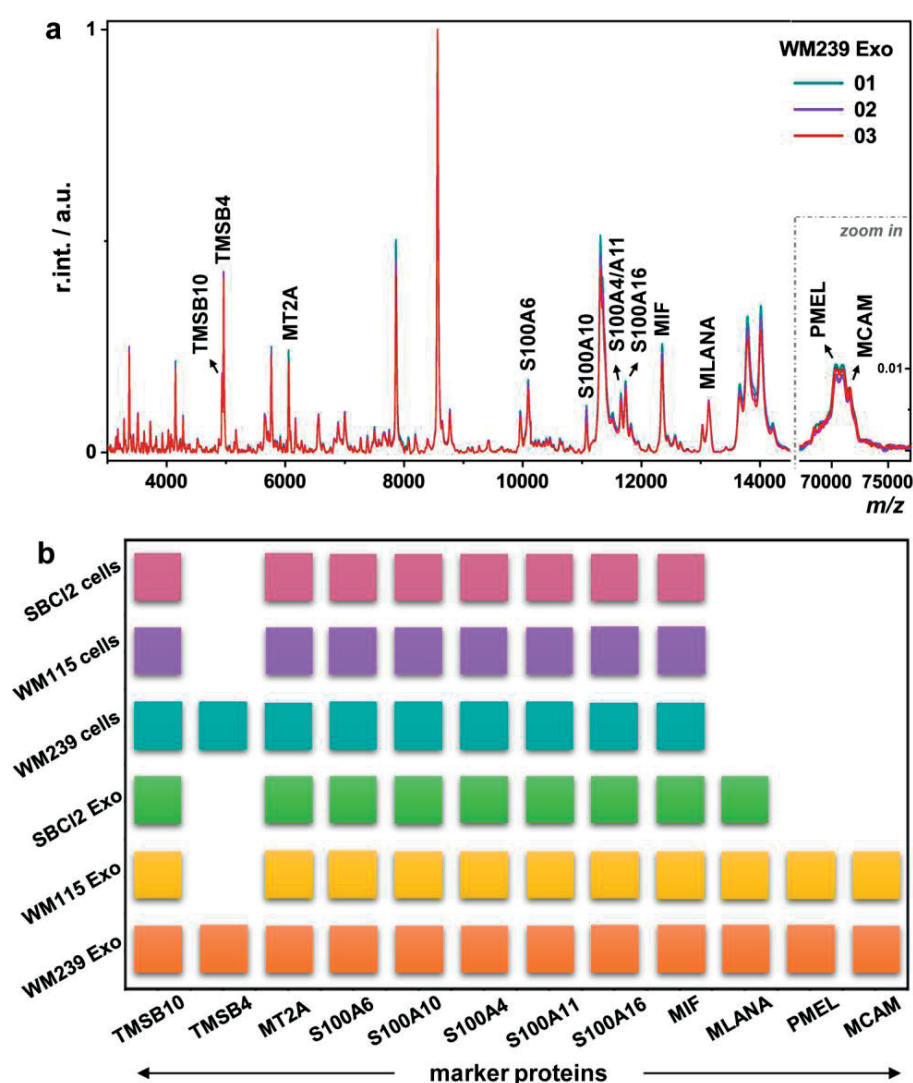


**Figure 5.9** (**a**) Read-out of melanoma marker proteins from WM239 exosome fingerprints, with the exosomes derived from WM239 cells at three culture passages. (**b**) Summary of melanoma marker proteins read from the fingerprints of SBCl2 cells, WM115 cells, WM239 cells, SBCl2 exosomes, WM115 exosomes and WM239 exosomes, with the coloured squares representing successful marker protein read-out.

Through the above procedure, a panel of well-known melanoma marker proteins were recognized from the exosome fingerprints. Taking WM239 exosomes as an example, the detected marker proteins are listed in **Figure 5.9 a**. Similarly, marker proteins detected from SBCl2 exosomes, WM115 exosomes, as well as SBCl2 cells, WM115 cells and WM239 cells are listed in **Appendix Figure**, with all the detected markers summarized in **Figure 5.9 b**. Specifically, thymosin beta 10 (TMSB10, 4,933 *m/z*), metallothionein-2 (MT2A, 6,052 *m/z*) and macrophage migration inhibitory factor (MIF, 12,337 *m/z*), three melanoma prognostic markers involved in the regulation of cellular migration, angiogenesis or inflammation, were detected from all the exosomes and their parental cells.[22-24] The S100 calcium binding protein family, a widely used marker for melanoma diagnosis, was also read from all the samples, with S100A6 observed at 10,084 *m/z*, S100A10 at 11,064 *m/z*, S100A4 & S100A11 at 11,640 *m/z* and S100A16 at 11,705 *m/z*.[25] Thymosin beta 4 (TMSB4, 4,960 *m/z*), a prognostic factor which stimulates tumour metastasis by activating cell migration and angiogenesis, was detected only from the metastatic melanoma WM239 cells and exosomes, not from the primary melanoma SBCl2 and WM115.[26] Some markers were read only from the exosome fingerprints, not from the parental cell fingerprints. They were melan-A (MLANA, 13,030 *m/z*, a melanoma differentiation antigen used for melanoma diagnosis), premelanosome protein (PMEL, 70,250 *m/z*, a melanoma diagnostic marker involved in melanosome maturation from stage I to stage II) and melanoma cell adhesion molecule (MCAM, 71,580 *m/z*, a cell surface glycoprotein promoting melanoma progression and associated with poor patient prognosis).[27,28] These three proteins are integral membrane proteins. Their enrichment in the secreted exosomes could be explained by the preferential sorting of cell membrane proteins into exosomes.[29] Among them, PMEL and MCAM were detected only from advanced melanoma (WM115, WM239), not from the non-tumorigenic primary melanoma (SBCl2). Detailed proteomic information supporting the protein assignment is given in **Appendix Note II**. To be mentioned, all the mass values mentioned in the present work were peak centre mass values averaged from multiple measurements. Herein a conclusion can be drawn that melanoma-derived exosomes are valuable sources of biomarkers, which are readable directly from the exosome fingerprints. Mass spectrometry detection of exosomes is thus a possible method for melanoma diagnosis and probably melanoma stage determination.

## 3.5. Exosome-mediated intercellular communication

As shown in **Figure 5.1**, exosomes contain surface molecules that facilitate their targeting to recipient cells. Upon attachment, exosomes can induce signaling through receptor-ligand interaction or can be internalized by endocytosis, phagocytosis or direct fusion with the cell membrane to deliver their contents into the recipient cells. Exosome
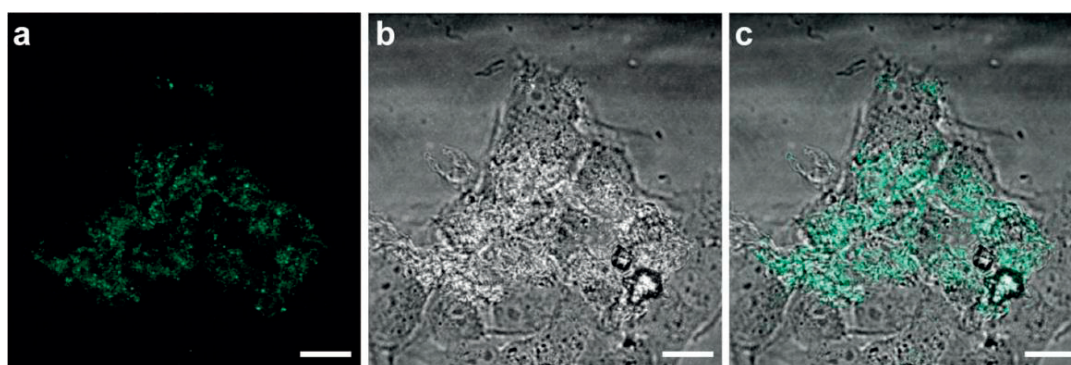
**Figure 5.10** Confocal microscopy images of SBCl2 cells co-incubated with exosomes derived from WM239 cells that have been transfected with GFP gene-containing plasmid (EGFP-N1 plasmid) to express green fluorescence protein in the cytoplasm. The images were taken in (**a**) fluorescence mode, (**b**) bright field mode and (**c**) the merge mode after 24 h of co-incubation with the exosomes, with 488 nm excitation and 510 nm emission. Scale bar, 20 μm.

contents such as mRNAs, miRNAs, DNAs, (signaling) proteins and bioactive lipids potentially function in the recipient cells and thereby alter the physiological state of the recipient cells.[30] In order to observe the active role of exosomes in cell-to-cell communication and cancer progression, an exosome transfer experiment was conducted. The non-tumorigenic radial growth phase primary melanoma cells SBCl2 were co-incubated with exosomes derived from the metastatic melanoma cells WM239. Sufficient amount of exosomes was used for the incubation to ensure an uptake of exosomes. The same transfer assay was conducted in triplicates to assess the reproducibility of the transfer results. Successful uptake of exosomes was demonstrated by confocal fluorescence microscopy observation (**Figure 5.10**). After 48 h of co-incubation with WM239 exosomes, the SBCl2 cells were analysed with MALDI-TOF MS, and the obtained fingerprints were compared with that of normal non-transferred SBCl2 cells. As shown in **Figure 5.11**, fingerprints of the recipient cells were changed, with some peaks newly detected or obviously elevated in intensity. As a contrast, no significant fingerprint difference was observed for the SBCl2 cells after co-incubation with WM115 exosomes (WM115 is a vertical growth phase primary melanoma cell line) (**Figure 5.12 a**). The fingerprint difference was neither observed for the control assay where SBCl2 cells were co-incubated with exosomes derived from the SBCl2 cells grown in a different passage (**Figure 5.12 b**). MALDI-TOF MS measurements are 'ion counting' processes, with the peak intensities greatly dependent on the numbers of ions reaching the detector. During the measurement of a mixture sample like the exosome entities in the present work, the normalized relative peak

intensities reflect, to a large extend, the relative abundance of the exosome components. Therefore, the newly detected or obviously elevated peaks in **Figure 5.11** indicate the up-regulation or possibly new expression of the corresponding proteins in the recipient cells. The results show that metastatic melanoma-derived exosomes can be taken up by primary non-tumorigenic melanoma cells, whose protein profile can thus be modified. Such kind of modulation could hardly happen when the exosomes are derived from less malignant cells. The superior activity of the metastatic cancer exosomes could be attributed to their high cargo level of functional biomolecules like mRNAs involved in cancer migration and metastasis.[31]
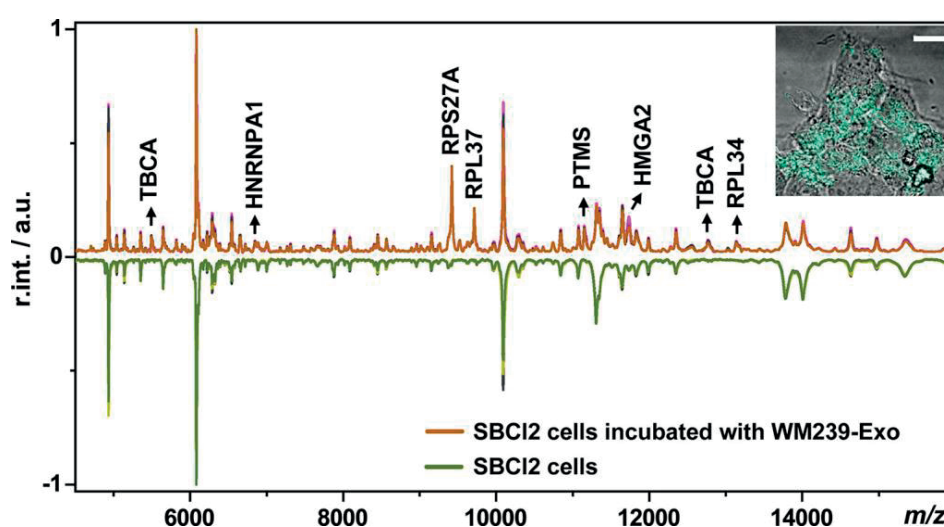


**Figure 5.11** Metastatic melanoma exosomes modulate protein profile of non-tumorigenic primary melanoma cells. Comparison of MALDI-TOF mass spectra generated from non-tumorigenic primary melanoma cells SBCl2 and the SBCl2 cells that have been co-incubated 48 h with exosomes secreted by metastatic melanoma cells WM239. Protein identity of differentially detected peaks were tentatively assigned by top-down and bottom-up proteomic analysis of the cells. Each panel of spectra is the overlapping of three spectra, coming from triplicate assays. The insert graph comes from Figure 5.10 c. demonstrating the successful internalization of exosomes in the recipient cells (scale bar, 20 μm). Each spectrum was obtained from ~ $10^3$ intact cells.

The differentially detected peaks in **Figure 5.11** were tentatively assigned to proteins by correlation with top-down and bottom-up proteomic analysis, and most of the proteins were found to be related with cancer progression. Specifically, the tubulin folding cofactor A (TBCA, 5,495 *m/z* (fragment) & 12,760 *m/z*), participating in tubulin
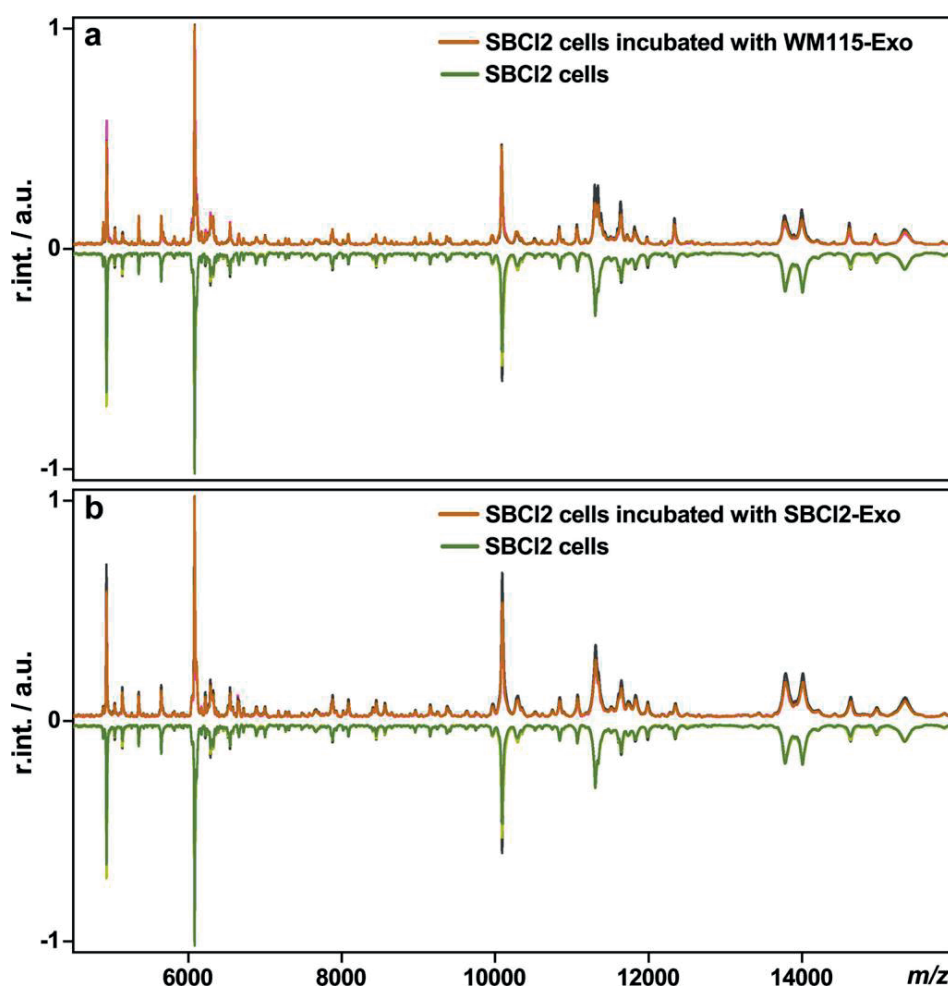
**Figure 5.12 (a)** Comparison of fingerprints generated from SBCl2 cells and SBCl2 cells after 48 h co-incubation with WM115 cells-derived exosomes. **(b)** Comparison of fingerprints generated from SBCl2 cells and SBCl2 cells after 48 h co-incubation with exosomes derived from the SBCl2 cells grown at different passages. Each panel of spectra contained the overlapping of three spectra, coming from triplicate assays.

folding pathway and α/β-tubulin heterodimer polymerization, can promote cancer cell migration and invasion by modulating cytoskeleton integration and cell cycle progress.[32] Heterogeneous nuclear ribonucleoprotein A1 (HNRNPA1, fragment, 6,845 *m/z*) is a RNA-binding protein involved in multiple aspects of mRNA metabolism and transport, and is associated with the metastasis of different cancers.[33] The ribosomal proteins including RPS27A (9,411 *m/z*), RPL37 (9,715 *m/z*) and RPL34 (13,150 *m/z*) have various cellular functions. Beside of the essential roles in ribosome assembly and mRNA translation, they take part in cancer cell migration and invasion, and are found

upregulated or overexpressed in advanced cancer phases.[34-37] Due to their important roles in nucleic acid management, HNRNPA1 and the three ribosomal proteins might be also related with the translation of exosomal genetic materials like mRNAs in the recipient cells.[38] Parathymosin (PTMS, 11,148 $m/z$) can regulate cell proliferation, apoptosis and cell cycle progress, and is correlated to malignant growth, progression and metastasis in the context of tumours.[39] The high mobility group AT-hook 2 (HMGA2, 11,734 $m/z$) is also related with cell proliferation and migration, whose overexpression has been suggested as a biomarker for melanoma progression and poor prognosis.[40] Detailed proteomic information supporting the protein assignment is given in **Appendix Note III**. The proteomic analyses showed that RPL37 and PTMS were present only in the exosome-transferred SBCl2 cells and the exosome parental cells WM239 but not in the non-transferred SBCl2 cells, while the other proteins were present in all cells. Combining the proteomic and the MALDI-TOF MS analysis results, it can be concluded that RPL37 and PTMS were most probably newly expressed and the other proteins were up-regulated in the exosome-transferred SBCl2 cells. Overall, the results show that metastatic melanoma-derived exosomes could modulate the protein profile of non-tumorigenic primary melanoma cells by increasing the expression of proteins involved in cancer progression. This finding is consistent with two recent reports, which demonstrated the enhancement of migration behaviour and metastatic capability of the exosome-transferred cells by fluorescence microscopy observation and intravital imaging.[31,41]

## 3.6. Monitoring of melanoma by detecting bloodstream-circulating exosomes

As illustrated above, exosomes play an active role in cancer progression. They are also valuable sources of cancer biomarkers, which are protected by the outermost lipid bilayer from rapid degradation. I predict that MALDI-TOF MS detection of exosomes circulating in the bloodstream, the most accessible and informative body fluid, could be a fast and convenient method for cancer disease monitoring. In clinical practice, the 1000-year-old biopsy is the current gold standard for cancer diagnosis and metastasis confirmation, which allows histological definition of cancer diseases.[42] But the sampling process is invasive and risky for patients and hard to be conducted repeatedly for dynamic cancer monitoring, especially when the patients are in poor performance status. Moreover, information obtained from a single biopsy provides a spatially and temporally limited snap-shot of a tumour, which is insufficient to reflect the tumour heterogeneity.[43] Liquid biopsy, a non-invasive procedure based on genetic and/or proteomic detection of circulating tumour DNA or circulating tumour cells in human blood, has been proposed as an alternative for cancer detection and post-diagnosis management. It has shown potentials in the assessment of prognosis, detection of disease recurrence and prediction

of response to treatment.[44,45] At the same time of obtaining clear success in different types of cancer, the liquid biopsy is nevertheless considerably costly, time-intensive or practically difficult.[46,47] In the case of melanoma, the situation is more complicated. Decades of investigation indicate that early detection of melanoma based on blood testing is hardly achievable, even using the highly sensitive circulating tumour DNA genotyping method. For instance, the optimal DNA concentration required by the ultrasensitive Sequenom® MassARRAY® detection platform is $\sim$ 30 ng·mL$^{-1}$ in blood plasma, but the average level of circulating melanoma DNA is only $\sim$ 7 ng·mL$^{-1}$, making the early detection difficult.[46,48] Here, exosomes circulating in patient bloodstream were investigated as the target biomaterial for melanoma monitoring. Instead of specifically detecting melanoma-derived exosomes, which might be limited in abundance and not easy to be separated from other circulating exosomes using current methods, all types of exosomes circulating in the bloodstream were measured together to give a panoramic view of the whole cancer burden in an individual sufferer.

The proposed approach was firstly tested with a mouse model of subcutaneous B16 melanoma, a model commonly used for *in vivo* melanoma study. Five wild-type mice of the same age and same gender were subcutaneously injected with B16 cells to develop localized melanoma.[49] The mice were maintained for tumour growth, and blood was drawn from the mice for exosome isolation on day 5, day 12 and day 19 after subcutaneous B16 cell injection. Regular observation of the mice found that a palpable tumour was formed in each of the mice on day 12, and the tumour reached the average size of 1 cm$^3$ on day 19. During blood collection, the blood was drawn from each mouse with tail vein sampling procedure, and the obtained five aliquots of blood plasma were mixed together for the isolation of 'averaged' circulating exosomes, which could represent the averaged physiological state of the five mice. Exosomes were isolated from the blood plasma using a commercial ExoQuick$^{TM}$ kit, which allows fast exosome precipitation and has been demonstrated efficient in performance by many users.[10] The obtained intact exosomes were measured with MALDI-TOF MS, and the generated fingerprints were compared with that from healthy mice. The whole process, from blood drawing to fingerprint generation, was completed within 2.5 h. As shown in **Figure 5.13**, exosome fingerprints obtained from the healthy mice on the three dates bear a high similarity (spectrum cosine similarity higher than 90% between each two of them) (**Figure 5.13 a, b, c**), meaning the stable physiological state of the mice. Compared to the healthy mice, clear fingerprint difference was observed for exosomes collected from melanoma-bearing mice (**Figure 5.13 d, e, f**). In the early stage of tumour growth, for instance, on day 5, the peak at 8,113 *m/z* and 8,878 *m/z* were found greatly elevated, which remained in high intensity on day 12 and day 19. They were tentatively assigned to platelet factor 4 (Pf4, 8,113 *m/z*) and complement component 3 (C3, 8,878 *m/z*) by
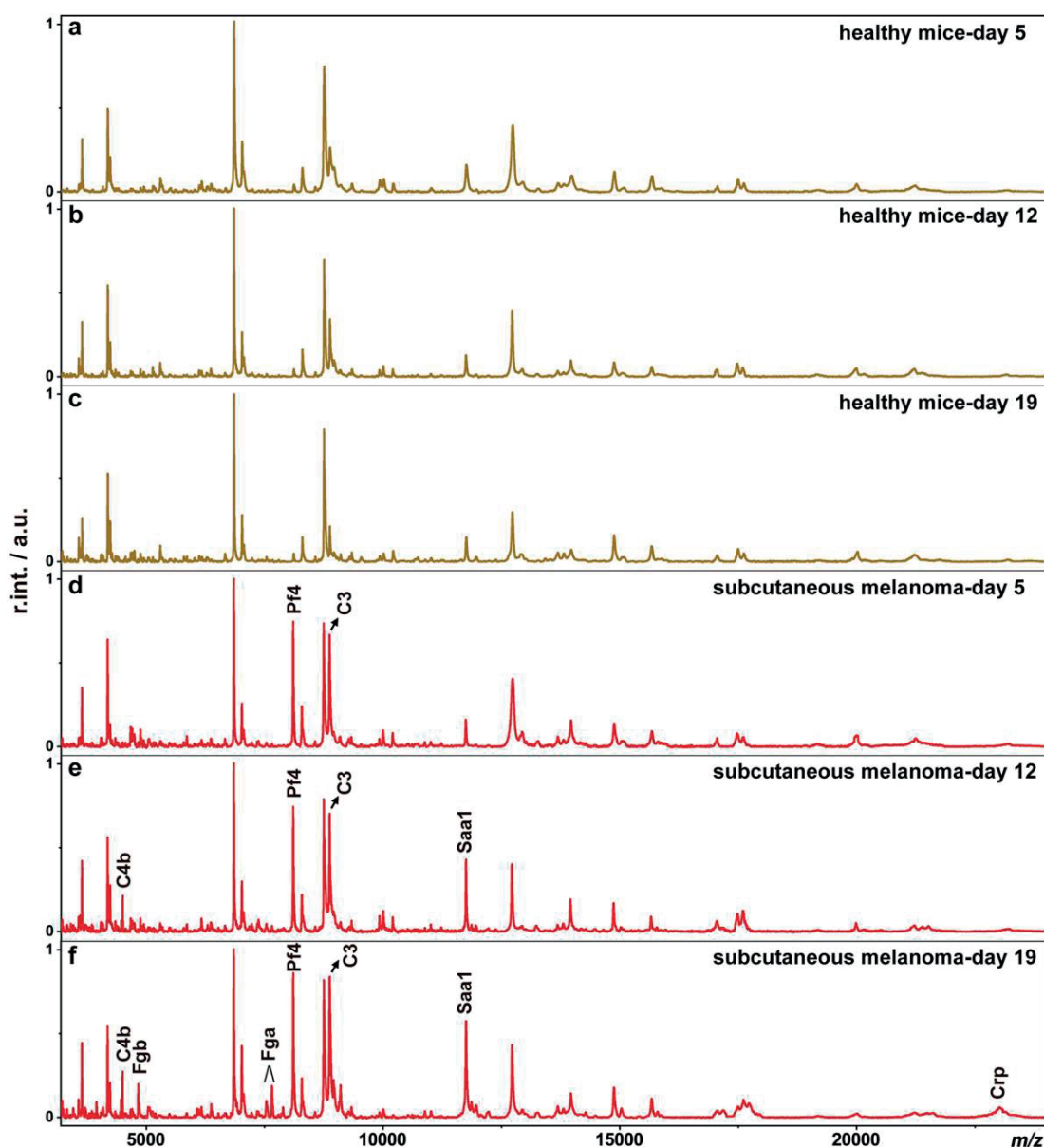
**Figure 5.13** Detection of bloodstream-circulating exosomes for the monitoring of murine melanoma growth. The healthy group and the subcutaneous melanoma group contained respectively five C57BL/6 mice of the same age and same gender. The displayed MALDI-TOF MS fingerprints correspond to (**a**) exosomes from healthy mice on day 5, (**b**) exosomes from healthy mice on day 12, (**c**) exosomes from healthy mice on day 19, (**d**) exosomes from melanoma-carrying mice on day 5, (**e**) exosomes from melanoma-carrying mice on day 12, (**f**) exosomes from melanoma-carrying mice on day 19, respectively. Protein identity of fingerprint peaks differentially detected from the melanoma-carrying mice were tentatively assigned by top-down and bottom-up proteomic analysis. Each spectrum was obtained from $\sim 5 \cdot 10^7$ exosome particles.

correlation with top-down and bottom-up proteomic analysis. The upregulation of Pf4 has been suggested as a potential marker of early tumour growth, as tumour growth can induce platelet activation, aggregation and thus trigger the release of Pf4 that is previously stored in the α-granules of platelets.[50,51] C3 plays a central role in the activation of complement system, which is a crucial part of the immune system. Early stages of complement activation in the tumour microenvironment is favourable to tumour growth.[52] For instance, secretion of C3 from CD8^{+} tumour-infiltrating lymphocytes (CD8^{+} TILs) and complement activation in the vicinity of CD8^{+} TILs can suppress the anti-tumour immunity of CD8^{+} TILs, and thus promote melanoma progression.[53] Increased level of C3 thus could also be an early sign of tumour growth. Along with the tumour development, complement component 4-B (C4b, fragment, 4,512 *m/z*), another important protein involved in complement activation through the classical and lectin pathways, was found obviously up-regulated on day 12 and on day 19.[54] Tumour development was also accompanied with the up-regulation of acute-phase proteins including fibrinogen beta chain (Fgb, fragment, 4,836 *m/z*), fibrinogen alpha chain (Fga, fragment, 7,538 & 7,666 *m/z*), serum amyloid A-1 (Saa1, 11,750 *m/z*) and C-reactive protein (Crp, 23,080 *m/z*). Their elevated level in the circulating exosomes should be caused by tissue inflammation during tumour growth.[55] Among them, fibrinogen has multiple functions in tumour development, including regulating inflammatory cell recruitment, providing structure to tumour stroma and inducing angiogenesis.[56] Serum amyloid A-1 and C-reactive protein are important biomarkers for melanoma prognosis, recurrence detection and treatment response prediction.[57,58] Accumulated evidence also supports the active roles of both proteins in tumour progression. For example, serum amyloid A probably acts as an extracellular matrix adhesive protein to hamper the adhesion of tumour cells on the extracellular matrix and thus to increase the migration ability of tumour cells. While C-reactive protein binds with complement protein C1q to initiate the classical pathway of complement activation in the tumour microenvironment and therefore to promote tumour growth.[59,60] Detailed proteomic information supporting the protein assignment is given in **Appendix Note IV**.

Encouraged by the positive feedback from the mouse model of melanoma, the proposed circulating exosome detection approach was further used for human melanoma investigation. Due to the difficulty in early melanoma detection, current liquid biopsy is mainly used for the monitoring of disease status in advanced melanoma patients. For example, circulating tumour DNA-based assays can reach the diagnostic sensitivity of 50-89% for stage IV melanoma patients.[61] And the detection rate of circulating tumour cells based on multi-marker RT-PCR assays is 10-35% from stage III melanoma patients and 54-86% from stage IV melanoma patients.[62] Here, three stage IV melanoma patients and three healthy adults were tested with the proposed approach. MALDI-TOF MS
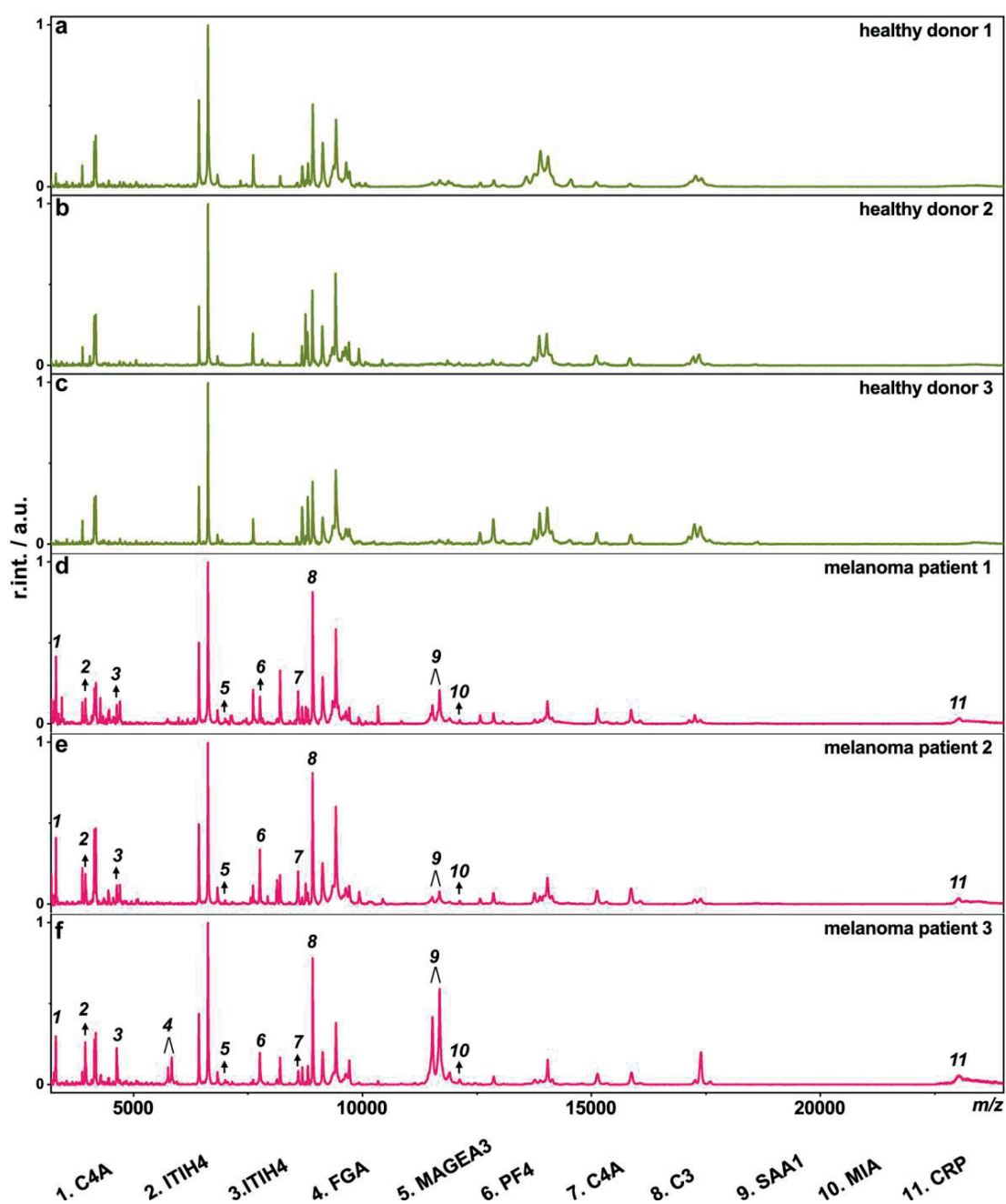
**Figure 5.14** Detection of bloodstream-circulating exosomes for the investigation of human melanoma. The displayed MALDI-TOF MS fingerprints correspond to (**a**) exosomes from healthy donor 1, (**b**) exosomes from healthy donor 2, (**c**) exosomes from healthy donor 3, (**d**) exosomes from melanoma patient 1, (**e**) exosomes from melanoma patient 2, (**f**) exosomes from melanoma patient 3, respectively. Protein identity of fingerprint peaks differentially detected from melanoma patients were tentatively assigned by correlation with top-down proteomic analysis. Each spectrum was obtained from ~ $5 \cdot 10^7$ exosome particles.

fingerprints of the bloodstream-circulating exosomes are shown in **Figure 5.14**. Each spectrum was an accumulation of totally 900 laser shots from three sample spots to make the detection result as reliable as possible. As displayed in **Figure 5.14 a, b, c,** exosomes from the three healthy adults shared most of the fingerprint peaks, with cosine similarity scores higher than 82%. Slight changes in intensities were observed for some of the peaks, associated with individual variations in physiological conditions. Compared to the healthy controls, melanoma patient exosomes displayed clear fingerprint difference. The differentially detected peaks were tentatively assigned by correlation with proteomic analysis. As listed in **Figure 5.14 d, e, f**, some of the proteins upregulated in melanoma-bearing mice were also upregulated in the melanoma patients, including the fibrinogen alpha chain (FGA, fragment, 5,802 & 5,898 *m/z, peak 4* in Figure 5.14), platelet factor 4 (PF4, 7,764 *m/z, peak 6* in Figure 5.14), complement component 3 (C3, 8,932 *m/z, peak 8* in Figure 5.14), serum amyloid A-1 (SAA1, 11,518 &11,675 *m/z, peak 9* in Figure 5.14) and C-reactive protein (CRP, 23,030 *m/z, peak 11* in Figure 5.14). Fibrinogen has been demonstrated a crucial determinant of tumour metastatic potential, with the elevated level significantly correlated with advanced cancer stage.[63,64] Increased expression of both SAA1 and CRP simultaneously highly predicts poor survival of melanoma patients.[58] The melanoma patient exosomes also carried increased level of inter alpha-trypsin inhibitor heavy chain family member 4 (ITIH4, fragment, 3,952 & 4,639 *m/z, peak 2 & 3* in Figure 5.14), another marker protein involved in acute-phase response.[65] In addition to the complement C3, one more protein related to the complement activation was up-regulated in the melanoma patients, *i.e.* complement component 4A (C4A, 3,312 (fragment) & 8,602 *m/z, peak 1 & 7* in Figure 5.14), which is the activation product of complement component 4.[66] Two melanoma-specific marker proteins were also detected from the patient exosomes, *i.e.* melanoma-associated antigen 3 (MAGEA3, fragment, 7,001 *m/z, peak 5* in Figure 5.14) and melanoma inhibitory activity (MIA, 12,112 *m/z, peak 10* in Figure 5.14). As one of the best characterized immunogenic antigens of melanoma, MAGEA3 has been frequently used for melanoma diagnosis, prognosis, metastasis indication and immunotherapy targeting.[62,67] MIA is also a valuable marker for melanoma diagnosis, which is secreted mainly from advanced primary or metastatic melanoma but not from normal melanocytes. The cancer cells are able to detach from some of their extracellular matrix contacts through secreting MIA to enhance their capability to migration, invasion and metastasis.[68,69] Detailed proteomic information supporting the above protein assignment is given in **Appendix Note V**. These differentially expressed proteins are hard to be detected by directly fingerprinting the blood plasma. Because blood plasma contains an extremely wide concentration range of proteins with more than 98% of the plasma mass represented by the several most abundant proteins like albumin,
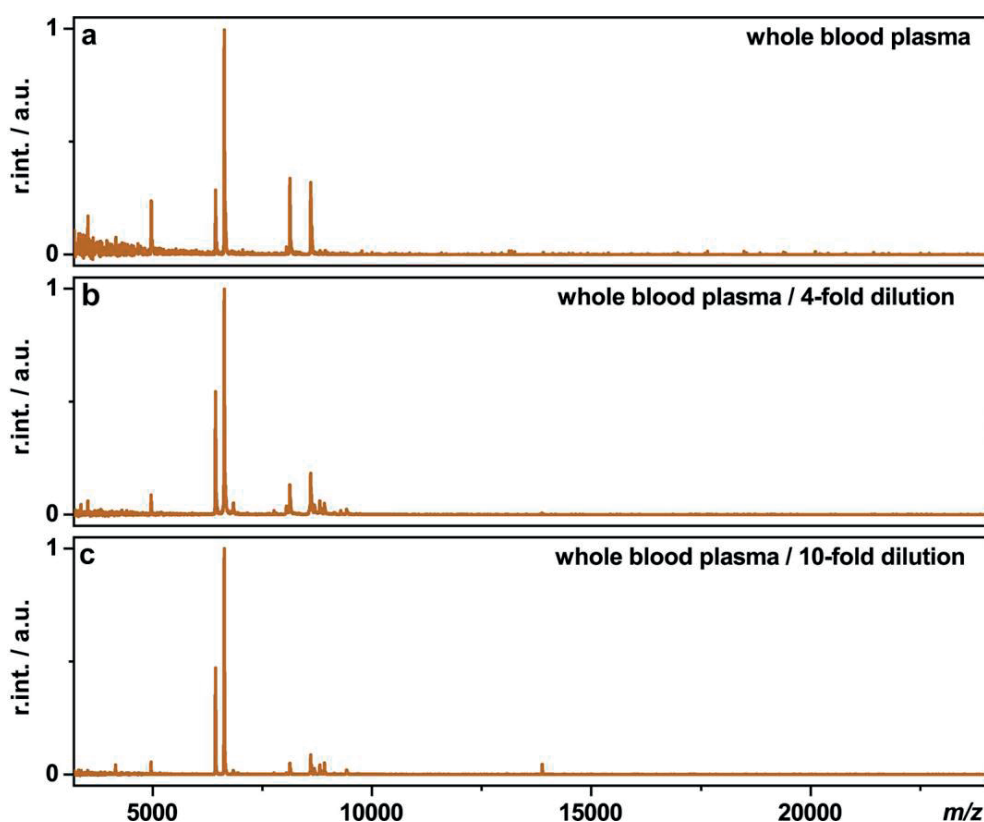
**Figure 5.15** MALDI-TOF MS detection of whole human blood plasma. The mass spectra were generated from whole blood plasma from the healthy donor 1 mentioned in Figure 5.14. The measurements were conducted under the following conditions: (**a**) the whole blood plasma was measured directly without any pre-treatment; (**b**) the whole blood plasma was measured after 4-fold dilution with deionized water; (**c**) the whole blood plasma was measured after 10-fold dilution with deionized water.

transthyretin and apolipoproteins, which dominate the mass spectra and greatly suppress the signals from other low abundant components (**Figure 5.15**).[70]

The above results show that MALDI-TOF mass spectrometry detection of bloodstream-circulating exosomes is potentially a very interesting method for melanoma diagnosis and the disease status monitoring. Based on nanoparticle tracking analysis, exosomes are circulating in human blood with high concentration, *i.e.* more than $10^{10}$ particles per mL of blood. And the exosome quantity required for one MALDI-TOF mass spectrometry measurement is only $\sim 5 \cdot 10^7$ particles. Each test therefore needs only a small volume of human blood (less than 1 mL). Owing to the availability of commercial kits for fast exosome precipitation and the use of mass spectrometry for rapid exosome measurement, the whole detection process, from blood drawing to mass

spectra generation, requires less than 3 h. The data analyses comprise reading and comparing mass spectral fingerprints, which are rather straightforward. Surely, many of the marker proteins remain to be validated *via* largescale studies, and the proposed method needs to be tested with many more patients from different melanoma stages with rigorous experimental design and statistical analysis. This will be the focus of my future work.

## 4. Conclusions

Overall, I present here a potential tool for cancer analysis by MALDI-TOF mass spectrometry detection of exosomes. Using melanoma as a cancer model, it has been shown that the tool can be applied for the classification of cancer cells, tracking of target proteins, detection of cancer biomarkers and exploring cancer progression *via* exosome-mediated intercellular communication. The tool also displays promise for melanoma diagnosis and the disease status monitoring by detecting bloodstream-circulating exosomes. In addition to melanoma, I expect that the proposed tool can be expanded to other cancer types after validation of corresponding biomarkers. Current methods for cancer analysis are often costly in time and money, or complex in experimental procedures and data analyses. The present tool could serve as a fast, convenient and less expensive supplement. Nowadays MALDI-TOF mass spectrometers have been installed in numerous hospitals for rapid diagnosis of infectious diseases, paving the way for their future applications in cancer diseases.

## Appendix Note I

**Exosome-associated proteins detected by bottom-up proteomic analysis.** These marker proteins were detected from all the exosome samples, *i.e.* SBCl2 exosomes, WM115 exosomes, WM239 exosomes. Results obtained from the WM115 exosomes are present here as examples.

**1.** CD63_CD63 molecule [Homo sapiens (human)], 100% identification, UniProt accession number P08962, 10 exclusive unique peptides, 19 exclusive unique spectra, 32 total spectra, 82/238 amino acids (34% coverage), recovered sequence shown below (highlighted with underline):

```
MAVEGGMKCV KFLLYVLLLA FCACAVGLIA VGVGAQLVLS QTIIQGATPG SLLPVVIIAV
GVFLFLVAFV GCCGACKENY CLMITFAIFL SLIMLVEVAA AIAGYVFRDK VMSEFNNNFR
QQMENYPKNN HTASILDRMQ ADFKCCGAAN YTDWEKIPSM SKNRVPDSCC INVTVGCGIN
FNEKAIHKEG CVEKIGGWLR KNVLVVAAAA LGIAFVEVLG IVFACCLVKS IRSGYEVM
```

**2.** CD81_CD81 molecule [Homo sapiens (human)], 100% identification, UniProt accession number P60033, 15 exclusive unique peptides, 30 exclusive unique spectra, 127 total spectra, 104/236 amino acids (44% coverage), recovered sequence shown below (highlighted with underline):

```
MGVEGCTKCI KYLLFVFNFV FWLAGGVILG VALWLRHDPQ TTNLLYLELG DKPAPNTFYV
GIYILIAVGA VMMFVGFLGC YGAIQESQCL LGTFFTCLVI LFACEVAAGI WGFVNKDQIA
KDVKQFYDQA LQQAVVDDDA NNAKAVVKTF HETLDCCGSS TLTALTTSVL KNNLCPSGSN
IISNLFKEDC HQKIDDLFSG KLYLIGIAAI VVAVIMIFEM ILSMVLCCGI RNSSVY
```

**3.** CD9_CD9 molecule [Homo sapiens (human)] fragment, 100% identification, UniProt accession number G8JLH6, 13 exclusive unique peptides, 26 exclusive unique spectra, 58 total spectra, 67/228 amino acids (29% coverage), recovered sequence shown below (highlighted with underline):

```
MPVKGGTKCI KYLLFGFNFI FWLAGIAVLA IGLWLRFDSQ TKSIFEQETN NNNSSFYTGV
YILIGAGALM MLVGFLGCCG AVQESQCMLG LATKRTMFPP FLEDHVCFFS LNPQFFGFLL
VIFAIEIAAA IWGYSHKDEV IKEVQEFYKD TYNKLKTKDE PQRETLKAIH YALNCCGLAG
GVEQFISDIC PKKDVLETFT VKSCPDAIKE VFDNKFHIIG AVGIGIAV
```

**4.** ALIX (PDCD6IP)_programmed cell death 6-interacting protein [Homo sapiens (human)], 100% identification, UniProt accession number **Q8WUM4,** 49 exclusive unique peptides, 71 exclusive unique spectra, 108 total spectra, 535/868 amino acids (62% coverage), recovered sequence shown below (highlighted with underline):

```
MATFISVQLK KTSEVDLAKP LVKFIQQTYP SGGEEQAQYC RAAEELSKLR RAAVGRPLDK
HEGALETLLR YYDQICSIEP KFPFSENQIC LTFTWKDAFD KGSLFGGSVK LALASLGYEK
SCVLFNCAAL ASQIAAEQNL DNDEGLKIAA KHYQFASGAF LHIKETVLSA LSREPTVDIS
PDTVGTLSLI MLAQAQEVFF LKATRDKMKD AIIAKLANQA ADYFGDAFKQ CQYKDTLPKE
VFPVLAAKHC IMQANAEYHQ SILAKQQKKF GEEIARLQHA AELIKTVASR YDEYVNVKDF
SDKINRALAA AKKDNDFIYH DRVPDLKDLD PIGKATLVKS TPVNVPISQK FTDLFEKMVP
VSVQQSLAAY NQRKADLVNR SIAQMREATT LANGVLASLN LPAAIEDVSG DTVPQSILTK
SRSVIEQGGI QTVDQLIKEL PELLQRNREI LDESLRLLDE EEATDNDLRA KFKERWQRTP
SNELYKPLRA EGTNFRTVLD KAVQADGQVK ECYQSHRDTI VLLCKPEPEL NAAIPSANPA
KTMQGSEVVN VLKSLLSNLD EVKKEREGLE NDLKSVNFDM TSKFLTALAQ DGVINEEALS
VTELDRVYGG LTTKVQESLK KQEGLLKNIQ VSHQEFSKMK QSNNEANLRE EVLKNLATAY
```

155

```
DNFVELVANL KEGTKFYNEL TEILVRFQNK CSDIVFARKT ERDELLKDLQ QSIAREPSAP
SIPTPAYQSS PAGGHAPTPP TPAPRTMPPT KPQPPARPPP PVLPANRAPS ATAPSPVGAG
TAAPAPSQTP GSAPPPQAQG PPYPTYPGYP GYCQMPMPMG YNPYAYGQYN MPYPPVYHQS
PGQAPYPGPQ QPSYPFPQPP QQSYYPQQ
```

**5.** TSG101_tumor susceptibility gene 101 protein [Homo sapiens (human)], 100% identification, UniProt accession number Q99816, 13 exclusive unique peptides, 19 exclusive unique spectra, 29 total spectra, 139/390 amino acids (36% coverage), recovered sequence shown below (highlighted with underline):

```
MAVSESQLKK MVSKYKYRDL TVRETVNVIT LYKDLKPVLD SYVFNDGSSR ELMNLTGTIP
VPYRGNTYNI PICLWLLDTY PYNPPICFVK PTSSMTIKTG KHVDANGKIY LPYLHEWKHP
QSDLLGLIQV MIVVFGDEPP VFSRPISASY PPYQATGPPN TSYMPGMPGG ISPYPSGYPP
NPSGYPGCPY PPGGPYPATT SSQYPSQPPV TTVGPSRDGT ISEDTIRASL ISAVSDKLRW
RMKEEMDRAQ AELNALKRTE EDLKKGHQKL EEMVTRLDQE VAEVDKNIEL LKKKDEELSS
ALEKMENQSE NNDIDEVIIP TAPLYKQILN LYAEENAIED TIFYLGEALR RGVIDLDVFL
KHVRLLSRKQ FQLRALMQKA RKTAGLSDLY
```

# Appendix Note II

**Protein identity of peaks listed in Figure 5.9.** Top-down and bottom-up proteomic analysis were conducted for all the following samples: SBCl2 cells, SBCl2 exosomes, WM115 cells, WM115 exosomes, WM239 cells, WM239 exosomes. Results obtained from WM239 exosomes are present here as examples.

**1.** TMSB10_thymosin beta 10 [*Homo sapiens* (human)], UniProt accession number P63313;

*a).* MALDI-TOF MS peak: 4,933 *m/z*;

*b).* Top-down proteomic analysis: adjusted precursor mass 4933.52296 Da, precursor mass 4933.515908 Da, number of matched fragment ions 29, E value 1.47E-27, P value 5.43E-35, sequence shown below:

```
M.(A)[Acetyl]DKPDMGEIASFDKAKLKKTETQEKNTLPTKETIEQEKRSEIS.
```

*c).* Bottom-up proteomic analysis: 100% identification, 2 exclusive unique peptides, 2 exclusive unique spectra, 2 total spectra, 22/44 amino acids (50% coverage), recovered sequence shown below (highlighted with underline):

```
MADKPDMGEI ASFDKAKLKK TETQEKNTLP TKETIEQEKR SEIS
```

**2.** TMSB4_thymosin beta 4 [*Homo sapiens* (human)], UniProt accession number P62328;

*a).* MALDI-TOF MS peak: 4,960 *m/z*;

*b).* Top-down proteomic analysis: adjusted precursor mass 4960.48624 Da, precursor mass 4960.495208 Da, number of matched fragment ions 17, E value 9.86E-19, P value 3.64E-19, sequence shown below:

```
M.(S)[Acetyl]DKPDMAEIEKFDKSKLKKTETQEKNPLPSKETIEQEKQAGES.
```

*c).* Bottom-up proteomic analysis: 100% identification, 1 exclusive unique peptides, 2 exclusive unique spectra, 2 total spectra, 14/44 amino acids (32% coverage), recovered sequence shown below (highlighted with underline):

```
MSDKPDMAEI EKFDKSKLKK TETQEKNPLP SKETIEQEKQ AGES
```

(Both Top-down and bottom-up proteomic analysis confirmed that TMSB4 was present only in metastatic melanoma WM239 cells and exosomes, not in the primary non-metastatic melanoma SBCl2 and WM115.)

**3.** MT2A_metallothionein-2 [*Homo sapiens* (human)], UniProt accession number P02795;

*a).* MALDI-TOF MS peak: 6,052 *m/z*;

*b).* Top-down proteomic analysis: adjusted precursor mass 6052.397438 Da, precursor mass 6052.217438 Da, number of matched fragment ions 13, E value 9.86E-19, P value 3.64E-19, sequence shown below:

```
.(MDPNCSCAA)[15.20132]GDSCTCAGSCKCKECKCTSCKKSCCSCCPVGCAKCAQGCICK
GASDKCSCCA.
```

*c).* Bottom-up proteomic analysis: 100% identification, 4 exclusive unique peptides, 4 exclusive unique spectra, 6 total spectra, 41/61 amino acids (67% coverage), recovered sequence shown below (highlighted with underline):

```
MDPNCSCAAG DSCTCAGSCK CKECKCTSCK KSCCSCCPVG CAKCAQGCIC KGASDKCSCC
A
```

**4.** S100A6_S100 calcium binding protein A6 [*Homo sapiens* (human)], UniProt accession number P06703;

*a).* MALDI-TOF MS peak: 10,084 *m/z*;

*b).* Top-down proteomic analysis: adjusted precursor mass 10084.31242 Da, precursor mass 10084.30133 Da, number of matched fragment ions 26, E value 1.79E-11, P value 6.59E-19, sequence shown below:

```
M.(A)[Acetyl]CPLDQAIGLLVAIFHKYSGREGDKHTLSKKELKELIQKELTIGSKLQDAEI
ARLMEDLDRNKDQEVNFQEYVTFLGALALIYNEALKG.
```

*c).* Bottom-up proteomic analysis: 100% identification, 9 exclusive unique peptides, 14 exclusive unique spectra, 27 total spectra, 81/90 amino acids (90% coverage), recovered sequence shown below (highlighted with underline):

```
MACPLDQAIG LLVAIFHKYS GREGDKHTLS KKELKELIQK ELTIGSKLQD AEIARLMEDL
DRNKDQEVNF QEYVTFLGAL ALIYNEALKG
```

**5.** S100A10_S100 calcium binding protein A10 [*Homo sapiens* (human)], UniProt accession number P60903;

*a).* MALDI-TOF MS peak: 11,064 *m/z*;

*b).* Top-down proteomic analysis: adjusted precursor mass 11064.47058 Da, precursor mass 11064.45679 Da, number of matched fragment ions 25, E value 3.35E-25, P value 1.23E-32, sequence shown below:

```
M.PSQMEHAMETMMFTFHKFAGDKGYLTKEDLRVLMEKEFPGFLENQKDPLAVDKIMKDLDQCR
DGKVGFQSFFSLIAGLTIACNDYFVVHMKQKGKK.
```

*c).* Bottom-up proteomic analysis: 100% identification, 5 exclusive unique peptides, 8 exclusive unique spectra, 22 total spectra, 44/97 amino acids (45% coverage), recovered sequence shown below (highlighted with underline):

```
MPSQMEHAME TMMFTFHKFA GDKGYLTKED LRVLMEKEFP GFLENQKDPL AVDKIMKDLD
QCRDGKVGFQ SFFSLIAGLT IACNDYFVVH MKQKGKK
```

**6.** S100A4_S100 calcium binding protein A4 [*Homo sapiens* (human)], UniProt accession number P26447;

*a).* MALDI-TOF MS peak: 11,640 *m/z*;

*b).* Top-down proteomic analysis: adjusted precursor mass 11631.70198 Da, precursor mass 11631.71462 Da, number of matched fragment ions 42, E value 4.00E-24, P value 1.48E-31, sequence shown below:

```
M.(A)[Acetyl]CPLEKALDVMVSTFHKYSGKEGDKFKLNKSELKELLTRELPSFLGKRTDEA
AFQKLMSNLDSNRDNEVDFQEYCVFLSCIAMMCNEFFEGFPDKQPRKK.
```

*c).* Bottom-up proteomic analysis: 100% identification, 5 exclusive unique peptides, 10 exclusive unique spectra, 16 total spectra, 37/101 amino acids (37% coverage), recovered sequence shown below (highlighted with underline):

```
MACPLEKALD VMVSTFHKYS GKEGDKFKLN KSELKELLTR ELPSFLGKRT DEAAFQKLMS
NLDSNRDNEV DFQEYCVFLS CIAMMCNEFF EGFPDKQPRK K
```

**7.** S100A11_S100 calcium binding protein A11 [*Homo sapiens* (human)], UniProt accession number P31949;

*a).* MALDI-TOF MS peak: 11,640 *m/z*;

*b).* Top-down proteomic analysis: adjusted precursor mass 11643.79502 Da, precursor mass 11643.78516 Da, number of matched fragment ions 42, E value 8.22E-32, P value 3.02E-39, sequence shown below:

```
M.(A)[Acetyl]KISSPTETERCIESLIAVFQKYAGKDGYNYTLSKTEFLSFMNTELAAFTKN
QKDPGVLDRMMKKLDTNSDGQLDFSEFLNLIGGLAMACHDSFLKAVPSQKRT.
```

*c).* Bottom-up proteomic analysis: 100% identification, 10 exclusive unique peptides, 23 exclusive unique spectra, 46 total spectra, 87/105 amino acids (83% coverage), recovered sequence shown below (highlighted with underline):

```
MAKISSPTET ERCIESLIAV FQKYAGKDGY NYTLSKTEFL SFMNTELAAF TKNQKDPGVL
DRMMKKLDTN SDGQLDFSEF LNLIGGLAMA CHDSFLKAVP SQKRT
```

**8.** S100A16_S100 calcium binding protein A16 [*Homo sapiens* (human)], UniProt accession number Q96FQ6;

*a).* MALDI-TOF MS peak: 11,705 *m/z*;

*b).* Top-down proteomic analysis: adjusted precursor mass 11704.93878 Da, precursor mass 11704.94767 Da, number of matched fragment ions 29, E value 1.64E-27, P value 6.06E-35, sequence shown below:

```
M.(S)[Acetyl]DCYTELEKAVIVLVENFYKYVSKYSLVKNKISKSSFREMLQKELNHMLSDT
GNRKAADKLIQNLDANHDGRISFDEYWTLIGGITGPIAKLIHEQEQQSSS.
```

*c).* Bottom-up proteomic analysis: 100% identification, 6 exclusive unique peptides, 8 exclusive unique spectra, 18 total spectra, 66/103 amino acids (64% coverage), recovered sequence shown below (highlighted with underline):

```
MSDCYTELEK AVIVLVENFY KYVSKYSLVK NKISKSSFRE MLQKELNHML SDTGNRKAAD
KLIQNLDANH DGRISFDEYW TLIGGITGPI AKLIHEQEQQ SSS
```

**9.** MIF_macrophage migration inhibitory factor [*Homo sapiens* (human)], UniProt accession number P14174;

*a).* MALDI-TOF MS peak: 12,337 *m/z*;

*b).* Top-down proteomic analysis: adjusted precursor mass 12337.17865 Da, precursor mass 12337.19735 Da, number of matched fragment ions 23, E value 6.36E-11, P value 2.34E-18, sequence shown below:

```
M.PMFIVNTNVPRASVPDGFLSELTQQLAQATGKPPQYIAVHVVPDQLMAFGGSSEPCALCSLH
SIGKIGGAQNRSYSKLLCGLLAERLRISPDRVYINYYDMNAANVGWNNSTFA.
```

***c).*** Bottom-up proteomic analysis: 100% identification, 10 exclusive unique peptides, 23 exclusive unique spectra, 91 total spectra, 73/115 amino acids (63% coverage), recovered sequence shown below (highlighted with underline):

```
MPMFIVNTNV PRASVPDGFL SELTQQLAQA TGKPPQYIAV HVVPDQLMAF GGSSEPCALC
SLHSIGKIGG AQNRSYSKLL CGLLAERLRI SPDRVYINYY DMNAANVGWN NSTFA
```

**10.** MLANA_melan-A (melanoma antigen recognized by T-cells 1) [*Homo sapiens* (human)], UniProt accession number Q16655;

***a).*** MALDI-TOF MS peak: 13,030 *m/z*;

***b).*** Top-down proteomic analysis: adjusted precursor mass 13025.75389 Da, precursor mass 13025.76345 Da, number of matched fragment ions 29, E value 1.82E-13, P value 6.69E-21, sequence shown below:

```
M.PREDAHFIYGYPKKGHGHSYTTAEEAAGIGILTVILGVLLLIGCWYCRRRNGYRALMDKSLH
VGTQCALTRRCPQEGFDHRDSKVSLQEKNCEPVVPNAPPAYEKLSAEQSPPPYSP.
```

***c).*** Bottom-up proteomic analysis: 100% identification, 10 exclusive unique peptides, 20 exclusive unique spectra, 45 total spectra, 71/118 amino acids (60% coverage), recovered sequence shown below (highlighted with underline):

```
MPREDAHFIY GYPKKGHGHS YTTAEEAAGI GILTVILGVL LLIGCWYCRR RNGYRALMDK
SLHVGTQCAL TRRCPQEGFD HRDSKVSLQE KNCEPVVPNA PPAYEKLSAE QSPPPYSP
```

**11.** PMEL_premelanosome protein [*Homo sapiens* (human)], UniProt accession number P40967;

***a).*** MALDI-TOF MS peak: 70,250 *m/z*;

***b).*** Top-down proteomic analysis: adjusted precursor mass 70304.187114 Da, precursor mass 70304.19145 Da, number of matched fragment ions 31, E value 2.29E-14, P value 8.44E-22, sequence shown below:

```
.(M)[Acetyl]DLVLKRCLLHLAVIGALLAVGATKVPRNQDWLGVSRQLRTKAWNRQLYPEWT
EAQRLDCWRGGQVSLKVSNDGPTLIGANASFSIALNFPGSQKVLPDGQVIWVNNTIINGSQVWG
GQPVYPQETDDACIFPDGGPCPSGSWSQKRSFVYVWKTWGQYWQVLGGPVSGLSIGTGRAMLGT
HTMEVTVYHRRGSRSYVPLAHSSSAFTITDQVPFSVSVSQLRALDGGNKHFLRNQPLTFALQLH
DPSGYLAEADLSYTWDFGDSSGTLISRALVVTHTYLEPGPVTAQVVLQAAIPLTSCGSSPVPGT
TDGHRPTAEAPNTTAGQVPTTEVVGTTPGQAPTAEPSGTTSVQVPTTEVISTAPVQMPTAESTG
MTPEKVPVSEVMGTTLAEMSTPEATGMTPAEVSIVVLSGTTAAQVTTTEWVETTARELPIPEPE
```

```
GPDASSIMSTESITGSLGPLLDGTATLRLVKRQVPLDCVLYRYGSFSVTLDIVQGIESAEILQA
VPSGEGDAFELTVSCQGGLPKEACMEISSPGCQPPAQRLCQPVLPSPACQLVLHQILKGGSGTY
CLNVSLADTNSLAVVSTQLIMPGQEAGLGQVPLIVGILLVLMAVVLASLIYRRRLMKQDFSVPQ
LPHSSSHWLRLPRIFCSCPIGENSPLLSGQQV.
```

*c).* Bottom-up proteomic analysis: 100% identification, 17 exclusive unique peptides, 43 exclusive unique spectra, 82 total spectra, 187/661 amino acids (28% coverage), recovered sequence shown below (highlighted with underline):

```
MDLVLKRCLL HLAVIGALLA VGATKVPRNQ DWLGVSRQLR TKAWNRQLYP EWTEAQRLDC
WRGGQVSLKV SNDGPTLIGA NASFSIALNF PGSQKVLPDG QVIWVNNTII NGSQVWGGQP
VYPQETDDAC IFPDGGPCPS GSWSQKRSFV YVWKTWGQYW QVLGGPVSGL SIGTGRAMLG
THTMEVTVYH RRGSRSYVPL AHSSSAFTIT DQVPFSVSVS QLRALDGGNK HFLRNQPLTF
ALQLHDPSGY LAEADLSYTW DFGDSSGTLI SRALVVTHTY LEPGPVTAQV VLQAAIPLTS
CGSSPVPGTT DGHRPTAEAP NTTAGQVPTT EVVGTTPGQA PTAEPSGTTS VQVPTTEVIS
TAPVQMPTAE STGMTPEKVP VSEVMGTTLA EMSTPEATGM TPAEVSIVVL SGTTAAQVTT
TEWVETTARE LPIPEPEGPD ASSIMSTESI TGSLGPLLDG TATLRLVKRQ VPLDCVLYRY
GSFSVTLDIV QGIESAEILQ AVPSGEGDAF ELTVSCQGGL PKEACMEISS PGCQPPAQRL
CQPVLPSPAC QLVLHQILKG GSGTYCLNVS LADTNSLAVV STQLIMPGQE AGLGQVPLIV
GILLVLMAVV LASLIYRRRL MKQDFSVPQL PHSSSHWLRL PRIFCSCPIG ENSPLLSGQQ
V
```

(Both Top-down and bottom-up proteomic analysis confirmed that PMEL was present only in advance melanoma WM115 and WM239 cells and exosomes, not in the non-tumorigenic primary melanoma SBCl2. With MALDI-TOF MS fingerprinting approach, PMEL was detected only from WM115 exosomes and WM239 exosomes, not from their parental cells, indicating the enrichment of PMEL in the secreted exosomes.)

**12.** MCAM_melanoma cell adhesion molecule [*Homo sapiens* (human)], UniProt accession number P43121;

*a).* MALDI-TOF MS peak: 71,580 *m/z*;

*b).* Top-down proteomic analysis failed to detect this protein. But bottom-up proteomic analysis of the SDS-PAGE gel band around ~72 kDa revealed that the most high abundant protein within this gel band was MCAM, whose theoretical molecular weight is 71,607 Da (provided by Uniprot database). Moreover, bottom-up analysis showed that this protein was present only in the WM115 exosomes and WM239 exosomes, not from the SBCl2 exosomes, consistent with the detection result provided by MALDI-TOF MS (the peak at 71,580 *m/z* was detected only from the WM115 exosomes and WM239 exosomes, not from the SBCl2 exosomes). Overall, the MALDI-TOF MS peak at 71,580 *m/z* has very high chance to come from the protein MCAM. By the way, bottom-up proteomic

analysis showed MCAM was also present in WM115 cells and WM239 cells, but the MALDI-TOF MS peak at 71,580 *m/z* was not observed from the two parental cells, indicating the enrichment of MCAM in the secreted exosomes.

*c).* Bottom-up proteomic analysis: 100% identification, 21 exclusive unique peptides, 38 exclusive unique spectra, 110 total spectra, 258/646 amino acids (40% coverage), recovered sequence shown below (highlighted with underline):

```
MGLPRLVCAF LLAACCCCPR VAGVPGEAEQ PAPELVEVEV GSTALLKCGL SQSQGNLSHV
DWFSVHKEKR TLIFRVRQGQ GQSEPGEYEQ RLSLQDRGAT LALTQVTPQD ERIFLCQGKR
PRSQEYRIQL RVYKAPEEPN IQVNPLGIPV NSKEPEEVAT CVGRNGYPIP QVIWYKNGRP
LKEEKNRVHI QSSQTVESSG LYTLQSILKA QLVKEDKDAQ FYCELNYRLP SGNHMKESRE
VTVPVFYPTE KVWLEVEPVG MLKEGDRVEI RCLADGNPPP HFSISKQNPS TREAEEETTN
DNGVLVLEPA RKEHSGRYEC QGLDLDTMIS LLSEPQELLV NYVSDVRVSP AAPERQEGSS
LTLTCEAESS QDLEFQWLRE ETGQVLERGP VLQLHDLKRE AGGGYRCVAS VPSIPGLNRT
QLVNVAIFGP PWMAFKERKV WVKENMVLNL SCEASGHPRP TISWNVNGTA SEQDQDPQRV
LSTLNVLVTP ELLETGVECT ASNDLGKNTS ILFLELVNLT TLTPDSNTTT GLSTSTASPH
TRANSTSTER KLPEPESRGV VIVAVIVCIL VLAVLGAVLY FLYKKGKLPC RRSGKQEITL
PPSRKSELVV EVKSDKLPEE MGLLQGSSGD KRAPGDQGEK YIDLRH
```

## Appendix Note III

**Protein identity of peaks listed in Figure 5.11.** SBCl2 cells, SBCl2 cells after 48 h co-incubation with exosomes derived from WM239 cells, as well as WM239 cells, were conducted top-down and bottom-up proteomic analysis to tentatively assign the newly detected or obviously elevated MALDI-TOF MS peaks in **Figure 5.11**. The proteomic analysis results showed that most of the assigned proteins were found to be involved in cancer progression, related with cancer cell migration, invasion and metastasis. Among the proteins, RPL37 and PTMS were present only in the exosome-transferred SBCl2 cells and WM239 cells, not in the normal (non-transferred) SBCl2 cells. The other proteins were present in all the three cells. Combining the proteomic and the MALDI-TOF MS analysis results, it can be concluded that RPL37 and PTMS were most probably newly expressed and the other proteins were up-regulated in the exosome-transferred SBCl2 cells. The data present below were obtained from the exosome-transferred SBCl2 cells.

**1.** TBCA_tubulin folding cofactor A [*Homo sapiens* (human)], UniProt accession number O75347;

*a).* MALDI-TOF MS peak: 5,495 *m/z*, 12,760 *m/z*;

***b).*** Top-down proteomic analysis: adjusted precursor mass 5495.972528 Da, precursor mass 5495.767756 Da, fragment of TBCA, number of matched fragment ions 20, E value 4.66E-14, P value 1.72E-21, sequence shown below:

```
D.PRVRQIKIKTGVVKRLVKEKVMYEKEAKQQEEKIEKMRAEDGEN(Y)[-50.01390]D.I
```

Top-down proteomic analysis: adjusted precursor mass 12758.08114 Da, precursor mass 12757.70114 Da, number of matched fragment ions 19, E value 4.39E-18, P value 2.08E-25, sequence shown below:

```
D.PRVRQIKIKTGVVKRLVKEKVMYEKEAKQQEEKIEKMRAEDGENYDIKKQAEILQESRM(MI
PD)[228.47496]CQRRLEAAYLDLQRILENEKDLEEAEEYKEARLVLDSVKLEA.
```

***c).*** Bottom-up proteomic analysis: 100% identification, 13 exclusive unique peptides, 22 exclusive unique spectra, 26 total spectra, 66/108 amino acids (61% coverage), recovered sequence shown below (highlighted with underline):

```
MADPRVRQIK IKTGVVKRLV KEKVMYEKEA KQQEEKIEKM RAEDGENYDI KKQAEILQES
RMMIPDCQRR LEAAYLDLQR ILENEKDLEE AEEYKEARLV LDSVKLEA
```

**2.** HNRNPA1_heterogeneous nuclear ribonucleoprotein A1 [*Homo sapiens* (human)], fragment, UniProt accession number P09651;

***a).*** MALDI-TOF MS peak: 6,845 *m/z*;

***b).***Top-down proteomic analysis: adjusted precursor mass 6845.111776 Da, precursor mass 6844.906776 Da, number of matched fragment ions 23, E value 7.62E-17, P value 1.16E-24, sequence shown below:

```
N.FGGGGSYND(F)[53.14232]GNYNNQSSNFGPMKGGNFGGRSSGPYGGGGQYFAKPRNQG
GYGGSSSSSSYGSGRRF.
```

***c).*** Bottom-up proteomic analysis: 100% identification, 19 exclusive unique peptides, 43 exclusive unique spectra, 59 total spectra, 181/372 amino acids (49% coverage), recovered sequence shown below (highlighted with underline):

```
MSKSESPKEP EQLRKLFIGG LSFETTDESL RSHFEQWGTL TDCVVMRDPN TKRSRGFGFV
TYATVEEVDA AMNARPHKVD GRVVEPKRAV SREDSQRPGA HLTVKKIFVG GIKEDTEEHH
LRDYFEQYGK IEVIEIMTDR GSGKKRGFAF VTFDDHDSVD KIVIQKYHTV NGHNCEVRKA
LSKQEMASAS SSQRGRSGSG NFGGGRGGGF GGNDNFGRGG NFSGRGGFGG SRGGGGYGGS
GDGYNGFGND GGYGGGGPGY SGGSRGYGSG GQGYGNQGSG YGGSGSYDSY NNGGGGGFGG
GSGSNFGGGG SYNDFGNYNN QSSNFGPMKG GNFGGRSSGP YGGGGQYFAK PRNQGGYGGS
SSSSSYGSGR RF
```

**3.** RPS27A_chain [77-156] in ubiquitin-40S ribosomal protein S27a [*Homo sapiens* (human)], UniProt accession number P62979;

*a).* MALDI-TOF MS peak: 9,411 *m/z*;

*b).* Top-down proteomic analysis: adjusted precursor mass 9411.885315 Da, precursor mass 9411.898116 Da, number of matched fragment ions 32, E value 5.52E-25, P value 6.19E-33, sequence shown below:

```
G.AKKRKKKSYTTPKKNKHKRKKVKLAVLKYYKVDENGKISRLRRECPSDECGAGVFMASHFDR
HYCGKCCLTYCFNKPEDK.
```

*c).* Bottom-up proteomic analysis: 100% identification, 11 exclusive unique peptides, 22 exclusive unique spectra, 34 total spectra, 94/156 amino acids (60% coverage), recovered sequence shown below (highlighted with underline):

```
MQIFVKTLTG KTITLEVEPS DTIENVKAKI QDKEGIPPDQ QRLIFAGKQL EDGRTLSDYN
IQKESTLHLV LRLRGGAKKR KKKSYTTPKK NKHKRKKVKL AVLKYYKVDE NGKISRLRRE
CPSDECGAGV FMASHFDRHY CGKCCLTYCF NKPEDK
```

**4.** RPL37_60S ribosomal protein L37 [*Homo sapiens* (human)], UniProt accession number D6RG19;

*a).* MALDI-TOF MS peak: 9,715 *m/z*;

*b).* Top-down proteomic analysis: adjusted precursor mass 9722.41189 Da, precursor mass 9722.42185 Da, number of matched fragment ions 15, E value 1.52E-12, P value 1.12E-14, sequence shown below:

```
.MTKGTSSFGKRRNKTHTLCRRCGSKAYHLQKSTCGKCGYPAKRKRKYNWSAKAKRRNTTGTGR
MRHLKIVYRRFRYSLYVRS.
```

*c).* Bottom-up proteomic analysis: 100% identification, 2 exclusive unique peptides, 2 exclusive unique spectra, 2 total spectra, 16/82 amino acids (20% coverage), recovered sequence shown below (highlighted with underline):

```
MTKGTSSFGK RRNKTHTLCR RCGSKAYHLQ KSTCGKCGYP AKRKRKYNWS AKAKRRNTTG
TGRMRHLKIV YRRFRYSLYV RS
```

**5.** PTMS_parathymosin [*Homo sapiens* (human)], UniProt accession number P20962;

*a).* MALDI-TOF MS peak: 11,148 *m/z*;

*b).* Top-down proteomic analysis: adjusted precursor mass 11148.02989 Da, precursor mass 11148.02015 Da, number of matched fragment ions 20, E value 8.05E-10, P value 1.39E-17, sequence shown below:

```
M.(S)[Acetyl]EKSVEAAAELSAKDLKEKKEKVEEKASRKERKKEVVEEEENGAEEEEEETA
EDGEEEDEGEEEDEEEEEDDEGPALKRAAEEEDEADPKRQKTEN.G
```

*c).* Bottom-up proteomic analysis: 100% identification, 2 exclusive unique peptides, 2 exclusive unique spectra, 3 total spectra, 25/102 amino acids (24% coverage), recovered sequence shown below (highlighted with underline):

```
MSEKSVEAAA ELSAKDLKEK KEKVEEKASR KERKKEVVEE EENGAEEEE ETAEDGEEED
EGEEEDEEEE EEDDEGPALK RAAEEEDEAD PKRQKTENGA SA
```


**6.** HMGA2_high mobility group AT-hook 2 [*Homo sapiens* (human)], UniProt accession number P52926;

*a).* MALDI-TOF MS peak: 11,734 *m/z*;

*b).* Top-down proteomic analysis: adjusted precursor mass 11739.455315 Da, precursor mass 11739.461855 Da, number of matched fragment ions 18, E value 2.24E-10, P value 8.27E-17, sequence shown below:

```
M.(S)[Acetyl]ARGEGAGQPSTSAQGQPAAPAPQKRGRGRPRKQQQEPTGEPSPKRPRGRPK
GSKNKSPSKAAQKKAEATGEKRPRGRPRKWPQQVVQKKPAQEETEETSSQESAEED
```

*c).* Bottom-up proteomic analysis: 100% identification, 4 exclusive unique peptides, 8 exclusive unique spectra, 9 total spectra, 58/109 amino acids (51% coverage), recovered sequence shown below (highlighted with underline):

```
MSARGEGAGQ PSTSAQGQPA APAPQKRGRG RPRKQQQEPT GEPSPKRPRG RPKGSKNKSP
SKAAQKKAEA TGEKRPRGRP RKWPQQVVQK KPAQEETEET SSQESAEED
```


**7.** RPL34_60S ribosomal protein L34 [*Homo sapiens* (human)], UniProt accession number P49207;

*a).* MALDI-TOF MS peak: 13,150 *m/z*;

*b).* Top-down proteomic analysis: adjusted precursor mass 13153.43159 Da, precursor mass 13153.45013 Da, number of matched fragment ions 22, E value 2.26E-11, P value 8.34E-19, sequence shown below:

```
M.VQRLTYRRRLSYNTASNKTRLSRTPGNRIVYLYTKKVGKAPKSACGVCPGRLRGVRAVRPKV
LMRLSKTKKHVSRAYGGSMCAKCVRDRIKRAFLIEEQKIVVKVLKAQAQSQKAK.
```

*c).* Bottom-up proteomic analysis: 100% identification, 5 exclusive unique peptides, 5 exclusive unique spectra, 5 total spectra, 43/117 amino acids (37% coverage), recovered sequence shown below (highlighted with underline):

```
MVQRLTYRRR LSYNTASNKT RLSRTPGNRI VYLYTKKVGK APKSACGVCP GRLRGVRAVR
PKVLMRLSKT KKHVSRAYGG SMCAKCVRDR IKRAFLIEEQ KIVVKVLKAQ AQSQKAK
```

## Appendix Note IV

**Protein identity of peaks listed in Figure 5.13.** All the exosome samples present in **Figure 5.13** were conducted top-down and bottom-up analyses to tentatively assign the differentially detected peaks from the melanoma-bearing mice. The data obtained from the melanoma-carrying mice on day 19 were present below as examples.

**1.** C4b_complement component 4B [*Mus musculus* (house mouse)], fragment, UniProt accession number P01029;

*a).* MALDI-TOF MS peak: 4,512 *m/z*;

*b).* Top-down proteomic analysis: adjusted precursor mass 4512.408795 Da, precursor mass 4512.413494 Da, number of matched fragment ions 25, E value 3.05E-23, P value 1.32E-30, sequence shown below:

```
R.NGLKTHGLHLNNHQVKGLEEELKFSLGSTISVKVEGNSKGTL.K
```

*c).* Bottom-up proteomic analysis: 100% identification, 104 exclusive unique peptides, 245 exclusive unique spectra, 593 total spectra, 1238/1738 amino acids (71% coverage), recovered sequence shown below (highlighted with underline):

```
MRLLWGLAWV  FSFCASSLQK  PRLLLFSPSV  VNLGTPLSVG  VQLLDAPPGQ  EVKGSVFLRN
PKGGSCSPKK  DFKLSSGDDF  VLLSLEVPLE  DVRSCGLFDL  RRAPHIQLVA  QSPWLRNTAF
KATETQGVNL  LFSSRRGHIF  VQTDQPIYNP  GQRVRYRVFA  LDQKMRPSTD  FLTITVENSH
GLRVLKKEIF  TSTSIFQDAF  TIPDISEPGT  WKISARFSDG  LESNRSTHFE  VKKYVLPNFE
VKITPWKPYI  LMVPSNSDEI  QLDIQARYIY  GKPVQGVAYT  RFALMDEQGK  RTFLRGLETQ
AKLVEGRTHI  SISKDQFQAA  LDKINIGVRD  LEGLRLYAAT  AVIESPGGEM  EEAELTSWRF
VSSAFSLDLS  RTKRHLVPGA  HFLLQALVQE  MSGSEASNVP  VKVSATLVSG  SDSQVLDIQQ
STNGIGQVSI  SFPIPPTVTE  LRLLVSAGSL  YPAIARLTVQ  APPSRGTGFL  SIEPLDPRSP
SVGDTFILNL  QPVGIPAPTF  SHYYYMIISR  GQIMAMGREP  RKTVTSVSVL  VDHQLAPSFY
FVAYFYHQGH  PVANSLLINI  QSRDCEGKLQ  LKVDGAKEYR  NADMMKLRIQ  TDSKALVALG
AVDMALYAVG  GRSHKPLDMS  KVFEVINSYN  VGCGPGGGDD  ALQVFQDAGL  AFSDGDRLTQ
TREDLSCPKE  KKSRQKRNVN  FQKAVSEKLG  QYSSPDAKRC  CQDGMTKLPM  KRTCEQRAAR
VPQQACREPF  LSCCKFAEDL  RRNQTRSQAH  LARNNHNMLQ  EEDLIDEDDI  LVRTSFPENW
LWRVEPVDSS  KLLTVWLPDS  MTTWEIHGVS  LSKSKGLCVA  KPTRVRVFRK  FHLHLRLPIS
IRRFEQFELR  PVLYNYLNDD  VAVSVHVTPV  EGLCLAGGGM  MAQQVTVPAG  SARPVAFSVV
PTAAANVPLK  VVARGVFDLG  DAVSKILQIE  KEGAIHREEL  VYNLDPLNNL  GRTLEIPGSS
DPNIVPDGDF  SSLVRVTASE  PLETMGSEGA  LSPGGVASLL  RLPQGCAEQT  MIYLAPTLTA
SNYLDRTEQW  SKLSPETKDH  AVDLIQKGYM  RIQQFRKNDG  SFGAWLHRDS  STWLTAFVLK
ILSLAQEQVG  NSPEKLQETA  SWLLAQQLGD  GSFHDPCPVI  HRAMQGGLVG  SDETVALTAF
VVIALHHGLD  VFQDDDAKQL  KNRVEASITK  ANSFLGQKAS  AGLLGAHAAA  ITAYALTLTK
ASEDLRNVAH  NSLMAMAEET  GEHLYWGLVL  GSQDKVVLRP  TAPRSPTEPV  PQAPALWIET
```

```
TAYALLHLLL  REGKGKMADK  AASWLTHQGS  FHGAFRSTQD  TVVTLDALSA  YWIASHTTEE
KALNVTLSSM  GRNGLKTHGL  HLNNHQVKGL  EEELKFSLGS  TISVKVEGNS  KGTLKILRTY
NVLDMKNTTC  QDLQIEVKVT  GAVEYAWDAN  EDYEDYYDMP  AADDPSVPLQ  PVTPLQLFEG
RRSRRRREAP  KVVEEQESRV  QYTVCIWRNG  KLGLSGMAIA  DITLLSGFHA  LRADLEKLTS
LSDRYVSHFE  TDGPHVLLYF  DSVPTTRECV  GFGASQEVVV  GLVQPSSAVL  YDYYSPDHKC
SVFYAAPTKS  QLLATLCSGD  VCQCAEGKCP  RLLRSLERRV  EDKDGYRMRF  ACYYPRVEYG
FTVKVLREDG  RAAFRLFESK  ITQVLHFRKD  TMASIGQTRN  FLSRASCRLR  LEPNKEYLIM
GMDGETSDNK  GDPQYLLDSN  TWIEEMPSEQ  MCKSTRHRAA  CFQLKDFLME  FSSRGCQV
```

**2.** Fgb_fibrinogen beta chain [*Mus musculus* (house mouse)], fragment, UniProt accession number Q8K0E8;

*a).* MALDI-TOF MS peak: 4,836 *m/z*;

*b).* Top-down proteomic analysis: adjusted precursor mass 4836.407896 Da, precursor mass 4836.262896 Da, number of matched fragment ions 23, E value 1.15E-17, P value 9.95E-25, sequence shown below:

```
A.(AD)[80.11018]DDYDEPTDSLDARGHRPVDRRKEEPPSLRPAPPPISGGGYR.A
```

*c).* Bottom-up proteomic analysis: 100% identification, 58 exclusive unique peptides, 155 exclusive unique spectra, 507 total spectra, 406/481 amino acids (84% coverage), recovered sequence shown below (highlighted with underline):

```
MRHLWLLLLL  CVFSVQTQAA  DDDYDEPTDS  LDARGHRPVD  RRKEEPPSLR  PAPPPISGGG
YRARPAKATA  NQKKVERRPP  DAGGCLHADT  DMGVLCPTGC  TLQQTLLNQE  RPIKSSIAEL
NNNIQSVSDT  SSVTFQYLTL  LKDMWKKKQA  QVKENENVIN  EYSSILEDQR  LYIDETVNDN
IPLNLRVLRS  ILEDLRSKIQ  KLESDISAQM  EYCRTPCTVS  CNIPVVSGKE  CEEIIRKGGE
TSEMYLIQPD  TSIKPYRVYC  DMKTENGGWT  VIQNRQDGSV  DFGRKWDPYK  KGFGNIATNE
DAKKYCGLPG  EYWLGNDKIS  QLTRMGPTEL  LIEMEDWKGD  KVKAHYGGFT  VQNEASKYQV
SVNKYKGTAG  NALMDGASQL  VGENRTMTIH  NGMFFSTYDR  DNDGWVTTDP  RKQCSKEDGG
GWWYNRCHAA  NPNGRYYWGG  LYSWDMSKHG  TDDGVVWMNW  KGSWYSMRRM  SMKIRPFFPQ
Q
```

**3.** Fga_fibrinogen alpha chain [*Mus musculus* (house mouse)], fragment, UniProt accession number E9PV24;

*a).* MALDI-TOF MS peak: 7,538 *m/z*, 7,666 *m/z*;

*b).* Top-down proteomic analysis: adjusted precursor mass 7538.478495 Da, precursor mass 7538.481763 Da, number of matched fragment ions 48, E value 8.22E-32, P value 3.03E-39, sequence shown below:

```
R.GPRVVERHQSQCKDSDWPFCSDDDWNHKCPSGCRMKGLIDEANQDFTNRINKLKNSLFDFQR
NN.K
```

Top-down proteomic analysis: adjusted precursor mass 7666.573455 Da, precursor mass 7666.583978 Da, number of matched fragment ions 29, E value 8.36E-24, P value 3.08E-31, sequence shown below:

```
R.GPRVVERHQSQCKDSDWPFCSDDDWNHKCPSGCRMKGLIDEANQDFTNRINKLKNSLFDFQR
NNK.D
```

*c).* Bottom-up proteomic analysis: 100% identification, 60 exclusive unique peptides, 143 exclusive unique spectra, 447 total spectra, 543/789 amino acids (69% coverage), recovered sequence shown below (highlighted with underline):

```
MLSLRVTCLI LSVASTVWTT DTEDKGEFLS EGGGVRGPRV VERHQSQCKD SDWPFCSDDD
WNHKCPSGCR MKGLIDEANQ DFTNRINKLK NSLFDFQRNN KDSNSLTRNI MEYLRGDFAN
ANNFDNTYGQ VSEDLRRRIE ILRRKVIEKA QQIQALQSNV RAQLIDMKRL EVDIDIKIRS
CKGSCSRAVN REINLQDYEG HQKQLQQVIA KELLPTKDRQ YLPALKMSPV PDLVPGSFKS
QLQEAPPEWK ALTEMRQMRM ELERPGKDGG SRGDSPGDSR GDSRGDFATR GPGSKAENPT
NPGPGGSGYW RPGNSGSGSD GNRNPGTTGS DGTGDWGTGS PRPGSDSGNF RPANPNWGVF
SEFGDSSSPA TRKEYHTGKA VTSKGDKELL IGKEKVTSSG TSTTHRSCSK TITKTVTGPD
GRREVVKEVI TSDDGSDCGD ATELDISHSF SGSLDELSER HPDLSGFFDN HFGLISPNFK
EFGSKTHSDS DILTNIEDPS SHVPEFSSSS KTSTVKKQVT KTYKMADEAG SEAHREGETR
NTKRGRARAR PTRDCDDVLQ TQTSGAQNGI FSIKPPGSSK VFSVYCDQET SLGGWLLIQQ
RMDGSLNFNR TWQDYKRGFG SLNDKGEGEF WLGNDYLHLL TLRGSVLRVE LEDWAGKEAY
AEYHFRVGSE AEGYALQVSS YRGTAGDALV QGSVEEGTEY TSHSNMQFST FDRDADQWEE
NCAEVYGGGW WYNSCQAANL NGIYYPGGTY DPRNNSPYEI ENGVVWVPFR GADYSLRAVR
MKIRPLVGQ
```

**4.** Pf4_platelet factor 4 [*Mus musculus* (house mouse)], UniProt accession number Q9Z126;

*a).* MALDI-TOF MS peak: 8,113 *m/z*;

*b).* Top-down proteomic analysis: adjusted precursor mass 8113.54185 Da, precursor mass 8113.55182 Da, number of matched fragment ions 22, E value 4.19E-9, P value 3.65E-16, sequence shown below:

```
M.(S)[Acetyl]VAAVFRGLRPSPELLLLGLLFLPAVVAVTSAGPEESDGDLSCVCVKTISSG
IHLKHITSLEVIKAGRHCAVPQLIAT.L
```

*c).* Bottom-up proteomic analysis: 100% identification, 2 exclusive unique peptides, 2 exclusive unique spectra, 2 total spectra, 18/77 amino acids (23% coverage), recovered sequence shown below (highlighted with underline):

```
MSVAAVFRGL RPSPELLLLG LLFLPAVVAV TSAGPEESDG DLSCVCVKTI SSGIHLKHIT
SLEVIKAGRH CAVPQLIATL KNGRKICLDR QAPLYKKVIK KILES
```

**5.** C3_complement component 3 [*Mus musculus* (house mouse)], fragment, UniProt accession number P01027;

*a).* MALDI-TOF MS peak: 8,878 *m/z*;

*b).* Top-down proteomic analysis: adjusted precursor mass 8878.353145 Da, precursor mass 8878.354766 Da, number of matched fragment ions 23, E value 3.97E-12, P value 2.96E-14, sequence shown below:

```
R.SVQLMERRMDKAGQYTDKGLRKCCEDGMRDIPMRYSCQRRARLITQGENCIKAFIDCCNHIT
KLREQHRRDHVLG.L
```

*c).* Bottom-up proteomic analysis: 100% identification, 203 exclusive unique peptides, 512 exclusive unique spectra, 2334 total spectra, 1473/1663 amino acids (89% coverage), recovered sequence shown below (highlighted with underline):

```
MGPASGSQLL VLLLLLASSP LALGIPMYSI ITPNVLRLES EETIVLEAHD AQGDIPVTVT
VQDFLKRQVL TSEKTVLTGA SGHLRSVSIK IPASKEFNSD KEGHKYVTVV ANFGETVVEK
AVMVSFQSGY LFIQTDKTIY TPGSTVLYRI FTVDNNLLPV GKTVVILIET PDGIPVKRDI
LSSNNQHGIL PLSWNIPELV NMGQWKIRAF YEHAPKQIFS AEFEVKEYVL PSFEVRVEPT
ETFYYIDDPN GLEVSIIAKF LYGKNVDGTA FVIFGVQDGD KKISLAHSLT RVVIEDGVGD
AVLTRKVLME GVRPSNADAL VGKSLYVSVT VILHSGSDMV EAERSGIPIV TSPYQIHFTK
TPKFFKPAMP FDLMVFVTNP DGSPASKVLV VTQGSNAKAL TQDDGVAKLS INTPNSRQPL
TITVRTKKDT LPESRQATKT MEAHPYSTMH NSNNYLHLSV SRMELKPGDN LNVNFHLRTD
PGHEAKIRYY TYLVMNKGKL LKAGRQVREP GQDLVVLSLP ITPEFIPSFR LVAYYTLIGA
SGQREVVADS VWVDVKDSCI GTLVVKGDPR DNHLAPGQQT TLRIEGNQGA RVGLVAVDKG
VFVLNKKNKL TQSKIWDVVE KADIGCTPGS GKNYAGVFMD AGLAFKTSQG LQTEQRADLE
CTKPAARRRR SVQLMERRMD KAGQYTDKGL RKCCEDGMRD IPMRYSCQRR ARLITQGENC
IKAFIDCCNH ITKLREQHRR DHVLGLARSE LEEDIIPEED IISRSHFPQS WLWTIEELKE
PEKNGISTKV MNIFLKDSIT TWEILAVSLS DKKGICVADP YEIRVMQDFF IDLRLPYSVV
RNEQVEIRAV LFNYREQEEL KVRVELLHNP AFCSMATAKN RYFQTIKIPP KSSVAVPYVI
VPLKIGQQEV EVKAAVFNHF ISDGVKKTLK VVPEGMRINK TVAIHTLDPE KLGQGGVQKV
DVPAADLSDQ VPDTDSETRI ILQGSPVVQM AEDAVDGERL KHLIVTPAGC GEQNMIGMTP
TVIAVHYLDQ TEQWEKFGIE KRQEALELIK KGYTQQLAFK QPSSAYAAFN NRPPSTWLTA
YVVKVFSLAA NLIAIDSHVL CGAVKWLILE KQKPDGVFQE DGPVIHQEMI GGFRNAKEAD
VSLTAFVLIA LQEARDICEG QVNSLPGSIN KAGEYIEASY MNLQRPYTVA IAGYALALMN
KLEEPYLGKF LNTAKDRNRW EEPDQQLYNV EATSYALLAL LLLKDFDSVP PVVRWLNEQR
YYGGGYGSTQ ATFMVFQALA QYQTDVPDHK DLNMDVSFHL PSRSSATTFR LLWENGNLLR
SEETKQNEAF SLTAKGKGRG TLSVVAVYHA KLKSKVTCKK FDLRVSIRPA PETAKKPEEA
KNTMFLEICT KYLGDVDATM SILDISMMTG FAPDTKDLEL LASGVDRYIS KYEMNKAFSN
KNTLIIYLEK ISHTEEDCLT FKVHQYFNVG LIQPGSVKVY SYYNLEESCT RFYHPEKDDG
MLSKLCHSEM CRCAEENCFM QQSQEKINLN VRLDKACEPG VDYVYKTELT NIELLDDFDE
YTMTIQQVIK SGSDEVQAGQ QRKFISHIKC RNALKLQKGK KYLMWGLSSD LWGEKPNTSY
IIGKDTWVEH WPEAEECQDQ KYQKQCEELG AFTESMVVYG CPN
```

**6.** Saa1_serum amyloid A-1 [*Mus musculus* (house mouse)], UniProt accession number P05366;

*a).* MALDI-TOF MS peak: 11,750 *m/z*;

*b).* Top-down proteomic analysis: adjusted precursor mass 11751.74895 Da, precursor mass 11751.74185 Da, number of matched fragment ions 25, E value 3.58E-16, P value 1.32E-23, sequence shown below:

```
G.GFFSFVHEAFQGAGDMWRAYTDMKEANWKNSDKYFHARGNYDAAQRGPGGVWAAEKISDGRE
AFQEFFGRGHEDTIADQEANRHGRSGKDPNYYRPPGLPDKY.
```

*c).* Bottom-up proteomic analysis: 100% identification, 2 exclusive unique peptides, 2 exclusive unique spectra, 2 total spectra, 29/122 amino acids (24% coverage), recovered sequence shown below (highlighted with underline):

```
MKLLTSLVFC SLLLGVCHGG FFSFVHEAFQ GAGDMWRAYT DMKEANWKNS DKYFHARGNY
DAAQRGPGGV WAAEKISDGR EAFQEFFGRG HEDTIADQEA NRHGRSGKDP NYYRPPGLPD
KY
```

**7.** Crp_C-reactive protein [*Mus musculus* (house mouse)], UniProt accession number P14847;

*a).* MALDI-TOF MS peak: 23,080 *m/z*;

*b).* Top-down proteomic analysis: adjusted precursor mass 23089.14285 Da, precursor mass 23089.15185 Da, number of matched fragment ions 17, E value 2.68E-5, P value 2.33E-12, sequence shown below:

```
G.HEDMFKKAFVFPKESDTSYVSLEAESKKPLNTFTVCLHFYTALSTVRSFSVFSYATKKNSND
ILIFWNKDKQYTFGVGGAEVRFMVSEIPEAPTHICASWESATGIVEFWIDGKPKVRKSLHKGYT
VGPDASIILGQEQDSYGGDFDAKQSLVGDIGDVNMWDFVLSPEQISTVYVGGTLSPNVLNWRAL
NYKAQGDVFIKPQLWS.
```

*c).* Bottom-up proteomic analysis: 100% identification, 9 exclusive unique peptides, 11 exclusive unique spectra, 18 total spectra, 168/225 amino acids (75% coverage), recovered sequence shown below (highlighted with underline):

```
MEKLLWCLLI MISFSRTFGH EDMFKKAFVF PKESDTSYVS LEAESKKPLN TFTVCLHFYT
ALSTVRSFSV FSYATKKNSN DILIFWNKDK QYTFGVGGAE VRFMVSEIPE APTHICASWE
SATGIVEFWI DGKPKVRKSL HKGYTVGPDA SIILGQEQDS YGGDFDAKQS LVGDIGDVNM
WDFVLSPEQI STVYVGGTLS PNVLNWRALN YKAQGDVFIK PQLWS
```

## Appendix Note V

**Protein identity of peaks listed in Figure 5.14.** Due to the limited volume of available melanoma patient blood plasma (~90-100 uL), this group of exosomes were conducted top-down proteomic analysis only, not the bottom-up proteomic analysis. The fingerprint peaks differentially detected from melanoma patients compared to healthy donors were tentatively assigned by correlation with the proteomic analysis. Among the assigned proteins, MAGEA3 and MIA were present only in the melanoma patient exosomes. The data obtained from melanoma patient 3 mentioned in Figure 5.14 were present below as examples.

**1.** C4A_complement component 4A [*Homo sapiens* (human)], fragment, UniProt accession number P0C0L4;

*a).* MALDI-TOF MS peak: 3,312 *m/z*;

*b).* Top-down proteomic analysis: adjusted precursor mass 3312.732675 Da, precursor mass 3312.744354 Da, number of matched fragment ions 21, E value 7.59E-20, P value 2.80E-22, sequence shown below:

```
R.NGFKSHALQLNNRQIRGLEEELQFSLGSK.I
```

**2.** ITIH4_inter-alpha-trypsin inhibitor heavy chain H4 [*Homo sapiens* (human)], fragment, UniProt accession number Q14624;

*a).* MALDI-TOF MS peak: 3,952 *m/z*;

*b).* Top-down proteomic analysis: adjusted precursor mass 3952.956625 Da, precursor mass 3952.971625 Da, number of matched fragment ions 24, E value 3.91E-12, P value 1.44E-19, sequence shown below:

```
R.(QAGAAGSRMNFR)[-17.02762]PGVLSSRQLGLPGPPDVPDHAAYHPF.R
```

**3.** ITIH4_inter-alpha-trypsin inhibitor heavy chain H4 [*Homo sapiens* (human)], fragment, UniProt accession number Q14624;

*a).* MALDI-TOF MS peak: 4639 *m/z*;

*b).* Top-down proteomic analysis: adjusted precursor mass 4639.326745 Da, precursor mass 4639.34064 Da, number of matched fragment ions 32, E value 4.18E-20, P value 1.54E-27, sequence shown below:

```
R.RGWNRQAGAAGSRMNFRPGVLSSRQLGLPGPPDVPDHAAYHPF.R
```

**4.** FGA_fibrinogen alpha chain [Homo sapiens (human)], fragment, UniProt accession number P02671;

*a).* MALDI-TOF MS peak: 5,802 *m/z*, 5,898 *m/z*;

*b).* Top-down proteomic analysis: adjusted precursor mass 5801.627245 Da, precursor mass 5800.640314 Da, number of matched fragment ions 10, E value 3.11E-7, P value 1.15E-14, sequence shown below:

```
K.SSSYSKQFTSSTSYNRGDSTFESKSYKMADEAGSEADHEGTHSTKRGHAKSRP.V
```

Top-down proteomic analysis: adjusted precursor mass 5900.695655 Da, precursor mass 5900.711424 Da, number of matched fragment ions 38, E value 1.80E-31, P value 6.62E-38, sequence shown below:

```
K.SSSYSKQFTSSTSYNRGDSTFESKSYKMADEAGSEADHEGTHSTKRGHAKSRPV.R
```

**5.** MAGEA3_melanoma-associated antigen 3 [*Homo sapiens* (human)], fragment, UniProt accession number P43357;

*a).* MALDI-TOF MS peak: 7,001 *m/z*;

*b).* Top-down proteomic analysis: adjusted precursor mass 7001.356295 Da, precursor mass 7001.347401 Da, number of matched fragment ions 11, E value 2.28E-6, P value 8.40E-14, sequence shown below:

```
K.PEEGLEARGEALGLVGAQAPATEEQEAASSSSTLVEVTLGEVPAAESPDPPQSPQGASSLPT
TMNYPLW.S
```

**6.** PF4_ platelet factor 4 [*Homo sapiens* (human)], UniProt accession number P02776;

*a).* MALDI-TOF MS peak: 7,764 *m/z*;

*b).* Top-down proteomic analysis: adjusted precursor mass 7764.208155 Da, precursor mass 7763.218418 Da, number of matched fragment ions 27, E value 3.05E-23, P value 1.13E-30, sequence shown below:

```
A.EAEEDGDLQCLCVKTTSQVRPRHITSLEVIKAGPHCPTAQLIATLKNGRKICLDLQAPLYKK
IIKKLLES.
```

**7.** C4A_complement component 4A [*Homo sapiens* (human)], UniProt accession number P0C0L4;

*a).* MALDI-TOF MS peak: 8,602 *m/z*;

*b).* Top-down proteomic analysis: adjusted precursor mass 8602.222825 Da, precursor

mass 8602.208875 Da, number of matched fragment ions 22, E value 9.39E-14, P value 3.46E-21, sequence shown below:

```
R.NVNFQKAINEKLGQYASPTAKRCCQDGVTRLPMMRSCEQRAARVQQPDCREPFLSCCQFAES
LRKKSRDKGQAGLQ.R
```

**8.** C3_complement component 3 [*Homo sapiens* (human)], UniProt accession number P01024;

*a).* MALDI-TOF MS peak: 8,932 *m/z*;

*b).* Top-down proteomic analysis: adjusted precursor mass 8932.483395 Da, precursor mass 8932.492015 Da, number of matched fragment ions 27, E value 4.54E-18, P value 1.67E-25, sequence shown below:

```
R.SVQLTEKRMDKVGKYPKELRKCCEDGMRENPMRFSCQRRTRFISLGEACKKVFLDCCNYITE
LRRQHARASHLGLA.R
```

**9.** SAA1_serum amyloid A1 [*Homo sapiens* (human)], UniProt accession number P0DJ18;

*a).* MALDI-TOF MS peak: 11,518 *m/z*, 11,675 *m/z*;

*b).* Top-down proteomic analysis: adjusted precursor mass 11519.39166 Da, precursor mass 11519.4444 Da, number of matched fragment ions 13, E value 2.56E-8, P value 9.45E-16, sequence shown below:

```
R.SFFSFLGEAFDGARDMWRAYSDMREANYIGSDKYFHARGNYDAAKRGPGGVWAAEAISDARE
NIQRFFGHGAEDSLADQAANEWGRSGKDPNHFRPAGLPEKY.
```

Top-down proteomic analysis: adjusted precursor mass 11675.49278 Da, precursor mass 11675.54697 Da, number of matched fragment ions 28, E value 4.79E-14, P value 1.77E-21, sequence shown below:

```
S.RSFFSFLGEAFDGARDMWRAYSDMREANYIGSDKYFHARGNYDAAKRGPGGVWAAEAISDAR
ENIQRFFGHGAEDSLADQAANEWGRSGKDPNHFRPAGLPEKY.
```

**10.** MIA_melanoma-derived growth regulatory protein [*Homo sapiens* (human)], UniProt accession number Q16674;

*a).* MALDI-TOF MS peak: 12,112 *m/z*;

*b).* Top-down proteomic analysis: adjusted precursor mass 12109.93825 Da, precursor mass 12109.94875 Da, number of matched fragment ions 26, E value 2.67E-17, P value 9.85E-25, sequence shown below:

```
G.GPMPKLADRKLCADQECSHPISMAVALQDYMAPDCRFLTIHRGQVVYVFSKLKGRGRLFWGG
SVQGDYYGDLAARLGYFPSSIVREDQTLKPGKVD VKTDKWDFYCQ.
```

**11.** CRP_ C-reactive protein [*Homo sapiens* (human)], UniProt accession number P02741;

*a).* MALDI-TOF MS peak: 23,030 *m/z*;

*b).* Top-down proteomic analysis: adjusted precursor mass 23047.14875 Da, precursor mass 23047.18155 Da, number of matched fragment ions 25, E value 4.79E-14, P value 1.77E-21, sequence shown below:

```
G.QTDMSRKAFVFPKESDTSYVSLKAPLTKPLKAFTVCLHFYTELSSTRGYSIFSYATKRQDNE
ILIFWSKDIGYSFTVGGSEILFEVPEVTVAPVHICTSWESASGIVEFWVDGKPRVRKSLKKGYT
VGAEASIILGQEQDSFGGNFEGSQSLVGDIGNVNMWDFVLSPDEINTIYLGGPFSPNVLNWRAL
KYEVQGEVFTKPQLWP.
```

# Appendix Figure

**Read-out of melanoma marker proteins from exosome and cell fingerprints.** Marker proteins commonly used for the diagnosis and prognosis of melanoma were recognized from MALDI-TOF MS fingerprints of intact melanoma cells (*i.e.* SBCl2 cells, WM115 cells, WM239 cells) and intact exosomes derived from the melanoma cells (*i.e.* SBCl2 exosomes, WM115 exosomes, WM239 exosomes). Protein identity of the mass spectral peaks were tentatively assigned by matching them with the protein profiles obtained from top-down and bottom-up proteomic analysis of the cells and exosomes. To facilitate the peak reading, the mass spectra were displayed in the mass range of (**a**) 2,000-20,000 *m/z* and (**b**) 20,000-80,000 *m/z*, respectively. Proteomic information supporting the protein assignment is present in Appendix Note II.

1. TMSB10    2. TMSB4    3. MT2A    4. S100A6    5. S100A10    6. S100A4    7. S100A11    8. S100A16    9. MIF    10. MLANA    11. PMEL    12. MCAM
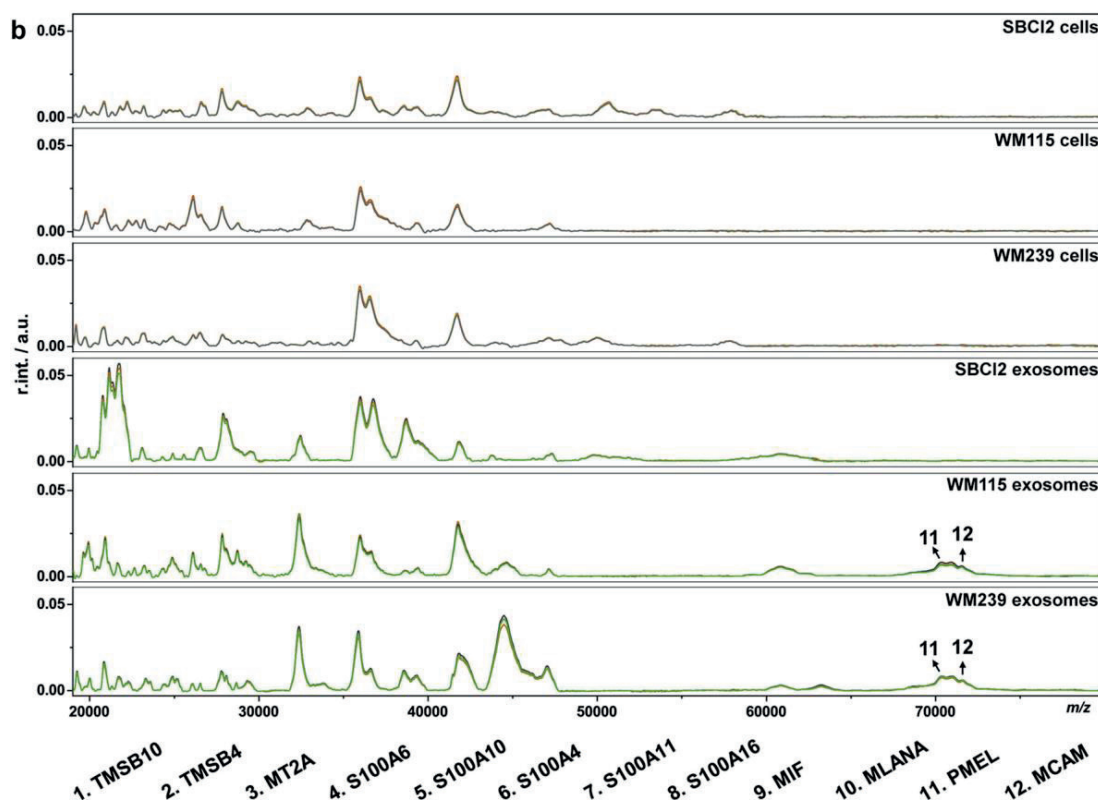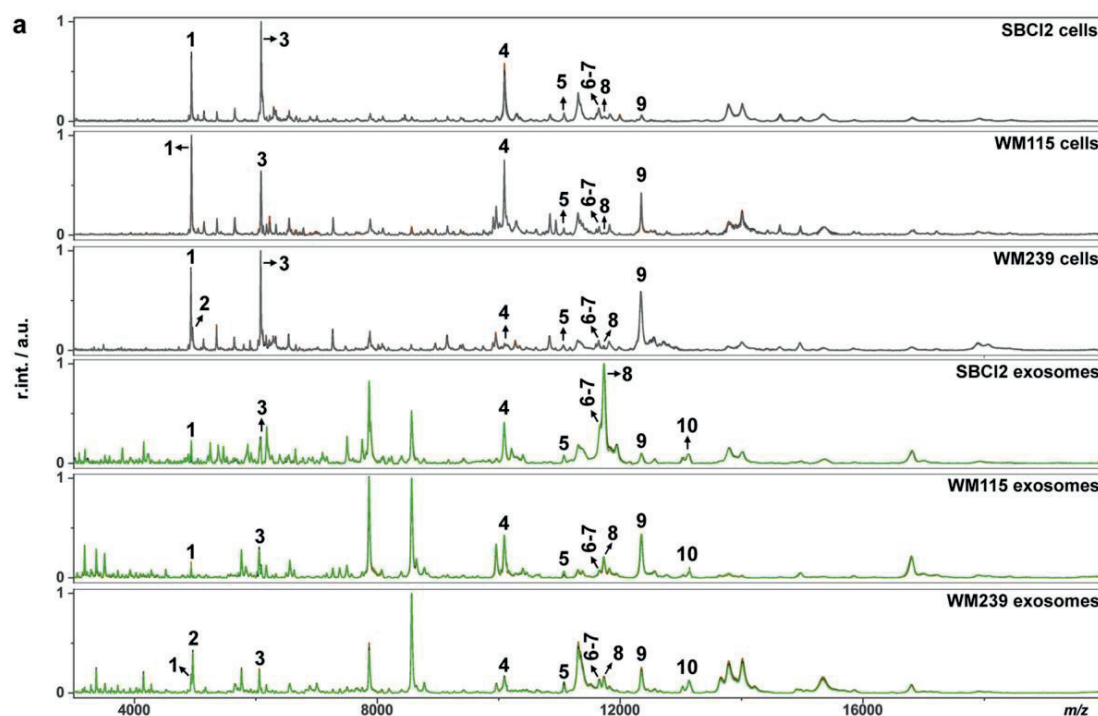
# Reference

1. Keller, S., Ridinger, J., Rupp, A.K., Janssen, J.W.G. & Altevogt, P. Body fluid derived exosomes as a novel template for clinical diagnostics. *J Transl Med* 9 (2011).
2. Colombo, M., Raposo, G. & Thery, C. Biogenesis, Secretion, and Intercellular Interactions of Exosomes and Other Extracellular Vesicles. *Annu Rev Cell Dev Bi* 30, 255-289 (2014).
3. Thery, C., Zitvogel, L. & Amigorena, S. Exosomes: Composition, biogenesis and function. *Nat Rev Immunol* 2, 569-579 (2002).
4. Takahashi, A*., et al.* Exosomes maintain cellular homeostasis by excreting harmful DNA from cells. *Nat Commun* 8 (2017).
5. Balaj, L*., et al.* Tumour microvesicles contain retrotransposon elements and amplified oncogene sequences. *Nat Commun* 2 (2011).
6. Becker, A*., et al.* Extracellular Vesicles in Cancer: Cell-to-Cell Mediators of Metastasis. *Cancer Cell* 30, 836-848 (2016).
7. Costa-Silva, B*., et al.* Pancreatic cancer exosomes initiate pre-metastatic niche formation in the liver. *Nat Cell Biol* 17, 816-826 (2015).
8. Sheridan, C. Exosome cancer diagnostic reaches market. *Nat Biotechnol* 34, 358-359 (2016).
9. Li, P., Kaslan, M., Lee, S.H., Yao, J. & Gao, Z.Q. Progress in Exosome Isolation Techniques. *Theranostics* 7, 789-804 (2017).
10. Ding, M*., et al.* Comparison of commercial exosome isolation kits for circulating exosomal microRNA profiling. *Anal Bioanal Chem* 410, 3805-3814 (2018).
11. Coumans, F.A.W*., et al.* Methodological Guidelines to Study Extracellular Vesicles. *Circ Res* 120, 1632-1648 (2017).
12. Patel, R. MALDI-TOF MS for the Diagnosis of Infectious Diseases. *Clin Chem* 61, 100-111 (2015).
13. Ossio, R., Roldan-Marin, R., Martinez-Said, H., Adams, D.J. & Robles-Espinoza, C.D. Melanoma: a global perspective. *Nat Rev Cancer* 17, 393-394 (2017).
14. Schaider, H*., et al.* Differential response of primary and metastatic melanomas to neutrophils attracted by IL-8. *Int J Cancer* 103, 335-343 (2003).
15. Herlyn, M*., et al.* Primary melanoma cells of the vertical growth phase: similarities to metastatic cells. *J Natl Cancer Inst* 74, 283-289 (1985).
16. Yoshioka, Y*., et al.* Ultra-sensitive liquid biopsy of circulating extracellular vesicles using ExoScreen. *Nat Commun* 5 (2014).
17. Zhu, Y.D*., et al.* Detection of antimicrobial resistance-associated proteins by titanium dioxide-facilitated intact bacteria mass spectrometry. *Chem Sci* 9, 2212-2221 (2018).
18. Raposo, G. & Stoorvogel, W. Extracellular vesicles: exosomes, microvesicles, and friends. *J Cell Biol* 200, 373-383 (2013).
19. Henry, N.L. & Hayes, D.F. Cancer biomarkers. *Mol Oncol* 6, 140-146 (2012).
20. Catherman, A.D., Skinner, O.S. & Kelleher, N.L. Top Down proteomics: Facts and perspectives. *Biochem Bioph Res Co* 445, 683-693 (2014).
21. Gillet, L.C., Leitner, A. & Aebersold, R. Mass Spectrometry Applied to Bottom-Up Proteomics: Entering the High-Throughput Era for Hypothesis Testing. *Annu Rev Anal Chem* 9, 449-472 (2016).
22. Weterman, M.A.J., Vanmuijen, G.N.P., Ruiter, D.J. & Bloemers, H.P.J. Thymosin Beta-10 Expression in Melanoma Cell-Lines and Melanocytic Lesions - a New Progression Marker for Human Cutaneous Melanoma. *Int J Cancer* 53, 278-284 (1993).
23. Weinlich, G*., et al.* Metallothionein - overexpression as a highly significant prognostic factor in melanoma: a prospective study on 1270 patients. *Brit J Cancer* 94, 835-841 (2006).
24. Shimizu, T*., et al.* High expression of macrophage migration inhibitory factor in human melanoma cells and its role in tumor cell growth and angiogenesis. *Biochem Bioph Res Co*

264, 751-758 (1999).

25. Gaynor, R., Irie, R., Morton, D. & Herschman, H.R. S100 Protein Is Present in Cultured Human-Malignant Melanomas. *Nature* 286, 400-401 (1980).

26. Cha, H.J., Jeong, M.J. & Kleinman, H.K. Role of thymosin beta(4) in tumor metastasis and angiogenesis. *J Natl Cancer Inst* 95, 1674-1680 (2003).

27. Weinstein, D., Leininger, J., Hamby, C. & Safai, B. Diagnostic and prognostic biomarkers in melanoma. *J Clin Aesthet Dermatol* 7, 13-24 (2014).

28. Lei, X., Guan, C.W., Song, Y. & Wang, H. The multifaceted role of CD146/MCAM in the promotion of melanoma progression. *Cancer Cell Int* 15 (2015).

29. van Niel, G.*, et al.* The Tetraspanin CD63 Regulates ESCRT-Independent and -Dependent Endosomal Sorting during Melanogenesis. *Dev Cell* 21, 708-721 (2011).

30. Tkach, M. & Thery, C. Communication by Extracellular Vesicles: Where We Are and Where We Need to Go. *Cell* 164, 1226-1232 (2016).

31. Zomer, A.*, et al.* In Vivo Imaging Reveals Extracellular Vesicle-Mediated Phenocopying of Metastatic Behavior. *Cell* 161, 1046-1057 (2015).

32. Zhang, P.*, et al.* Tubulin cofactor A functions as a novel positive regulator of ccRCC progression, invasion and metastasis. *Int J Cancer* 133, 2801-2811 (2013).

33. Geuens, T., Bouhy, D. & Timmerman, V. The hnRNP family: insights into their role in health and disease. *Hum Genet* 135, 851-867 (2016).

34. Wang, H.C.*, et al.* RPS27a promotes proliferation, regulates cell cycle progression and inhibits apoptosis of leukemia cells. *Biochem Bioph Res Co* 446, 1204-1210 (2014).

35. Kleivi, K.*, et al.* Gene expression profiles of primary colorectal carcinomas, liver metastases, and carcinomatoses. *Mol Cancer* 6 (2007).

36. Wei, F.*, et al.* Ribosomal protein L34 promotes the proliferation, invasion and metastasis of pancreatic cancer cells. *Oncotarget* 7, 85259-85272 (2016).

37. Daftuar, L., Zhu, Y., Jacq, X. & Prives, C. Ribosomal proteins RPL37, RPS15 and RPS20 regulate the Mdm2-p53-MdmX network. *Plos One* 8, e68667 (2013).

38. Villarroya-Beltri, C.*, et al.* Sumoylated hnRNPA2B1 controls the sorting of miRNAs into exosomes through binding to specific motifs. *Nat Commun* 4 (2013).

39. Hannappel, E. & Huff, T. The thymosins - Prothymosin alpha, parathymosin, and beta-thymosins: Structure and function. *Vitam Horm* 66, 257-296 (2003).

40. Raskin, L.*, et al.* Transcriptome Profiling Identifies HMGA2 as a Biomarker of Melanoma Progression and Prognosis. *J Invest Dermatol* 133, 2585-2592 (2013).

41. Lazar, I.*, et al.* Proteome characterization of melanoma exosomes reveals a specific signature for metastatic cell lines. *Pigm Cell Melanoma R* 28 (2015).

42. Lyman, G.H.*, et al.* Sentinel Lymph Node Biopsy for Patients With Early-Stage Breast Cancer: American Society of Clinical Oncology Clinical Practice Guideline Update. *J Clin Oncol* 35, 561-564 (2017).

43. Gerlinger, M.*, et al.* Intratumor Heterogeneity and Branched Evolution Revealed by Multiregion Sequencing. *New Engl J Med* 366, 883-892 (2012).

44. Alix-Panabieres, C. & Pantel, K. Clinical Applications of Circulating Tumor Cells and Circulating Tumor DNA as Liquid Biopsy. *Cancer Discov* 6, 479-491 (2016).

45. Diaz, L.A. & Bardelli, A. Liquid Biopsies: Genotyping Circulating Tumor DNA. *J Clin Oncol* 32, 579-586 (2014).

46. Crowley, E., Di Nicolantonio, F., Loupakis, F. & Bardelli, A. Liquid biopsy: monitoring cancer-genetics in the blood. *Nat Rev Clin Oncol* 10, 472-484 (2013).

47. Heitzer, E., Ulz, P. & Geigl, J.B. Circulating Tumor DNA as a Liquid Biopsy for Cancer. *Clin Chem* 61, 112-123 (2015).

48. Perkins, G.*, et al.* Multi-Purpose Utility of Circulating Plasma DNA Testing in Patients with Advanced Cancers. *Plos One* 7, e47020 (2012).

49. Overwijk, W.W. & Restifo, N.P. B16 as a mouse model for human melanoma. *Current protocols in immunology* 39, Unit-20.21. (2000).

50. Pilatova, K.*, et al.* Role of platelet chemokines, PF-4 and CTAP-III, in cancer biology. *J Hematol Oncol* 6 (2013).

51. Cervi, D.*, et al.* Platelet-associated PF-4 as a biomarker of early tumor growth. *Blood* 111, 1201-1207 (2008).

52. Afshar-Kharghan, V. The role of the complement system in cancer. *J Clin Invest* 127, 780-789 (2017).

53. Wang, Y.*, et al.* Autocrine Complement Inhibits IL10-Dependent T-cell-Mediated Antitumor Immunity to Promote Tumor Progression. *Cancer Discov* 6, 1022-1035 (2016).

54. Mortensen, S.*, et al.* Structural basis for the function of complement component C4 within the classical and lectin pathways of complement. *J Immunol* 194, 5488-5496 (2015).

55. Jain, S., Gautam, V. & Naseem, S. Acute-phase proteins: As diagnostic tool. *J Pharm Bioallied Sci* 3, 118 (2011).

56. Simpson-Haidaris, P. & Rybarczyk, B. Tumors and fibrinogen. *Ann N Y Acad Sci* 936, 406-425 (2001).

57. Fang, S.Y.*, et al.* C-Reactive Protein As a Marker of Melanoma Progression. *J Clin Oncol* 33, 1389-1396 (2015).

58. Findeisen, P.*, et al.* Serum Amyloid A As a Prognostic Marker in Melanoma Identified by Proteomic Profiling. *J Clin Oncol* 27, 2199-2208 (2009).

59. Malle, E., Sodin-Semrl, S. & Kovacevic, A. Serum amyloid A: An acute-phase protein involved in tumour pathogenesis. *Cell Mol Life Sci* 66, 9-26 (2009).

60. Mihlan, M.*, et al.* Monomeric C-reactive protein modulates classic complement activation on necrotic cells. *Faseb J* 25, 4198-4210 (2011).

61. Calapre, L., Warburton, L., Millward, M., Ziman, M. & Gray, E.S. Circulating tumour DNA (ctDNA) as a liquid biopsy for melanoma. *Cancer Lett* 404, 62-69 (2017).

62. Huang, S.K. & Hoon, D.S.B. Liquid biopsy utility for the surveillance of cutaneous malignant melanoma patients. *Mol Oncol* 10, 450-463 (2016).

63. Palumbo, J.S.*, et al.* Fibrinogen is an important determinant of the metastatic potential of circulating tumor cells. *Blood* 96, 3302-3309 (2000).

64. Yu, X.F.*, et al.* Serum fibrinogen levels are positively correlated with advanced tumor stage and poor survival in patients with gastric cancer undergoing gastrectomy: a large cohort retrospective study. *Bmc Cancer* 16 (2016).

65. Subbannayya, Y.*, et al.* Identification of differentially expressed serum proteins in gastric adenocarcinoma. *J Proteomics* 127, 80-88 (2015).

66. Wang, H., Ricklin, D. & Lambris, J.D. Complement-activation fragment C4a mediates effector functions by binding as untethered agonist to protease-activated receptors 1 and 4. *P Natl Acad Sci USA*, 201707364 (2017).

67. Liu, W., Cheng, S., Asa, S.L. & Ezzat, S. The melanoma-associated antigen A3 mediates fibronectin-controlled cancer progression and metastasis. *Cancer Res* 68, 8104-8112 (2008).

68. Bosserhoff, A.K.*, et al.* Melanoma-inhibiting activity, a novel serum marker for progression of malignant melanoma. *Cancer Res* 57, 3149-3153 (1997).

69. Bosserhoff, A.K. Melanoma inhibitory activity (MIA): an important molecule in melanoma development and progression. *Pigm Cell Res* 18, 411-416 (2005).

70. Hortin, G.L. The MALDI-TOF mass spectrometric view of the plasma proteome and peptidome. *Clin Chem* 52, 1223-1237 (2006).

# CHAPTER VI. Tape stripping mass spectrometry method for skin cell analysis

## Abstract

A method combining tape stripping sampling and MALDI-TOF mass spectrometry detection was designed for quick and non-invasive diagnosis of skin diseases like skin cancers. The method proposed to recover skin cells from the epidermis layer of a suspicious skin region using adhesive tapes *via* the tape stripping sampling procedure. Without any pretreatment, skin cells recovered on the adhesive tapes are analysed directly by the technique of MALDI-TOF mass spectrometry.

# 1. Introduction

Skin cancers, especially cutaneous malignancies like melanoma, attack millions of people worldwide. The survival rate of skin cancer patient increases with early detection when the cancer is still superficial and can be removed through minor surgery. Therefore, reliable methodologies for early diagnosis of skin cancers are of great importance.[1,2]

Dermatologists usually examine suspicious skin areas, which are potentially cancerous, by dermoscopy technique according to the "ABCDE" criteria.[3] The 'ABCDE' refers to the characteristics of 'asymmetry', 'border irregularity', 'colour variegation', 'diameter greater than 6 mm' and 'evolving (lesions that have changed over a relatively short time)'. However, visual ABCDE signs are often not effective for early stage diagnosis. Thus, a skin biopsy is usually performed, in which a piece of skin is removed from the patient and sectioned into thin slices, and then subjected to microscopic analysis. Commonly used methods for microscopic analysis include immunohistochemistry, fluorescence *in situ* hybridization, or comparative genomic hybridization.[4-6] These methods usually require expensive antibodies and probes to target cancer-specific biomolecules. For example, the immunohistochemistry method uses a primary antibody for the specific binding to a target melanoma-associated antigen in the skin tissue, and then uses a secondary antibody conjugated with a "signal producing" enzyme to recognize the primary antibody. The "colour producing" enzyme, often a phosphatase or a peroxidase, catalyzes in-solution reactions to produce colour or fluorescence signals.[4] The employment of antibodies or other probes could introduce background noise, depending on the specificity of the target molecule binding process. Furthermore, the invasive biopsy sampling methods may cause painful wounds and high risks of infection. Recently, different modalities have been developed for the purpose of safer and more efficient skin cancer diagnosis. For instance, pigmentation patterns of suspicious melanoma areas can be examined by multispectral digital dermoscopy, confocal scanning laser microscopy, as well as optical coherence tomography.[7-9] Despite the versatility of these optical modalities, the pigmentation can only represent a part of the skin cancer characteristics, unable to provide clear molecular information.[10]

Over the years, MALDI-TOF mass spectrometry has become a convenient and powerful technique for the analysis of biomolecules. It can be used not only for global proteome profiling but also for specific molecule measuring according to the predicted molecular weight.[11-14] This technique allows the analysis of complex samples without the need of prior target molecule labelling. It allows skin state checking and cancer prediction/detection by following up in-tissue protein changes that are associated with the transition from normal skin cells to mediate cells and the final cancer cells. Furthermore, protein signatures or profiles of the skin tissues can be used to classify skin

cancers, to provide valuable insights into prognostic evaluation and to stratify patients by the risk of recurrence.[15] Current limitation in skin cancer diagnosis using MALDI-TOF mass spectrometry stems from the need for invasive skin biopsy sampling methods to obtain biomaterials for testing.

Recently, non-invasive sampling methods have been extensively proposed to improve the detection of skin diseases. For instance, a tape stripping procedure was used to collect DNA or messenger RNA from the outer skin layer (the stratum corneum) for genomic analysis.[16-19] The method provides accurate molecular information for analysis of pathological skin state. But a polymerase chain reaction is required for amplifying the trace nucleic acid, which is time consuming, costly and labor intensive. Tandem mass spectrometry has also been used to analyse the recovered skin biomaterials for cancer biomarker identification.[20] But the method required preparatory biomolecule extraction prior to mass spectrometry measurements. In this chapter, a quick and non-invasive technique is proposed for skin cancer diagnosis by direct MALDI-TOF mass spectrometry measuring of skin cells recovered from suspicious skin regions *via* tape stripping.

## 2. Materials and methods

### 2.1. Preparation of skin samples from healthy human

Normal skin regions and skin moles from three adult volunteers (Persons A, B, C) were selected for the collection of skin cells by the tape stripping sampling procedure. The selected regions were firstly rinsed with water and then cleaned with 70% ethanol aqueous solution with lint-free tissues to remove dust, lipids or other materials adherent on the skin surface. The adhesive tapes used for sampling are the commercial Adhesive Skin Collection Kit provided by DermTech (La Jolla, California, USA). The tapes are single-sided adhesive, with the adhesive layer stuck to a thin inert plastic film. The effective sampling area on each tape is a round region with a diameter of 20 mm, and the total thickness of each tape is ~ 0.1 mm. During the sampling process, the tape was adhered onto a selected skin region with the adhesive side and applied with a slight pressure for a certain period of time (approximately 30 s) to achieve good attachment between the adhesive layer and the skin cells. The region to be measured was outlined with a marking pen on the plastic topside. The tape was then slowly stripped from the skin surface, and skin cells were thus recovered on the adhesive layer of the tape. At least four operations of such tape stripping sampling were applied to an individual skin region, and a new adhesive tape was used for each sampling. The tapes bearing the recovered skin cells were transferred to a MALDI target for immediate mass spectrometry measurement, or carefully stored at 4 °C in a fridge for later measurement

within one week.

## 2.2. Preparation of mimic human melanoma samples

Three different human melanoma cell lines, *i.e.* SBCl2, WM115, WM239, were grown *in vitro* in Petri dishes. The cells were then harvested by trypsinization and centrifugation. Details for the cell culture and harvesting were illustrated in Chapter V. The harvested cells were suspended in ice-cold deionized water to reach a final concentration of $10^5$ cells·mL$^{-1}$. The pure intact cells were deposited onto the tapes that have been previously stripped from a normal skin region of Person A. In such a way, the recovered normal skin cells were doped and/or covered with melanoma cells, and mimic human melanoma samples were thus generated.

## 2.3. Preparation of normal skin samples and melanoma samples from mice

One healthy mouse and two mice carrying localized melanoma tumours were provided by the Ludwig Centre for Cancer Research in Epalinges, Switzerland. The tumour formation time for the two mice was 4.5 weeks and 6 weeks, respectively. Before conducting tape stripping sampling, the tumour region of each mouse was shaved carefully to remove the hairs, and then cleaned gently with 70% ethanol to remove dusters, lipids or other materials adherent on skin surface. The cleaned skin surface was then pasted with an adhesive tape for the collection of skin cells. Four times of tape stripping sampling were applied to each tumour region. The same sampling procedure was also applied to a normal skin region of the healthy mouse to form a healthy control skin sample.

## 2.4. Preparation of mouse melanoma reference

A murine melanoma cell line B16, an often-used model for the study of solid tumour formation, was cultured *in vitro*. The cells were harvested by trypsinization and centrifugation, and suspended in ice-cold deionized water to reach the final concentration of $10^5$ cells·mL$^{-1}$. The pure intact cells were deposited onto a non-used adhesive tape to form the mouse melanoma reference sample. The deposition of every 4 μL of the intact cells resulted in a reference spot with the diameter of ~3 mm. Three such reference spots were prepared in parallel for triplicated measurement.

## 2.5. MALDI-TOF MS measurement and data analysis

The adhesive tapes bearing human or mouse skin cells were transferred onto an electrically conductive MALDI target plate for mass spectrometry measurement. During the transfer process, the tapes were stuck to the MALDI target using an additional adhesive layer (double-sided Scotch sticky tape, product No. 34-8509-3289-7, MN

55144-1000, less than 0.1 mm thickness, 3M Science, USA). Sinapinic acid, 20 mg·mL⁻¹ dissolved in 50/49.9/0.1% (volume percentage) acetonitrile/water/trifluoroacetic acid, was used as matrix. The matrix was deposited onto the adhesive tape to cover the skin cells, and dried at room temperature (~ 5 min) to form cells/matrix co-crystals. Every 4 µL of matrix resulted in a sample spot with the diameter of ~ 3 mm. Thereafter, the target plate was loaded into the MALDI-TOF mass spectrometer for measurements under linear positive mode. Details about mass calibration and measurement parameters are explained in CHAPTER II of this thesis. The obtained mass spectra were analysed by pattern matching *via* the open access software BacteriaMS. Cosine correlation algorithm was used to calculate the similarity scores between each two spectra.[27] Cluster analysis was conducted for the simultaneous comparison of more than two mass spectra. It could divide samples into different groups (clusters) according to the mass spectrum similarity scores. The grouping results were shown in the form of heat-maps, in which colour darkness corresponded to mass spectrum similarity scores.

## 3. Results and discussion

### 3.1. Illustration of the tape stripping mass spectrometry method

The method comprised a non-invasive skin cell sampling procedure and a MALDI-TOF mass spectrometry whole cell fingerprinting approach. As shown in **Figure 6.1**, it includes following steps, *i*) pasting an adhesive tape onto a suspicious
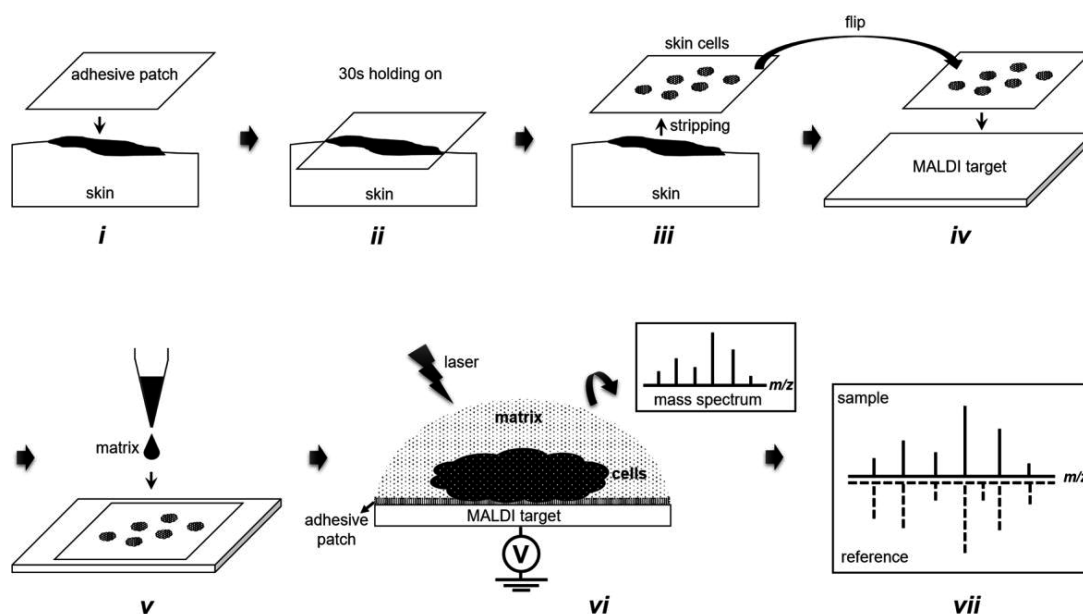


**Figure 6.1** Scheme of tape stripping mass spectrometry method for skin cell analysis.

skin region, ***ii***) applying a slight pressure onto the top of the tape for a certain period of time (~ 30 s) to achieve good attachment between skin cells and the adhesive layer of hthe tape, ***iii***) slowly stripping the tape from the skin surface to recover skin cells, ***iv***) transferring the skin cells-bearing tape onto a MALDI target using an additional adhesive layer, ***v***) depositing a MALDI matrix on the tape to cover the skin cells to form a condensed phase of cells/matrix mixture, ***vi***) conducting MALDI-TOF mass spectrometry measurements and ***vii***) analyzing the generated mass spectra *via* pattern matching and/or peak picking by comparing the mass spectra with reference mass spectra corresponding to healthy controls or cancerous controls. Throughout this procedure, the recovered skin cells were measured in their intact whole state directly after the tape stripping sampling, without any sample pretreatment like cell lysis, preparatory cellular component extraction or enzymatic digestion.

The adhesive tapes used for skin cell sampling came from the commercial Adhesive Skin Collection Kit (DermTech, La Jolla, California, USA). The kit is designed to reliably collect cells from the skin layer, mainly the stratum corneum layer, from nearly all locations of the body, with the exception of palmar, plantar, mucosal surfaces and areas with excessive non-vellus hair.[18] **Figure 6.2** shows the MALDI-TOF mass spectrum generated from a non-used adhesive tape within 2,000-20,000 *m/z*, a mass range that was used for skin cell analysis in the present work. It turned that no mass spectral peaks were generated within the selected mass range, indicating that the adhesive tape itself will not bring any interference to mass spectrometry analysis of the skin cells.
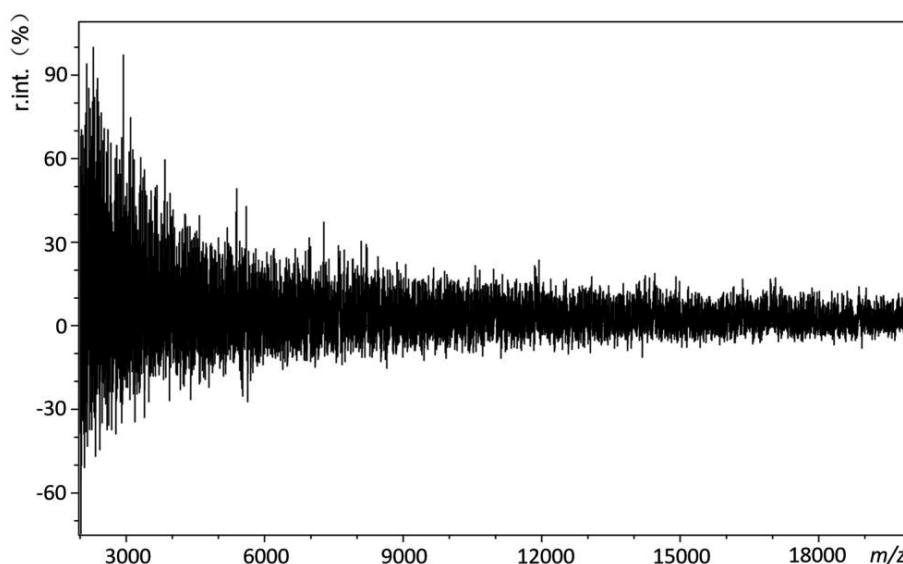


**Figure 6.2** MALDI-TOF mass spectrum of a non-used adhesive tape, using sinapinic acid as matrix.

### 3.2. Analysis of skin samples from healthy human

The tape stripping MALDI-TOF mass spectrometry method was firstly tested with three healthy adult donors. A normal skin region and/or a skin mole was selected from each of the donors for the recovery of skin cells, by applying at least four times the tape stripping sampling method on each selected skin region. **Figure 6.3** compared the microscopy images of a non-used adhesive tape (**Figure 6.3 a**) and an adhesive tape after skin cell sampling (**Figure 6.3 b**). It was clear that skin cells were indeed recovered on the adhesive tape. The adhesive tapes bearing the recovered skin cells from the three healthy donors were subjected to MALDI-TOF mass spectrometry measurements, and the generated mass spectra were displayed in **Figure 6.4-6.8**.
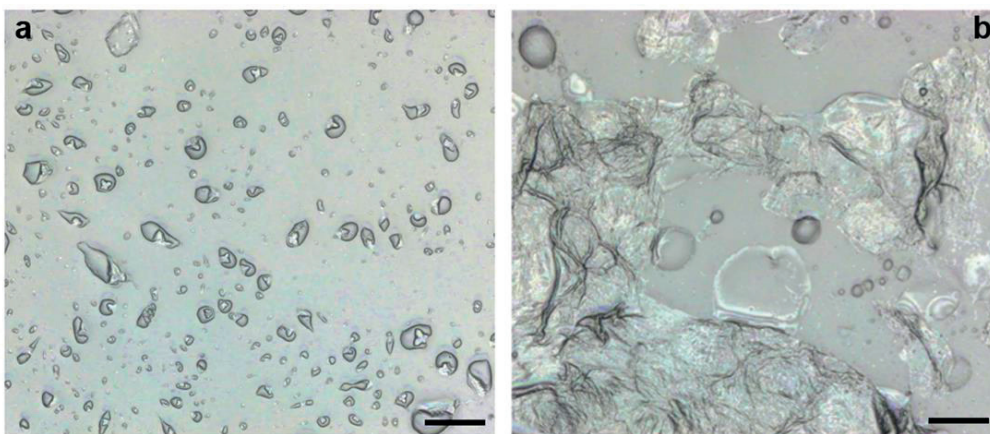


**Figure 6.3** Microscope images of the surface of (**a**) a non-used adhesive tape and (**b**) an adhesive tape that has been used to collect skin cells from a normal skin region on the right forearm of a healthy adult (scale bare 30 μm).

**Figure 6.4** and **Figure 6.5** correspond to a normal skin region and a skin mole (~ 3 mm in diameter), respectively, on the right forearm of Person A, a male donor from Germany in his 30's. **Figure 6.6** and **Figure 6.7** correspond to a normal skin region and a skin mole (~ 3.5 mm in diameter), respectively, on the waist of Person B, a female donor from East Asia in her late 20's. **Figure 6.8** comes from a tiny skin mole (~ 1 mm in diameter) on the right forearm of Person C, a female donor from East Asia in her early 30's, with seven samplings. For all the skin regions, many well-shaped peaks were detected in the mass range of 2,000-20,000 *m/z*. These peaks mainly came from proteins and possibly peptides within the recovered skin cells. Proteins larger than 20 kDa were hardly detected in the present system, most probably due to the reduced detection
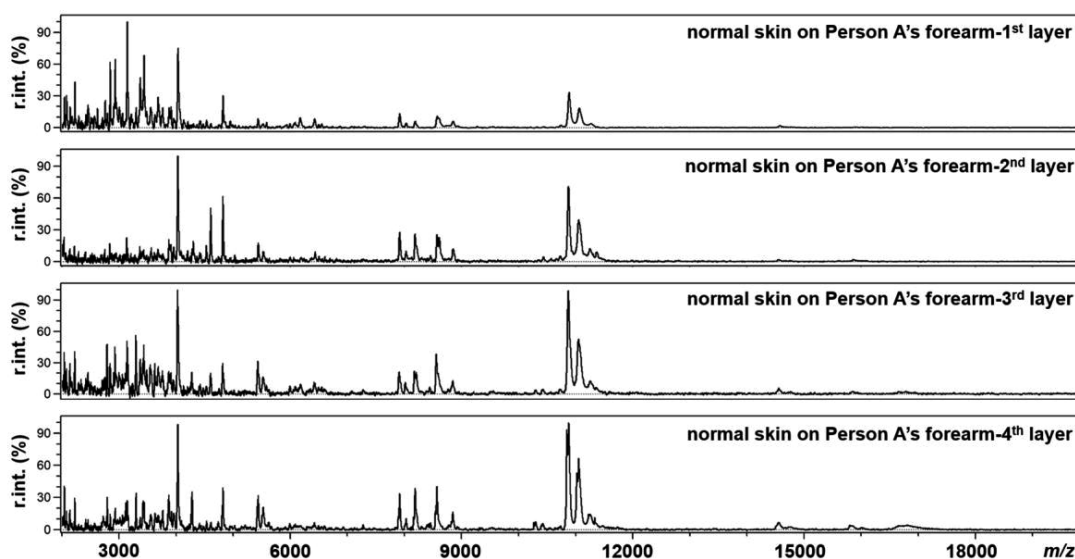
**Figure 6.4** Mass spectra of a normal skin region on the right forearm of Person A, a male donor from Germany in his 30's.
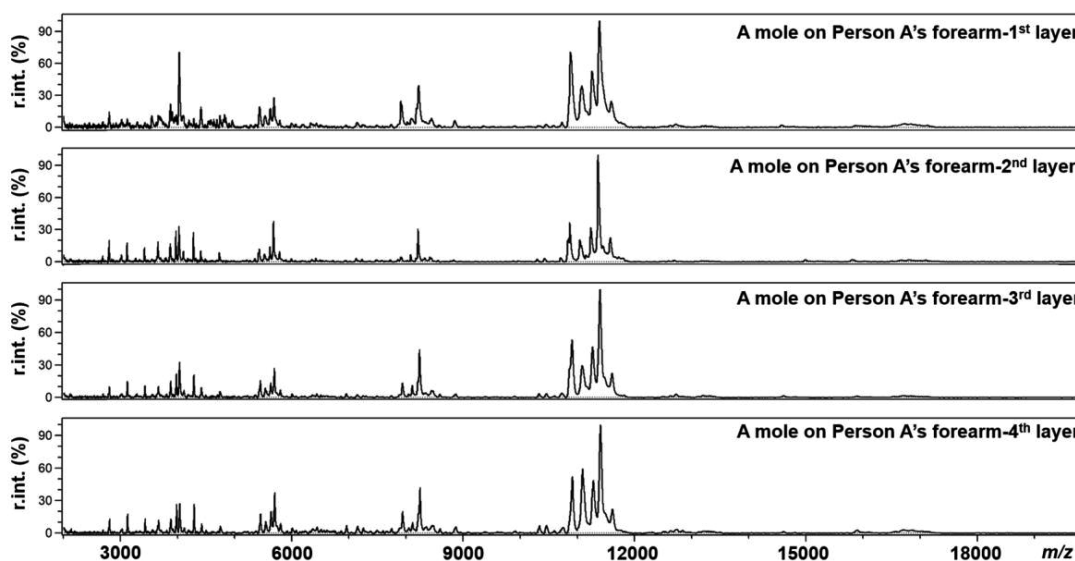


**Figure 6.5** Mass spectra of a skin mole on the right forearm of Person A, a male donor from Germany in his 30's.

sensitivity resulting from the utilization of non-conductive adhesive tapes. As shown in **Figure 6.4**, the four mass spectra obtained from four samplings on the same skin region are similar to each other, especially the two spectra obtained from the third and fourth sampling. The same phenomenon were observed in **Figure 6.5**, **Figure 6.6**, **Figure 6.7** and **Figure 6.8** (third to seventh sampling), indicating the high reproducibility and

reliability of the present procedure for skin cell collection and detection. Overall, the results show that the tape stripping sampling and transfer procedure is compatible with MALDI-TOF mass spectrometry measurements and the recovered skin cells can be measured directly without the need of any pre-treatment.
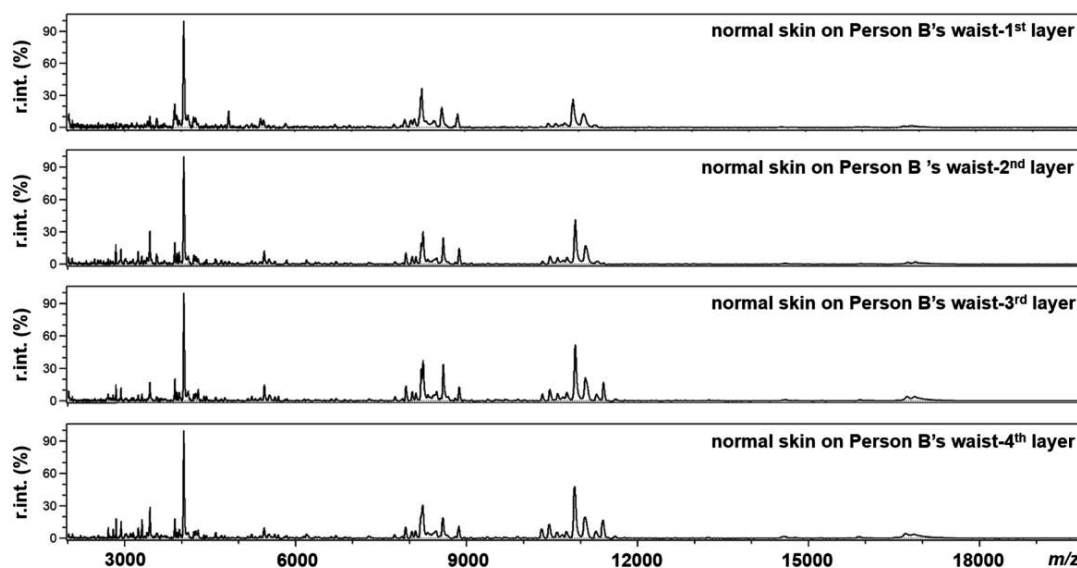
**Figure 6.6** Mass spectra of a normal skin region on the waist of Person B, a female donor from East Asia in her late 20's.
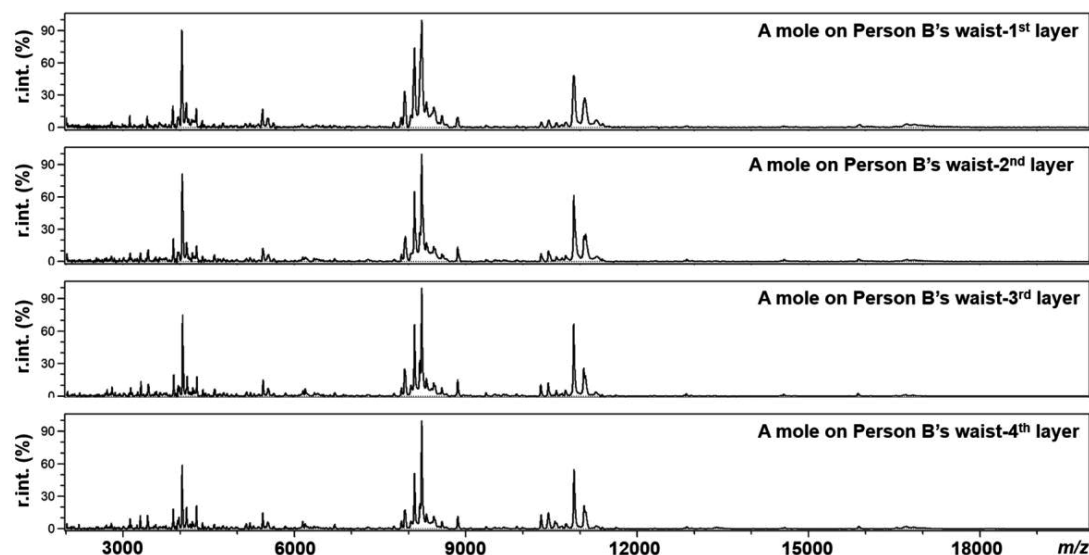
**Figure 6.7** Mass spectra of a skin mole on the waist of Person B, a female donor from East Asia in her late 20's.
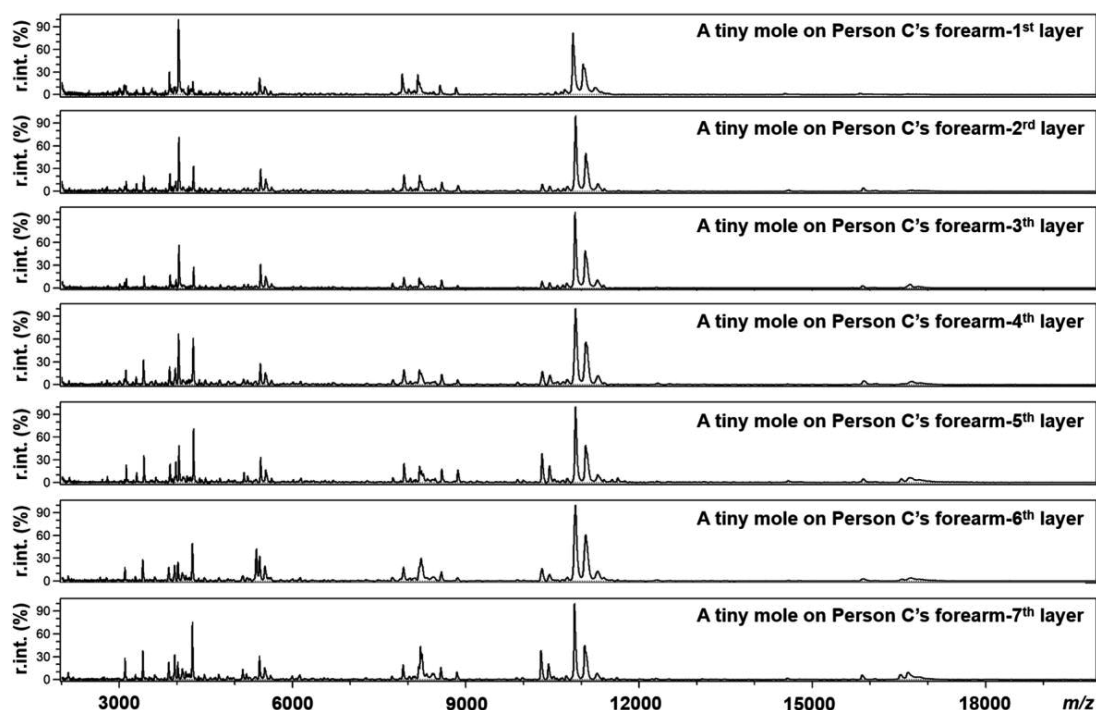
**Figure 6.8** Mass spectra of a tiny skin mole on the right forearm of Person C, a female donor from East Asia in her early 30's.

### 3.3. Analysis of mimic human melanoma samples

In order to mimic real human melanoma, the normal skin region of Person A was subjected to four times tape stripping sampling, and the obtained four pieces of normal skin cells-bearing adhesive tapes were spiked with *in vitro* grown human melanoma cells. In such a way, the recovered normal skin cells were doped and/or covered with malignant skin cells. Such kind of mimic human melanoma samples were prepared with three different melanoma cell lines, *i.e.* primary melanoma cell line SBCl2 (radial growth phase), primary melanoma cell line WM115 (vertical growth phase) and metastatic melanoma cell line WM239. The samples were then subjected to mass spectrometry measurements. And the resulting mass spectra were displayed in **Figure 6.9** for SBCl2 cells, **Figure 6.10** for WM115 cells and **Figure 6.11** for WM239 cells. In each figure, the four mass spectra show high similarity to each other, indicating high reproducibility of the measurements.

In order to investigate the difference among the normal skin regions, skin moles and the mimic melanoma samples, the mass spectra generated from the third sampling in **Figure 6.4-6.11** were visually compared, as shown in **Figure 6.12**.
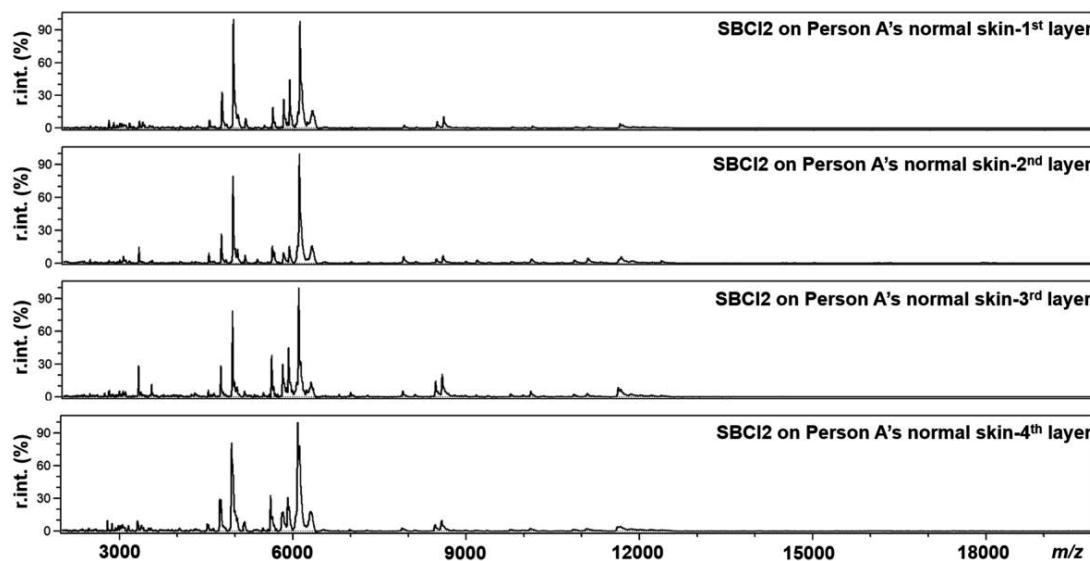
**Figure 6.9** Mass spectra of mimic human melanoma samples, prepared by spiking primary (radial growth phase) human melanoma cells SBCl2 on to adhesive tapes bearing normal skin cells stripped from the right forearm of Person A. The same skin region of Person A was subjected to four times tape stripping sampling.
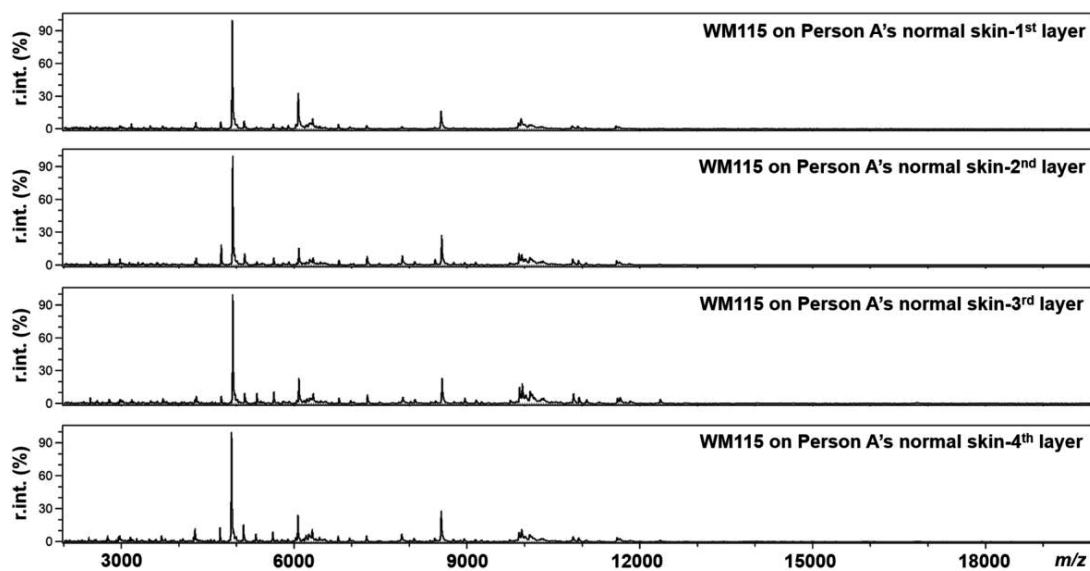


**Figure 6.10** Mass spectra of mimic human melanoma samples, prepared by spiking primary (vertical growth phase) human melanoma cells WM115 on to adhesive tapes bearing normal skin cells stripped from the right forearm of Person A. The same skin region of Person A was subjected to four times tape stripping sampling.
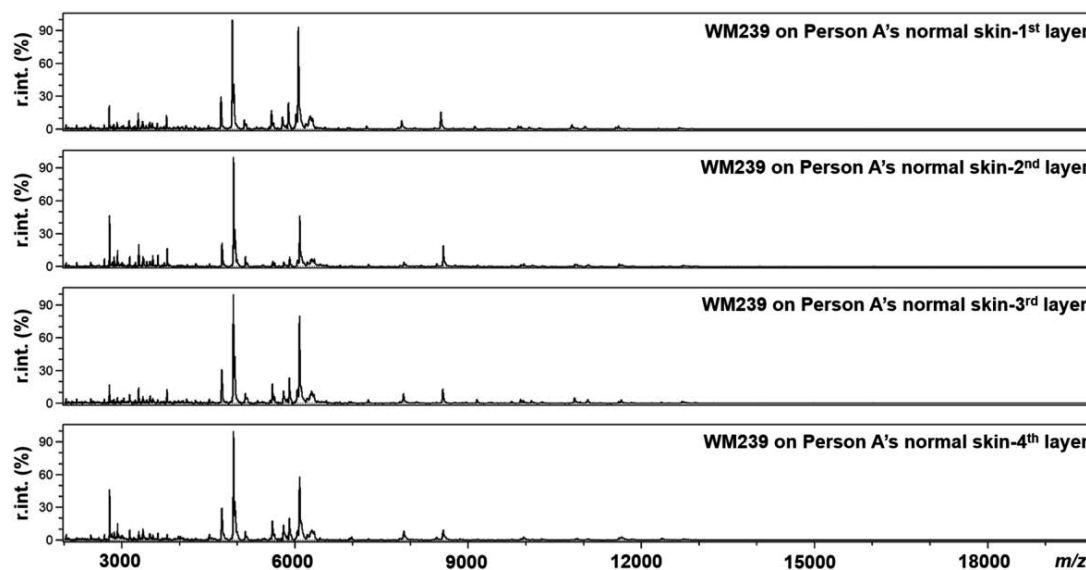
**Figure 6.11** Mass spectra of mimic human melanoma samples, prepared by spiking metastatic human melanoma cells WM239 on to adhesive tapes bearing normal skin cells stripped from the right forearm of Person A. The same skin region of Person A was subjected to four times tape stripping sampling.

**Figure 6.12** shows that the mass spectra generated from normal skin regions, or skin moles, share many of the highly intensive peaks, meaning that the collected cells share many of their high abundant cellular proteins. Similarly, the three mimic human melanoma samples also shared high mass spectrum similarity between each other, indicating the expression of similar proteins within different stages of melanoma. However, mass spectra of the mimic melanoma samples were greatly different from that of normal skin regions or skin moles, which should be attributed to the different protein compositions between the malignant and the non-malignant skin cells. The epidermis of normally skin, or the outermost layer of the skin, contains mainly Merkel cells and keratinocytes, with the presence of some melanocytes and Langerhans cells. A skin mole is a benign growth of melanocytes, a type of cells that give skin dark colour. The melanocytes within skin moles grow in a group rather than individually. Although in very few cases the skin mole become malignant, abnormal moles can develop into melanoma over time. Melanoma is one type of most aggressive skin cancers, resulting from the un-controllable growth of melanocytes. Observation of **Figure 6.12** finds that several mass spectral peaks were specific to the mimic melanoma samples. As shown in Chapter V of this thesis, top-down proteomic analysis of the three *in vitro* grown melanoma cell lines revealed that some of peaks came from marker proteins used for

diagnosis or prognosis of human melanoma. As labelled in **Figure 6.12**, Peak 1 at 4,933 *m/z* (mass value observed at the peak centre, averaged from four measurements) came from thymosin beta 10, a melanoma progression marker, which is involved in the regulation of cellular motility, angiogenesis and inflammation.[21] Peak 2 at 6,052 *m/z* was from metallothionein-2, which has been used for melanoma prognosis.[22] Peak 3 at 10,084 *m/z* and peak group 4 (peak at 11,640 *m/z* and 11,750 *m/z*) corresponded to S100 calcium binding proteins, a protein family widely used for melanoma dianosis.[23] These maker proteins can be used to distinguish cancer cells and normal proliferating cells. The mass spectra in **Figure 6.12** were then compared with cluster analysis according to the cosine similarity between each of the two spectra, and the resulting heat-map is displayed in **Figure 6.13**. The heat-map clearly divided the eight samples into two
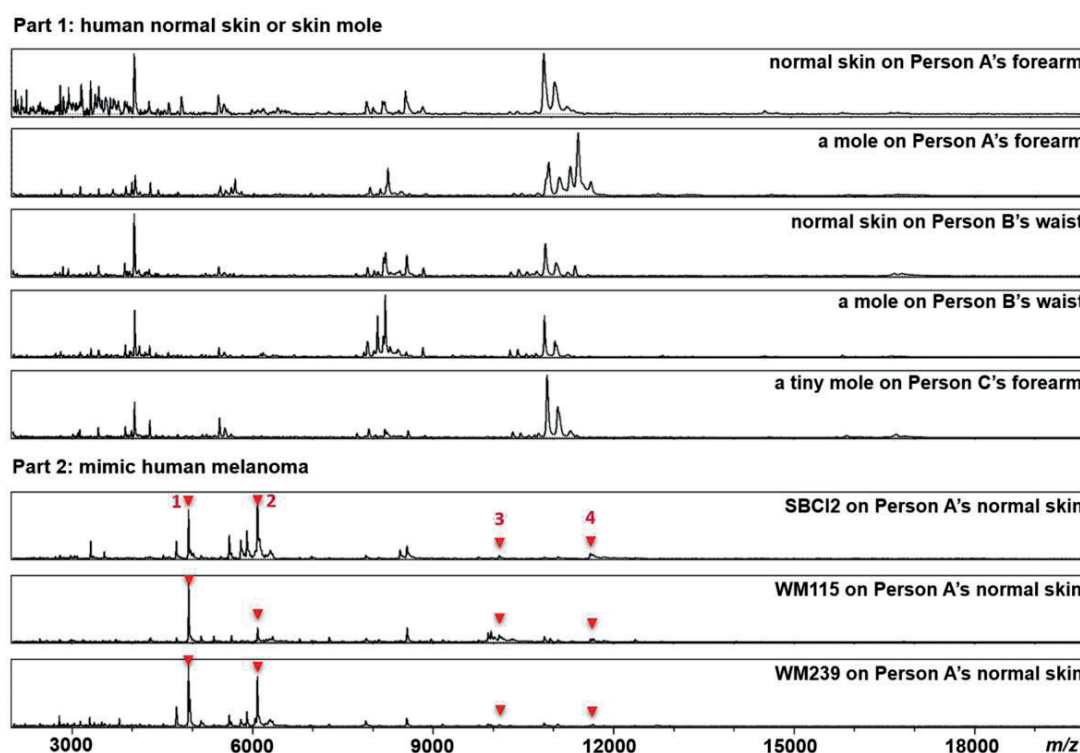


**Figure 6.12** Comparison of mass spectra generated from normal skin regions, skin moles and mimic human melanoma samples. Each of the spectra corresponds to the third spectrum in **Figure 6.4-6.11**. Peak 1 at 4,933 *m/z* came from thymosin beta-10. Peak 2 at 6,052 *m/z* was from metallothionein-2. Peak 3 at 10,084 *m/z* and peak group 4 (peak at 11,640 *m/z* and 11,750 *m/z*) corresponded to S100 calcium binding proteins. The above mass values were the averaged mass value at the peak center resulting from four measurements.
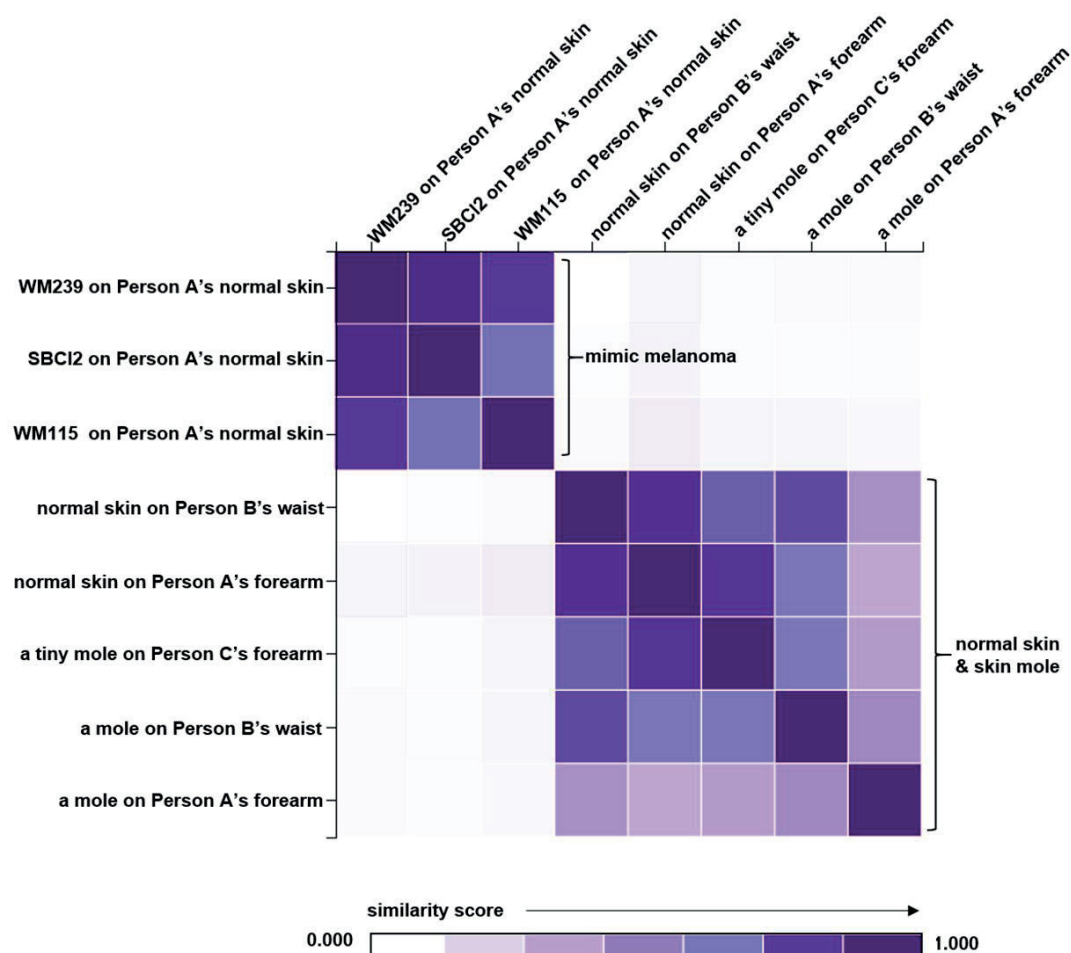
**Figure 6.13** Cluster analysis of normal skin regions, skin moles and mimic human melanoma samples.

groups. One group was comprised of normal skin regions or skin moles from the three healthy donors, and the other was comprised of the three mimic human melanoma samples. The similarity scores between group-crossing samples were mostly lower than 0.05. The above results show that the proposed tape stripping mass spectrometry method is promising for the prediction and detection of skin cancers or other types of skin diseases.

## 3.4. Mouse melanoma testing

The proposed tape stripping mass spectrometry method was employed to analyse mouse melanoma. Melanoma tumour was introduced into mice by genetically introducing a BRAF V600E mutation (a common mutation in more than 40% of human melanoma patients) and the deletion of PTEN. This mouse model melanoma has been
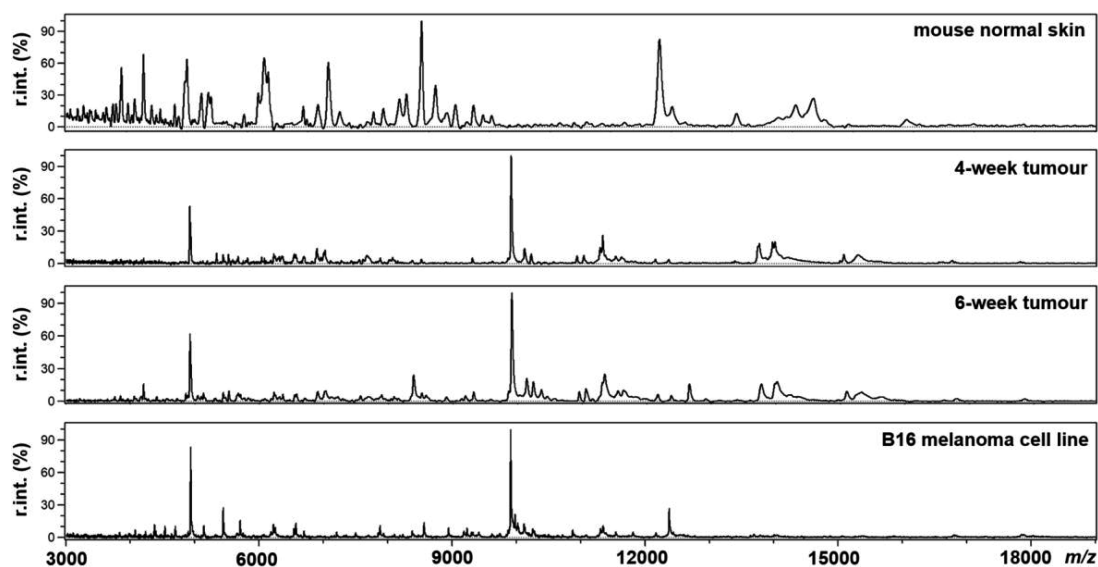
**Figure 6.14** Mass spectra generated from a normal skin region on mouse back, tumour regions on melanoma-carrying mice and mouse melanoma reference (*in vitro* grown B16 cells).

frequently used to mimic pathophysiology and tumorigenesis in human melanomas.[24] The tumour was allowed to develop for 4 weeks and 6 weeks, respectively. Skin cells were recovered from the tumour regions of the melanoma-carrying mice and a normal skin region of a healthy mouse through the tape stripping sampling procedure. Each skin region was continuously sampled four times. The first three samples were contaminated with a lot of mice hairs, which interfered with skin cell analyses. The contamination was less for the fourth samples, which were afterwards analysed with MALDI-TOF mass spectrometry. The generated mass spectra, together with a mouse melanoma reference mass spectrum (collected from *in vitro* grown mouse melanoma cell line B16, a genetically irrelevant melanoma cell line), are shown in **Figure 6.14**. It was clear that the mass spectra generated from the mouse tumour regions were quite different from the normal skin region, but showed high similarity to the *in vitro* grown melanoma cell line B16. This result indicates the presence of melanoma cells on the tumour surface of the melanoma-carrying mice, and demonstrated the recovery of those melanoma cells on the adhesive tapes *via* the tape stripping sampling procedure.

## 4. Summary

In this chapter, a method combining tape stripping sampling and MALDI-TOF mass spectrometry whole cell fingerprinting was proposed for fast and non-invasive analysis

of skin cells. The method shows potentials in prediction and detection of skin cancers or other types of skin diseases. A primary test conducted with melanoma-carrying mice showed its possibility in clinical practice. Due to the heavy contamination from the mouse hairs, I didn't test the method with more mouse samples. Instead, I have contacted a dermatologists in Switzerland and applied for a testing approval of melanoma patients. At the same time, more assays will be designed and conducted to further improve the performance of this method, aiming to make it a useful and convenient diagnosis tool.

# Reference

1. Gray-Schopfer, V., Wellbrock, C. & Marais, R. Melanoma biology and new targeted therapy. *Nature* 445, 851-857 (2007).
2. Rothberg, B.E.G., Bracken, M.B. & Rimm, D.L. Tissue biomarkers for prognosis in cutaneous melanoma: a systematic review and meta-analysis. *J Natl Cancer Inst* 101, 452-474 (2009).
3. Abbasi, N.R.*, et al.* Early diagnosis of cutaneous melanoma: revisiting the ABCD criteria. *Jama* 292, 2771-2776 (2004).
4. Bethune, G.C., Pettit, A.S., Veldhuijzen van Zanten, D. & Barnes, P.J. Well-differentiated invasive breast cancers with equivocal HER 2 immunohistochemistry: what is the yield of routine reflex in-situ hybridization testing? *Histopathology* 70, 966-974 (2017).
5. Frickmann, H.*, et al.* Fluorescence in situ hybridization (FISH) in the microbiological diagnostic routine laboratory: a review. *Crit Rev Microbiol* 43, 263-293 (2017).
6. Vishwanathan, N.*, et al.* A comparative genomic hybridization approach to study gene copy number variations among chinese hamster cell lines. *Biotechnol Bioeng* 114, 1903-1908 (2017).
7. Marghoob, A.A.*, et al.* Instruments and new technologies for the in vivo diagnosis of melanoma. *J Am Acad Dermatol* 49, 777-797 (2003).
8. Goodson, A.G. & Grossman, D. Strategies for early melanoma detection: Approaches to the patient with nevi. *J Am Acad Dermatol* 60, 719-735 (2009).
9. Wadhawan, T., Situ, N., Lancaster, K., Yuan, X. & Zouridakis, G. SkinScan©: a portable library for melanoma detection on handheld devices. in *Biomedical Imaging: From Nano to Macro,* 133-136, 2011 IEEE International Symposium (2011).
10. Zonios, G.*, et al.* Melanin absorption spectroscopy: new method for noninvasive skin investigation and melanoma detection. *J Biomed Opt* 13, 014017 (2008).
11. Chughtai, K. & Heeren, R.M. Mass spectrometric imaging for biomedical tissue analysis. *Chem Rev* 110, 3237-3277 (2010).
12. Cornett, D.S.*, et al.* A novel histology-directed strategy for MALDI-MS tissue profiling that improves throughput and cellular specificity in human breast cancer. *Mol Cell Proteomics* 5, 1975-1983 (2006).
13. Kang, H.S.*, et al.* Protein and lipid MALDI profiles classify breast cancers according to the intrinsic subtype. *Bmc Cancer* 11, 465 (2011).
14. Bondarenko, A.*, et al.* Aluminium foil as a single-use substrate for MALDI-MS fingerprinting of different melanoma cell lines. *Analyst* 141, 3403-3410 (2016).
15. Gross, J.H. *Mass spectrometry: a textbook*. Springer Science & Business Media (2006).
16. Benson, N.R. Tape stripping methods for analysis of skin disease and pathological skin state. U.S. Patent Application (2007).
17. Vogt, T. Method for detection of melanoma. U.S. Patent (2007).
18. Rheins, L.A. & Morhenn, V.B. Methods and kits for obtaining and analyzing skin samples for the detection of nucleic acids. U.S. Patent (2005).
19. Rheins, L.A. & Morhenn, V.B. Method for detection of biological factors in epidermis. U.S. Patent (2004).
20. Mehul, B., Laffet, G. & Russo, L. Non-invasive method for collecting biological data for establishing a diagnosis of a cutaneous pathology. U.S. Patent Application (2010).
21. Weterman, M.A.J., Vanmuijen, G.N.P., Ruiter, D.J. & Bloemers, H.P.J. Thymosin Beta-10 Expression in Melanoma Cell-Lines and Melanocytic Lesions - a New Progression Marker for Human Cutaneous Melanoma. *Int J Cancer* 53, 278-284 (1993).
22. Weinlich, G.*, et al.* Metallothionein - overexpression as a highly significant prognostic factor in melanoma: a prospective study on 1270 patients. *Brit J Cancer* 94, 835-841 (2006).
23. Gaynor, R., Irie, R., Morton, D. & Herschman, H.R. S100 Protein Is Present in Cultured

Human-Malignant Melanomas. *Nature* 286, 400-401 (1980).

24. Hodis, E.*, et al.* A landscape of driver mutations in melanoma. *Cell* 150, 251-263 (2012).

# CHAPTER VII. Summary & Perspective

## 1. Summary of this thesis

On October 1st 2014, the first day I started PhD study, my thesis director Prof. Hubert H. Girault and co-director Dr. Liang Qiao told me that my thesis would focus on the topic of bacterial detection by mass spectrometry. At that time I was not too happy, as I thought that bacteria are smelly, disgusting and dangerous. My educational background was mainly in material science and to some extent analytical chemistry, not at all in microbiology. But, as a Chinese student who has been taught since the age of 5 to respect teachers whenever, I decided to accept this thesis topic. However, my opinion about bacterial research changed when I started to learn about it. Now, I feel very fortunate that I did not give it up.

Bacterial infections greatly threaten public health, especially when the pathogens are antimicrobial-resistant. If left uncontrolled, antimicrobial-resistance genes are easily transported among bacteria, and the resulting human deaths are expected to reach 10 million globally every year in 2050s, even more than the current deaths caused by cancers which are 8.2 million per year (data come from The Review on Antimicrobial Resistance, chaired by Jim O'neill, May 2016).[1] The prevalence of antimicrobial resistance is largely caused by the misuse and overuse of antimicrobial drugs. The drugs thus should be prescribed properly to relieve the resistance crisis. For this purpose, a change in the current diagnosis is needed. Today in many cases doctors still prescribe drugs based only on their immediate assessment of patient's symptoms, just like in the 1950s when antibiotics were still new in hospitals. The main reason is the lack of cheap and rapid diagnostic tests. As introduced in CHAPTER I, current diagnostic standards are often time-consuming. It would be meaningful to improve human health if I could find some ways to speed up and simplify the diagnosis process.

"*Today, antibiotics are rarely prescribed based on a definitive diagnosis. Diagnostic tests can show whether or not an antibiotic is actually needed, and which one. Having rapid, low-cost, and readily available diagnostics is an essential part of the solution to this urgent problem.*"

Dr Margaret Chan
Director General of the World Health Organization

My thesis was then carried out with this motivation. During the first half of my PhD study, I developed three methods to facilitate bacterial infection diagnosis, including:

*i)* an immuno-affinity MALDI-TOF mass spectrometry method to provide a rapid identification of bacteria from human blood, as shown in CHAPTER II;

*ii)* a titanium dioxide-assisted MALDI-TOF mass spectrometry method to detect antimicrobial resistance proteins from intact bacteria, as shown in CHAPTER III;

*iii)* an immuno-affinity amperometric method to achieve bacterial species determination, living bacteria quantification and antimicrobial susceptibility testing, as shown in CHAPTER IV;

As bacterial cells and mammalian cells share many similarities, my thesis topic was extended to cancer cells during the second half of my PhD study. Two tools were proposed for cancer analysis, including:

*i)* a potential tool for quick cancer analysis based on MALDI-TOF mass spectrometry detection of exosomes, as shown in CHAPTER V;

*ii)* a potential tool for non-invasive skin disease monitoring based on MALDI-TOF mass spectrometry detection of skin cells, as shown in CHAPTER VI.

For each of the above works, some aspects remain to be continued or improved. A brief discussion is given below.

## 2. Perspective

In CHAPTER II, bacterial reference mass spectra were collected from low numbers (10-100) of bacterial cells to help species identification from human blood contaminated with low concentration of bacterial pathogens and thus to facilitate quick diagnosis. Currently, the reference spectra were collected from three bacterial species only, and more bacterial species should be included to enlarge the reference spectrum database. The present strategy relies on the use of bacterial species-specific antibody to isolate and enrichment bacterial pathogens. In clinical practice, magnetic beads coated with a mixture of antibodies against common bacterial pathogens can be prepared for the isolation of unknown pathogens. Taking bloodstream infections as an example, bacterial pathogens like *Escherichia coli*, *Staphylococcus aureus*, *Staphylococcus epidermidis*, *Pseudomonas aeruginosa*, *Klebsiella spp.*, *Enterococcus spp.* and *Enterobacter cloacae* account for more than 70% of the infection episodes. Commercial antibodies against all the above species are currently available, and a cocktail of these antibodies is efficient for the diagnosis in most cases. The immuno-affinity capture can be further improved by using non-specific affinity probes. Instead of using bacterial species-specific antibodies,

ligands bearing affinity to universally all bacterial species or multi-species could be employed to blindly capture all bacterial cells from infected blood. The collected bacteria can then be identified by MALDI-TOF mass spectrometry fingerprinting. This blind capture strategy is extremely suitable for single-species infections. If the infections are caused by more than one species, the identification could be achievable by adjusting the mathematical algorithm for pattern matching.[2] In such a way, there would be no need to prepare different bacterial antibodies, which will greatly reduce the testing time and cost. Such ligands could be found by systematically analysing the bacterial surface structures and compositions. Attentions should be focused on the similarities among different bacterial species, as well as the difference between bacterial cells and blood cells. It is ideal that the ligands have affinity to every kind of bacteria, but have no or very minimal interaction with blood components. Currently such ligands have not yet been reported, but the potential candidates could include mannose-binding lectin, DNA binding ligands, eosinophil cationic protein, Zn(II)-dipicolylamine and mammalian immunoglobulin G.[3-7] All of them have been reported showing affinity to multiple bacterial species.

In addition to be used for the detection of antimicrobial resistance-associated proteins, the titanium dioxide-modified MALDI target plates present in CHAPTER III also show potentials to boost bacterial identification. Current reference spectra are limited within the mass range of 2,000-20,000 *m/z*. Any fingerprint peak beyond this mass range could be useful to improve the identification accuracy, for instance, to distinguish between *Shigella* species and *Escherichia coli* whose fingerprints share quite high similarities.[8] The peaks in high mass range could also enable bacterial identification at the sub-species level or the strain level. Relatively few fingerprint peaks, normally 5-10 peaks, are required for species identification, whereas many more peaks are needed for subspecies or strain identification, which is a long-time challenge for the MALDI-TOF mass spectrometry fingerprinting approach.[9] Moreover, my colleagues are making efforts to simplify the manufacture of the titanium dioxide-modified target, aiming at producing disposable plates with robot to reduce the fabrication time and cost. Beside of bacteria analysis, the plates have many other mass spectrometry applications. Examples include on-plate phosphopeptide enrichment and in-source photocatalytic redox reactions for inducing peptide fragmentation.[10,11] Also, the application of MALDI-TOF mass spectrometry in the testing of antimicrobial resistance could be further explored. For instance, the fingerprinting procedure could be used to follow up the physiological state of bacterial cells under antibiotic treatment, targeting the changes in their protein profiles or metabolic profiles. The initial bacterial cell concentration, antibiotic concentration and the treatment time are expected to make influence. Such kind of follow-up might be able to distinguish between resistant bacteria and susceptible bacteria. In addition to MALDI-TOF mass

spectrometry, ESI mass spectrometry also could be used for the detection of antimicrobial resistance. For example, by coupling with specially designed microchips, the ESI mass spectrometry might enable the dynamic monitoring of antibiotic degradation caused by resistant bacteria. Our laboratory has experience in such kind of microchip-mass spectrometer combination strategy.[12,13]

Many researchers are interested in the amperometric method presented in CHAPTER IV, as it allows not only bacterial species determination and living bacteria quantification but also antimicrobial susceptibility testing. The method can be used in point-of-care diagnosis, which is gaining increasing clinical significance during the last decade. A point-of-care diagnosis is performed at the time and site of an initial encounter with the health care system. The rapid diagnosis would reduce the patient visit time and allow a quick delivery of appropriate antibiotic therapy.[14] The company SENSàSION has the plan to commercialize the detection system to bring it into the real life. Of course, many aspects remain to be improved. For instance, more universal ligands could be developed to replace the bacterial species-specific antibodies to simplify the bacterial isolation process, as mentioned previously. The use of non-specific ligands will disable the determination of bacterial identity, but still enables the antimicrobial susceptibility testing which is the most important part of clinical diagnosis. Besides, the metabolite activity indicators should receive more attention. In the current work, I have clarified a group of potentially useful indicators, but didn't compare their performance systematically. Well-designed experiments should be conducted to find out the best ones for clinical practice. So far around 4-6 h of blood culture is still needed to enlarge the bacterial cell numbers to a detectable level. This 4-6 h of culture time is definitely not the bottleneck, which is possibly to be further shorten by improving the bacterial isolation process. Techniques like microfluidic or acoustofluidic separation might help.[15,16] The electrode-imbedded microtiter plates produced by our group are currently comprised of 8 channels, not enough for a practical susceptibility testing which often involves around 10-20 different antibiotics simultaneously. My colleagues are making efforts to increase the microtiter plate channels to 16, 24 or as many as 96 ideally. If achieved, it would greatly increase the analysis throughput and shorten the overall testing time. In addition to bloodstream infection diagnosis, the above mass spectrometry and amperometry methods are also applicable for urine infection diagnosis, blood product quality control and food quality control. Similar to the diagnosis of bloodstream infections, the key factor influence the testing is the utilization of appropriate affinity probes for isolation and enrichment of the bacterial cells.

The blood-circulating exosome detection approach present in CHAPTER V is clinically meaningful. It provides a fast, convenient and non-invasive way to monitor melanoma diseases. Currently the detection is limited in murine melanoma and stage IV

human melanoma patients. I am going to conduct the tests with more patients in earlier melanoma stages. I have contacted collaborators in Ludwig Cancer Research Lausanne Branch and University Hospital of Basel, who will provide more blood serum samples from stage II and III melanoma patients. Through largescale studies and statistical analysis, it would be possible to validate exosome fingerprint markers for melanoma diagnosis, prognosis (evaluation of the disease state) and patient post-treatment follow-up. The validation of biomarkers relies on the correlation between MALDI-TOF MS fingerprints and top-down proteomic analysis. To facilitate the validation, it is important to improve MALDI-TOF MS measurements to generated fingerprint peaks with high resolution. It is also crucial to find an efficient way for protein assignment, especially when several proteins with almost the same molecular weight are detected from a single sample. To solve this problem, it is necessary to consult experts in the field of proteomics. In the present work, all types of exosomes circulating in the bloodstream were measured together, providing an overview of the patient physiological state under cancer pressure. But it would lead to the loss of melanoma detection sensitivity, due to the interference from non-melanoma-derived exosomes which are present in much higher concentrations than the melanoma-derived exosomes. Immuno-affinity separation combined with MALDI-TOF mass spectrometry is a potential way to solve this problem. For example, a recent publication in November 2018 reports that antibodies against chondroitin sulfate proteoglycan 4 (CSPG4) have high affinity to melanoma-derived exosomes.[17] CSPG4 is a transmembrane proteoglycan originally identified as a highly immunogenic tumour antigen. It has been found on the surface of more than 80% of melanoma cells and the secreted exosomes, but not on normal (non-cancerous) cells. My experimental results also show that CSPG4 are present on all the three melanoma exosomes, *i.e.* exosome secreted by SBCl2 cells (radial growth phase primary melanoma), WM115 cells (vertical growth phase primary melanoma) and WM239 cells (metastatic melanoma), as was confirmed by bottom-up proteomic analysis. This type of anti-CSPG4 antibodies conjugated with a suitable size of magnetic beads might be an efficient immuno-affinity probe to separate melanoma-derived exosomes from other blood-circulating exosomes. In addition to melanoma, the proposed exosome detection method can be expanded to other types of cancers like lung cancer, breast cancer, prostate cancer, colorectal cancer or pancreatic cancer. These types of cancers are the top deadliest cancers around the world, highly demanding an improvement to the diagnostic techniques.

The skin cell analysis tool present in CHAPTER VI is not yet well developed. At the moment, it has been proven feasible for healthy human skin and mimic human melanoma samples. A tentative test on melanoma-carrying mouse found that mouse hairs recovered on the adhesive tapes during the tape stripping sampling process would

interfere with the skin cell detection. Compared to human skin, mouse skin is full of long, thick, dark-coloured non-vellus hairs, making the sampling process difficult. I plan to continue the tests with nude mice or directly with human melanoma patients, depending on the outcome of a future discussion with my collaborators. I have contacted my collaborators in the University of Lausanne and Lausanne cancer research centre for the preparation of a group of melanoma-carrying mice, which will be used for the testing at different cancer stages. My advisor has also helped me contact a dermatologist in Sierre, Switzerland to apply for human testing approval. We are now waiting for the testing permit and volunteer patients. To be mentioned, in order to make sure the detection reliability, around three or four times of the sampling are suggested to be applied on each suspicious skin region to recovery as many skin cells as possible. Another possible application of this tape stripping mass spectrometry method is the analysis of biofilms on human skin or public contact surfaces like door handles where microorganisms are easily accumulated. Frequently isolated microbes from the biofilms include species like *Staphylococcus aureus*, *Staphylococcus epidermidis*, *Propionibacterium acnes*, *Escherichia coli*, *Malassezia spp.*, *micrococcus spp.*, *Salmonella spp.* and *Klebsiella spp.*[18,19] Many of them are associated with infectious diseases. Analysis of the biofilms would help the study of human-microbe or microbe-microbe interaction and the prevention of probable infections.

As two of the most important human health concerns, cancers and microorganism infections have attracted the attention from a great number of scientists. Tremendous efforts have been made over the past few decades to improve the diagnosis conditions. Such kind of efforts will be continued in at least the next decades. As a PhD student in analytical chemistry, I feel honoured to be involved in this scientific research. The ending of this thesis is the point to restart. I am happy to go deeper in the related fields with the aim to develop more practically useful methods to improve clinical diagnosis.

# Reference

1. *Tackling drug-resistant infections globally: final report and recommendations*. Review on Antimicrobial Resistance (2016).
2. Yang, Y., Lin, Y. & Qiao, L. Direct MALDI-TOF MS Identification of Bacterial Mixtures. *Anal Chem* 90, 10400-10408 (2018).
3. Kaizerman, J.A*., et al.* DNA binding ligands targeting drug-resistant bacteria: Structure, activity, and pharmacology. *J Med Chem* 46, 3914-3929 (2003).
4. Torrent, M., Navarro, S., Moussaoui, M., Nogués, M.V. & Boix, E. Eosinophil cationic protein high-affinity binding to bacteria-wall lipopolysaccharides and peptidoglycans. *Biochemistry* 47, 3544-3555 (2008).
5. Yi, J*., et al.* Identification of pathogenic bacteria in human blood using IgG-modified Fe 3 O 4 magnetic beads as a sorbent and MALDI-TOF MS for profiling. *Microchimica Acta* 185, 542 (2018).
6. Neth, O*., et al.* Mannose-binding lectin binds to a range of clinically relevant microorganisms and promotes complement deposition. *Infection and immunity* 68, 688-693 (2000).
7. Lee, J.J*., et al.* Synthetic Ligand-Coated Magnetic Nanoparticles for Microfluidic Bacterial Separation from Blood. *Nano Lett* 14, 1-5 (2014).
8. Paauw, A*., et al.* Rapid and reliable discrimination between Shigella species and Escherichia coli using MALDI-TOF mass spectrometry. *Int J Med Microbiol* 305, 446-452 (2015).
9. Dieckmann, R., Helmuth, R., Erhard, M. & Malorny, B. Rapid Classification and Identification of Salmonellae at the Species and Subspecies Levels by Whole-Cell Matrix-Assisted Laser Desorption Ionization-Time of Flight Mass Spectrometry. *Appl Environ Microb* 74, 7767-7778 (2008).
10. Qiao, L*., et al.* Photocatalytic Redox Reactions for In-Source Peptide Fragmentation. *Chem-Eur J* 15, 6711-6717 (2009).
11. Qiao, L*., et al.* Specific on-plate enrichment of phosphorylated peptides for direct MALDI-TOF MS analysis. *J Proteome Res* 6, 4763-4769 (2007).
12. Gasilova, N., Qiao, L., Momotenko, D., Pourhaghighi, M.R. & Girault, H.H. Microchip Emitter for Solid-Phase Extraction-Gradient Elution-Mass Spectrometry. *Anal Chem* 85, 6254-6263 (2013).
13. Gasilova, N., Yu, Q.L., Qiao, L. & Girault, H.H. On-Chip Spyhole Mass Spectrometry for Droplet- Based Microfluidics. *Angew Chem Int Edit* 53, 4408-4412 (2014).
14. Gauglitz, G. Point-of-care platforms. *Annu Rev Anal Chem* 7, 297-315 (2014).
15. Li, S.X*., et al.* Acoustofluidic bacteria separation. *J Micromech Microeng* 27(2017).
16. D'Amico, L., Ajami, N., Adachi, J., Gascoyne, P. & Petrosino, J. Isolation and concentration of bacteria from blood using microfluidic membraneless dialysis and dielectrophoresis. *Lab Chip* 17, 1340-1348 (2017).
17. Sharma, P*., et al.* Immunoaffinity-based isolation of melanoma cell-derived exosomes from plasma of patients with melanoma. *J Extracell Vesicles* 7(2018).
18. Brandwein, M., Steinberg, D. & Meshner, S. Microbial biofilms and the human skin microbiome. *NPJ biofilms and microbiomes* 2, 3 (2016).
19. Onwubiko, N.E. & Chinyeaka, A. Isolation and identification of bacterial Contaminants from door handles in a Tertiary institution in Umuahia, Abia State, Nigeria. *Nigerian Journal of Microbiology* 29, 3139-3147 (2015).

CURRICULUM VITAE

# Yingdi ZHU

**Birth: December 10th 1988, China**

**E-mail: yingdi.zhu@epfl.ch**

**Tel: +41 78 900 1855**

**Chemin des Collines 41, CH-1950 Sion, Valais, Switzerland**

## Education

**09.2007 – 07.2011     Bachelor in Material Science**

College of Engineering and Applied Sciences, Nanjing University, P. R. China

GPA: 4.49/5.00; GPA Rank: 2 / 120

**09.2011 – 07.2014     Master in Chemistry**

State Key Laboratory of Analytical Chemistry for Life Science

School of Chemistry and Chemical Engineering, Nanjing University, P. R. China

Thesis: Application of Nanomaterials in Electrochemical and Fluorescent Immunoassays

Thesis director: Prof. Junjie Zhu, Prof. Liping Jiang

**10.2014 – 12.2018     Ph.D. in Chemistry**

Laboratory of Physical and Analytical Electrochemistry

Institute of Chemistry and Chemical Engineering

École Polytechnique Fédérale de Lausanne, Switzerland

Thesis: Mass Spectrometry Methods for Bacterial Infection Diagnosis and Cancer Analysis

Thesis director: Prof. Hubert H. Girault, Dr. Liang Qiao

## Scientific Research Experience

- Synthesis of functionalized nanomaterials like copper sulphate nanoparticles, ceria mesoporous nanospheres, metal ion functionalized titanium phosphate nanospheres;
- Immunoassays based on fluorescence spectroscopy and electrochemical sensors;

- Fabrication of PDMS-based microfluidic devices for the analysis of mammalian cells;
- Magnetic separation/Immuno-affinity capture and enrichment of bacteria from complex matrices like human blood;
- Identification of bacteria by MALDI-TOF mass spectrometry;
- Analysis of bacterial cells, mammalian cells and cell-derived exosomes by MALDI-TOF mass spectrometry;
- Antimicrobial susceptibility testing using broth dilution and redox indicators-facilitated amperometric sensors;
- Correlation of MALDI-TOF mass spectrometry with top-down and bottom-up proteomics for the discovery and detection of biomarkers;
- Real-time monitoring of antibiotic degradation by resistant bacteria using microchip-coupled ESI mass spectrometry;

## Awards and Honors

| Year 2008–2010 | China National Scholarship for Undergraduates |
|---|---|
| Year 2008–2010 | Jiangsu Province 'Renmin' Scholarship Award-First Prize |
| Year 2010 | Excellent Social Practice Project of Nanjing University |
| Year 2011 | Outstanding Undergraduate of Nanjing University |
| Year 2012 | Outstanding Minister of Nanjing University Student Union |
| Year 2013 | Outstanding Student Cadre of Nanjing University |
| Year 2012–2013 | Nanjing University Scholarship for Excellent Master Students |
| Year 2014–2018 | Scholarship for PhD Study Abroad–China Scholarship Council |
| Year 2018 | EPFL-Stanford University Exchange Program Fellowship (Firmenich) |

## Patent Applications

**Yingdi Zhu**, Milica Jović, Andreas Lesch, Tzu-En Lin, Horst Pick, Ping-Chih. Ho and Hubert H. Girault, École Polytechnique Fédérale de Lausanne, EPFL-TTO/EPFL Innovation Park, *Skin Cell Analysis,* GB Patent Application No. 1813449.4, 2018.

**Yingdi Zhu**, Milica Jović, Andreas Lesch, Horst Pick and Hubert H. Girault, École Polytechnique Fédérale de Lausanne, EPFL-TTO/EPFL Innovation Park, *Detection of Bacteria,* GB Patent Application No. 1806361.0, 2018.

# Publications

- **Yingdi Zhu**, Horst Pick, Natalia Gasilova, Xiaoyun Li, Tzu-En Lin, Heinz Philipp Laeubli, Alfred Zippelius, Ping-chih Ho and Hubert H. Girault, MALDI detection of exosomes: a potential tool for cancer studies, in submission.

- **Yingdi Zhu**, Milica Jović, Andreas Lesch, Lysiane Tissières Lovey, Michel Prudent, Horst Pick and Hubert H. Girault, Immunoaffinity Amperometric Detection of Bacterial infections, *Angewandte Chemie International Edition*, 2018, 57, 14942-14946.

- **Yingdi Zhu**, Milica Jović, Andreas Lesch, Lysiane Tissières Lovey, Michel Prudent, Horst Pick and Hubert H. Girault, Immunaffine amperometrische Detektion bakterieller Infektionen, *Angewandte Chemie*, 2018, 130, 15158-15162.

- **Yingdi Zhu**, Natalia Gasilova, Milica Jović, Liang Qiao, Baohong Liu, Lysiane Tissières Lovey, Horst Pick and Hubert H. Girault, Detection of antimicrobial resistance-associated proteins by titanium dioxide-facilitated intact bacteria mass spectrometry, *Chemical Science*, 2018, 9, 2212-2221.

- **Yingdi Zhu**, Liang Qiao, Michel Prudent, Alexandra Bondarenko, Natalia Gasilova, Siham Beggah Möller, Niels Lion, Horst Pick, Tianqi Gong, Zhuoxin Chen, Pengyuan Yang, Lysiane Tissières Lovey and Hubert H. Girault, Sensitive and fast identification of bacteria in blood samples by immunoaffinity mass spectrometry for quick BSI diagnosis, *Chemical Science* (front cover), 2016, **7**, 2987-2995.

- **Yingdi Zhu**, Juan Peng, Liping Jiang, Junjie Zhu, Fluorescent immunosensor based on CuS nanoparticles for sensitive detection of cancer biomarker, *Analyst*, 2014, 139, 649-655.

- Andreas Lesch, Milica Jović, Marie Baudoz, **Yingdi Zhu**, Philippe Tacchini, Frédéric Gumy, Hubert Girault, Point-of-Care Diagnostics with Inkjet-Printed Microchips, *ECS Transactions*, 2017, 77(7), 73-81, invited.

- Milica Jović, **Yingdi Zhu**, Andreas Lesch, Alexandra Bondarenko, Fernando Cortés-Salazar, Frédéric Gumy, Hubert H. Girault, Inkjet-printed microtiter plates for portable electrochemical immunoassays, *Journal of Electroanalytical Chemistry*, 2017, 786, 69-76.

- Alexandra Bondarenko, **Yingdi Zhu**, Liang Qiao, Fernando Cortés Salazar, Horst Pick and Hubert. H. Girault, Aluminium foil as single-use substrate for MALDI-MS fingerprinting of different melanoma cell lines, *Analyst*, 2016, 6, 141, 3403-3410.

- Juan Peng, **Yingdi Zhu**, Xinghua Li, Liping Jiang, E. S. Abdel-Halim, Junjie Zhu, Electrochemical immunoassay for the prostate specificantigen using ceria mesoporous nanospheres, *Microchimica Acta*, 2014, 181, 1505-1512.

- Juntao Cao, **Yingdi Zhu**, Rohit Kumar Ranab and Junjie Zhu, Microfluidic chip integrated with flexible PDMS-based electrochemical cytosensor for dynamic analysis of drug-induced apoptosis on HeLa cells, *Biosensors and Bioelectronics*, 2014, 51, 97-102.

- Juntao Cao, Xiaoyao Hao, **Yingdi Zhu**, Ken Sun, and Junjie Zhu, Microfluidic platform for the evaluation of multi-glycan expressions on living cells using electrochemical gimpedance spectroscopy and optical microscope, *Analytical Chemistry*, 2012, 84, 6775-6782.

- Lina Feng, Juan Peng, **Yingdi Zhu**, Liping Jiang and Junjie Zhu, Synthesis of $Cd^{2+}$-functionalized titanium phosphate nanoparticles and application as labels for electrochemical immunoassays, *Chemical Communications*, 2012, 48, 4474-4476.

- Lina Feng, Zhiping Bian, Juan Peng, Fang Jiang, Guohai Yang, **Yingdi Zhu**, Liping Jiang, Junjie Zhu, Ultrasensitive Electrochemical Immunoassay Based on Metal Ion Functionalized Titanium Phosphate Nanospheres, *Analytical Chemistry*, 2012, 84, 7810-7815.